

Dissertation
submitted to the
Combined Faculty of Natural Sciences and Mathematics
of the Ruperto Carola University Heidelberg, Germany
for the degree of
Doctor of Natural Sciences

Presented by
M. Sc. Benjamin Roman Spreng
Born in: Stuttgart, Germany
Oral examination: 12th October 2018

The role of microtubules in *Plasmodium berghei*
sporozoite development, morphology, motility and
infectivity

First examiner: Prof. Dr. Ulrich Schwarz

Second examiner: Prof. Dr. Friedrich Frischknecht

Affidavit

I hereby declare, that the experiments for this work were conducted between April 2014 and July 2018 in the laboratory of Prof. Dr. Friedrich Frischknecht at the parasitology unit of the centre of infectious diseases at the Ruperto-Carola University in Heidelberg.

I further declare that I wrote this thesis independently and that I used no resources other than those indicated in my thesis.

Heidelberg, 29.07.2018

Benjamin R. Spreng

Summary

Malaria is caused by a unicellular parasite of the genus *Plasmodium* which has a complex life cycle involving an *Anopheles* mosquito vector and a vertebrate host. The development in the mosquito vector is crucial for the parasite to be transmitted to new hosts and to ensure genetic diversity. This requires parasite motility, crossing of barriers and persistence for long periods of time. Especially the sporozoite stage which develops in the mosquito gut has to overcome all these challenges to assure transmission back to the vertebrate host. Among others, this demands a very stable but flexible composition of the cytoskeleton. Besides actin filaments and intermediate filaments, microtubules (MTs) are one of the building blocks of the eukaryotic cytoskeleton. MTs are hollow cylinders composed of α - and β -tubulin heterodimers that are essential for many cellular processes, including intracellular transport, chromosome segregation, cell polarity, and migration. In most eukaryotes, the number and length of microtubules is variable whereas the highly polarized and crescent shaped *Plasmodium* sporozoites contain a special subset of cytosolic microtubules called subpellicular microtubules (sMTs) that are well defined in number and length. However, the significance of both parameters has not been studied to date. Little is known about the two α -tubulin isotypes existing in *Plasmodium* that are required for sMT polymerization in sporozoites as well as the influence of sMT parameters (e.g. number, length, arrangement) on sporozoite development and infectivity. In addition, other microtubule subsets such as hemispindle microtubules (hMTs), required for chromosome segregation during sporozoite budding, have been sparsely investigated due to difficulties in labelling MTs within insect stages. In this study, I quantitatively examine the impact of MT number and length in *Plasmodium berghei* by using state of the art gene manipulation strategies and imaging techniques. I could show, that $\alpha 1$ -tubulin is essential for hMT and sMT formation during sporozoite budding, while replacement of $\alpha 1$ -tubulin with $\alpha 2$ -tubulin partially rescued microtubule polymerization. My data show, that microtubules are not essential for nuclear division and onset of sporozoite budding during sporogenesis. However, deletion of $\alpha 1$ -tubulin led to severely deformed sporozoites unable to detach of the sporoblast after budding. Modifications of $\alpha 1$ -tubulin regulatory elements resulted in reduced tubulin expression levels that highly correlated with the number of sMTs found in sporozoites. Reduced sMT numbers impaired sporozoite formation, motility and infectivity. Only sporozoites with 10 or more sMTs were infectious to mice. Replacement of $\alpha 1$ -tubulin with $\alpha 2$ -tubulin resulted in shortened sMTs leading to shorter sporozoites with increased curvature. Parasite lines with reduced MT length and/or number showed reduced transmission

efficiencies when mice were bitten by infected mosquitoes while parasites containing shortened sMTs displayed also delayed prepatencies when mice were infected by intravenous injections indicating also a reduced efficacy in liver infection. Taken together, my findings emphasize the importance of defined microtubule numbers and length in a unicellular organism to ensure efficient transmission as well as functional and transcriptional differences of the two α -tubulin isotypes found in *Plasmodium berghei*.

Zusammenfassung

Die Tropenkrankheit Malaria wird durch einzellige Parasiten der Gattung *Plasmodium spp.* verursacht, welche einen sehr komplexen Lebenszyklus innerhalb von *Anopheles* Mücken und Wirbeltieren aufweisen. Die Entwicklung innerhalb von Moskitos ist entscheidend für die Übertragung des Parasiten auf neue Wirte und die Gewährleistung der genetischen Vielfalt. Dies erfordert jedoch eine Überwindung von mehreren Barrieren, Beweglichkeit und Beständigkeit über längere Zeiträume hinweg. Insbesondere das Sporozoiten-Stadium, das sich im Moskito-Darm entwickelt, muss all diese Herausforderungen meistern, um die Übertragung auf den Wirbeltierwirt zu gewährleisten. Dies erfordert unter anderem einen sehr stabilen aber auch flexiblen Aufbau des Sporozoiten-Zytoskeletts. Neben Aktinfilamenten und Intermediärfilamenten sind Mikrotubuli (MTs) eine der Hauptbestandteile des eukaryotischen Zytoskeletts. MTs sind helikale Hohlkörper, gebildet aus α - und β -Tubulin-Heterodimeren, die für viele zelluläre Prozesse essentiell sind, einschließlich intrazellulärem Transport, Chromosomentrennung, Zellpolarität und Migration. In den meisten Eukaryoten ist die Anzahl und Länge dieser Mikrotubuli variabel, wohingegen die polaren und halbmondförmigen *Plasmodium*-Sporozoiten eine definierte Anzahl und Länge an speziellen zytosolischen Mikrotubuli enthalten, die subpellikuläre Mikrotubuli (sMT) genannt werden. Es ist nur wenig über ihre Funktion als auch über die Bedeutung der genau definierten Anzahl, Länge und Anordnung von sMT auf die Sporozoiten-Entwicklung und deren Infektiosität bekannt. Außerdem ist nicht bekannt, welcher der beiden α -Tubulin-Isotypen existierend in *Plasmodium* für die Bildung dieser Mikrotubuli Verwendung findet. Darüber hinaus wurden Hemispindel-Mikrotubuli (hMT), die für die Chromosomenteilung während der Sporozoiten-Entwicklung benötigt werden, aufgrund von Schwierigkeiten bei der Einfärbung von Mikrotubuli in Insektenstadien nur spärlich untersucht. Die vorliegende Arbeit erforscht zum einen die Bedeutung einer definierten Anzahl und Länge an Mikrotubuli und zum anderen deren besondere Funktion hinsichtlich der Sporozoiten-Entwicklung und Infektiosität mithilfe des Modellorganismus *Plasmodium berghei*. Dabei wurden Genmanipulationsstrategien und bildgebende Verfahren des aktuellsten Stands der Technik verwendet. Es konnte gezeigt werden, dass $\alpha 1$ -Tubulin essentiell für die hMT- und sMT-Bildung während der Sporozoiten-Entwicklung ist, jedoch der Austausch von $\alpha 1$ -Tubulin durch $\alpha 2$ -Tubulin diese Mikrotubuli-Bildung nur teilweise ermöglicht. Die Daten zeigen außerdem, dass Mikrotubuli für die Chromosomenteilung und den Beginn der Sporozoiten-Entwicklung während der Sporogenese nicht essentiell sind. Die Deletion von $\alpha 1$ -Tubulin führte jedoch zu stark deformierten Sporozoiten, die nicht in der Lage waren, sich vom Sporoblasten abzulösen. Modifikationen

von α 1-Tubulin-regulatorischen Elementen führten zu verringerten Tubulin-Expressionsspiegeln, die stark mit der Anzahl an sMT in Sporozoiten korrelierten. Reduzierte sMT-Zahlen beeinträchtigten die Entwicklung, Motilität und Infektiosität von Sporozoiten. Nur Sporozoiten mit 10 oder mehr sMT waren infektiös für Mäuse. Der Austausch von α 1-Tubulin durch α 2-Tubulin führte zu verkürzten sMTs, die wiederum zu kürzeren Sporozoiten mit erhöhter Krümmung führten. Parasitenlinien mit verringerter MT-Länge und/oder MT-Anzahl zeigten eine verminderte Übertragungseffizienz, sobald Mäuse von infizierten Moskitos gebissen wurden. Parasiten, die verkürzte sMTs besaßen, zeigten jedoch auch eine verzögerte Präpatenz, wenn Mäuse durch intravenöse Injektionen infiziert wurden. Zusammengefasst zeigen meine Ergebnisse die Wichtigkeit einer genau regulierten Anzahl und Länge an Mikrotubuli in einem einzelligen Organismus, um eine effiziente Übertragung zu gewährleisten. Darüber hinaus zeigen meine Daten funktionelle und transkriptionelle Unterschiede der beiden α -Tubulin-Isotypen in *Plasmodium berghei* auf.

Table of contents

Summary	VII
Zusammenfassung	IX
Table of contents	XI
Abbreviations	XVI
1. Introduction	1
1.1. Malaria	1
1.1.1. The complex life cycle of <i>Plasmodium</i>	1
1.1.2. Gliding motility of <i>Plasmodium</i> sporozoites	4
1.1.3. The cytoskeleton of <i>Plasmodium</i> sporozoites	5
1.2. Microtubules	8
1.2.1. Microtubule subsets in <i>Plasmodium</i> spp.	9
1.2.2. Tubulin isotypes in <i>Plasmodium</i> spp.	10
1.2.3. Microtubule associated proteins in <i>Plasmodium</i>	13
1.3. Regulation of protein expression in <i>Plasmodium</i> spp.	14
1.4. Aim of this study	16
2. Materials & Methods	17
2.1. Material	17
2.1.1. Chemicals, enzymes, buffers & consumables	17
2.1.2. Media, buffers and solutions	20
2.1.3. Devices	21
2.1.4. Software and websites	22
2.2. Molecular & microbiological methods	24
2.2.1. Polymerase chain reaction	24
2.2.2. Primer design	25
2.2.1. Agarose gel electrophoresis	25
2.2.2. DNA fragment extraction	25
2.2.3. Restriction enzyme digest	26
2.2.4. DNA fragment end modification	26
2.2.5. DNA ligation	26
2.2.6. NEBuilder® HiFi DNA Assembly	26

Table of contents

2.2.7.	Transformation _____	26
2.2.8.	Bacterial overnight cultures _____	27
2.2.9.	Sequencing _____	27
2.2.10.	Bioinformatic analysis _____	27
2.3.	Parasitological methods _____	27
2.3.1.	Determination of parasitemia _____	27
2.3.2.	Cardiac puncture _____	27
2.3.3.	Schizont culture _____	28
2.3.4.	<i>P. berghei</i> schizont transfection _____	28
2.3.5.	Parasite positive and negative selection _____	28
2.3.6.	Parasite storage _____	29
2.3.7.	Isolation of genomic DNA _____	29
2.3.8.	Generation of isogenic lines (limiting dilution) _____	29
2.3.9.	Mosquito infection _____	29
2.3.10.	Analysis of oocyst development _____	29
2.3.11.	Sporozoite isolation and counting _____	30
2.3.12.	Sporozoite movement, length and gliding diameter analysis _____	30
2.3.13.	Fluorescence assay of sporozoites _____	31
2.3.14.	Quantification of microtubule length and intensity _____	31
2.3.15.	Transmission electron microscopy (TEM) _____	32
2.3.16.	Scanning electron microscopy (SEM) _____	33
2.3.17.	Sporozoite tomography _____	33
2.3.18.	Expression levels of $\alpha 1$ -tubulin and $\alpha 2$ -tubulin _____	33
2.3.19.	Mouse infection by mosquito bites or intravenous sporozoite injection _____	34
2.3.20.	Parasite blood stage growth _____	34
2.3.21.	Parasite strain _____	34
2.3.22.	Mosquito strain _____	35
2.3.23.	Ethics statement _____	35
2.3.24.	Statistics _____	35
3.	Results _____	36
3.1.	Generation of genetically modified <i>P. berghei</i> parasites _____	36
3.1.1.	Plasmid vector design _____	36
3.1.2.	Generation of parasite lines _____	39
3.2.	Microtubules in oocyst and sporozoite development of <i>Plasmodium berghei</i> _____	44
3.2.1.	SiR-tubulin can label microtubules <i>in vivo</i> in mosquito midgut oocysts _____	44
3.2.2.	Oocysts can develop intracellularly in mosquito midgut cells _____	49

Table of contents

3.2.3.	Late oocysts show subpellicular and very long hemispindle microtubules _____	50
3.2.4.	Subpellicular microtubules are dynamic during sporozoite budding and beyond ___	52
3.2.5.	<i>α1-tubulin</i> is the predominantly expressed <i>α-tubulin</i> isotype during oocyst development _____	53
3.3.	<i>α1-tubulin</i> is only essential for sporozoite formation _____	55
3.3.1.	Deletion of <i>α1-tubulin</i> has no impact on blood stage growth and oocyst numbers __	56
3.3.2.	Deletion of <i>α1-tubulin</i> does not affect <i>α2-tubulin</i> and <i>CSP</i> expression during early oocyst development but delays oocyst/sporozoite maturation during sporozoite budding _____	56
3.3.3.	Nuclear replication, segregation and membrane alignment appear to fundamentally function in the absence of <i>α1-tubulin</i> during early oocyst development but nuclei distribution to budding sporozoites is strongly impaired _____	58
3.3.4.	Sporozoite budding is initiated and proceeds in <i>α1(-)</i> parasites which lack subpellicular and hemispindle microtubules resulting in aberrant sporozoites and life cycle arrest _____	64
3.3.5.	Complementation of <i>α1(-)</i> with wild-type <i>α1-tubulin</i> reverses the <i>α1(-)</i> phenotype_	72
3.4.	Reduced expression of <i>α1-tubulin</i> leads to fewer subpellicular microtubules and aberrantly formed sporozoites _____	74
3.4.1.	<i>α1-tubulin</i> expression can be reduced by deletion of introns and by codon modification of exons _____	74
3.4.2.	Reduced <i>α1-tubulin</i> expression leads to malformed sporozoites with fewer subpellicular microtubules, variable sporozoite thickness and nuclei size _____	75
3.5.	Specific <i>α-tubulin</i> amino acids define microtubule length whereas <i>α-tubulin</i> expression levels mediate microtubule numbers _____	83
3.5.1.	Introduction of <i>α2-tubulin</i> elements does not affect oocyst numbers _____	83
3.5.2.	Complementation of the <i>α1(-)</i> strain by a set of <i>α2-tubulin</i> constructs results in grading aberrant sporozoites with less and shorter subpellicular microtubules _____	84
3.6.	Subpellicular microtubule length and number define sporozoite overall morphology including length, curvature and thickness _____	94
3.6.1.	Subpellicular microtubule numbers or <i>α2-tubulin</i> expression have no impact on apical polar ring tilt _____	94
3.6.2.	A reduced number of subpellicular microtubules leads to IMC & plasma membrane extrusions _____	95
3.6.3.	Subpellicular MTs stabilize the IMC and force nuclei into elongated formation ___	97
3.6.4.	Parasite lines with short maximum microtubule length have shorter sporozoites ___	99
3.6.5.	<i>α2-tubulin</i> chimeras have an increased sporozoite curvature _____	100

Table of contents

3.6.6.	A reduced number of subpellicular microtubules negatively influences gliding motility of sporozoites _____	100
3.6.7.	Attachment to the subpellicular network and the distance between neighboring subpellicular microtubules is changed in $\alpha 2$ -tubulin chimeras and $\alpha 1^{\Delta c-term}$ _____	102
3.1.	Subpellicular microtubule length and number define sporozoite infectivity	103
3.1.1.	Subpellicular microtubule numbers define salivary gland invasion efficiency ____	103
3.1.2.	At least 10 subpellicular MTs are necessary to invade mosquito salivary glands __	104
3.1.3.	A reduced number and shortening of subpellicular microtubules lowers parasite infectivity in mice _____	105
4.	Discussion _____	106
4.1.	Nuclear segregation can occur in the absence of microtubules but microtubules are important to sustain nuclear integrity _____	108
4.1.1.	Hemispindle microtubules are most likely important to sustain nuclear integrity _	109
4.1.2.	Cell cycle checkpoints seem to be absent during oocyst development _____	111
4.2.	$\alpha 1$-tubulin is essential for sporozoite formation but the deletion of $\alpha 1$-tubulin can be partially rescued by $\alpha 2$-tubulin _____	112
4.2.1.	$\alpha 1$ -tubulin has no important function during blood stage development _____	112
4.2.2.	$\alpha 1$ -tubulin is essential for nuclei packaging and microneme positioning into sporozoites _____	112
4.2.3.	Sporozoite “budding” might be sporozoite “invagination” _____	115
4.2.4.	Complementation of the $\alpha 1(-)$ parasite line with WT $\alpha 1$ -tubulin or a set of $\alpha 2$ -tubulin constructs rescues sporozoite formation _____	115
4.3.	Reduced α-tubulin expression levels lead to fewer subpellicular microtubules (sMTs) while the α-tubulin isotype expressed defines sMT length _____	116
4.3.1.	$\alpha 1$ -tubulin introns might be important for base line tubulin expression _____	116
4.3.2.	$\alpha 1$ -tubulin codon modification strongly reduces $\alpha 1$ -tubulin RNA levels _____	116
4.3.3.	$\alpha 2$ -tubulin regulatory elements affect α -tubulin expression levels _____	117
4.3.4.	α -tubulin expression levels highly correlate with the number of subpellicular microtubules _____	118
4.3.5.	Isotypic differences between the two α -tubulins are suggested to define sMT length and the C-terminus might represent one major functional difference _____	120
4.4.	Subpellicular microtubules stabilize sporozoite morphology _____	122
4.5.	The apical polar ring is not restricted to 17 microtubule nucleation sites ____	123
4.6.	Subpellicular microtubules are dynamic _____	123

Table of contents

4.7.	Microtubule length mediates sporozoite length and curvature	123
4.8.	Microtubule length and number influences sporozoite motility	126
4.9.	Subpellicular microtubule length and number define sporozoite infectivity	127
4.9.1.	Microtubule numbers and length define salivary gland invasion efficiency	127
4.9.2.	Microtubule length defines sporozoite infectivity in mice	129
4.10.	Do $\alpha 1$-tubulin and $\alpha 2$-tubulin have different functionalities?	131
4.11.	Conclusion	132
5.	References	133
6.	Publications	153
7.	Acknowledgements	153
8.	Appendix	153
8.1.	Primers	155
8.1.1.	Generation of $\alpha 1^{cm\&\Delta introns}$	155
8.1.2.	Generation of $\alpha 1^{\Delta introns}$	155
8.1.3.	Generation of $\alpha 1^{WTcompl.}$	155
8.1.4.	Generation of $\alpha 2^{+++}$	155
8.1.5.	Generation of $\alpha 2^{++}$	156
8.1.6.	Generation of $\alpha 2^{+}$	156
8.1.7.	Generation of $\alpha 1^{\Delta c-term}$	157
8.1.8.	Genotyping primers	157
8.1.9.	qRT-PCR primers	157
8.2.	Macros	158
8.2.1.	Crop of EM images	158
8.2.2.	Spinning Disc image analysis	158

Abbreviations

Sizes and volumes are indicated according to the “international system of units“ (SI).

5-FC	5-fluorocytosine
ADP	adenosine diphosphate
APR	apical polar ring
ATP	adenosine triphosphate
BSA	bovine serum albumin
C-terminus	carboxy-terminus
cm	codon modified
CSP	circumsporozoite protein
ddH ₂ O	double distilled water
DHFS	dihydrofolate synthase
DIC	differential interference contrast
DNA	deoxyribonucleic acid
dNTP	deoxynucleotide triphosphates
<i>E. coli</i>	<i>Escherichia coli</i>
EB	End binding protein
<i>efl</i> α	elongation factor 1 α
F-actin	filamentous actin
G-actin	globular actin
gDNA	genomic deoxyribonucleic acid
GFP	green fluorescent protein
hDHFR	human dihydrofolate reductase
HEPES	4-(2-hydroxyethyl)-1-piperazineethanesulfonic acid
HL	hemolymph
hMT	hemispindle microtubule
HP1	heterochromatin protein 1
i.p.	intraperitoneal
i.v.	intravenous
IMC	inner membrane complex
lncRNA	long non-coding RNA
mRNA	messenger RNA
MT	microtubule
MTOC	Microtubule organizing center
ncRNA	non-coding RNA

Abbreviations

NMRI	Naval Medical Research Institute
NP-40	Nonidet P-40
ORF	open reading frame
<i>Pb</i>	<i>Plasmodium berghei</i>
PBS	phosphate buffered saline
PCR	polymerase chain reaction
<i>Pf</i>	<i>Plasmodium falciparum</i>
PFA	paraformaldehyde
PM	plasma membrane
qRT-PCR	quantitative real-time PCR
RBP	RNA binding protein
RNA	ribonucleic acid
rpm	rotations per minute
RPMI-1640	Roswell Park Memorial Institute medium 1640
RT	room temperature
SD	standard deviation
SFA	striated fiber assemblin
SG	salivary gland
sMT	subpellicular microtubule
SPN	subpellicular network
SPP	spindle pole plaque
<i>spp.</i>	<i>species pluralis</i>
T-medium	transfection medium
<i>T. gondii</i>	<i>Toxoplasma gondii</i>
Taq	<i>Thermus aquaticus</i> polymerase
<i>Tg</i>	<i>Toxoplasma gondii</i>
U	units
UTR	untranslated region
v/v	volume / volume
w/v	weight / volume
WT	wild-type (refers to <i>P. berghei</i> ANKA strain)
yFCU	yeast cytosine deaminase and uridyl phosphoribosyl transferase

1. Introduction

1.1. Malaria

The disease malaria is caused by the unicellular protist of the genus *Plasmodium spp.* It causes a serious health and economic burden especially in sub-Saharan Africa. The World Health Organization (WHO) estimates 216 million cases of malaria with 445,000 deaths in 2016, which is an increase of 5 million cases over 2015 (WHO, 2017). This indicates that after a long and successful period of malaria control progress has stalled.

Plasmodium spp. belong to the phylum of apicomplexan which also includes other unicellular parasites such as *Toxoplasma gondii*. Five different human infecting *Plasmodium* species are known: *P. falciparum*, *P. vivax*, *P. knowlesi*, *P. ovale* and *P. malariae* (Kantele and Jokiranta, 2011). *P. knowlesi* is also categorized as a zoonotic simian species because it can infect humans and macaques, but transmission can only occur from macaques to mosquitos (Ramasamy, 2014). Most *Plasmodium* infections are asymptomatic due to acquired immunity of persons living in endemic regions. Indeed, mostly children under the age of five and travelers, which have not acquired immunity suffer from severe malaria with symptoms like high fevers, chills, anemia and neuronal and respiratory impairments. This is caused by massive erythrocyte lysis and clogging of blood capillaries in the brain or lung. Among the five species, *P. falciparum* causes over 90% of all malaria cases, is responsible for most severe malaria cases (WHO, 2017) and most deaths.

Attempts to generate a fully protective vaccine against *Plasmodium* were not successful to date. The complexity of the parasite life cycle, its perfect adaption and exploitation of weaknesses of its host combined with the lack of knowledge especially in terms of malaria immunity are major reasons for this failure (Stanisic and Good, 2015; Long and Zavala, 2017). However, partial success was achieved with the first licensed malaria vaccine RTS,S (Olotu et al., 2016). Yet this vaccine only protects 30-50% of children after 4 immunizations and immunity wanes after just one year (RTS, 2015).

1.1.1. The complex life cycle of *Plasmodium*

Plasmodium is an obligate parasite with a complex life cycle (**Figure 1.1**) which involves a mosquito host and a vertebrate host. It is transmitted by an infected female *Anopheles* mosquito which deposits approximately 10-100 sporozoites into the vertebrate dermis during a blood meal (Frischknecht et al., 2004; Vanderberg and Frevert, 2004; Medica and Sinnis, 2005;

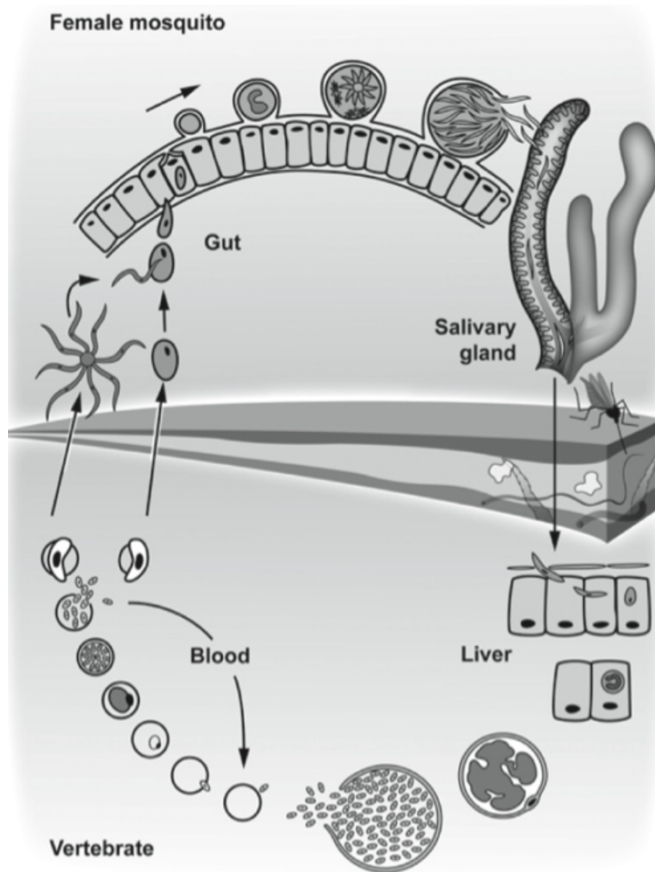


Figure 1.1. The *Plasmodium* life cycle. Sporozoites are injected into the skin of a vertebrate host during a blood meal of an infected *Anopheles* mosquito. Sporozoites migrate, invade a blood capillary and are passively transported towards the liver. Sporozoites enter into hepatocytes and transform into thousands of merozoites which are released into the blood and infect erythrocytes. Besides asexual replication within erythrocytes, also gametocytes are formed for sexual reproduction. After the uptake by a mosquito, gametes can fuse to a zygote form which an ookinete emerges which traverses the midgut epithelium. Below the basal lamina, it develops into an oocyst which produces hundreds to thousands of sporozoites. Sporozoites egress into the hemolymph and invade the mosquito salivary glands where they rest to be injected during a mosquito blood meal. Figure from (Frischknecht, Hellmann, and Singer, 2011)

Amino et al., 2006; Hellmann et al., 2011; Hopp et al., 2015). Once injected, sporozoites actively search and invade blood capillaries which can take at least 15 min (Sidjanski and Vanderberg, 1997; Matsuoka et al., 2002). Sporozoites are then passively transported to the liver via the circular blood system (Douglas et al., 2015) and enter the liver via Kupffer cells and endothelial cells (Frevort et al., 2005; Baer, Roosevelt, et al., 2007; Tavares et al., 2013). Sporozoites first traverse several cells before transforming into an extra-erythrocytic stage within an intracellular parasitophorous vacuole (Mota et al., 2001; Risco-Castillo et al., 2015). During liver stage development, enormous replication is performed by schizogony, a special form of parasite multiplication which first includes several rounds of nuclear divisions and only a final round of daughter cell assembly therefore temporarily resulting in multinucleated cells (Striepen et al., 2007; Francia and Striepen, 2014). Nuclear replication is performed by the parasite via endomitosis which involves nuclei replication without disintegration of the nuclear membrane (Striepen et al., 2007; Arnot, Ronander, and Bengtsson, 2011; Francia and Striepen, 2014). In *P. vivax* and *P. ovale*, some liver stages can develop into hypnozoites, a dormant parasite stage that can lead to new malaria symptoms years after the first outbreak (Dembélé et al., 2014). Once schizogony is completed, thousands of the so-called merozoites are released into the blood stream (Prudêncio, Rodriguez, and Mota, 2006) within vesicles called

merosomes (Sturm et al., 2006). These eventually rupture (Baer, Klotz, et al., 2007) and release the merozoites into the blood stream where they subsequently invade erythrocytes (Dvorak et al., 1975). Similar to the extra-erythrocytic stages, erythrocytic stages develop within a parasitophorous vacuole and undergo asexual replication via schizogony (Francia and Striepen, 2014). This includes the transformation of the merozoite into a ring, trophozoite and finally into a schizont stage leading to newly developed merozoites. Especially during schizont development, erythrocytes are strongly remodeled by the parasite. The parasite uses a protein export system to secrete proteins through the parasitophorous vacuole into the erythrocytic cytosol (De Koning-Ward et al., 2016). One such protein is PfEMP-1, which is involved in forming knob-structures on the erythrocyte plasma membrane, important for cytoadherence to the endothelium of blood vessels to avoid clearance in the spleen (Langreth and Peterson, 1985; Tilley, Dixon, and Kirk, 2011; Elsworth et al., 2014). Depending on the *Plasmodium* species, merozoites egress out of erythrocytes after 24 to 72 hours. Erythrocytic development including the rupture of erythrocytes is responsible for malaria symptoms (Boyle et al., 2014), whereas cytoadherence of parasitic blood stages is related to cerebral malaria (van der Heyde et al., 2006).

Besides erythrocytic asexual replication, *Plasmodium* also undergoes sexual commitment by forming into male and female gametocytes (Josling and Llinás, 2015). Following a blood meal of a female mosquito, male gametocytes can sense the drop in pH, temperature and increase in xanthurenic acid in the mosquito midgut (Billker et al., 1998) which initiates the formation of eight motile microgametes (Sinden and Croll, 1975; Sinden, Canning, and Spain, 1976; Janse, van der Klooster, et al., 1986; Janse, Van Der Klooster, et al., 1986). These fuse with female macrogametes to form zygotes and subsequently develop into ookinetes. Motile ookinetes can cross the mosquito midgut wall (Garnham, Bird, and Baker, 1962; Garnham et al., 1969; Dessens et al., 1999; Vinetz, 2005) and develop into an oocyst below the basal lamina (Garnham et al., 1969; Vlachou et al., 2006; Angrisano et al., 2012). Oocysts form a capsule around their plasma membrane and enlarge progressively (Vanderberg and Rhodin, 1967; Garnham et al., 1969). In *P. berghei*, oocysts maturation takes about 2 weeks depending on the *Plasmodium* species (Smith and Barillas-Mury, 2016). Similar to erythrocytic and liver stage development, parasite multiplication is performed by schizogony, here also called sporogony. First, multiple asynchronous nuclear divisions occur in the absence of cytokinesis until approximately a thousand nuclei are formed within the multinucleate oocyst. From day 10 post blood meal, the plasma membrane invaginates followed by nuclei alignment to the membrane (Thathy et al., 2002; Burda et al., 2017). Thereupon, hundreds to thousands of uninucleate sporozoites form

during the process of sporozoite budding (Terzakis, Sprinz, and Ward, 1967; Vanderberg and Rhodin, 1967; Sinden and Garnham, 1973; Schrével, Asfaux-Foucher, and Bafort, 1977; Sinden and Strong, 1978; Aikawa, 1988; Thathy et al., 2002; Kappe, Kaiser, and Matuschewski, 2003; Schrevel et al., 2007). This involves the formation of the apical polar ring, its tethering via the rootlet fiber to the spindle pole plaque of the aligned nucleus and the formation of the inner membrane complex (IMC). The IMC is a bilaminar layer formed along the inside of the budding sporozoite by fusing flattened Golgi-derived vesicles. Subsequently, subpellicular microtubules (sMTs) along the IMC and pre-rhoptries are formed while the budding sporozoite increases in length. After the sporozoite reaches approximately half its final length, the nucleus is pulled into the budding sporozoite and pre-micronemes are formed. Each budding sporozoite is finally invaded by a mitochondrion and an apicoplast. Upon full formation, sporozoites actively egress from the oocyst into the surrounding mosquito hemolymph. This process is performed by proteolysis of the oocyst wall and active sporozoite movement (Aly and Matuschewski, 2005; Klug and Frischknecht, 2017). Sporozoites are passively transported via the mosquito hemolymph to the mosquito salivary glands (Douglas et al., 2015) where they actively traverse the acinar cells by forming a transient parasitic vacuole and subsequently enter into the secretory cavities of the salivary glands (Sterling, Aikawa, and Vanderberg, 1973; Pimenta, Touray, and Miller, 1994; Rodriguez and Hernández-Hernández, 2004; Ghosh et al., 2009). Here, sporozoites rest until injection into a new host (Frischknecht et al., 2004; Douglas et al., 2015).

1.1.2. Gliding motility of *Plasmodium* sporozoites

At several stages of the parasite life cycle, active movement is necessary for successful parasite transmission such as sporozoite migration through the vertebrate host skin to find a blood capillary, merozoite motility after schizont rupture to find an erythrocyte, microgamete motility in the mosquito midgut to find a female macrogamete or during ookinete transition of the mosquito midgut epithelium (Douglas et al., 2015). Despite the lack of cilia or flagella, *Plasmodium* sporozoites can glide with an average speed of 1-2 $\mu\text{m/s}$ in 2D and 3D environments (Vanderberg, 1974; Amino et al., 2006; Hellmann et al., 2011; Hopp et al., 2015). In comparison, this is 10 times faster than the speed of neutrophil granulocytes, which are one of the first responding cells of the innate immune system to infections (Lämmermann et al., 2013). This speed is achieved by a special form of locomotion called gliding motility which is unique to apicomplexans (Heintzelman, 2015). The forces needed for gliding are generated in the so called glideosome located in the supra-alveolar space between the plasma membrane

(PM) and the inner membrane complex (IMC) which is subtending the PM (Keeley and Soldati, 2004; Heintzelman, 2015; Frischknecht and Matuschewski, 2017). The IMC and PM function as important anchor sites for the glideosome. Gliding forces are generated via an actin-myosin based motor complex (Baum et al., 2008; Heintzelman, 2015). Myosin are anchored via adapter proteins to the IMC/SPN whereas actin filaments (F-actin) are assumed to be connected to transmembrane adhesins of the PM (Gaskins et al., 2004; Baum et al., 2006; Sanders et al., 2007; Bullen et al., 2009; Jacot et al., 2016). Adhesins are incorporated into the plasma membrane by microneme secretion at the anterior end of the sporozoite (Morahan, Wang, and Coppel, 2009). Adhesins of the PM in turn are binding to extracellular host receptors. During gliding, myosins are pushing filamentous actin (F-actin) and its connected adhesins towards the rear of the parasite which results in retrograde flow and a forward movement of the sporozoite (Münter et al., 2009; Quadt et al., 2016). The required counterforce is accomplished by the IMC and its connection to the subpellicular network (SPN) which in turn is stabilized by sMTs (Kudryashev et al., 2010). To accomplish continuous gliding, actin-adhesin complexes have to be disassembled before accumulation at the rear of the sporozoite. It is suggested that this is mainly achieved by the intrinsic properties of *Plasmodium* actin, which is predominantly found in its globular (G-actin) state. Actin state alterations induced by actin stabilizing or destabilizing drugs (e.g. Jasplakinolide, Cytochalasin D) or introduced parts of rabbit actin as actin chimera parasites have shown to impair parasite gliding and invasion (Wetzel, Håkansson, and Hu, 2003; Münter et al., 2009; Skillman et al., 2011)(Ross Douglas, unpublished work). This glideosome model is the most logical to date. However, there is still ongoing debate (Meissner, Ferguson, and Frischknecht, 2013; Whitelaw et al., 2017).

1.1.3. The cytoskeleton of *Plasmodium* sporozoites

Sporozoites (**Figure 1.2**) are the only parasite stage which have to cross several barriers (salivary gland, skin, blood capillary, hepatocytes) whereas all other *Plasmodium* stages have to only cross one barrier or no barrier at all; e.g. merozoites have to invade erythrocytes by forming a parasitophorous vacuole (no barrier crossing) and ookinetes have to traverse the mosquito midgut epithelium. Sporozoites have to last for weeks while waiting within the mosquito salivary glands until the mosquito takes a blood meal. Therefore, the requirements on sporozoites are tremendous, including to be long-lasting, stable and flexible. It is suggested, that the sporozoite rigidity and flexibility is strongly dependent on sMTs but also on the IMC and SPN (Morrissette and Sibley, 2002a; Cyrklaff et al., 2007; Kudryashev et al., 2010). As mentioned above, the IMC is connected to and stabilized by the SPN consisting of intermediate

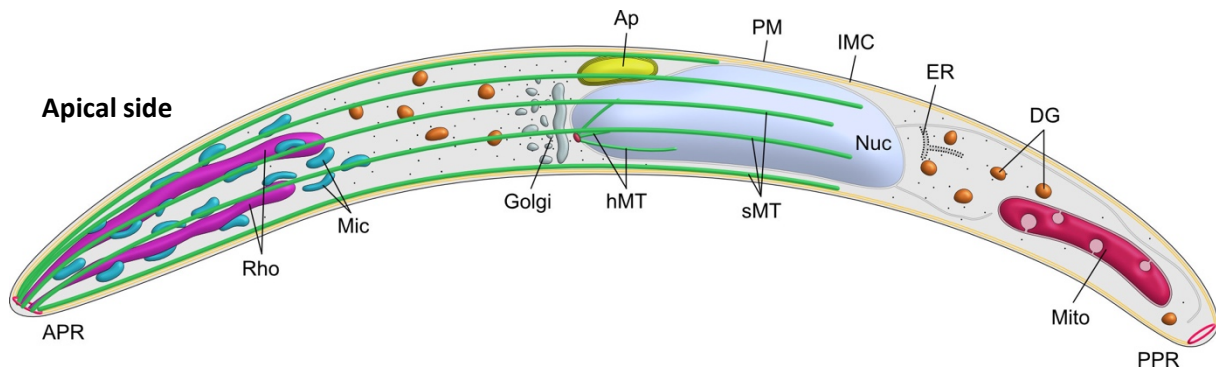


Figure 1.2. *Plasmodium* sporozoite. Sporozoites are extremely polarized cells (apical side, left). The plasma membrane (PM, black) is underlined by the inner membrane complex (IMC, yellow) and the subpellicular network (SPN, not shown). Subpellicular microtubules (sMTs, green) are attached to the apical polar ring (APR, red) and to the SPN and reach approximately 2/3 the length of the sporozoite. The apical end of the sporozoite contains rhoptries (Rho, purple) and micronemes (Mic, blue) which are important secretory organelles involved in adhesion, motility and sporozoite invasion, including formation of the parasitophorous vacuole. The Golgi apparatus (Golgi, grey) is located apical from the nucleus (Nuc, light blue) and the apicoplast (Ap, yellow) is usually found next to the nucleus. The nuclear membrane extends towards the posterior end of the sporozoite to form the endoplasmic reticulum (ER). In not fully mature sporozoites, hemispindle microtubules (hMTs, green) attached at the spindle pole plaque (centriolar plaque, MTOC, red) can be seen within the nucleus. Dense granules (DG, orange) and ribosomes (black dots) are spread over the entire sporozoite. One mitochondrion (Mito, dark red) is found at the posterior end of the sporozoite. The IMC emerging from the APR is attached to the posterior polar ring (PPR).

filaments (Mann and Beckers, 2001; Morrissette and Sibley, 2002a; Khater, Sinden, and Dessens, 2004). The SPN in turn is stabilized by sMTs which are tethered to the subpellicular network via yet an unknown linker protein (Kudryashev et al., 2010). Interestingly, the number of sMTs is highly regulated with 16 sMTs per sporozoite in case of *P. berghei* (Vanderberg, Rdodin, and Yoeli, 1967). sMTs reach about 2/3 the length of the sporozoite (Morrissette and Sibley, 2002a; Baum et al., 2008) and originate at the apical polar ring in an equally spaced manner but show a polar dorsoventral distribution towards the center of the sporozoite (Kudryashev et al., 2012)(**Figure 1.3**). When gliding on a 2D surface, the group of many microtubules is located at the substrate-facing side whereas a single microtubule is found on the opposite side of the sporozoite (Kudryashev et al., 2012). The apical polar ring (APR) is tilted towards the substrate suggesting its role in depositing adhesins on the substrate side thereby promoting directional gliding (Kudryashev et al., 2012). Sporozoites also show an overall crescent shape. *In vivo* experiments demonstrated that sporozoites meander around small blood capillaries before invasion (Amino et al., 2006; Srinivasan et al., 2006; Hopp et al., 2015) and *in vitro* micro-pillar arrays revealed a preferred pillar diameter of 10 μm for sporozoite gliding which is similar to peripheral blood capillaries (Muthinja et al., 2017). This

suggests, that the crescent shape found in sporozoites is adapted to blood capillaries of its vertebrate host but the underlying mechanism is not known to date.

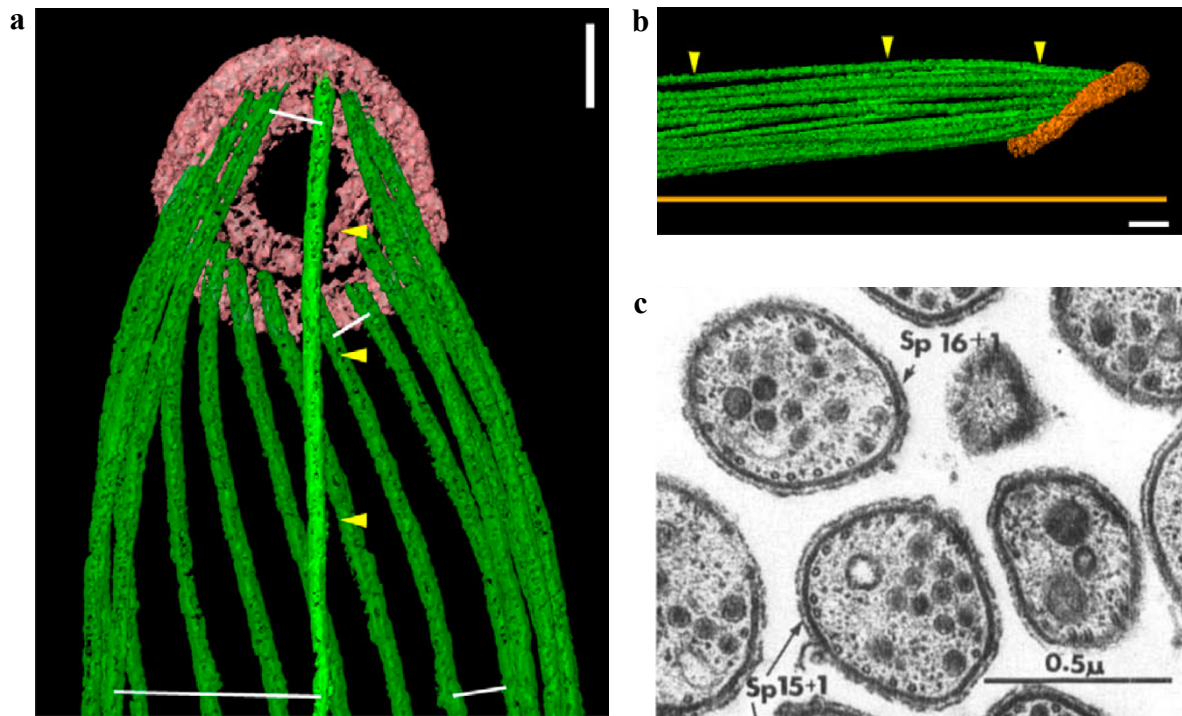


Figure 1.3. The number and arrangement of subpellicular microtubules (sMT) in *Plasmodium berghei* sporozoites. (a) Cryoelectron tomography shows the attachment of sMTs (green) to the apical polar ring (APR, red) and reveals the dorsoventral polarity of sMTs. The single sMT is indicated with yellow arrowheads (image from: Kudryashev et al., 2012). Scale bar corresponds to 100 nm. (b) Side view of a sporozoite indicating the APR (orange) tilt towards the substrate (orange bar) and the location of the single microtubule (yellow arrowheads) on the opposite side (image from: Kudryashev et al., 2012). Scale bar corresponds to 100 nm. (c) Transmission electron microscopy of apical sporozoite cross sections reveal sMTs below the pellicle of the sporozoites. The total number of sMTs is highly regulated to a median of 15+1 (image from: Vanderberg, Rdodin, and Yoeli, 1967).

Attempts to target the parasite cytoskeleton by microtubule disruption drugs were not successful. Microtubule disrupting drugs such as oryzalin or dinitroanilines have no effect on fully formed sMTs in extracellular parasites. However, during parasite development and nuclear division, microtubule disruption caused a lack of apical polarity and the incapability of parasite replication (Russell and Sinden, 1981; Bell, 1998; Morrissette and Sibley, 2002a).

1.2. Microtubules

Besides microfilaments (actin filaments) and intermediate filaments, microtubules are the building block of the eukaryotic cytoskeleton (Alberts et al., 2014). Microtubules (MTs) are essential for many cellular processes, including intracellular transport, chromosome segregation, establishment and maintenance of polarity, and migration (Fojo, 2008; Alberts et al., 2014). MTs are composed from protofilaments of α -tubulin and β -tubulin, which arrange into hollow cylinders with a diameter of 25 nm (Alberts et al., 2014). MTs are polar, with one end of the microtubule crowned by α -tubulins (minus end) and the other by β -tubulins (plus end). The minus end is usually anchored or capped in a microtubule organizing center (MTOC) such as a centrosome. The plus end is the more dynamic end of the MT (Alberts et al., 2014). MTs can spontaneously nucleate in case GTP-bound $\alpha\beta$ -tubulin heterodimer concentrations are high enough, however *in vivo*, nucleation is usually restricted to γ -tubulin ring complexes located within MTOCs (Sulimenko et al., 2017). Spontaneous microtubule nucleation is a kinetically restrained process which needs to overcome a high energy barrier. Increasing tubulin

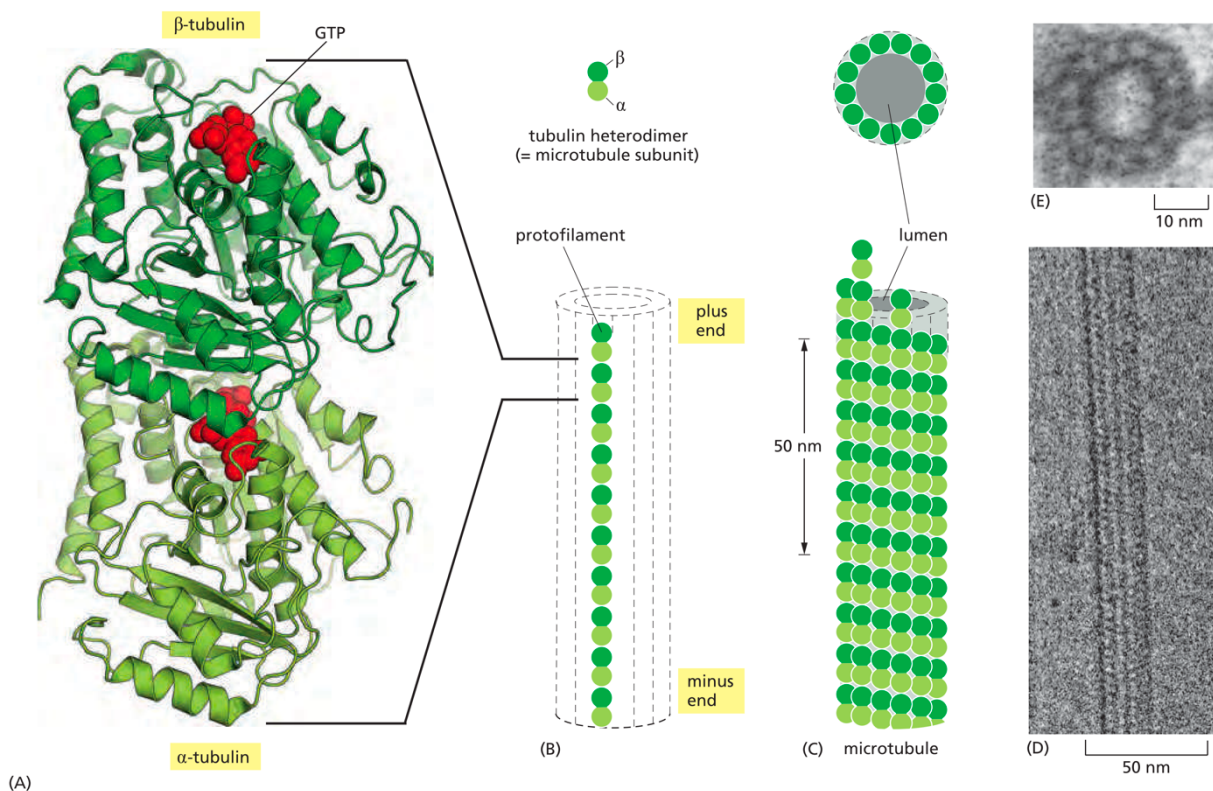


Figure 1.4. Microtubule structure. (a) α -tubulin and β -tubulin monomers are tightly bound to form an $\alpha\beta$ -tubulin heterodimer. Both tubulins can bind GTP (red), however, only β -tubulin can hydrolyze GTP to GDP+P_i, an important step in destabilizing already formed microtubules. (b) Microtubules are usually formed by 13 protofilaments which consist of adjacent tubulin heterodimers orientated in the same direction. (c) Microtubules are hollow tubes arranged from protofilaments. (d) Electron microscopy images (top and side view) showing a 13 protofilament microtubule. Figure from Alberts et al., 2014.

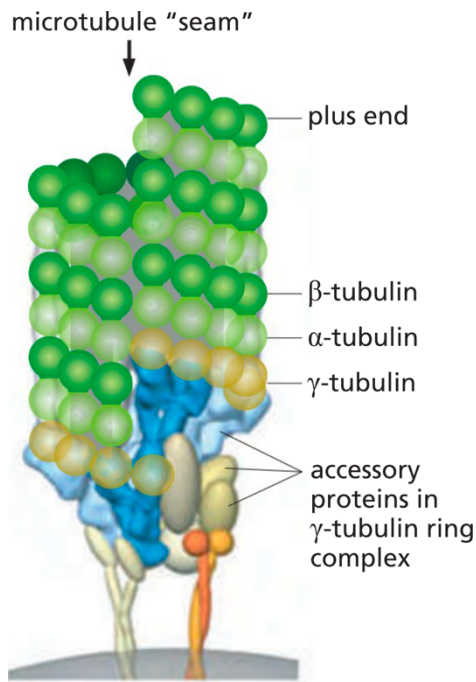


Figure 1.5. Microtubule nucleation is facilitated by a γ -tubulin ring complex. Spontaneous microtubule nucleation is a kinetically restrained process which needs to overcome a high energy barrier. Increasing tubulin concentrations can rise efficiency of nucleation. To allow microtubule nucleation in physiological environments, γ -tubulin ring complexes act as microtubule templates to reduce necessary tubulin concentration for nucleation. α -tubulins bind to the γ -tubulin ring complex, therefore defining the nucleation site as the microtubule minus end. Besides γ -tubulin, other accessory proteins are involved in microtubule nucleation. Figure from Alberts et al., 2014

concentrations can therefore rise efficiency of nucleation (Kuchnir Fygenon et al., 1995). For mammalian tubulin, approximately $>20 \mu\text{M}$ tubulin is required for spontaneous nucleation. This concentration can be reduced by template-initiated nucleation (centrosomes with bound γ -tubulin ring complexes) which only needs approximately $>6 \mu\text{M}$ tubulin for nucleation (Voter and Erickson, 1984; Wiczorek et al., 2015).

MTs are dynamic structures that are able to polymerize and depolymerize depending on the addition or loss of $\alpha\beta$ -tubulin heterodimers. The dynamic process of switching between MT shrinkage and growth is called dynamic instability (Mitchison and Kirschner, 1984). This is strongly influenced by the GTPase activity of tubulin itself (Carlier and Pantaloni, 1981), end-binding (EB) proteins and microtubule-associated proteins (MAPs) including microtubule polymerases and depolymerases and regulatory kinesins (Howard and Hyman, 2007; Akhmanova and Steinmetz, 2008, 2015; Brouhard and Rice, 2018).

1.2.1. Microtubule subsets in *Plasmodium spp.*

At least three functional classes of microtubules are found in *Plasmodium*, namely the subpellicular, spindle and axonemal microtubules (Bell, 1998).

Subpellicular microtubules (sMTs) are found in all motile stages of the parasite life cycle – the sporozoites, ookinetes and merozoites (Morrissette and Sibley, 2002a). As mentioned previously (chapter 1.1.3), sMTs are one of the key components of the parasites' cytoskeleton and thus contribute to parasite cell shape and integrity and are possibly involved in motility

(chapter 1.1.2) and infectivity (Bell, 1998; Morrissette and Sibley, 2002a). The number of sMTs differs among the parasite stages and species. While some *P. berghei* merozoites lack sMTs (Lemgruber and Kudryashev, unpublished data), all *P. falciparum* merozoites show 3-4 sMTs (often referred to as f-MAST) (Fowler et al., 1998) and merozoites of *P. fallax* even contain 24-26 sMTs (Aikawa, 1967). Ookinetes contain between 55-65 sMTs (*P. falciparum*: approximately 60 sMTs; *P. gallinaceum*: at least 55 sMTs; *P. cynomolgi*: at least 65 sMTs) (Garnham, Bird, and Baker, 1962; Morrissette and Sibley, 2002a). In sporozoites, a range between 11-17 sMTs are found among different species (*P. berghei*, 15-17 sMTs; *P. falciparum*: 13-17 sMTs; *P. vivax*: 11; *P. cynomolgi*: 11; *P. ovale*: 13, *P. bastianellii*: 11; *P. gallinaceum*: 12) (Garnham, Bird, and Baker, 1960, 1963; Garnham et al., 1961; Sinden and Strong, 1978).

Spindle microtubules are found during schizogony of replicating parasites. This implicates not only microtubules during nuclear segregation but also during daughter cell assembly. The so-called hemispindle microtubules stay intact until early budding in sporozoites (Morrissette and Sibley, 2002a; Schrevel et al., 2007). Due to endomitosis which involves nuclei replication without disintegration of the nuclear membrane, hemispindle microtubules are located inside the nucleus and are attached at a spindle pole plaque (also called centriolar plaque, MTOC) which is embedded in the nuclear membrane (Morrissette and Sibley, 2002a; Striepen et al., 2007; Arnot, Ronander, and Bengtsson, 2011; Gerald, Mahajan, and Kumar, 2011; Francia and Striepen, 2014).

Axonemal microtubules are exclusively found in microgametes in *Plasmodium*. They are the building block of the axoneme. Similar to other eukaryotic axonemes, the characteristic “9x2 + 2” microtubule arrangement is also found in the flagellum of microgametes in *Plasmodium* (Sinden, Canning, and Spain, 1976; Sinden et al., 1978; Nicastro et al., 2006). The flagellum is used for locomotion, to reach a macrogamete and accomplish efficient sexual replication.

1.2.2. Tubulin isotypes in *Plasmodium* spp.

The number of tubulin isotypes differs across eukaryotes **Figure 1.6**. Humans for instance express seven α - and eight β -tubulins whereas mice only express six α - and seven β -tubulins and yeast only expresses two α -tubulins and one β -tubulin (Ludueña and Banerjee, 2008; Brouhard and Rice, 2018). Already 40 years ago, Fulton and Simpson introduced the multi-tubulin hypothesis, which postulated that each isotype confers a specific function (Fulton and Simpson, 1976). Amino acid differences among isotypes are often highly conserved across species thus suggesting a functional significance. The most unambiguous experiments

	α	β
Plants & animals		
<i>Homo</i> (human)	7	8
<i>Mus</i> (mouse)	6	7
<i>Drosophila</i>	4	3
Fungi		
<i>Candida</i>	1	1
<i>Saccharomyces</i>	2	1
Protista		
<i>Toxoplasma</i>	3	3
<i>Plasmodium spp.</i>	2	1

Figure 1.6. Tubulin isotypes in eukaryotes and *Plasmodium spp.* The number of tubulin isotypes can vary widely across different species. In many multicellular organisms, tissue specific tubulin expression is observed. Data collected from (Ludueña and Banerjee, 2008).

supporting this hypothesis were acquired in the 90s when isotypes of *Drosophila* were altered and interchanged which eventually led to malfunctions (Hoyle and Raff, 1990; Matthews, Rees, and Kaufman, 1993). Around the same time, it was shown that purified isotypes can have different ligand-binding properties and assembly kinetics (Banerjee et al., 1990) giving cells the ability to regulate the dynamic behavior of microtubules not just by microtubule associated proteins or by posttranslational modifications but also by differential expression of tubulin isotypes. In contrast, also interchangeability of isotypes was shown in the case of yeast (Schatz, Solomon, and Botstein, 1986) and other studies as discussed in detail in (Ludueña and Banerjee, 2008). It can therefore be said, that the multi-tubulin hypothesis is fundamentally correct, but not all isotypes can be explained by it.

Only two α -tubulins (namely $\alpha 1$ -tubulin and $\alpha 2$ -tubulin) and one β -tubulin located on different chromosomes are identified in the *Plasmodium* genome (Delves et al., 1989; Holloway et al., 1989, 1990)(Figure 1.7). $\alpha 2$ -tubulin is predominantly expressed during *Plasmodium* blood

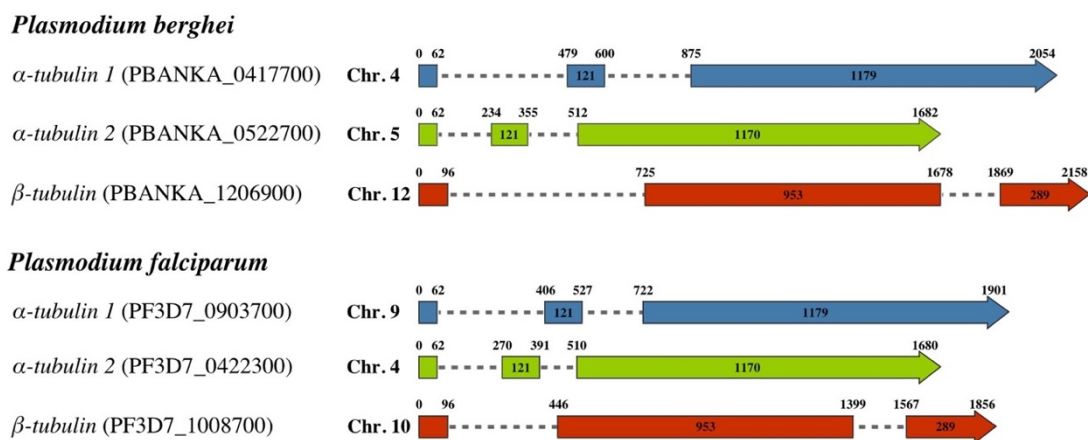


Figure 1.7. Genome localization and comparison of *Plasmodium* tubulin isotypes of *P. berghei* and *P. falciparum*. Colored boxes indicate exon regions and dashed lines indicate intron regions. Numbers within boxes reveal base pairs. The number of introns and the length of exons is identical between the two *Plasmodium* species. Only the intron lengths differ. Data obtained from PlasmoDB (version 36).

stage development and male gametocytes (Rawlings et al., 1992; Kooij et al., 2005; Otto et al., 2014). $\alpha 1$ -tubulin was also shown to be expressed in blood stages, however, it is suggested to be mainly expressed in mosquito stages (Kooij et al., 2005; Lasonder et al., 2008; S. E. Lindner et al., 2013). Alignment of the two α -tubulins only show very few differing regions (**Figure 1.8**) with an amino acid sequence identity of 95%. Major amino acid differences are found at a loop (38-45) which is facing into the lumen of the microtubule scaffold and is therefore a

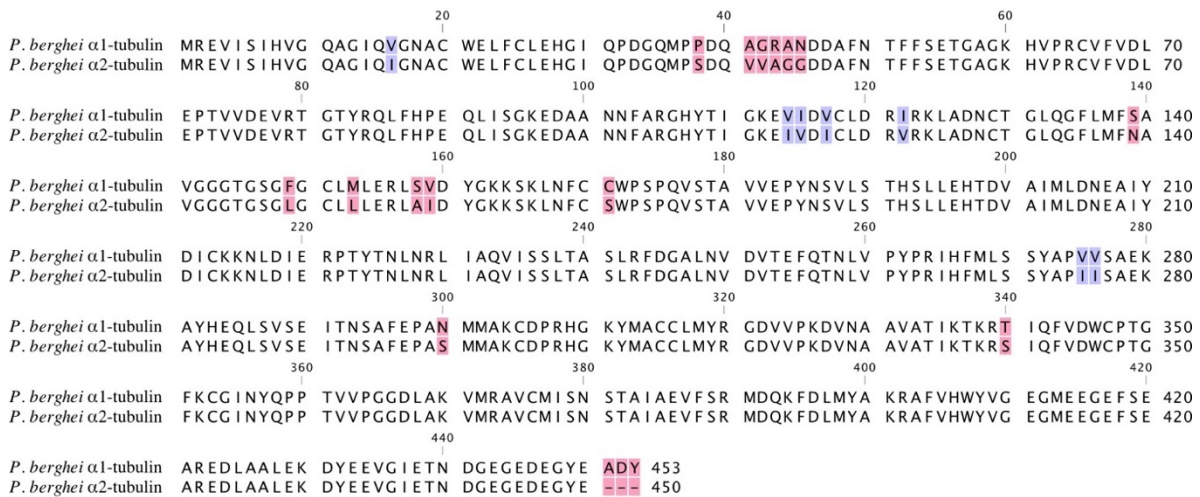


Figure 1.8. Differences between *P. berghei* α -tubulin isotypes. Alignment of $\alpha 1$ - and $\alpha 2$ -tubulin from *P. berghei* with highlighted divergent amino acids. Red highlights indicate the differences considered for the $\alpha 2^+$ chimera generated during this study. Most valine to isoleucine differences were not considered for this chimera. Sequences were retrieved from PlasmoDB (version 36).

potential binding site for microtubule associated proteins (MAPs). Luminal densities within sMTs of sporozoites are identified via cryo-electron tomography potentially indicating proteins bound to the inner surface of microtubules (Cyrklaff et al., 2007). Many eukaryotes contain a lysine at position 40 (K40), which can be post-translationally modified via acetylation (Akella et al., 2010; Kull and Sloboda, 2014; Szyk et al., 2014). Acetylation is correlating with stable and long-lasting microtubules (Shida et al., 2010; Kim et al., 2013; Neumann and Hilliard, 2014; Portran et al., 2017). However, in case of rodent *Plasmodium*, both $\alpha 1$ -tubulins contain a glutamine at this position (Q40), meaning both are continuously mimicking acetylated lysine. The variances between the two α -tubulin isotypes between 139-171 are located at the GTP binding site. Although GTP-hydrolysis is occurring in β -tubulin, one should not exclude that point mutations in α -tubulin cannot impact α/β -heterodimer conformational changes. In case of β -tubulin, it was experimentally shown by introduced point mutations in the β -tubulin core that catastrophe frequencies could be reduced two-fold by keeping the structural GTP-state although GTP-hydrolysis has occurred (Geyer et al., 2015). Further differences are found at N300S and T340S. These amino acids can be post-translationally modified (PTM) via phosphorylation (serine, threonine) or glycosylation (asparagine, serine, threonine). Phosphorylation was shown

to occur on α -tubulins and β -tubulins (Fojo, 2008). Interestingly, tubulin assembly is significantly decreased in the absence of phosphorylation, but only when MAPs are present (Khan and Ludueña, 1996). This suggests that phosphorylation can promote MAP binding and enhance tubulin assembly (Littauer et al., 1986). Glycosylation has not yet been identified for tubulin (Fojo, 2008; Janke and Chloë Bulinski, 2011). The most interesting difference between α 1-tubulin and α 2-tubulin is the C-terminus (**Figure 1.9**). α 2-tubulin is missing the three amino

Species	ID	Protein		420		440		
<i>H. sapiens</i>	(Q71U36)	tubulin α -1A	409	GEGMEEGEFS	EAREDMAALE	KDYEEVGVD	VEGEGEEEGE	E--Y 451
<i>S. cerevisiae</i>	(P09733)	tubulin α -1	410	GEGMEEGEFT	EAREDLAALE	RDYIEVGADS	YAEFEF---	---- 447
<i>P. berghei</i>	(PBANKA_0417700)	tubulin α -1	409	GEGMEEGEFS	EAREDLAALE	KDYEEVG IET	NDGEGEDEGY	EADY 453
<i>P. yoelii</i>	(PY17X_0420500)	tubulin α -1	409	GEGMEEGEFS	EAREDLAALE	KDYEEVG IET	NDGEGEDEGY	EADY 453
<i>P. chabaudi</i>	(PCHAS_0418600)	tubulin α -1	409	GEGMEEGEFS	EAREDLAALE	KDYEEVG IET	NDGEGEDEGY	EADY 453
<i>P. falciparum</i>	(PF3D7_0903700)	tubulin α -1	409	GEGMEEGEFS	EAREDLAALE	KDYEEVG IES	NEAEGEDEGY	EADY 453
<i>P. vivax</i>	(PVX_098630)	tubulin α -1	409	GEGMEEGEFS	EAREDLAALE	KDYEEVG IET	NEGEGEDEGY	EADY 453
<i>P. knowlesi</i>	(PKNH_0701400)	tubulin α -1	409	GEGMEEGEFS	EAREDLAALE	KDYEEVG IET	NEGEGEDEGY	EAEY 453
<i>H. sapiens</i>	(P68366)	tubulin α -4A	409	GEGMEEGEFS	EAREDMAALE	KDYEEVG IDS	Y--EDEDGE	E--- 448
<i>S. cerevisiae</i>	(P09734)	tubulin α -3	410	GEGMEEGEFT	EAREDLAALE	RDYIEVGADS	YAEFEF---	---- 445
<i>P. berghei</i>	(PBANKA_0522700)	tubulin α -2	409	GEGMEEGEFS	EAREDLAALE	KDYEEVG IET	NDGEGEDEGY	E--- 450
<i>P. yoelii</i>	(PY17X_0524100)	tubulin α -2	409	GEGMEEGEFS	EAREDLAALE	KDYEEVG IET	NDGEGEDEGY	E--- 450
<i>P. chabaudi</i>	(PCHAS_0522900)	tubulin α -2	409	GEGMEEGEFS	EAREDLAALE	KDYEEVG IET	NDGEGEDEGY	E--- 450
<i>P. falciparum</i>	(PF3D7_0422300)	tubulin α -2	409	GEGMEEGEFS	EAREDLAALE	KDYEEVG IES	NDGEGEDEGY	E--- 450
<i>P. vivax</i>	(PVX_090155)	tubulin α -2	409	GEGMEEGEFS	EAREDLAALE	KDYEEVG IET	NEGEGEDEGY	E--- 450
<i>P. knowlesi</i>	(PKNH_0514200)	tubulin α -2	409	GEGMEEGEFS	EAREDLAALE	KDYEEVG IET	NEGEGEDEGY	E--- 450

Figure 1.9. Alignment of α -tubulin C-termini across eukaryotes. Alignment of the C-terminus of α 1- and α 2-tubulin from different *Plasmodium* species, human (*Homo sapiens*) and yeast (*Saccharomyces cerevisiae*). Sequences were retrieved from PlasmoDB (version 36) and UniProt (2018).

acids ADY. The final tyrosine is known for providing mechanical resistance to microtubules (Robison et al., 2016). Due to its location at the outermost tail of α 1-tubulin, it is suggested to only affect the binding of microtubule binding proteins (MAPs). This is e.g. shown for kinesin-13 family members which prefer tyrosinated microtubules as their substrate (Peris et al., 2009). In *Plasmodium*, three putative tubulin tyrosine ligases are identified which are differently expressed in male and female gametocytes (Aurrecochea et al., 2009; Yeoh et al., 2017). However, no functional data and expression data for oocyst and sporozoite development was assessed yet.

1.2.3. Microtubule associated proteins in *Plasmodium*

Ultrastructural studies in the closely related *T. gondii* revealed that sMTs are heavily decorated with MAPs (Morrissette, Murray, and Roos, 1997; Hu, Roos, and Murray, 2002). One key protein decorating sMTs in *T. gondii* is the subpellicular microtubule binding protein SPM1. Deletion of SPM1 in *T. gondii* resulted in complete microtubule depolymerization upon cell lysis with detergents (Tran et al., 2012). A recent study on blood stage parasites of *P. berghei* revealed impaired schizont formation with unequally sized and reduced numbers of merozoites when SPM1 is deleted via CRISPR/Cas9 (Kiernan, 2017). However, no data was assessed during mosquito development yet. Other proteins such as TrxL1, TrxL2 and four TLAPs

(TrxL1-associated proteins) were found to form a protein complex binding SPM1 in *T. gondii*, therefore indirectly interacting with sMTs (Liu et al., 2013). These MAPs are suggested to collectively protect sMT stability (Liu et al., 2015). Knockout studies on TrxL1 in *P. berghei* revealed no phenotype in blood stages but ookinetes revealed less organized microtubules. However, ookinetes were still infectious (Kiernan, 2017).

1.3. Regulation of protein expression in *Plasmodium spp.*

Eukaryotic cells have several options to regulate protein expression levels. First, expression can be regulated by how often and when a gene is transcribed. Further, the resulting pre-mRNA can be controlled by splicing, processing and subsequent export into the cytosol. mRNA can be further selectively destabilized or stabilized by RNA binding proteins (RBPs) or non-coding RNA (ncRNA). However, the most reasonable way of regulating gene expression is by transcription control. Here, transcriptional regulators are either classified into transcriptional repressors or activators. These transcriptional regulators can identify specific DNA *cis*-regulatory sequences and e.g. in the case of an activator actively promote RNA polymerase binding by modifying the local chromatin structure. The signal sequences are mostly located upstream of a gene but are also found within the open reading frame and within exon regions of a gene (Ritter et al., 2012; Alberts et al., 2014).

In *Plasmodium*, mostly proteins of the ApiAP2 family are involved in transcriptional regulation and gene silencing (Painter, Campbell, and Llinás, 2011). AP2-G is a major transcriptional regulator of gametogenesis (Kafsack et al., 2014; Sinha et al., 2014). However, it became apparent in recent years that transcription control is limited in *P. falciparum* and *P. vivax* and that the number of transcription factors is low (Coulson, Hall, and Ouzounis, 2004; Balaji et al., 2005; Carlton et al., 2008; Bischoff and Vaquero, 2010). It appears, that the parasite predominantly uses post-transcriptional mechanism to regulate gene expression such as RBPs, which especially play a role in transmission stages. During transformation of the female gametocytes into ookinetes, RNA granules can be formed by the RBPs DOZI or CITH which repress the translation of hundreds of transcripts (Mair et al., 2006, 2010; Guerreiro et al., 2014). In sporozoites, latency and therefore maintaining translational repression is performed by the RNA-binding protein PUF2 (Zhang et al., 2010; Gomes-Santos et al., 2011; Müller, Matuschewski, and Silvie, 2011; Scott E. Lindner et al., 2013). However, RBPs are also found in other parasite stages such as blood stages. PfAlba1, PfSR1 and PfCAF-1 regulate hundreds of transcripts which are mainly involved in invasion or egress (Balu et al., 2011; Vembar et al., 2015). PfSR1 cannot just stabilize transcripts but also controls alternative splicing (Reddy et

al., 2015). However, studies on the mRNA-bound proteome did not reveal any RBPs for tubulin in infected red blood cells of *P. falciparum* (Bunnik et al., 2016) and little is known about RBPs involved during oocyst development. Thus, one cannot exclude the existence of RBPs for tubulin transcripts.

Besides RBPs, non-coding RNAs (ncRNAs) are also involved in transcript regulation in *Plasmodium spp.* *Var* gene activation was shown to depend on antisense long ncRNAs and GC-rich ncRNAs (Amit-Avraham et al., 2015; Guizetti, Barcons-Simon, and Scherf, 2016): Heterochromatin protein 1 (HP1) is silencing AP2-G expression and prevents sexual commitment (Kafsack et al., 2014; Sinha et al., 2014). HP1 on the other hand can be evicted from binding by the gametocyte development 1 protein (GDV1) and GDV1 is regulated by an antisense RNA (Filarsky et al., 2018). This nicely shows the interplay of several transcriptional regulators and antisense lncRNA involved in gene regulation of *Plasmodium*. lncRNAs were also identified for $\alpha 2$ -tubulin for *P. falciparum* blood stage parasites (Sorber, Dimon, and Derisi, 2011). Due to the fact, that $\alpha 2$ -tubulin is predominantly expressed during blood stages this might hint a similar effect during oocyst development where $\alpha 1$ -tubulin is suggested to be the predominant expressed α -tubulin.

1.4. Aim of this study

Sporozoites require active movement in order to glide in the vertebrate skin and to actively find blood capillaries, an essential step in establishing a new infection. Furthermore, sporozoites have to cross several barriers such as traversing the mosquito salivary glands and the endothelium of blood capillaries to enter the circulatory system. Sporozoites can also persist for weeks within the mosquito salivary glands, waiting for the mosquito vector to take a blood meal and to be injected into a new host. To cope with these extraordinary charges sporozoites developed a very stable but also flexible composition of the cytoskeleton. Microscopic studies revealed a high degree of organization of subpellicular microtubules (sMTs) suggesting a key role in stabilizing the sporozoite as well as its gliding machinery and are likely to be involved in establishing and maintaining sporozoite polarity (Baum et al., 2008; Kudryashev et al., 2010, 2012). Interestingly, sporozoites contain a highly regulated number and length of sMTs with a dorsoventral divergent distribution (Garnham, Bird, and Baker, 1963; Vanderberg, Rddin, and Yoeli, 1967; Kudryashev et al., 2012). However, these studies were mostly descriptive and little has been known about which of the two α -tubulin isotypes found in *Plasmodium* is required for forming MTs in sporozoites and what importance number, length and arrangement of sMTs play on sporozoite development and infectivity.

During this study, I aimed to better understand microtubule function on sporozoite formation, motility and infectivity by using a gene deletion and replacement strategy. I first aimed to identify, which of the two α -tubulin isotypes is used to form microtubules in sporozoites by deleting the $\alpha 1$ -tubulin locus. Additionally, I aimed to change tubulin expression levels by modifying $\alpha 1$ -tubulin regulatory elements. To investigate functional differences between the two isotypes, I generated several parasite lines which expressed $\alpha 2$ -tubulin or elements of $\alpha 2$ -tubulin in place of $\alpha 1$ -tubulin. I used the rodent malaria parasite *Plasmodium berghei* to be able to investigate the phenotypes of the transgenic parasite lines throughout the entire *Plasmodium* life cycle *in vivo* and *in vitro*. To assess correlations between morphological changes and parasite virulence, transgenic parasite lines were investigated by using electron microscopy (TEM, SEM) including tomography and confocal fluorescence microscopy combined with quantitative image analysis, qRT-PCR and transmission efficiency experiments in mice.

2. Materials & Methods

2.1. Material

2.1.1. Chemicals, enzymes, buffers & consumables

1 kb DNA ladder	New England Biolabs, Germany
10x Taq Buffer with (NH ₄) ₂ SO ₄	Thermo Scientific, Germany
2-Propanol	Sigma-Aldrich, Germany
24 well cell culture plate	Greiner Bio-One, Germany
5-Fluorocytosine (5-FC)	Sigma-Aldrich, Germany
5x Phusion HF buffer	Thermo Scientific, Germany
96 well optical plates	Thermo Scientific, USA
Accudenz	Accurate Chemical & Scientific Corp., USA
AccuPrep Plasmid Mini Extraction Kit	BioNeer, South Korea
Acetic acid	Sigma-Aldrich, Germany
Agarose NEEO ultra-quality	Carl Roth, Germany
Albumin Fraktion V (BSA)	Carl Roth, Germany
Alsever's solution	Sigma-Aldrich, Germany
Amaya Human T Cell Nucleofector Kit	Lonza, Germany
Amaya human T cell Nucleofector Kit	Lonza, Germany
Ampicillin sodium salt	Carl Roth, Germany
Cell culture dishes	Greiner Bio-One, Germany
Cell culture flasks	Greiner Bio-One, Germany
Chamber slides	Thermo Scientific, Denmark
CIP Alkaline Phosphatase	New England BioLabs, Germany
Cover slips	Roth, Germany
Cryo tubes	Greiner Bio-One, Germany
CutSmart buffer	New England BioLabs, Germany
DMEM	Invitrogen, Germany

Materials & Methods

DNeasy Blood & Tissue Kit	Qiagen, Germany
Ethanol > 99.8%	Sigma-Aldrich, Germany
Ethylenediaminetetraacetic acid (EDTA)	Sigma-Aldrich, Germany
Fetal bovine serum (FBS)	Invitrogen, Germany
Gel loading dye purple (6x)	New England Biolabs, Germany
Giemsa's azur eosin methylene blue solution	Merck, Germany
Glycerol 99%, water-free	Sigma-Aldrich, Germany
Glycine	AppliChem, Germany
HEPES	Carl Roth, Germany
High Pure PCR Product Purification Kit	Roche, Germany
Hydrochloric acid (HCl)	Merck, Germany
Immersion oil	ZEISS, Germany
Insulin syringes	Becton Dickinson, France
Ketamine hydrochloride solution	Sigma Aldrich, Germany
L-Glutamine	Sigma-Aldrich, Germany
Latex gloves	Semperit, Austria
Ligase	New England BioLabs, Germany
Ligase Buffer	New England BioLabs, Germany
Mattek glass bottom dishes	MatTEK corporation, USA
Mercurochrome	Sigma-Aldrich, Germany
Methanol	Sigma-Aldrich, Germany
MgCl ₂	Thermo Scientific, Germany
Microscope slides	Marienfeld
Midori Green	NIPPON Genetics EUROPE, Germany
NEBuilder® HiFi DNA Assembly kit	New England BioLabs, Germany
Needles	Becton Dickinson, Ireland
Nitrile gloves	Ansell, Belgium
Nonidet P40 (NP-40)	AppliChem, Germany

Materials & Methods

Nycodenz	Axis-Shield PoC, Norway
Paraffin	Carl Roth, Germany
Parafilm	Bemis, Belgium
Paraformaldehyde (PFA)	Riedel-de Haen, Germany
Pasteur pipettes	Corning, USA
PCR tubes	Thermo Scientific
Pestles	Bel-Art Products, USA
Phosphate-buffered saline (PBS) tablets	Thermo Fisher Scientific, Germany
Phusion HF polymerase	Thermo Fisher Scientific, Germany
Pipette tips	Steinbrenner Laborsysteme, Germany
Plastic pipettes 5 ml, 10 ml, 25 ml	Greiner Bio-One, Germany
Potassium chloride	Merck, Germany
ProLong Gold antifade reagent	Invitrogen, Germany
QIAprep Spin Miniprep Kit	Qiagen, Germany
Reaction tubes 0.5 ml, 1.5 ml, 15 ml, 50 ml	Sarstedt, Germany
Reaction tubes 2 ml	Greiner Bio-One, Germany
Restriction Endonucleases	New England BioLabs, Germany
RPMI-1640	PAA, Austria
Saponin	Sigma-Aldrich, Germany
SiR-tubulin	Spirochrome, tebu-bio, Germany
Sodium hydroxide (NaOH)	Merck, Germany
Sterile filter	Merck Millipore, Ireland
Syringes	Becton Dickinson, Spain
Taq DNA Polymerase (recombinant)	New England BioLabs, Germany
TRIS	Carl Roth, Germany
Tris-hydrochloride (HCl)	AppliChem, Germany
Triton X-100	Merck, Germany
Trypan blue	Sigma-Aldrich, Germany

Materials & Methods

Trypsin	c.c.pro, Germany
Tryptone	Sigma-Aldrich, Germany
XL1-Blue competent cells	Stratagene, La Jolla, USA
Xylazine hydrochloride solution	Sigma Aldrich, Germany
Yeast extract	Sigma-Aldrich, Germany

2.1.2. Media, buffers and solutions

5-FC drinking water	1 mg/ml in tap water
Accudenz	17% (w/v) Accudenz in ddH ₂ O
Ampicillin (1000x)	100 mg/ml Ampicillin in ddH ₂ O
Freezing solution	10% (v/v) glycerol in Alsever's solution
Giemsa staining solution	14% (v/v) Giemsa in Sørensen staining buffer
Ketamine/ Xylazine	10% Ketamine (v/v) 2% Xylazine (v/v) in PBS
LB agar	LB medium 1.5% (w/v) agarose
LB medium	1% (w/v) tryptone 0.5% (w/v) yeast extract 1% (w/v) NaCl adjusted to pH 7
Mercurochrome	0.1% (v/v) Mercurochrome in PBS
NP-40	1% (v/v) NP-40 in PBS
Nycodenz	276 g/l Nycodenz 10 mmol/l TrisHCl 6 mmol/l KCl 0.6 mmol/l Na ₂ EDTA adjusted to pH 7.5 with 5 M KOH or HCl
PFA	4% (w/v) PFA in PBS
Pyrimethamine drinking water	280 µM Pyrimethamine (stock) in tap water pH = 3.5-5.5 (preferably pH 5) with HCl

Materials & Methods

Pyrimethamine stock solution	28 mM Pyrimethamine in DMSO
RPMI-1640 + Pen/Strep	500 ml RPMI-1640 5 ml Pen/Strep (100x)
Saponin stock solution	2.8% (w/v) saponin in PBS
Sporozoite activating buffer	3% (w/v) BSA in RPMI-1640
Transfection medium (T-medium)	15 ml FBS (USA) 60 ml RPMI (with 25 mM HEPES) 22,5 µl Gentamycin Sterile filtered
Tris-acetate-EDTA buffer (TAE), 50x	242 g Tris 57,1 ml Acetic acid 50 ml 0.5 M EDTA add ddH ₂ O to 1 l

2.1.3. Devices

Amaxa Nucleofector II	Lonza, Germany
Analytic balance TE124S-OCE	Sartorius, Germany
Axiostar plus transmitted-light microscope	Zeiss, Germany
Axiovert 200M inverted microscope	Zeiss, Germany
Balance EW600-2M	Kern, Germany
Binocular SMZ 1500	Nikon, Japan
Centrifuge 5417 C	Eppendorf, Germany
Centrifuge Galaxy Mini	VWR, Germany
Centrifuge Labofuge 400e	Heraeus, Germany
Centrifuge Multifuge 1 S-R	Heraeus, Germany
Centrifuge Pico 17	Heraeus, Germany
CO ₂ incubator MCO-17AI	Sanyo, Japan
Electrophoresis power supply E831	Consort, Belgium
Electrophoresis power supply EV231	Consort, Belgium

Materials & Methods

Freezer -80°C	New Brunswick Scientific, USA
Freezers	Liebherr, Germany
Heat block neoBlock 1	neoLab, Germany
Hotplate stirrer CB162	Bibby Scientific, UK
Incubator MIR-253	Sanyo, Japan
Microcentrifuge Capsule HF-120	Tomy Seiko, USA
Microwave oven	Medion, Germany
Mosquito cages	BioQuip Products, USA
Neubauer improved chamber	Brand, Germany
Nikon coolpix 5400	Nikon, Japan
Pipettus	Abimed, Germany
Safety cabinet Herasafe KS 15	ThermoScientific, Germany
Shaking incubator Multitron 2	Infors, Switzerland
Thermal cycler 3Prime	Bibby Scientific, UK
Thermal cycler Mastercycler 5341	Eppendorf, Germany
UV-table UVT-28 L	Herolab, Germany
Vacuum pump N86KN.18	Neuberger, Germany
Vibrating Shaker REAX top	Heidolph, Germany
Waterbath Isotemp 210	Fischer Scientific, Germany

2.1.4. Software and websites

Adobe Photoshop CS5.1	Adobe Systems, USA
Affinity Designer 1.6.1	Serif Ltd., UK
AxioVision 4.6	Zeiss, Germany
CLC Main Workbench 8.0.1	Qiagen Advanced Genomics, USA
E.A.S.Y Win 32	Herolab, Germany
FFmpeg (vers. be1d324)	FFmpeg-project, ffmpeg.org
FIJI (version: 2.0.0-rc-64/1.51s)	Loci, USA

Materials & Methods

GeneDB	www.genedb.org/Homepage
GraphPad Prism 6h	GraphPad Software, USA
IMOD 4.9	Boulder Laboratory for 3-D Electron Microscopy of Cells, USA
Mendeley 1.19.1	Mendeley Ltd., USA
Microsoft Office Mac 16.14.1	Microsoft Corporation, USA
PlasmoDB	plasmodb.org/plasmo/
SerialEM 3.6	Boulder Laboratory for 3-D Electron Microscopy of Cells, USA
SnapGene 3.2.1	GSL Biotech, USA
UniProt	https://www.uniprot.org
Volocity 6.3	PerkinElmer, USA

2.2. Molecular & microbiological methods

2.2.1. Polymerase chain reaction

PCR was used to either amplify DNA fragments for cloning or to genotype transgenic parasite lines. For genotyping, *Taq* polymerase (NEB) was used. To amplify long constructs (> 6 kb), 50 μ l reactions were pipetted instead of 25 μ l reactions. For cloning, Phusion HF polymerase (Thermo Fisher Scientific) was used due to its proof-reading abilities. The pipetting volumes and thermocycler conditions are shown below:

Table 1. PCR pipetting scheme

Components	<i>Taq</i> polymerase (25 μ l)		Phusion HF polymerase (50 μ l)	
	Concentration	Volume [μ l]	Concentration	Volume [μ l]
Buffer	10x	2.5	5x	10
dNTPs	2 mM	2.5	2 mM	5
Primer forward	0.5 μ M	0.25	0.5 μ M	0.5
Primer reverse	0.5 μ M	0.25	0.5 μ M	0.5
MgCl ₂	25 mM	1.5	-	-
Template DNA		1		1
Polymerase		0.25		0.5
ddH ₂ O		16.75		32,5

Table 2. Thermocycler conditions used for *Taq* polymerase

Step	Temperature [°C]	Time	Cycles
Initial denaturation	94	2'	1
Denaturation	94	30''	
Annealing	Primer T _m	30''	30-35
Extension	60	1' per kb + 30'	
Final extension	60	10'	1
Pause	4	∞	

Table 3. Thermocycler conditions used for Phusion HF polymerase

Step	Temperature [°C]	Time	Cycles
Initial denaturation	98	2'	1
Denaturation	98	30''	
Annealing	Primer T _m	30''	30-35
Extension	60	1' per 2 kb	
Final extension	60	10'	1
Pause	4	∞	

2.2.2. Primer design

Primers used for genotyping, cloning, qPCR or NEBuilder® HiFi DNA Assembly were designed with SnapGene (version 3.2.1). Primer annealing temperatures of the program were used. Desalted primers were ordered from Thermo Fisher Scientific. All primer sequences are listed in the appendix.

2.2.1. Agarose gel electrophoresis

Depending on the fragment length, either 0.8% (fragments above 500 kb) or 2% (fragments below 500 kb) agarose gels were used. Agarose gels were prepared by mixing UltraPure Agarose (Invitrogen) powder in 1x TAE buffer. Following complete agarose dissolution via boiling, the Agarose-TAE mixture was stored in a 55°C heater. Agarose-TAE was poured into casting trays, allowed to solidify and was then transferred into an electrophoresis chamber containing 1x TAE buffer. Next, DNA samples were mixed with 6x loading dye (NEB) containing Midori Green Advanced DNASTain (Nippon Genetics Europe GmbH; 1:500) and loaded onto the gel. 5 µl of a molecular weight marker (1kb-Ladder, NEB) also containing Midori Green was loaded onto the gel as well. Gels were run at a voltage of 90 to 150 Volts until separated. For documentation, a picture was taken on a UV transilluminator (UVT-28 L, Herolab).

2.2.2. DNA fragment extraction

Desired PCR products or DNA fragments were extracted from agarose gels by using the PCR Product Purification Kit (Roche). DNA purification was performed in accordance to the manufacturer's protocol. Prior to purification of DNA fragments, agarose gel pieces that

contained desired DNA fragments were cut out, melted and transferred onto silica membrane columns. The DNA was finally eluted with 35 μ l ddH₂O and stored at -20°C.

2.2.3. Restriction enzyme digest

Buffers used for restrictions enzyme digests were used according to the manufacturer's instructions (NEB). Digests were either incubated over night at room temperature or for 3 hours at 37°C. Enzymes were used at concentrations between 2 – 5 U in 50 μ l reactions.

2.2.4. DNA fragment end modification

Linearized plasmid DNA was dephosphorylated using alkaline phosphatase, calf intestinal (CIP) enzyme thus preventing self-ligation. To this end, (10 U) CIP was added to the restriction enzyme digest mixture after 2 hours and thereafter incubated for 1 hour at 37°C.

2.2.5. DNA ligation

1 μ g of DNA fragments with a molar ratio of 1:3 (vector : insert) were mixed with 5 U T4-DNA ligase and 10x ligation buffer in a total volume of 10 μ l. The ligation mix was incubated over night at 16°C.

2.2.6. NEBuilder® HiFi DNA Assembly

Primers for NEBuilder® HiFi DNA Assembly were designed to have at least 20 bp overlaps with a minimum melting temperature of 50°C. Approximately 0.5 pmols of vector and insert (1:1 or 1:2 ratio) were used for assembly. Half of the reaction volume recommended by the manufacturer's protocol (NEB) was used and incubation was conducted at 50°C for 60 min. Reaction mix was directly used for transformation or stored at – 20°C.

2.2.7. Transformation

Plasmids were amplified in super-competent *E. coli* XL-1 Blue cells. Cells of a 20 μ l volume were thawed on ice, mixed with 1 μ g of DNA and kept for 30 min on ice. Cells were then heat-shocked at 42°C for 45 s and afterwards put on ice for 2 min. The transformation mixture was then plated on 0.1 mg/ml ampicillin LB-agar plates and incubated at 37°C overnight.

2.2.8. Bacterial overnight cultures

A colony picked from an LB-agar plate was inoculated into 5 ml of LB-media containing ampicillin. The bacteria were grown in a 37°C shaker overnight.

2.2.9. Sequencing

All vectors used in this study were sequenced before transfection into parasites. Furthermore, the correct and error-free integration of the GOI in the clonal parasites was sequenced. DNA and sequencing primers were sent to GATC. Sequences were aligned and analyzed with Snapgene (version 3.2.1).

2.2.10. Bioinformatic analysis

Sequence alignments were conducted with CLC Main Workbench 8 (Quiagen) or Snapgene 3.2.1 and sequences were retrieved from PlasmoDB (<http://plasmodb.org/plasmo/>, version 36) and UniProt (<http://www.uniprot.org>, 2018).

2.3. Parasitological methods

2.3.1. Determination of parasitemia

A drop of tail blood was smeared on a microscopy slide, air-dried and fixed for 10 s in 100% methanol. Slides were air-dried and stained with Giemsa solution (Merck) for 30-60 min. Eventually, the slides were rinsed with tap water and air-dried. Parasitemia was enumerated using a light microscope (Zeiss) with a 100x objective and calculated as follows:

$$\frac{\left(\frac{\text{counted parasites (all fields)}}{\text{number of fields}}\right)}{\text{counted erythrocytes of one field}} \times 100$$

2.3.2. Cardiac puncture

In case a blood volume greater than a drop from the tail was needed, a cardiac puncture was performed. This cardiac puncture provided the maximum blood volume. This is necessary for example during genomic DNA isolation, schizont culture, ookinete culture or cryopreservation of parasites. Cardiac punctures were routinely done on mice that presented greater than 2% parasitemia. These mice were anaesthetized with ketamine and xylazine (87.5 mg/kg ketamine

and 12.5 mg/kg xylazine) and blood was taken by cardiac puncture. Afterwards, mice were killed by cervical dislocation.

2.3.3. Schizont culture

Approximately 1 ml of blood infected with WT ANKA or receiver line parasites (> 2%) was mixed with 250 µl of heparin, added to 30 ml of pre-warmed T-medium and incubated at 37°C for 20-22 h. Schizont stage parasites were separated from uninfected erythrocytes and other parasite stages using a Nycodenz gradient. The schizont culture was transferred into a 50 ml Falcon and then underlaid with 10 ml 55% Nycodenz solution. The culture was centrifuged with 1.000 rpm (Heraeus Multifuge S1) at RT for 25 min and schizonts were collected from the top of the Nycodenz phase. Subsequently, schizonts were washed in T-medium and diluted depending on the number of transfections performed.

2.3.4. *P. berghei* schizont transfection

Isolated schizonts were mixed with linearized vector DNA and Nucleofector solution (Amaxa human T cell Nucleofector Kit, Lonza) on ice. The schizonts were then electroporated (program U-33, Amaxa Nucleofector II, Lonza) and injected into the tail vein of a naïve mouse. After 24 h, either pyrimethamine or 5-fluorocytosine treatment was started depending on the integration strategy used. When mice reached a parasitemia of at least 1%, blood was harvested via cardiac puncture and used for parasite storage in liquid nitrogen and isolation of genomic DNA.

2.3.5. Parasite positive and negative selection

The positive-negative selection marker *hDHFR-yFCU* allows for parasite selection and selection marker recycling. The human *dihydrofolate reductase* (*hDHFR*) confers resistance to pyrimethamine resulting in a predominant survival of parasites that integrated the construct of interest (positive selection). This is performed by adding 0.07 mg/ml pyrimethamine to the drinking water of mice. The *yFCU* fusion gene (*yeast cytosine deaminase* and *uridyl phosphoribosyl transferase*) metabolizes the 5-FC into the toxic 5-fluorocytosine triphosphate. Only parasites that lost the selection cassette via homology-based excision survive (negative selection). However, this involves a construct design with two homology regions flanking the selection cassette. 5-fluorocytosine (5-FC, 1 mg/ml) can also be added to the drinking water of mice.

2.3.6. Parasite storage

Parasites were stored/cryopreserved in liquid nitrogen. To this end, the blood of an infected mouse (100 μ l) was mixed with 200 μ l freezing solution on ice and directly frozen with liquid nitrogen.

2.3.7. Isolation of genomic DNA

Erythrocytes were lysed in 15 ml PBS containing 0.03% saponin on ice until solution was clear. After centrifugation and washing, the parasites were isolated using the Blood and Tissue kit (Quiagen) according to the manufacturer's protocol.

2.3.8. Generation of isogenic lines (limiting dilution)

Genomic DNA of positive mice was genotyped via PCR to test for correct construct integration following transfection and positive or negative parasite selection. Selection pressure with pyrimethamine or 5-FC does not eliminate all receiver line parasites and subsequently, parasites from transfections reflect a mixed population. A dilution series is necessary to further select for correct parasites. For that, one parental parasite stabilate was injected intraperitoneally into a naïve NMRI mouse. The blood of the mouse was harvested when a parasitemia of 0.5-1% was reached to minimize the number of double-infected erythrocytes. Then, blood was diluted to a concentration of 9 blood stage parasites per 1 ml PBS. 100 μ l of solution was injected in 5-10 naïve NMRI mice each. Blood was harvested from positive mice, stored and genotyped for correct construct integration by PCR and sequencing (GATC).

2.3.9. Mosquito infection

Frozen parasite stocks were injected intraperitoneally into 2-3 mice (100 - 150 μ l) and parasites were allowed to develop for 4-6 days. The infection rate was monitored by blood smears. When infected mice reached 2-3% parasitemia, mice were anesthetized as described previously and fed to mosquitoes for 45 min by turning the mouse every 5 min. Mosquitos were starved from sugar and salt solution overnight before feeding.

2.3.10. Analysis of oocyst development

Midguts of 10-20 mosquitoes were isolated in phosphate buffered saline (PBS) on ice at day 5, day 7, day 10, day 12, day 14 and day 19 post mosquito blood meal. Non-fluorescent oocysts were stained following a 0.1% mercurochrome staining (Moll et al., 2008) and counted by light

microscopy (Axiovert 200M, Zeiss) with a 10x objective (NA = 0.5, air). Fluorescent oocysts were counted using a stereomicroscope (SMZ1000, Nikon). To visualize microtubules, highly infected midguts were incubated in 100 μ l RPMI (supplemented with 50,000 units/l penicillin and 50 mg/l streptomycin) with 3 μ M SiR-tubulin (Spirochrome) and 3 μ M Hoechst 33342 (Thermo Scientific) for 30 min at 37°C. Midguts and a drop of medium were then transferred with a Pasteur pipette onto a microscopy slide, covered with a cover slip and sealed with paraffin. Samples were observed using a Nikon TE 2000-E microscope equipped with an Ultra View ERS spinning disc confocal unit (Perkin-Elmer) with 20x (NA = 0.85, oil) and 60x (NA = 1.49, oil) objectives. A minimum of duplicate mosquito feeds and a minimum of triplicate counts were performed. 3D reconstructions of oocysts were rendered from z-stack images (z-distance between 0.5 μ m and 1.5 μ m) with the 3D Opacity tool of Volocity 6.3 (Perkin-Elmer).

2.3.11. Sporozoite isolation and counting

Midgut (MG), hemolymph (HL) and salivary gland (SG) sporozoites of infected mosquitoes were isolated on day 14 and day 17 post mosquito blood meal. A minimum of 10 mosquitoes was dissected per count. HL sporozoites were isolated from immobilized mosquitoes (on ice) by cutting of the last segment of the abdomen and flushing the abdomen by injecting RPMI into the thorax and collecting drops containing the hemolymph sporozoites from the abdomen. For MG and SG sporozoites, MGs and SGs were dissected on ice and crushed before counting. Sporozoite numbers were counted using a Neubauer counting chamber. Sporozoites of the different compartments were collected from each mosquito to ensure a correct salivary gland invasion ratio calculation.

2.3.12. Sporozoite movement, length and gliding diameter analysis

HL and extracted salivary glands were collected in 50 μ l RPMI on ice between day 17-19. SG were smashed, centrifuged for 3 min at 1000 rpm (Thermo Fisher Scientific, Biofuge primo) to remove salivary gland fragments and the supernatant was collected. HL sporozoites were concentrated by centrifugation for 3 min at 10,000 rpm. HL and SG sporozoites were each mixed in a 1:1 ratio with RPMI containing 6% bovine serum albumin (ROTH) and were transferred into an optical bottom 96-well plate (Thermo Scientific). The plate was centrifuged for 3 min at 1000 rpm (Multifuge S1-R, Heraeus) and imaged using an epifluorescence microscope (Axiovert 200M, Zeiss) and the Axiovision 4.7.2 software (Zeiss). Movies were taken with either differential interference contrast (DIC) or in the mCherry channel using a 10x (NA 0.5, air) or 25x (NA 0.8, water) objective at a speed of 1 frame every 3 seconds. Videos

were analyzed for 100 seconds with Fiji (Version: 2.0.0 rc 64/1.51s). Gliding motility was categorized into three different patterns. Moving sporozoites moved at least a full circle during 100 seconds. Partially moving sporozoites moved for at least a sporozoite length and non-moving sporozoites were not moving at all. Non-moving also included attached, waving, twitching, patch gliding and floating sporozoites (Hegge et al., 2009). Moving sporozoites were further categorized into clockwise (CW) movers when sporozoites moved for at least two frames (6 seconds) in CW direction during the 100 s video. To assess the gliding diameter of sporozoites, 100 s videos were combined by maximum intensity z-projection and the diameter of the gliding circles was measured. Sporozoite length was measured with the segmented line tool of Fiji.

2.3.13. Fluorescence assay of sporozoites

Hemolymph or salivary gland sporozoites were isolated on day 14 post mosquito blood meal and purified as described above. Sporozoites were mixed in a 1:1 ratio with RPMI containing 6% bovine serum albumin (ROTH), 0,5 μ M SiR-tubulin and 3 μ g/ml Hoechst. Sporozoites were incubated for 10 min at room temperature and then diluted in a 1:5 ratio with RPMI. Sporozoites were centrifuged onto cover slips at 1500 rpm (Multifuge S1-R, Heraeus) for 5 min. Cells were directly fixed in 4% paraformaldehyde (PFA) solution (diluted in PBS) for 5 min and subsequently diluted by 1:4 in PBS and incubated for further 15 min. Cover slips were shortly air-dried and mounted to a microscopy slide with 5 μ l ProLong Gold anti-fade reagent (Invitrogen). After 24 hours at room temperature, images of sporozoites were taken with a Nikon TE 2000-E microscope equipped with an Ultra View ERS spinning disc confocal unit (Perkin-Elmer) using a 60x objective (NA 1.49, oil).

2.3.14. Quantification of microtubule length and intensity

Sporozoite images acquired from the fluorescence assay were analyzed with Volocity Analysis 6.3 (Perkin Elmer). First, a sporozoite was automatically identified by the cytoplasmic mCherry signal and the Hoechst staining of the nucleus. The dynamic range of the original SiR tubulin staining was adjusted to the weakest microtubule staining near the nucleus. The program quantifies original intensity levels of the SiR tubulin stain and maximal microtubule length by measuring the longest axis. Automatic measurements were compared to manual measurements acquired with ImageJ (**Figure 2.1**).

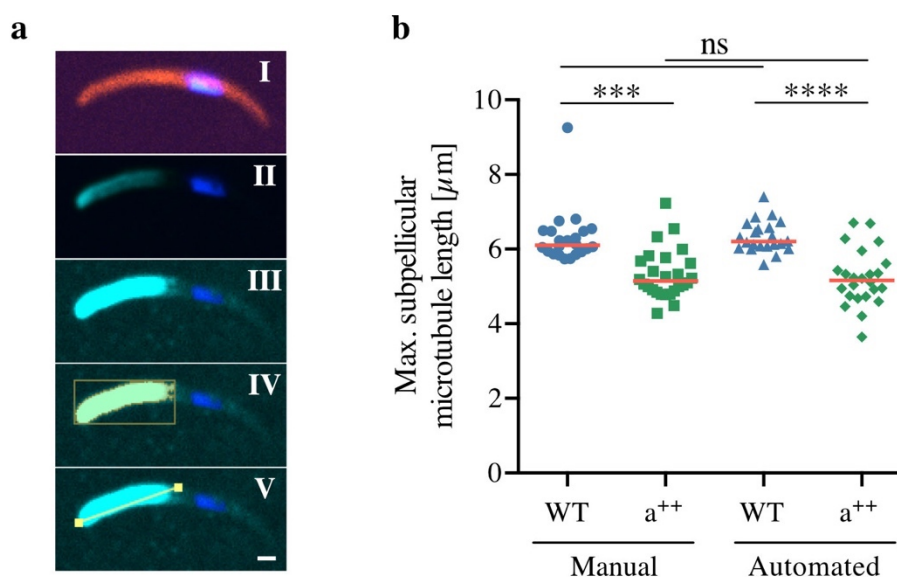


Figure 2.1. Quantification of microtubule length and intensity. (a) Spinning disc confocal images were semi-automatically analyzed with Velocity Analysis 6.3 (Perkin Elmer). Sporozoites were identified by their mCherry and Hoechst signal. Due to unequal intensity values of the microscope laser beam, only sporozoites located within a circle of 100 μm in diameter located at the center of the field of view were considered. The threshold of SiR-tubulin signal was manually adjusted to the weakest signal next to the sporozoite nucleus. However, the program considered original intensity values for calculating the SiR-tubulin fluorescence intensities. Background fluorescence was subtracted. Maximum SMT length was automatically measured by using the longest axis measurement tool. (b) Automatic data acquisition was compared to manual data assessment with ImageJ (version 2.0.0 rc 64/1.51s). Data was not significant when comparing the different methods but it was significant across different lines for both approaches. Scale bar: 1 μm

2.3.15. Transmission electron microscopy (TEM)

Highly infected MGs or SGs were fixed in 2% paraformaldehyde and 2% glutaraldehyde diluted in 100 mM sodium cacodylate buffer at 4 °C overnight. Fixed samples were washed three times in 100 mM sodium cacodylate buffer at room temperature (RT) for 5 min. A secondary fixation was performed in 1% osmium (in 100 mM sodium cacodylate buffer) at RT for 60 min. Samples were washed twice with 100 mM sodium cacodylate buffer and twice in ddH₂O and then contrasted with 1% uranyl acetate (in ddH₂O) at 4°C overnight. Samples were washed twice with ddH₂O for 10 min and then dehydrated by incubating in increasing concentrations of acetone (30%, 50%, 70%, 90%) for 10 min and two times in 100% for 10 min. Samples were adapted to ‘Spurr’ solution (23.6% epoxycyclohexylmethyl-3,4epoxycyclohexylcarboxylate (ERL); 14.2% ERL-4206 plasticizer; 61.3% nonenylsuccinic anhydride; 0.9% dimethylethanolamine) by incubating in increasing concentrations (25%, 50%, 75%) at RT for 45 min and at 100% at 4°C overnight. MGs were resin embedded with ‘Spurr’ at 60°C overnight. Embedded MGs were trimmed and 70 nm thick sections were imaged on a

transmission electron microscope at 80 kV (JEOL JEM-1400) using a TempCam F416 camera (Tietz Video and Image Processing Systems GmbH, Gautig).

2.3.16. Scanning electron microscopy (SEM)

Sporozoites were isolated as previously described and fixed in 2% glutaraldehyde and 4% PFA onto cover slips at RT for 1h or at 4°C overnight. Sporozoites were dehydrated with increasing ethanol concentrations (30%, 50%, 70%, 90% in water) at room temperature for 10 min and in 100% two times for 10 min. Ethanol was exchanged first by incubating the sample with 50% HMDS (hexamethyldisilazane) and 50% ethanol for 5 min and then by 100% HDMS for 10 min. The sample was kept under the fume hood until all HDMS was evaporated. Cover slips were mounted onto studs and sputter-coated with 5–10 nm gold. Sporozoites were imaged using a scanning electron microscope (Leo1530, Zeiss).

2.3.17. Sporozoite tomography

The tomograms were acquired from serial sections of resin embedded (Spurr) mosquito midguts. Each section was inspected for suitable objects and mapped using a JEOL JEM-1400 80 kV TEM. The tilt series were performed on a FEI Tecnai F30 300 kV TEM with the Gatan OneView sensor (Gatan Inc, Pleasanton, CA, USA) installed and controlled by SerialEM (Mastronarde, 2005). Each series ranged from ± 60 -70° with images at 2° increments at 9600x magnification. The tomogram volumetric reconstruction for each individual section was performed using the IMOD 4.9 software package (Kremer, Mastronarde, and McIntosh, 1996). Every image in the tilt series was aligned and tracked via patch tracking and the volume was reconstructed using weighted-back projection. The 3D reconstructions of the sections were flattened and trimmed before combining them into a single volume. For visual representation, the objects of interest in each tomogram were manually segmented in 3dmod (IMOD). The animations (**Figure 3.21** and **Figure 3.22**) were created by exporting frames in 3dmod and combining them using FFmpeg (FFmpeg Developers, version: be1d324).

2.3.18. Expression levels of *$\alpha 1$ -tubulin* and *$\alpha 2$ -tubulin*

Total RNA of 17 well infected mosquito midguts (> 1 million sporozoites) was isolated on day 5, 7, 10, 12 and 14 for WT and *$\alpha 1$ (-)* parasites and from day 7 and day 12 for all other parasite lines. RNA was isolated with Qiazol reagent according to the manufacturer's protocol (Invitrogen). RNA was treated with the Turbo DNA-free kit (Life Technologies) according to

the manufacturer's protocol and cDNA synthesis was generated using the First Strand cDNA synthesis kit (Thermo Scientific). The quantitative PCR reaction was performed using SYBR Green PCR Master Mix (Life Technologies) including ROX dye and was measured with the Abi 7500 Fast RT-PCR system (Applied Biosystems). The mRNA levels of *α1-tubulin* and *α2-tubulin* were normalized against 18S rRNA levels. Across run differences were normalized using a calibrator sample. The sequences of the primers used can be found in the appendix of this thesis.

2.3.19. Mouse infection by mosquito bites or intravenous sporozoite injection

We tested the ability of vector-to-host transmission of the generated parasite strains by either infecting naïve mice with infected mosquitoes or by injecting sporozoites intravenously. 10 preselected infected mosquitoes were put into cups and starved overnight. NMRI mice were anesthetized with ketamine and xylazine (87.5 mg/kg ketamine and 12.5 mg/kg xylazine) and one mouse was put on each cup. The eyes of the mice were covered with Bepanthen cream (Bayer) to prevent dehydration. Mosquitos were allowed to bite for 20 min. For intravenous injections, SG sporozoites were isolated in RPMI as described above, diluted to 10,000 sporozoites per 100 µl and the same volume was injected into the tail vein per mouse. Parasitemia of mice was monitored daily from day 3 to day 8 post mosquito blood meal or post *i.v.* injection via blood smears stained with Giemsa solution (Merck). Blood smears were counted via a light microscope (Zeiss) counting grid. The time until the first parasite was identified is stated as the prepatency.

2.3.20. Parasite blood stage growth

Blood stage growth was assessed by injecting intravenously 100 blood stage parasites per C57Bl/6 mouse. The injection volume was 100 µl. Mice were monitored from day 3 to day 10 post injection as described previously. Growth rate was calculated for day 7, when parasitemia was between 0.7% and 1.5%.

$$growth\ rate = \left(\frac{number\ of\ parasites}{number\ of\ injected\ parasites} \right)^{\frac{1}{day}}$$

2.3.21. Parasite strain

All genetic modifications were performed in *Plasmodium berghei* strain ANKA WT or in WT derived parasites.

2.3.22. Mosquito strain

During this study, *Anopheles stephensi* mosquitos of the strain FDA500 were used.

2.3.23. Ethics statement

Animal experiments were approved by the German authorities (Regierungspräsidium Karlsruhe, Germany) and were performed according to the FELASA and GV-SOLAS standard guidelines. All experiments were conducted in female NMRI mice (8-10 weeks of age) obtained from JANVIER. Only parasite blood stage growth was determined with female C57Bl/6 mice (8-10 weeks of age) obtained from Charles River Laboratories.

2.3.24. Statistics

Statistical significance was assessed using GraphPad Prism 6.0h and a one-way ANOVA test (Kruskal-Wallis test) or a Mann-Whitney test depending on the sample analyzed.

3. Results

3.1. Generation of genetically modified *P. berghei* parasites

3.1.1. Plasmid vector design

To genetically modify the *Plasmodium berghei* genome at the $\alpha 1$ -*tubulin* locus, a vector flanked by two homology regions is needed for stable double-homologous crossover integration into the parasites genome. Furthermore, a selection cassette is required to be able to select for successful integration. The *Pb262* vector (**Figure 3.1**, top left) (Singer et al., 2015) contains a *hDHFR-yFCU* positive-negative selection marker conferring resistance to pyrimethamine via a *human dihydrofolate reductase* (*hDHFR*; for positive selection) and toxicity to 5-fluorocytosine via a *yFCU* fusion gene (*yeast cytosine deaminase* and *uridyl phosphoribosyl transferase*; for negative selection) for parasite selection in mice and an ampicillin resistance cassette for plasmid selection in *E. coli*. This vector was modified so that it could be used for $\alpha 1$ -*tubulin* locus integrations. The chromosome 12 integration site (Chr12first), the *CSP* promoter, the *mCherry* and the *dhfs* 3'UTR were replaced by a native $\alpha 1$ -*tubulin* 5'UTR promoter region, the codon modified and intron-deleted $\alpha 1$ -*tubulin* gene and a $\alpha 1$ -*tubulin* 3'UTR. Furthermore, a longer sequence of the $\alpha 1$ -*tubulin* 3'UTR was inserted between the selection cassette and the second chromosome 12 integration site (**Figure 3.1**, top right). The $\alpha 1$ -*tubulin* 5'UTR and the long $\alpha 1$ -*tubulin* 3'UTR allowed for homologous recombination and integration into the endogenous $\alpha 1$ -*tubulin* gene locus. This vector was generated by Madlen Konert as described in detail in her Master's thesis (Konert, 2014). All vectors generated in this study originated from this vector.

To generate the $\alpha 1$ -*tubulin* knockout vector $\alpha 1(-)$, only the codon modified $\alpha 1$ -*tubulin* gene and its attached $\alpha 1$ -*tubulin* 3'UTR had to be removed. The *hDHFR-yFCU* selection cassette was kept flanked with the *Pbdhfr* 3'UTR to allow negative selection and subsequent selection cassette recycling. All other vectors also originated from the “v_{a1} Δ introns, cm” vector. The vectors were designed in a way, that they could be used with either the ‘gene insertion/marker out’ (GIMO) method (Lin et al., 2011) or via standard transfection protocols (Janse, Franke-Fayard, and Waters, 2006) (**Figure 3.2**). Only the ORF had to be replaced with the desired α -*tubulin* ORF constructs. In case of the $\alpha 2^{++}$ vector, the short $\alpha 1$ -*tubulin* 3'UTR had to be additionally replaced with a $\alpha 2$ -*tubulin* 3'UTR. For most vectors, the second chromosome 12 integration site was deleted to reduce vector size.

To be able to transfect parasites by using the GIMO method, a receiver parasite line is needed which cannot cycle out its selection marker. To generate this parasite line, a GIMO receiver

line vector was designed from the “v_a1 Δ introns, cm” vector (**Figure 3.1**). The short α -tubulin 3’UTR was replaced by a *dhfs* 3’UTR to eliminate the homology region. Furthermore, the *Pbdhfr* 3’UTR next to the *ef1 α* promoter was deleted to prevent the selection cassette from being cycled out during 5-fluorocytosine treatment (negative selection).

In case of the GIMO technique, plasmids were linearized before transfections by either SalI and KpnI to only integrate the gene of interest (GOI) and the 5’ and 3’ homology regions without any selection cassette. Otherwise, vectors were linearized with SalI and XhoI (or ScaI) to integrate everything except the vector backbone.

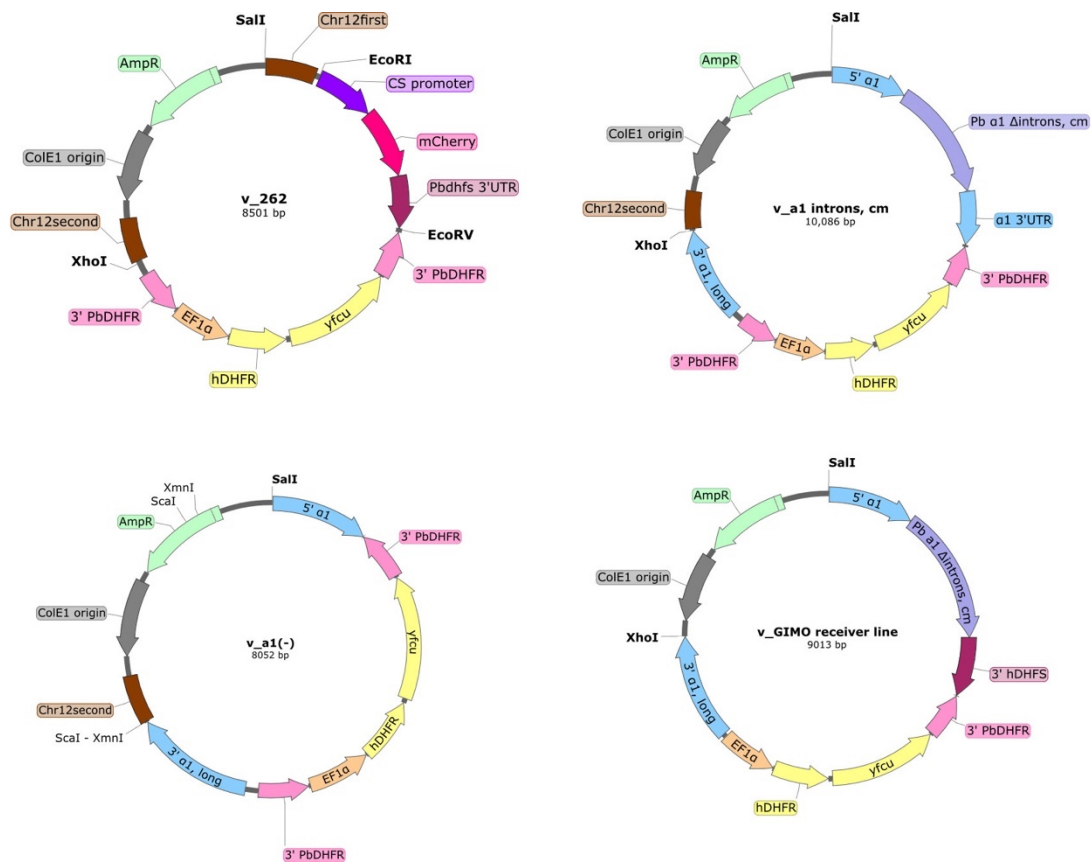


Figure 3.1. Transfection vector maps. α 1-tubulin promoter regions are named as 5’ α 1 untranslated regions (UTR) due to the unknown location of the promoter. 5’UTRs and 3’UTRs (3’ α 1) of α 1-tubulin are highlighted in blue. Open reading frames (ORFs) are shown in magenta for mCherry, purple for α 1-tubulin and in yellow for the selection cassette genes *human dihydrofolate reductase* and *yeast cytosine deaminase* and *uridyl phosphoribosyl transferase* (*hDHFR* and *yFCU*, respectively). Arrows point into the direction of promoter activity and gene orientation. Restriction enzyme sites for linearization are shown in black. (top, left) *Pb262* vector (Singer et al., 2015); (top, right) α 1^{cm Δ introns} vector (Konert, 2014); (bottom left) α 1(-) vector; (bottom right) ‘gene insertion/marker out’ vector.

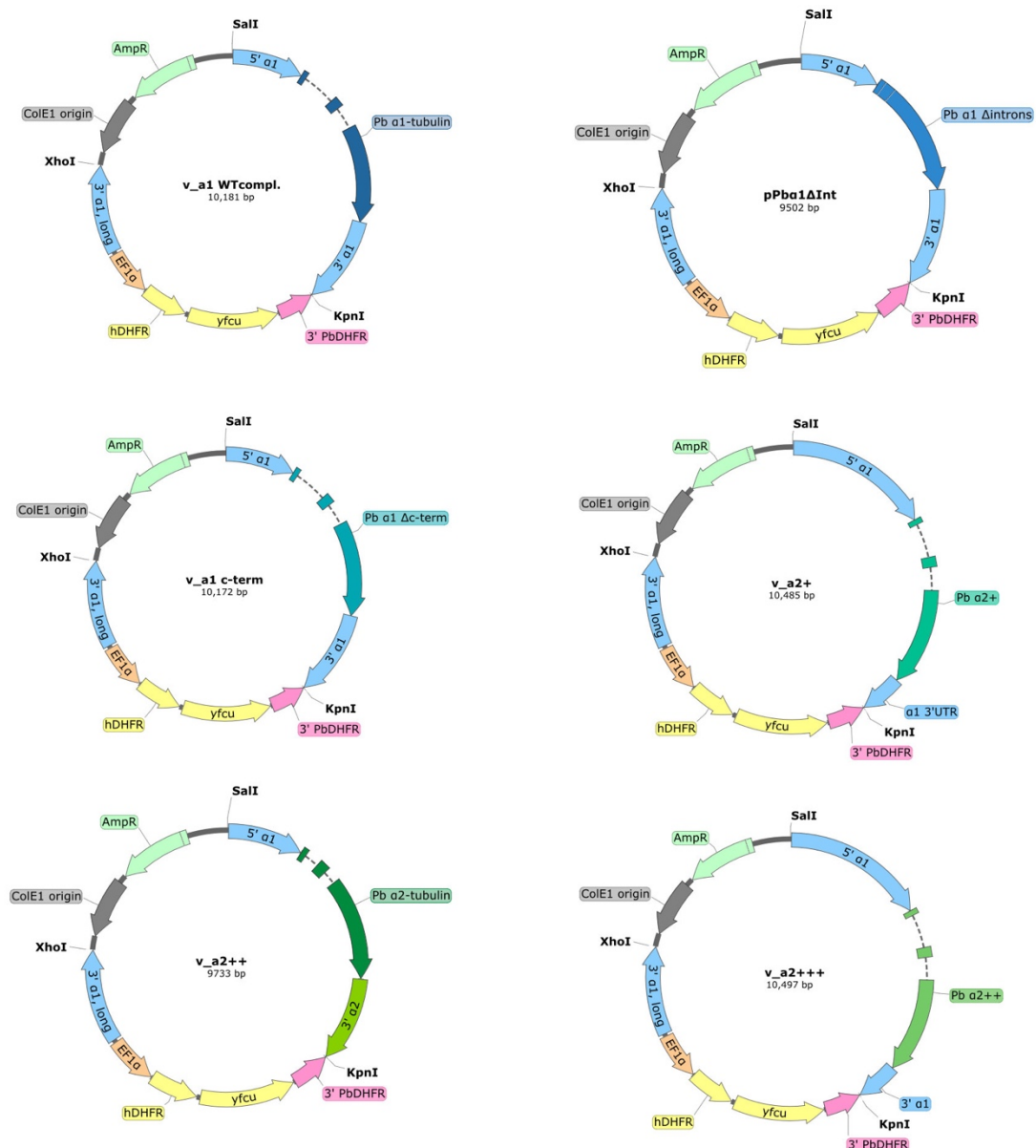


Figure 3.2 Transfection vector maps. To genetically modify the open reading frame (ORF) of the *α1-tubulin* locus, only the ORF of the $\alpha1^{cm\&\Delta introns}$ vector (**Figure 3.1**) had to be replaced whereas the integration sites and selection cassette could be kept identical. Only in case of the $\alpha2^{++}$ vector, the *α1-tubulin* 3'UTR was replaced by an *α2-tubulin* 3'UTR. This vector could not be used for the GIMO method. 5'UTRs and 3'UTRs of *α1-tubulin* are shown in blue. ORFs are highlighted in different bluish or greenish colors for the different *α1-tubulin* ORF modifications and in yellow for the selection cassette genes *hDHFR* and *yFCU*. Arrows point into the direction of promoter activity and gene orientation. Important restriction enzyme sites are shown in black. Note, that the vector $\alpha1^{WTcompl.}$ (top, left), $\alpha1^{\Delta introns}$ (top, right) and $\alpha2^{++}$ (bottom, left) were designed by me but generated under my supervision by Hannah Fleckenstein (Fleckenstein, 2016). The vector $\alpha2^{+}$ (center, right) was generated under my supervision by Claudia di Biagio (Di Biagio, 2017).

3.1.2. Generation of parasite lines

The linearized $\alpha I(-)$ vector was transfected into *P. berghei* strain ANKA (*PbANKA*) or *P. berghei* strain ANKA expressing *mCherry* under control of the *CS*-promoter and *GFP* under control of the *efl* α -promoter (*PbRG*; kindly provided by Dennis Klug) using standard protocols (Janse, Franke-Fayard, and Waters, 2006). Parasites that integrated the desired DNA construct were positively selected by administration of pyrimethamine (0.07 mg/ml) via the mouse drinking water. An isogenic population was obtained by a dilution series, which was then followed by elimination of the positive-negative selection marker *hdhfr-yfcu* by applying 5-fluorocytosine (1 mg/mL) (Lin, 2011) (**Figure 3.3**). The selection marker free $\alpha I(-)$ parasite lines (*PbANKA* and *PbRG*) were used for complementation approaches with wild type ($\alpha I^{WTcompl.}$, **Figure 3.4**), deletion of αI -*tubulin* introns ($\alpha I^{\Delta introns}$, **Figure 3.5**) and a set of $\alpha 2$ -*tubulin* chimera constructs ($\alpha 2^{+++}$, $\alpha 2^{++}$, $\alpha 2^{+}$, **Figure 3.5**). The αI -*tubulin* codon modified and intron-deleted construct ($\alpha I^{cm\&\Delta introns}$) was transfected directly into *P. berghei* strain ANKA. The GIMO receiver parasite line, only differing in the *dhfs* 3'UTR, was used to generate the C-terminally truncated αI -*tubulin* parasite line ($\alpha I^{\Delta c-term}$, **Figure 3.5**) via a 'gene insertion/marker out' approach. The GIMO method resulted in very inefficient transfections and subsequent difficulties in receiving a clonal parasite line. It was only successful for the $\alpha I^{\Delta c-term}$ parasite line, therefore, a standard integration approach was followed up for all other vectors/parasites by complementing the negatively selected $\alpha I(-)$ line or *PbANKA* WT in case of $\alpha I^{cm\&\Delta introns}$. The parasite lines $\alpha I^{WTcompl.}$, $\alpha I^{\Delta introns}$ and $\alpha 2^{++}$ were generated under my supervision by Hannah Fleckenstein (Fleckenstein, 2016) and the parasite line $\alpha 2^{+}$ was generated under my supervision by Claudia di Biagio (Biagio, 2017).

Results

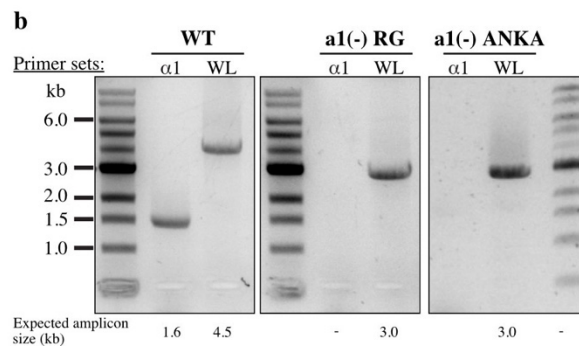
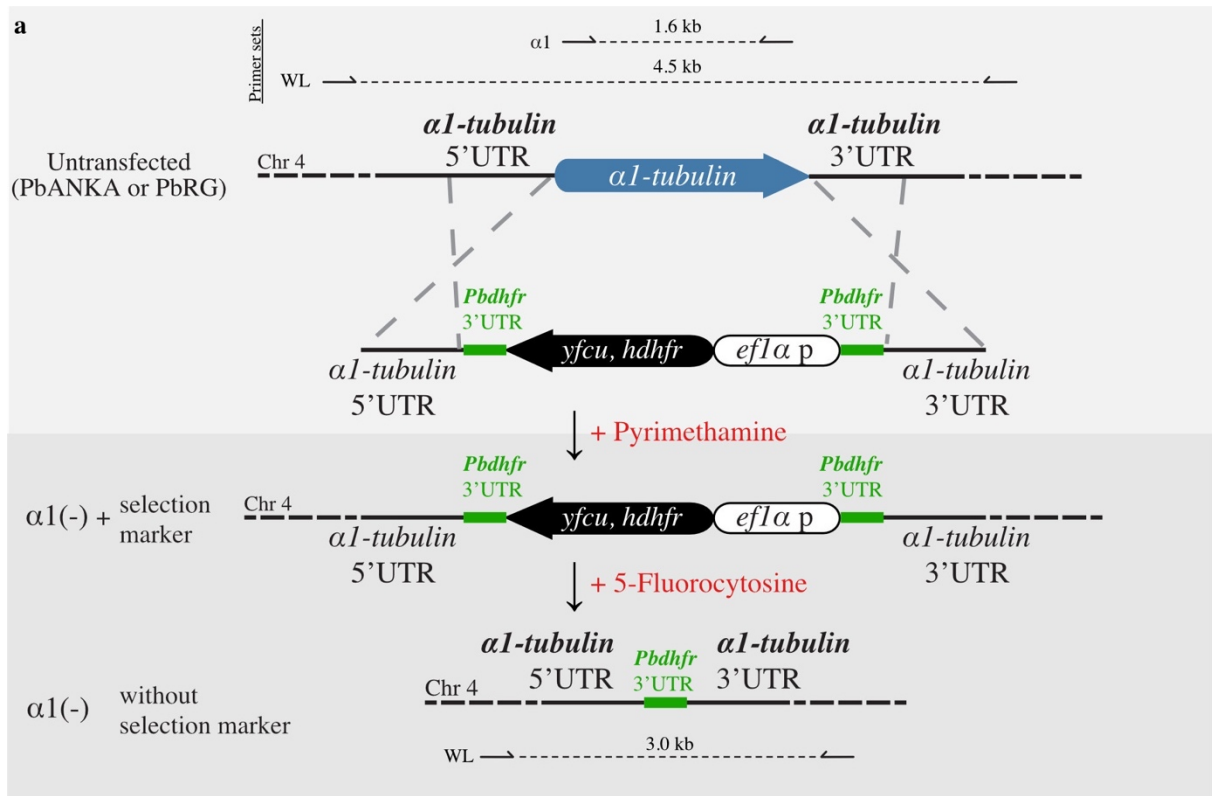


Figure 3.3. Generation of the $\alpha 1(-)$ parasite lines. (a) The strategy to delete $\alpha 1$ -tubulin from the genome of *P. berghei* is shown. The $\alpha 1$ -tubulin open reading frame (ORF) was replaced by the *hDHFR/yFCU* selection cassette integrating via double homologous recombination. Two independent $\alpha 1(-)$ parasite lines were generated via transfections into either the *PbANKA* or the *PbRG* line (kindly provided by Dennis Klug) which expresses two fluorescent proteins (*cs-mCherry* and *ef1 α -GFP*) at different stages of the *Plasmodium* life cycle. Parasites were positively selected via pyrimethamine and negatively selected via 5-fluorocytosine. (b) Correct integration was shown with PCR analysis. Expected amplicon sizes below the images and primer binding sites (a) are indicated. WL: whole locus; $\alpha 1$: $\alpha 1$ -tubulin.

Results

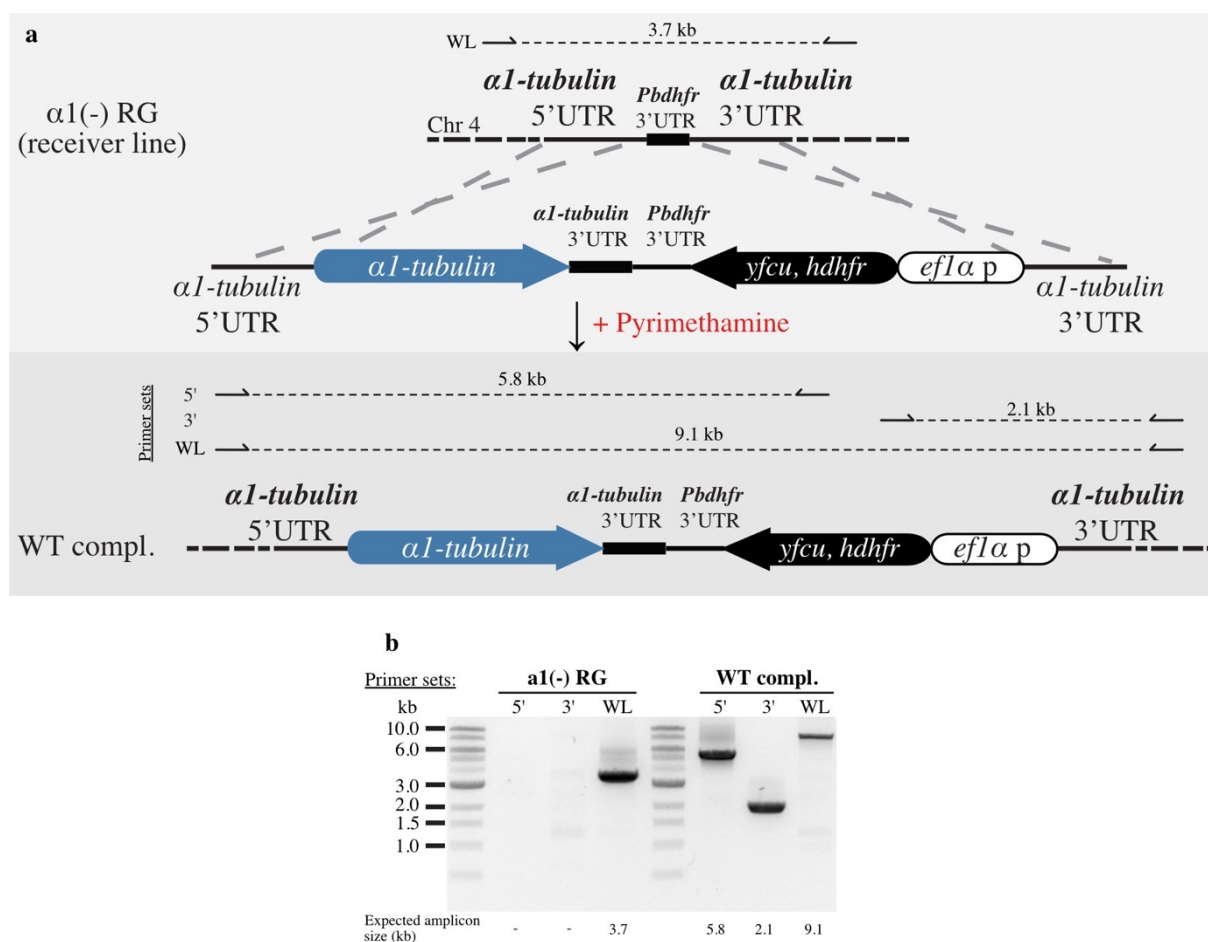
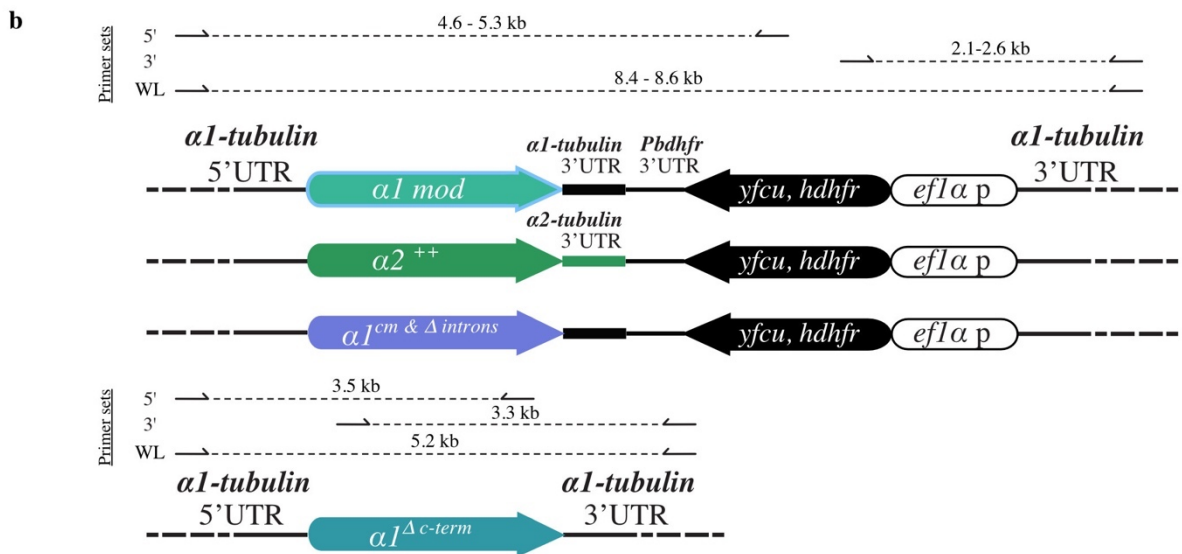
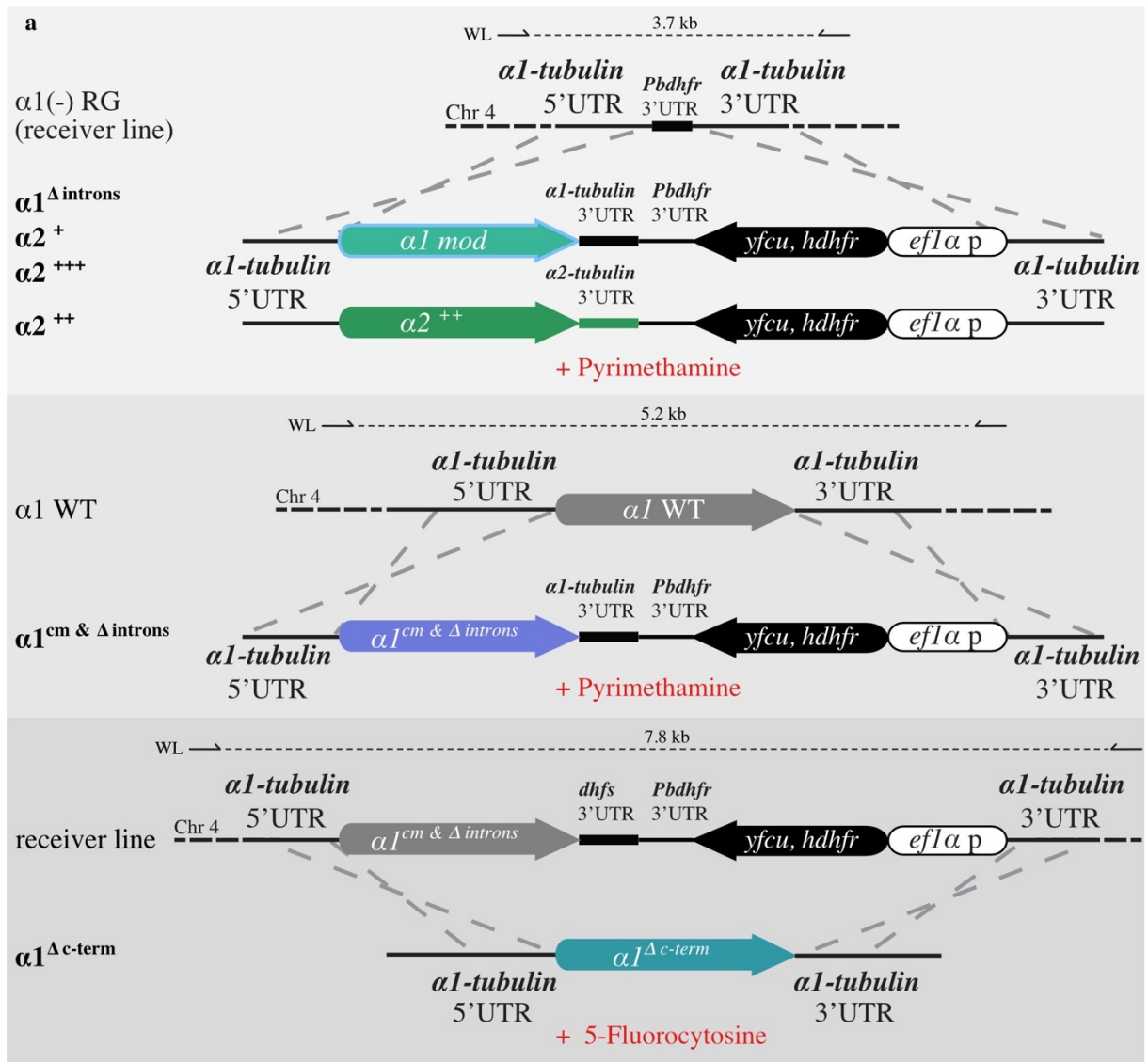


Figure 3.4. Complementation of the $\alpha 1(-)$ RG parasite line. (a) The negatively selected $\alpha 1(-)$ RG parasite line was complemented with a construct containing the WT $\alpha 1$ -tubulin ORF. $\alpha 1^{WTcompl.}$ parasites were positively selected via pyrimethamine. (b) Correct integration was shown with PCR analysis. Expected amplicon sizes below the images and primer binding sites (a) are indicated. 5': 5'UTR integration; 3': 3'UTR integration; WL: whole locus.

Results



Results

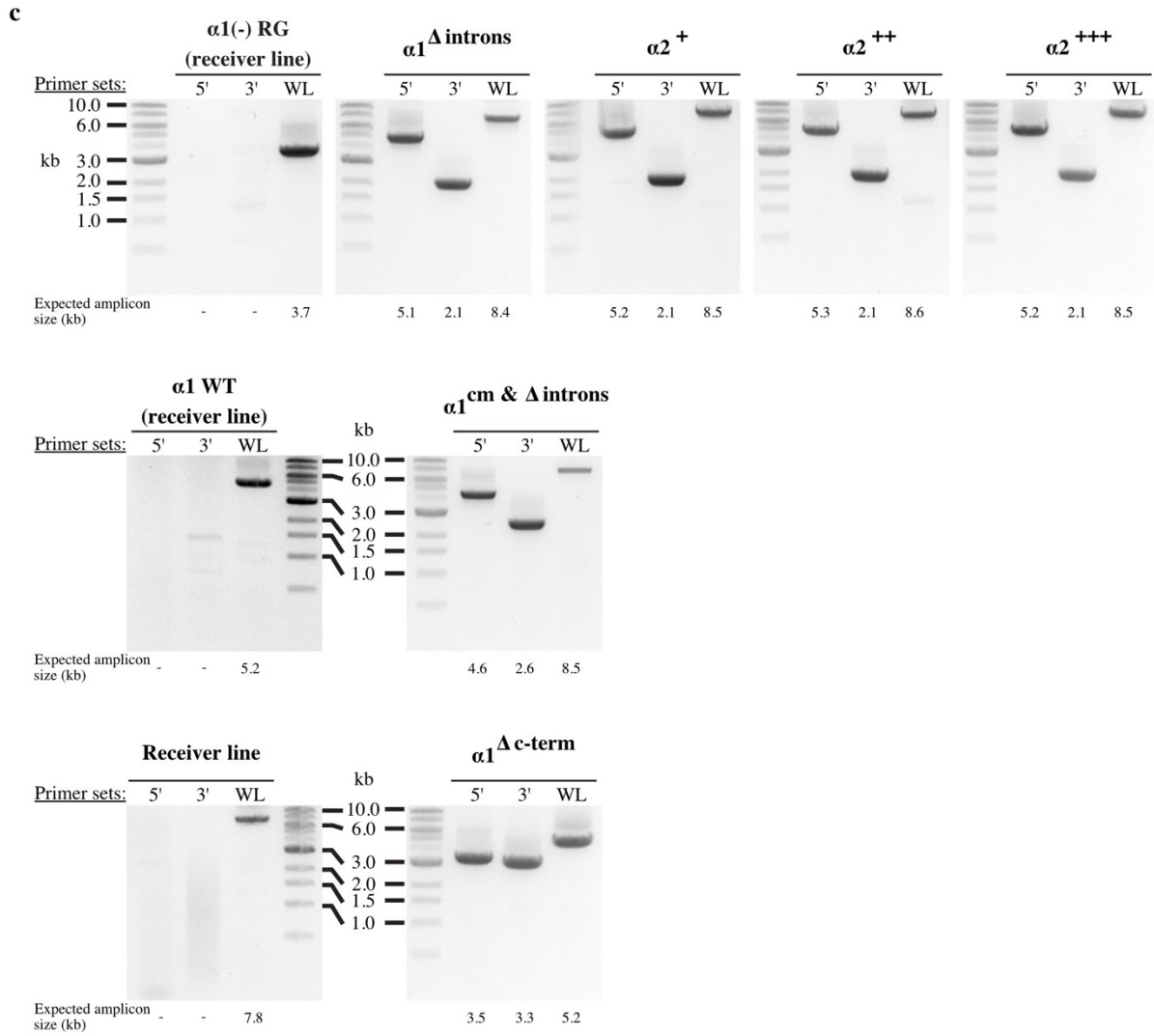


Figure 3.5. Generation of $\alpha 2^{+}$, $\alpha 2^{++}$, $\alpha 2^{+++}$, $\alpha 1^{\Delta \text{introns}}$, $\alpha 1^{cm \& \Delta \text{introns}}$ and $\alpha 1^{\Delta \text{c-term}}$ parasite lines. (a) The negatively selected $\alpha 1(-)$ RG parasite line was complemented with the constructs $\alpha 2^{+}$, $\alpha 2^{++}$, $\alpha 2^{+++}$ and $\alpha 1^{\Delta \text{introns}}$. In contrast, the $\alpha 1^{cm \& \Delta \text{introns}}$ parasite line was generated using a non-fluorescent *PbANKA* strain as a receiver line. Parasites were positively selected via pyrimethamine. Only the parasite line $\alpha 1^{\Delta \text{c-term}}$ was generated via the GIMO method by integrating the $\alpha 1^{\Delta \text{c-term}}$ construct into the GIMO receiver line and selecting with 5-FC. (c) Correct integration was shown with PCR analysis. Expected amplicon sizes below the images and primer binding sites (a, b) are indicated. 5': 5'UTR integration; 3': 3'UTR integration; WL: whole locus.

3.2. Microtubules in oocyst and sporozoite development of *Plasmodium berghei*

3.2.1. SiR-tubulin can label microtubules *in vivo* in mosquito midgut oocysts

As a first step to understand the presence and consequent role of microtubules during oocyst development, I tested several different approaches to visualize microtubules. Tubulin-specific antibodies were not successful possibly due to the inability of antibodies to penetrate the oocyst wall efficiently despite extensive oocyst permeabilization approaches. Tagging of any of the tubulins was previously shown to result in tagging-dependent phenotypes (Kooij et al., 2005), (Mirko Singer, data not shown). Therefore, an alternative method was necessary to visualize microtubules during parasite development in mosquitos. With the recently published dye SiR-tubulin (combining the microtubule ligand docetaxel with silicon-rhodamine), I was finally successful in staining microtubules throughout oocyst and sporozoite development (Lukinavičius et al., 2014), (**Figure 3.6**).

Very early oocysts (4 days post mosquito blood meal) showed remaining subpellicular microtubules (sMTs) of the preceding ookinete stage (**Figure 3.6 I**). From day 5 to day 10 post blood meal, oocysts replicated their nuclei (II – IV). Hemispindle microtubules (III, close up) or spindle pole bodies could only be detected when oocysts were detached from the midgut by pressing slightly on the cover slide despite using spinning disc confocal microscopy. Otherwise, the microtubule background signal of surrounding midgut cells was overexposing the faint signal of the hemispindle and spindle pole structures (II, III). From day 10 onwards, oocysts started to align their nuclei to the invaginating plasma membrane (not stained) followed by sMT formation at the sporoblast membrane next to each aligned nuclei (V). sMTs then elongated (VI a, b). Nuclei were pulled into the budding sporozoite when sMTs reached approximately 3 μm in length (VI c, d). Subpellicular MTs were extending beyond the nuclei in close proximity to mature midgut sporozoites (VII). When considering only a single oocyst, sporozoite budding occurs in a very synchronous manner. However, across many oocysts infecting one mosquito midgut, developmental progress can be very asynchronous. On day 12 post blood meal, some oocysts can still be replicating their nuclei while others are already containing mature sporozoites. Thus, categorizing oocyst development by time past blood meal can only be used as an approximate indication of oocyst development.

Oocyst images acquired with transmission electron microscopy (TEM) were in line with the previous description of oocyst development. During very early oocyst development (**Figure 3.7 I-III**, 5-10 days post blood meal), nuclear replication takes place and the number of nuclei (N) increases. This is followed by the plasma membrane (PM) detachment from the oocyst wall, the invagination of the PM and the synchronous onset of sporozoite budding (arrows heads, IV-

VI, 10-12 days post blood meal). Sporozoites are then elongated and sporoblast (Sb) size is reduced with increased sporozoites length (VIII-X).

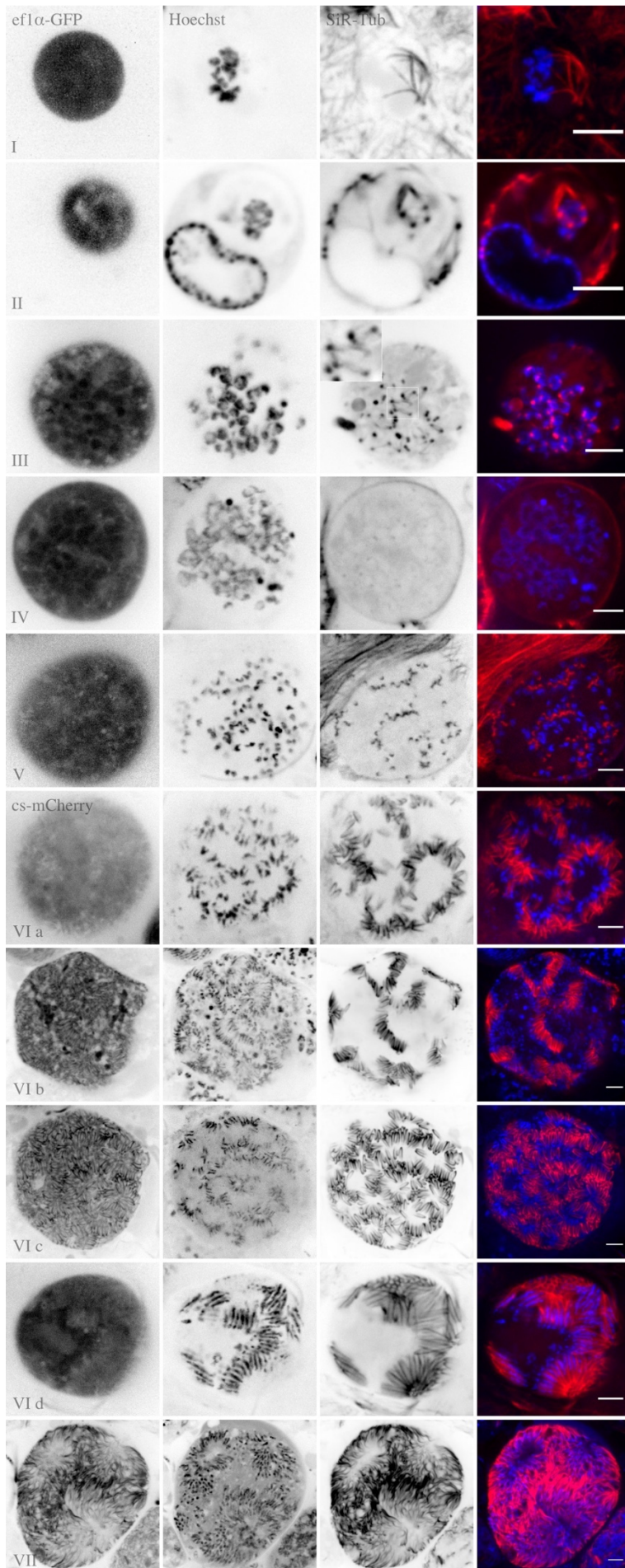
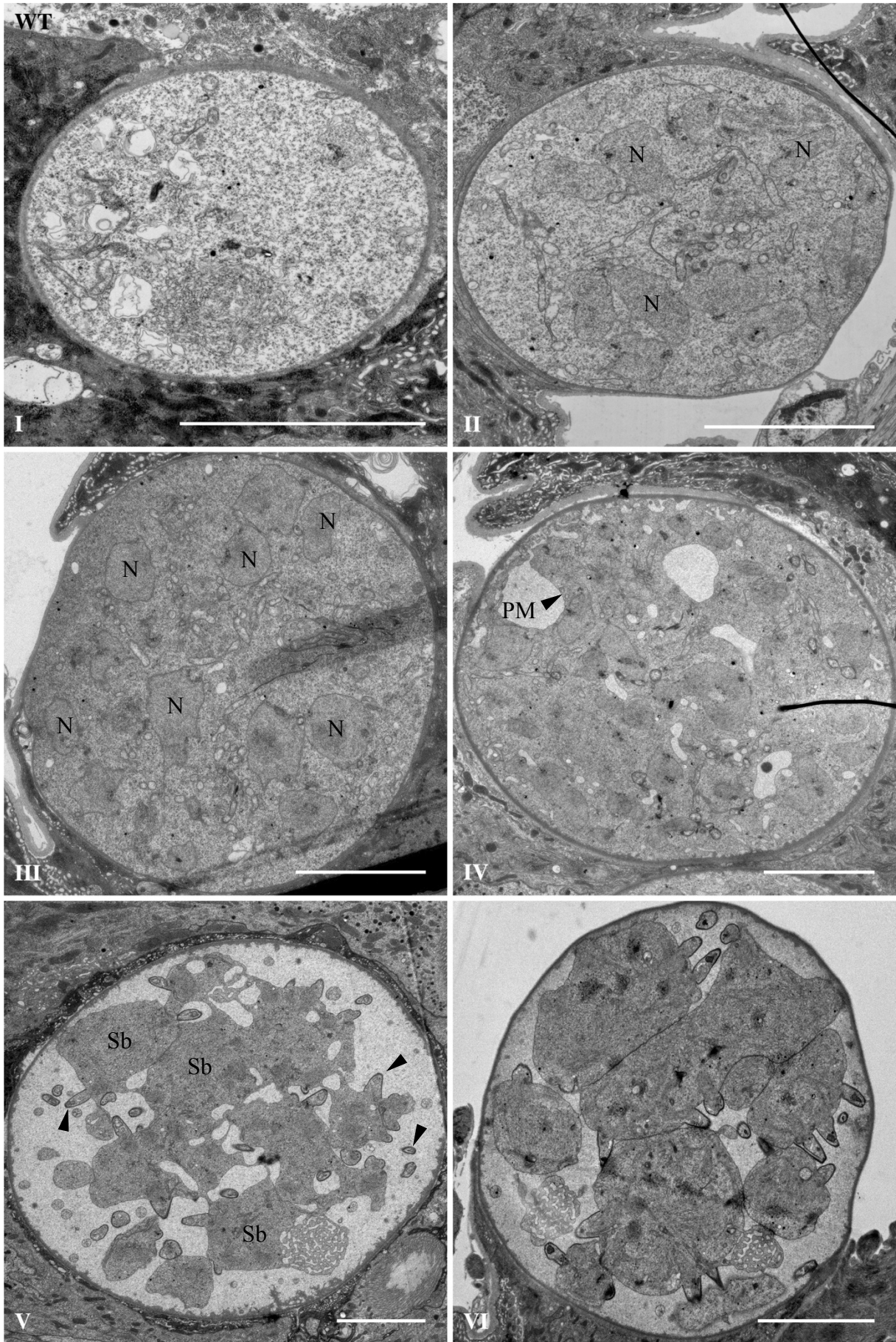


Figure 3.6. Oocyst development in the mosquito midgut. Life imaging of wild-type (WT) RG line oocysts expressing *eflα-GFP* (early and late oocysts) and *cs-mCherry* (late oocysts) to locate the oocyst cytoplasm. Microtubules were labeled with SiR-tubulin (red) and DNA with Hoechst 33342 (blue). Oocysts are shown in a chronological order from early to late development. I-IV show early oocyst development with remaining sMTs of the preceding ookinete stage (I) and subsequent DNA replication (II-IV). Followed by nuclear alignments to the invaginated plasma membrane (V) and budding of sporozoites (VI a-d). Note the strong SiR-tubulin signal showing the sporozoite sMTs. (VII) Oocyst ready to burst with fully formed sporozoites. Shown are single images or maximum projections of stacks in z-direction (I, 7,6μm; III, 2μm in z-direction). Scale bars: 5 μm.



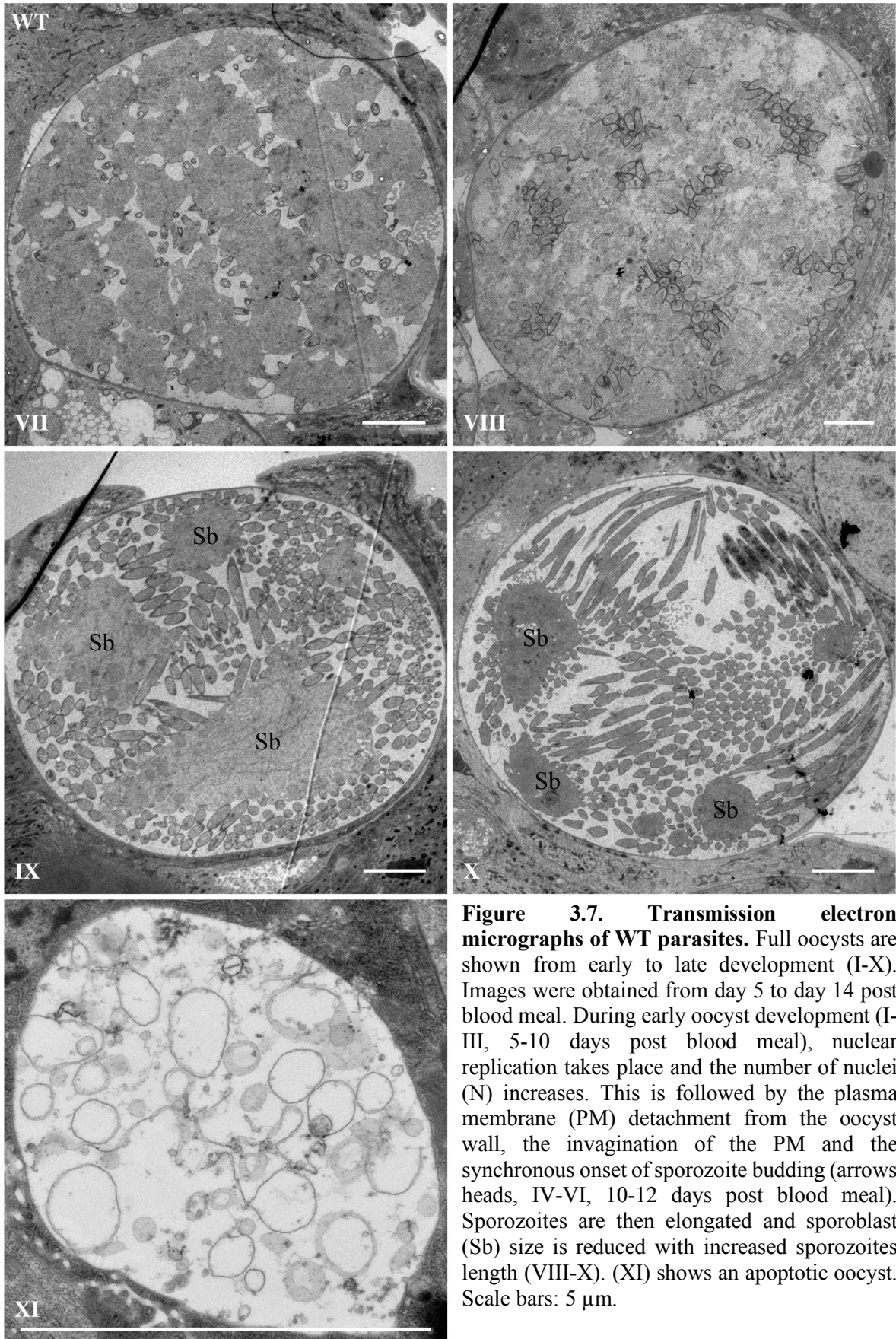
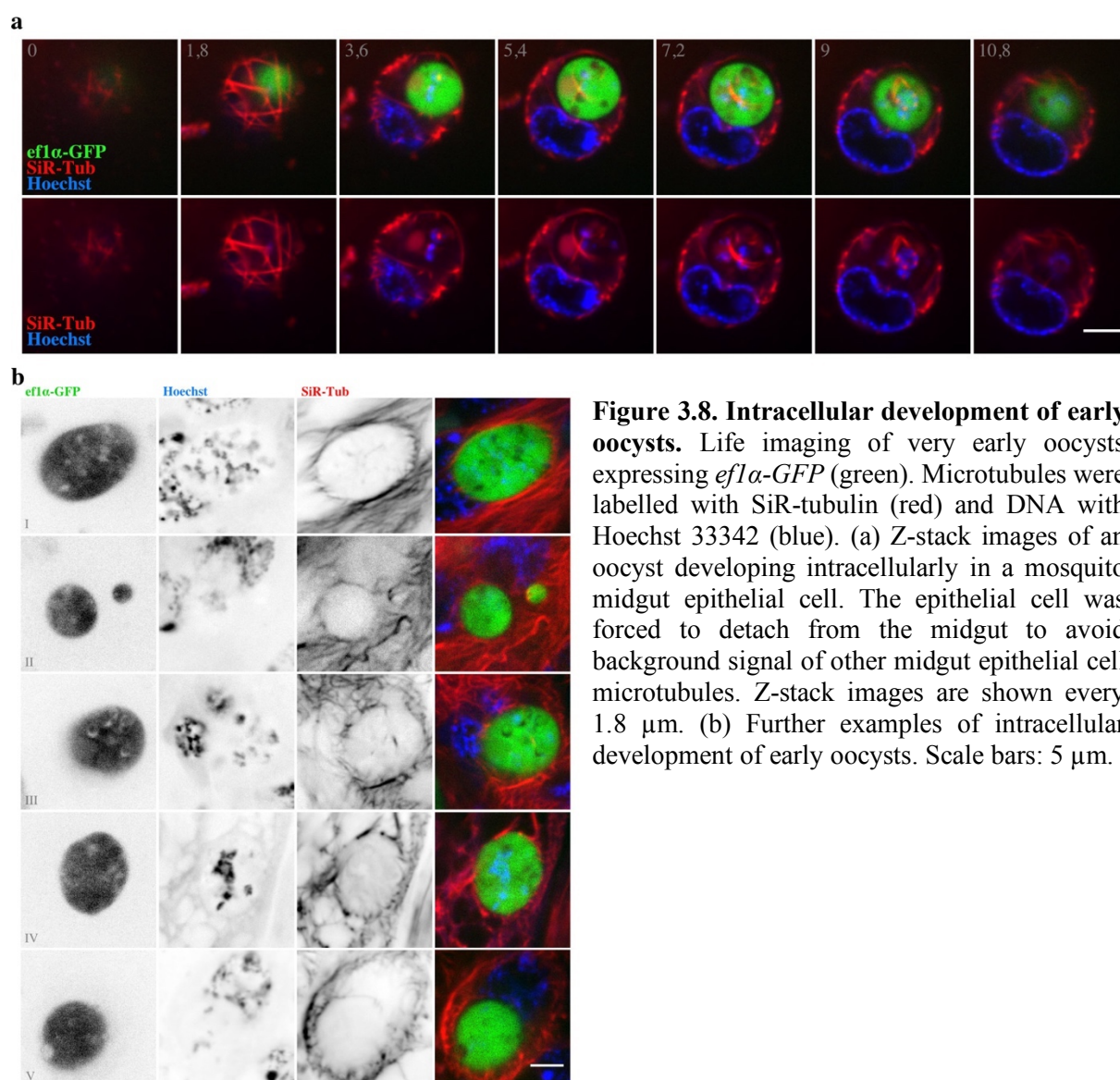


Figure 3.7. Transmission electron micrographs of WT parasites. Full oocysts are shown from early to late development (I-X). Images were obtained from day 5 to day 14 post blood meal. During early oocyst development (I-III, 5-10 days post blood meal), nuclear replication takes place and the number of nuclei (N) increases. This is followed by the plasma membrane (PM) detachment from the oocyst wall, the invagination of the PM and the synchronous onset of sporozoite budding (arrows heads, IV-VI, 10-12 days post blood meal). Sporozoites are then elongated and sporoblast (Sb) size is reduced with increased sporozoites length (VIII-X). (XI) shows an apoptotic oocyst. Scale bars: 5 μ m.

3.2.2. Oocysts can develop intracellularly in mosquito midgut cells

In the late 60s, Vanderberg et al. already showed via TEM approaches that oocyst occasionally develop intracellularly in mosquito midgut epithelial cells (Vanderberg, Rdodin, and Yoeli, 1967). These observations can now be supported by spinning disc confocal microscopy images of early oocysts as shown in **Figure 3.8**. (a) shows an oocyst developing intracellularly in a midgut epithelial cell. (b) shows further examples of intracellular developing early oocysts.



3.2.3. Late oocysts show subpellicular and very long hemispindle microtubules

Hemispindle microtubules (hMTs) are originating in a radial fashion from the nuclear spindle pole plaque (also called microtubule organizing center (MTOC) or centriolar plaque) which is embedded in the nuclear envelope. During early sporozoite budding, the spindle pole plaque is located at the basal site of the emerging sporozoite (Schrével, Asfaux-Foucher, and Bafort, 1977; Gerald, Mahajan, and Kumar, 2011). With serial sections, approximately 35 hMTs per hemispindle were identified (Sinden and Strong, 1978). However, the length could not be determined with electron microscopy to date. Visualizing and measuring the length of hMTs within SiR-tubulin stained oocyst is possible but difficult due to the strong SiR-tubulin signal of surrounding cells and sMTs. Oocysts have to be detached of the midgut by pressing slightly on the cover slide. Furthermore, it is advantageous to search for sporoblasts which are not located within the oocyst wall anymore (**Figure 3.9**). Hemispindles reached up to 14,5 μm into the sporoblast (**Figure 3.9 b**, left) and were surrounded by Hoechst staining at their endings (b, center left and right). As hMT are intra-nuclear as further described in Chapter 3.3.4 (**Figure 3.21**), this would suggest that this nuclear stain is part of the nucleus already aligned at the sporoblast membrane therefore indicating very elongated nuclei. This is further discussed in chapter 4.1.1.

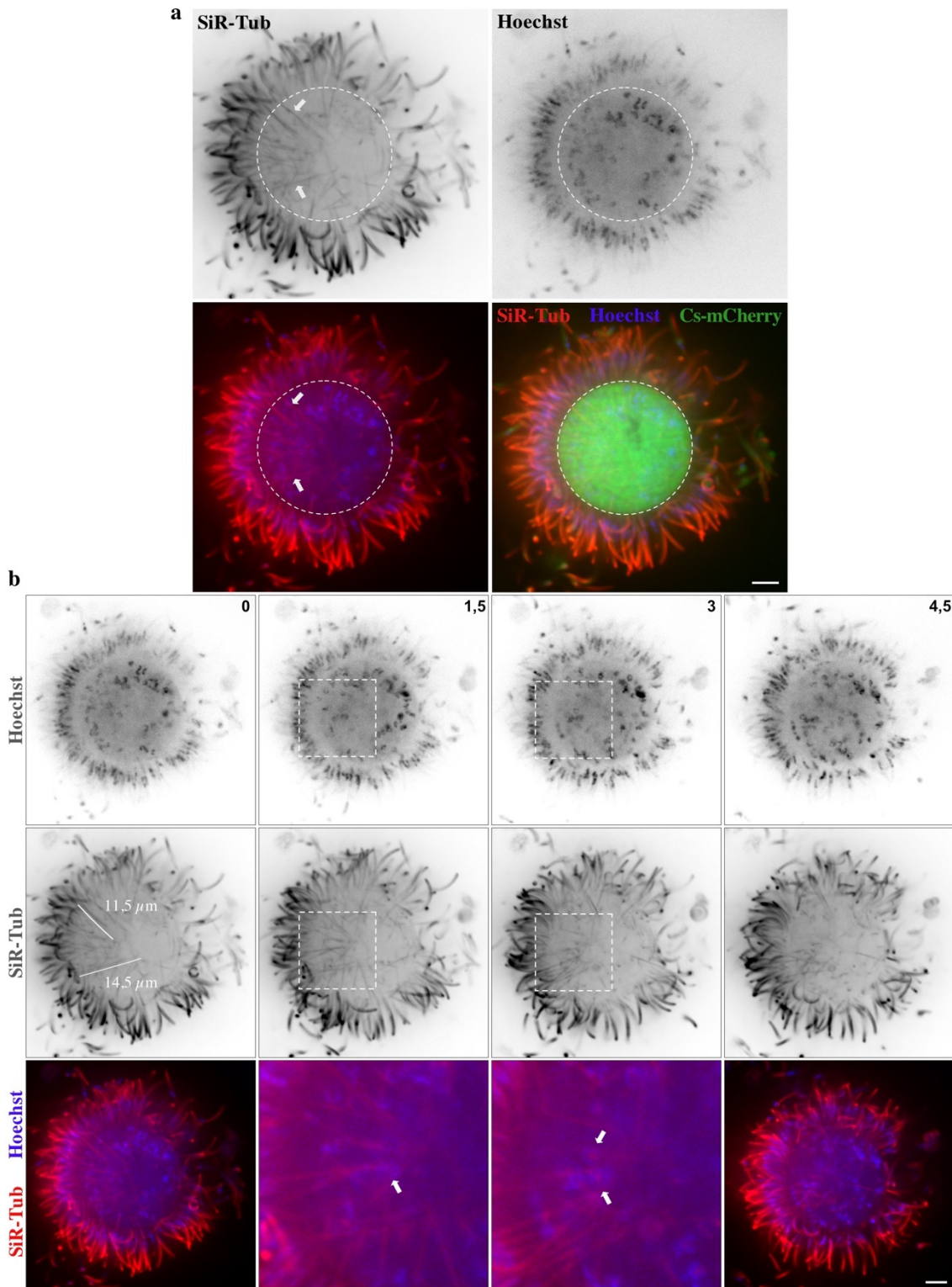


Figure 3.9. Late oocysts showing subpellicular and hemispindle microtubules (hMTs). (a) Life images of an oocyst sporoblast with attached budding sporozoites expressing cytoplasmic *cs-mCherry* (green; inside dotted circle). Microtubules were labelled with SiR-tubulin (red) and DNA with Hoechst (blue). The oocyst wall was removed to be able to identify single hemolymph sporozoites. Arrows point to hMTs whereas sMTs are outside the white circle. (b) hMTs can be up to 14,5 µm long and seem to end at nuclei. Bottom center left: longitudinal section; bottom center right: cross section of hemispindles and nuclei. Scale bars: 5 µm

3.2.4. Subpellicular microtubules are dynamic during sporozoite budding and beyond

Analyzing microtubule length during sporozoite budding was always limited for the reasons mentioned in chapter 3.2.1. As a result, no conclusions could be made about the dynamicity of sMTs in *Plasmodium*. It was long thought that once formed sMTs are not elongated or shortened (Cyrklaff et al., 2007). Strikingly, my investigations on late oocyst development showed, that microtubules reached full sporozoite length during late sporozoite budding but MT length was again reduced during sporozoite maturation (**Figure 3.10**). Spinning disc data showed SiR-tubulin signal along the entire length of the budding sporozoites and beyond sporozoite nuclei (a-I). Sporozoite cross sections acquired very closely to the sporoblast

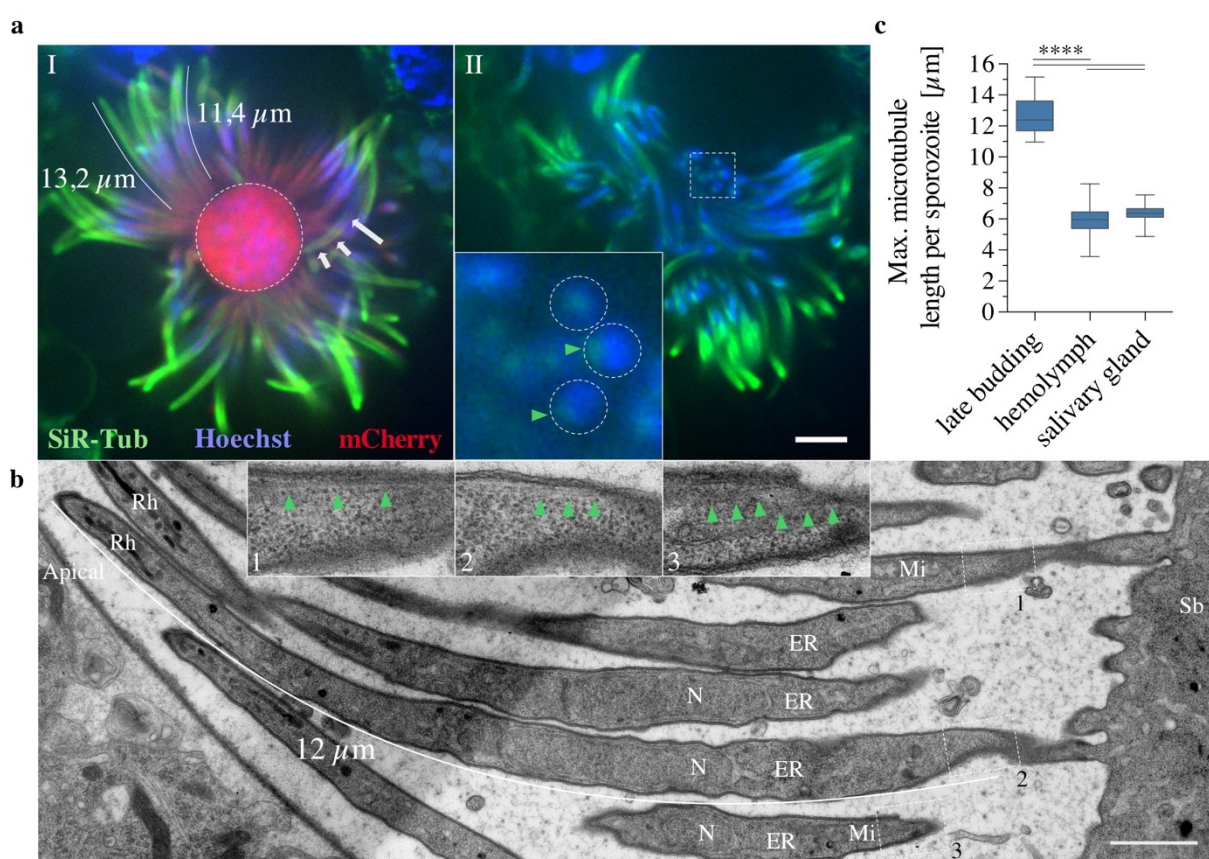


Figure 3.10. Sporozoite subpellicular microtubules increase and shorten in length during sporozoite development and maturation. (a) Subpellicular microtubules stained with SiR-tubulin (green) reached full sporozoite length during late sporozoite budding (I, small arrows). The sporoblast is visualized by cytoplasmic *mCherry* (red) expressed via the *cs*-promoter. The big arrow indicates the nucleus of the sporozoite. Cross section of sporozoites acquired very closely to the sporoblast showed SiR-tubulin staining next to the DNA staining (II, dotted circles indicate cross sections of sporozoites; green arrows indicate sMTs). (b) Longitudinal sections of late budding sporozoites. Organelles of several sporozoites are named to indicate simultaneous budding. Rh: rhoptry; N: nucleus; ER: endoplasmic reticulum; Mi: mitochondrion; Sb: sporoblast. Close up views of the posterior end of three sporozoites with microtubules (green arrows) are shown. (c) Quantification of sMT length of different sporozoite stages. SiR-tubulin stained samples were analyzed by semi-automated length measurement using Volocity 6.3 as described in chapter 2.3.14. Statistics were analyzed using a Kruskal-Wallis test. **** indicate $P < 0.0001$. Scale bar: a: 5 μm ; b: 1 μm .

membrane showed SiR-tubulin staining next to the DNA signal (a-II, close up: dotted circle indicates cross sections of sporozoites). TEM images supported these observations by showing microtubules that reached almost the entire length of the budding sporozoite (b). Due to never perfect longitudinal TEM sections of late budding sporozoites, a single microtubule could not be followed up throughout the entire sporozoite length. However, longitudinal cuts of neighboring sporozoites with identical developmental progress (identified by their organelle location) can be used to identify sMTs at different longitudinal positions and microtubule length could be estimated to about 12 μm . Close up views indicate microtubules (green arrows) of different budding sporozoites at their posterior end. Due to the fluorescent images and the knowledge that sMTs are attached at the apical polar ring (APR) and elongated towards the sporozoite posterior end (Kudryashev et al., 2012), we can assume that sMTs seen at the sporozoite posterior end originated at the APR. Comparing the sMT length of late budding midgut sporozoites with stages following oocyst development such as hemolymph sporozoites and salivary gland sporozoites showed a highly significant drop in length from 12 μm in late developing oocysts to 6 μm in hemolymph sporozoites followed by a slight elongation to 6.5 μm during sporozoite maturation to salivary gland sporozoites (c).

3.2.5. *$\alpha 1$ -tubulin* is the predominantly expressed *α -tubulin* isotype during oocyst development

RNA sequencing data revealed a predominant expression of *$\alpha 2$ -tubulin* during blood stage and ookinete development (Otto et al., 2014). Proteomic data showed, that both tubulins can be identified with mass spectrometry in hemolymph and salivary gland sporozoites, however, both publications did not consider the high amino acid sequence identity between *Plasmodium* tubulins and also between *Plasmodium* and *Anopheles* mosquito tubulins and therefore assignment of oligo peptide counts is likely wrong for both *α -tubulins*. Furthermore, quantitative conclusions are not possible with the methods used in the publications (Lasonder et al., 2008; S. E. Lindner et al., 2013). Due to the fact that there are no available specific antibodies for *$\alpha 1$ -tubulin* and *$\alpha 2$ -tubulin* and the general difficulty of performing a Western blot on oocyst stages, qRT-PCR was used to estimate mRNA levels during oocyst development as the best proxy for protein levels (**Figure 3.11**). Expression of *$\alpha 1$ -tubulin* increased during oocyst development and peaked at day 12 post mosquito blood meal (a). *$\alpha 2$ -tubulin* showed a similar pattern. However, already at day 12 post blood meal when sporozoite budding is occurring in most oocysts, *$\alpha 2$ -tubulin* expression was reduced and continued to drop to a level of day 7 on day 14 (b). When comparing *$\alpha 2$ -tubulin* expression levels to *$\alpha 1$ -tubulin*, *$\alpha 2$ -tubulin*

expression was approximately 100-fold lower until day 10 and then reduced to 200-fold on day 14. To put tubulin expression into relation to another strongly expressed gene during oocyst development, I tested expression levels of the *circumsporozoite protein (CSP)*, a surface protein strongly expressed during sporozoite budding and the most abundant protein found on the sporozoite surface (Ménard et al., 1997; Thathy et al., 2002). This revealed that *CSP* increased its expression throughout oocyst development and reached a 320-fold increase on day 14 if compared to its day 5 levels (d). Both proteins have very similar expression levels from day 10 to day 14 post blood meal when DNA replication is finished and sporozoite budding occurs (e). *CSP* is then (day 14) expressed about 2-3 times as abundantly as *$\alpha 1$ -tubulin* mRNA.

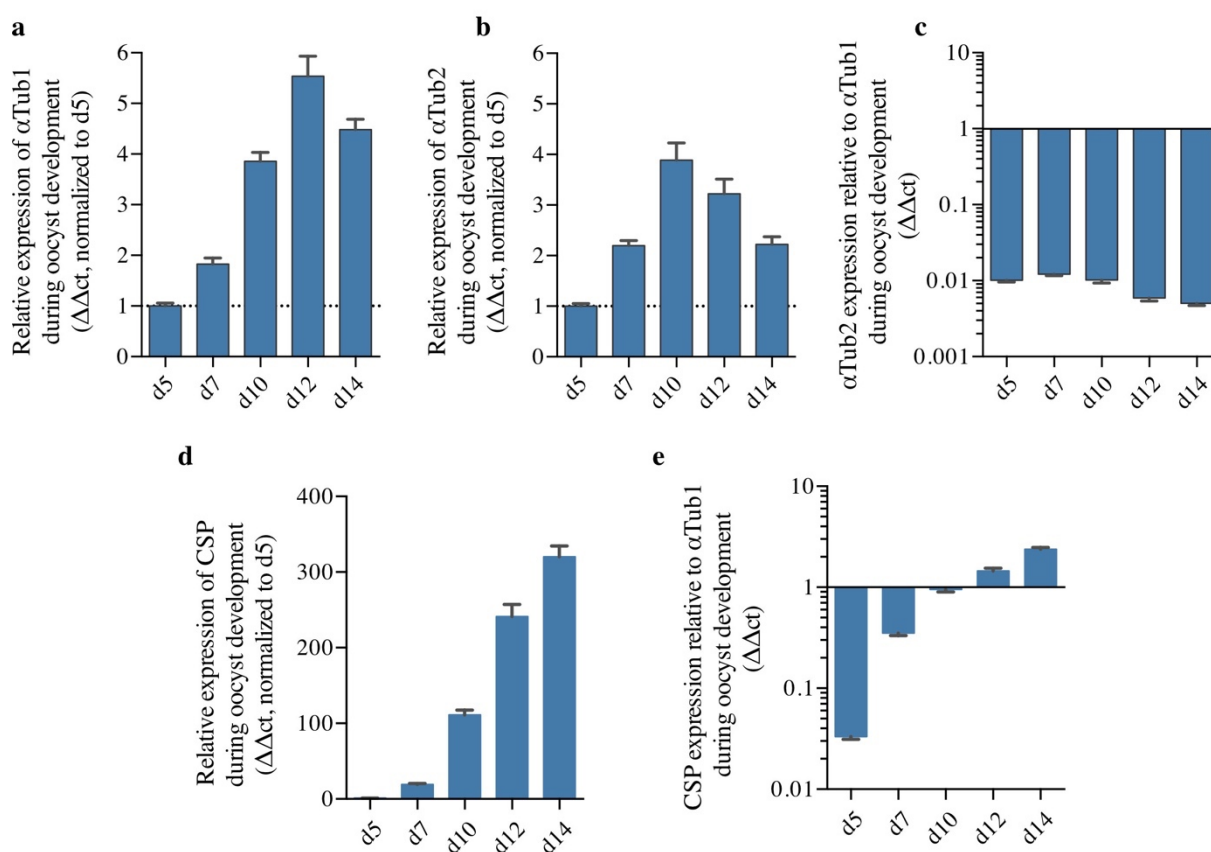


Figure 3.11. Relative expression of $\alpha 1$ -tubulin, $\alpha 2$ -tubulin and CSP during oocyst development. Days indicated represent days post mosquito blood meal. *18SrRNA* was used to eliminate sample and ROX dye for pipetting variances. Relative expression was calculated via the $\Delta\Delta Ct$ -method with error bars indicating the standard deviation of the mean calculated from technical duplicates. (a) $\alpha 1$ -tubulin relative expression. Samples of all days were normalized to day 5. (b) $\alpha 2$ -tubulin relative expression. Samples of all days were normalized to day 5. (c) $\alpha 2$ -tubulin expression relative to $\alpha 1$ -tubulin. Each $\alpha 2$ -tubulin time point was normalized to its corresponding $\alpha 1$ -tubulin time point. (d) CSP relative expression. Samples of all days were normalized to day 5. (e) CSP expression relative to $\alpha 1$ -tubulin. Each CSP time point was normalized to its corresponding $\alpha 1$ -tubulin time point.

3.3. $\alpha 1$ -tubulin is only essential for sporozoite formation

In contrast to a previous publication indicating that both α -tubulins are essential during blood stage development (Kooij et al., 2005), I was able to knock out $\alpha 1$ -tubulin in two independent ways, one parasite generated with wild type *PbANKA* as the recipient line and one with the *PbRG* line kindly provided by Dennis Klug.

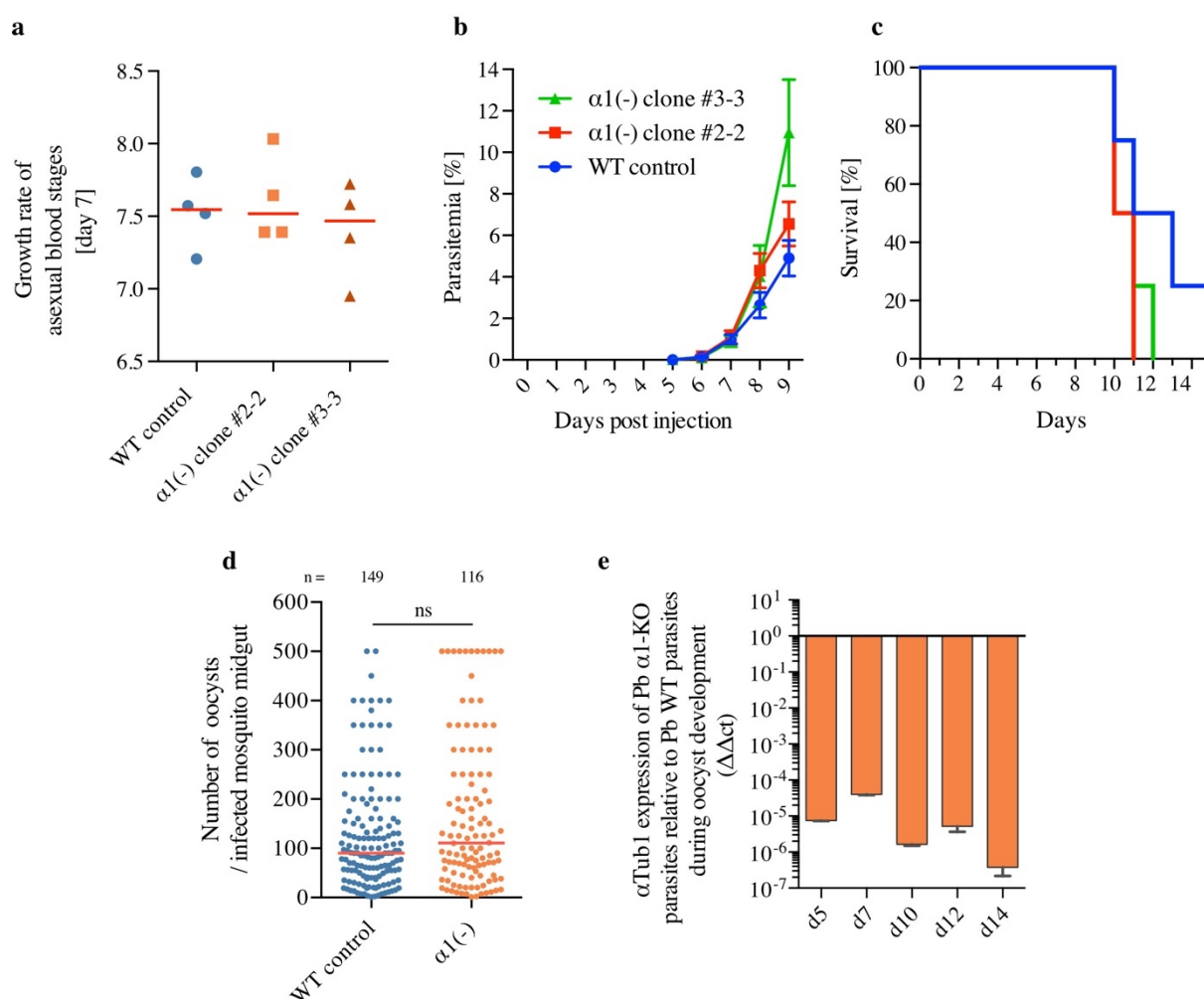


Figure 3.12. Blood stage growth and oocyst numbers are not affected in $\alpha 1(-)$ parasites. (a-c) Four C57BL/6 mice were infected with 100 blood stage parasites *i.v.* and monitored. (a) Parasite growth rate was calculated of day 7. No significant difference was seen across WT and $\alpha 1(-)$ parasites. Red bars indicate medians. (b) Parasitemia was monitored for 9 days. (c) All mice infected with $\alpha 1(-)$ parasites died within 12 days post infection. (d) Oocyst counts between d10 and d14 post mosquito blood meal of four independent cage feeds showed no significant difference. Statistics were analyzed using a Mann-Whitney test. The red lines indicate the median. (e) Quantitative real-time PCR (qRT-PCR) with $\alpha 1$ -specific primers on $\alpha 1(-)$ parasites put in relation to WT revealed loss of $\alpha 1$ -tubulin RNA. Relative expression was calculated via the $\Delta\Delta Ct$ -method with error bars indicating the standard deviation of the mean calculated from technical duplicates.

3.3.1. Deletion of *$\alpha 1$ -tubulin* has no impact on blood stage growth and oocyst numbers

No phenotype was observed during blood stage development and oocyst numbers in *$\alpha 1(-)$* parasites (**Figure 3.12**). Injection of 100 blood stage parasites *i.v.* to determine blood stage growth of two *$\alpha 1(-)$* clones showed no significant difference to WT (a). Prepatency as well as survival of infected mice was not affected either (b & c). Oocyst numbers had variances across mosquito cages. However, overall no significant difference could be determined (d). Quantitative real-time PCR showed, that no *$\alpha 1$ -tubulin* RNA can be found in *$\alpha 1(-)$* parasites.

3.3.2. Deletion of *$\alpha 1$ -tubulin* does not affect *$\alpha 2$ -tubulin* and *CSP* expression during early oocyst development but delays oocyst/sporozoite maturation during sporozoite budding

To test whether *$\alpha 1(-)$* leads to negative or positive feedback regulations potentially delaying parasite development, I plotted *$\alpha 2$ -tubulin* and *CSP* expression levels of *$\alpha 1(-)$* parasites in relation to WT (**Figure 3.13**). qRT-PCR data indicated, that *$\alpha 2$ -tubulin* expression in *$\alpha 1(-)$* parasites reached almost WT parasite levels, but expression slightly dropped to approximately ~70% on day 12 and day 14 post blood meal (a). *CSP* expression indicated a similar trend. Expression slightly dropped on day 12 post feed but during early development expression reached the same level or even higher levels than WT (b). To investigate whether the reduced amounts of RNA found for *$\alpha 2$ -tubulin* and *CSP* from day 12 onwards are of biological relevance, I investigated *CSP* expression and oocyst developmental progress via fluorescence microscopy at day 10 and day 12 post blood meal (c-e). Parasites used for quantification were generated in the *PbRG* background therefore expressing *mCherry* under control of the *cs*-promoter and *GFP* under control of the *efl α* -promoter. No difference in *CSP* fluorescence (expression) between WT control and *$\alpha 1(-)$* could be observed at day 10. Remarkably at day 12 post blood meal, ~37% of WT compared to ~28% of *$\alpha 1(-)$* showed weak *cs-mCherry* fluorescence and ~29% of WT compared to ~5% of *$\alpha 1(-)$* oocysts showed strong *cs-mCherry* fluorescence (c, d). A similar picture arose when categorizing oocysts into developmental stages to identify differences in developmental progress at a specific time point. The following categories were chosen and are named in a developmental ‘chronological’ manner: no nuclear alignment; nuclear alignment; early sporozoite formation; late sporozoite formation. While ~65% of WT oocysts had already started with sporozoite formation on day 12, only ~3% of *$\alpha 1(-)$* oocysts did. One has to mention, that categorizing *$\alpha 1(-)$* oocysts was more difficult due to the missing SiR-tubulin (subpellicular microtubules) signal. *$\alpha 1(-)$* oocysts could therefore only

Results

be categorized via the Hoechst signal (nuclei structures, sporoblast alignment) and overall oocyst morphology (GFP, mCherry).

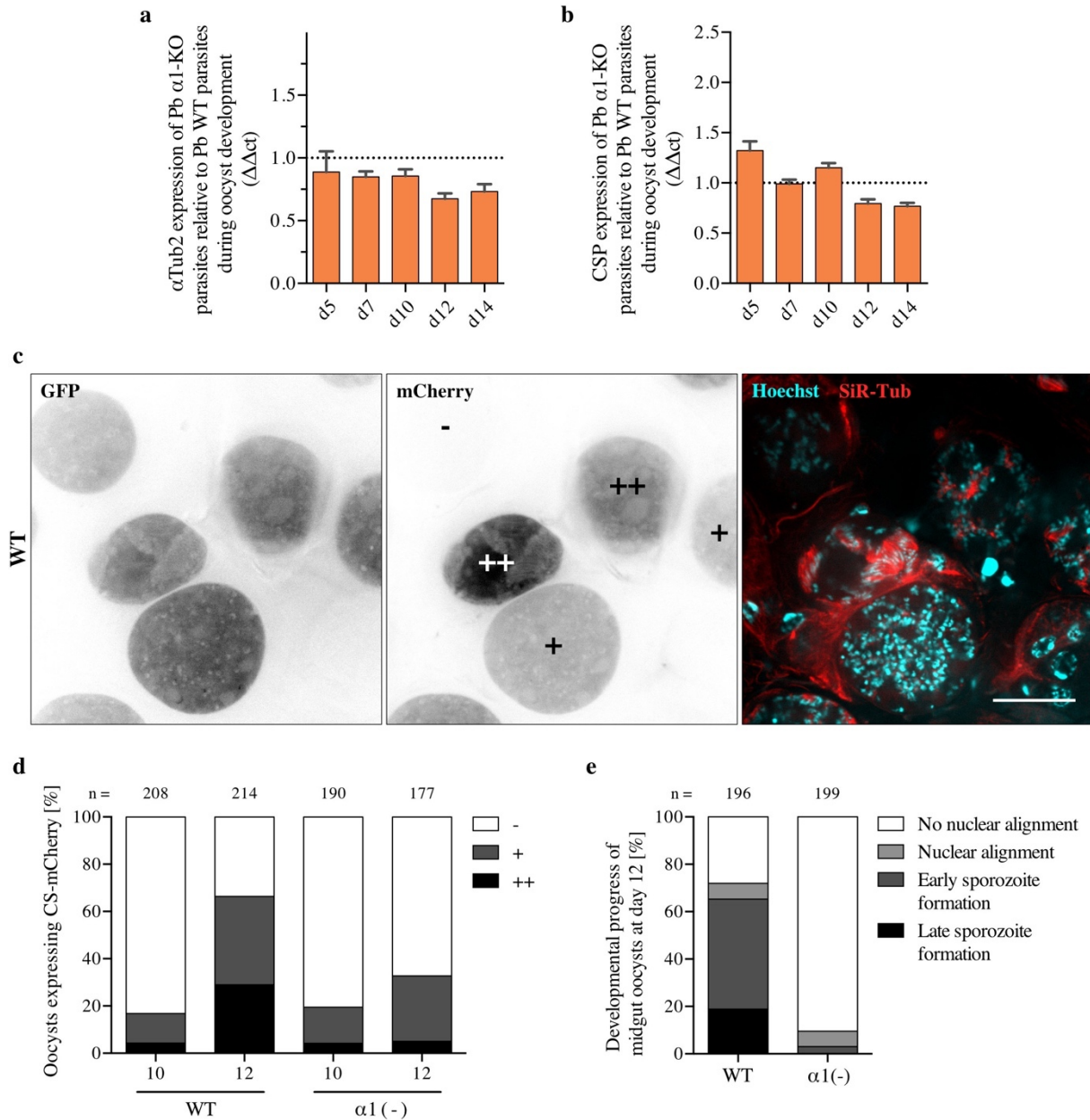


Figure 3.13. Effects of $\alpha 1$ -tubulin deletion on $\alpha 2$ -tubulin and CSP expression during oocyst development. (a) $\alpha 2$ -tubulin expression of $\alpha 1(-)$ parasites relative to WT on different days post mosquito blood meal. (b) CSP expression of $\alpha 1(-)$ parasites relative to WT on different days post mosquito blood meal. Relative expression was calculated via the $\Delta\Delta\text{Act}$ -method with error bars indicating the standard deviation of the mean calculated from technical duplicates. (c) Live images of oocysts expressing *efl* α -GFP and *cs*-mCherry. Microtubules were labelled with SiR-tubulin and DNA was labelled with Hoechst. Note that CSP expression is not seen in all oocysts and that oocysts with stronger CSP expression progressed further in development. (d) Quantification of oocysts expressing CSP on day 10 and day 12 post blood meal. (e) Classification and quantification of oocyst developmental progress on day 12 post blood meal. The number of oocysts is indicated above each column.

3.3.3. Nuclear replication, segregation and membrane alignment appear to fundamentally function in the absence of $\alpha 1$ -tubulin during early oocyst development but nuclei distribution to budding sporozoites is strongly impaired

As mentioned in chapter 3.2.5, $\alpha 1$ -tubulin was ~ 100 -fold stronger expressed than $\alpha 2$ -tubulin during early oocyst development, when DNA replication and segregation takes place. Hemispindle microtubules (hMTs) were formed during DNA replication (**Figure 3.15**, WT-III). hMTs were never seen in $\alpha 1(-)$ oocysts. However, during very early oocyst development, microtubules (I) and SiR-tubulin plaques next to nuclei (II, III) were visible. Later $\alpha 1(-)$ oocysts did not show any SiR-tubulin signal. The SiR-tubulin signal seen around midgut attached $\alpha 1(-)$ oocysts is belonging to microtubules of midgut epithelial cells (VI b, d). Independent of the missing hMTs, clearly definite nuclei increasing in numbers were seen in $\alpha 1(-)$ oocysts over time (**Figure 3.15** III-VIa & **Figure 3.14**). Moreover, nuclei aligned to the sporoblast membrane (V, VI-a, VI-b). In WT oocysts, nuclear alignment was followed by sporozoite budding identified by the SiR-tubulin staining of subpellicular microtubules (V-VII). SiR-tubulin signal was never seen in late $\alpha 1(-)$ oocysts, therefore, identification of the sporozoite budding onset was difficult to determine. However, sporozoite budding could also be estimated by looking at the mCherry or GFP signal. Both fluorescent proteins are expressed into the cytosol, therefore staining the oocyst sporoblast darker and budding sporozoites fainter due to extracellular space surrounding sporozoites (VI b-c, VII). Intriguingly, even very late $\alpha 1(-)$

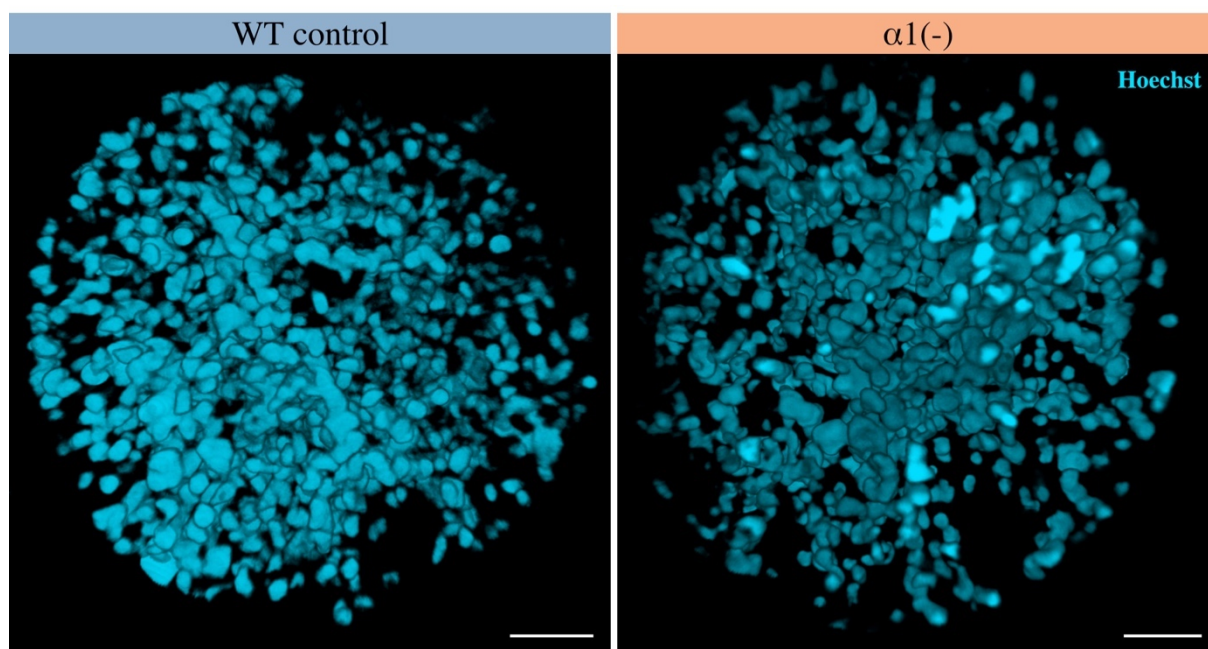


Figure 3.14. 3D reconstruction of oocyst nuclei. 3D reconstructions of early oocysts were rendered with Volocity 6.3 (3D Opacity) from z-stack images acquired with spinning disc confocal microscopy. DNA was labeled with Hoechst (cyan). Note the definite nuclei in WT as well as $\alpha 1(-)$ oocysts. Scale bars: 5 μ m.

oocysts (VI-d, day 21) still showed big sporoblasts whereas sporoblasts of WT oocysts strongly decreased their size over time. When sMTs reached $\sim 3 \mu\text{m}$ in length, nuclei were pulled into the emerging sporozoite resulting in elongated nuclei formations in WT (**Figure 3.15** VI a-d, **Figure 3.16**). In $\alpha 1(-)$ parasites, only very few nuclei were spotted inside budding sporozoites (**Figure 3.16**, late oocyst). The main nuclear mass was found within the sporoblast even in very late developed oocysts (**Figure 3.15** VI-c, VI-d, VII).

3D reconstructions of sporoblasts with emerging/budding sporozoites were rendered with Volocity 6.3 (using 3D Opacity) from z-stack images acquired with spinning disc confocal microscopy (**Figure 3.17**). The oocysts were slightly squeezed beforehand to release their sporoblasts out of the surrounding oocyst wall. Outstretched budding sporozoites still connected to the sporoblast could then be visualized. Cytoplasm is depicted in yellow (*cs-mCherry* expression), microtubules in red (SiR-tubulin labelling) and DNA in blue/cyan (Hoechst 33342 labelling). On top of each 3D reconstruction, a z-stack image representing the raw data is shown. The WT sporoblast showed emerging sporozoites from its surface with sMTs (red) emerging from the outer/apical end of the sporozoites towards the sporoblast membrane, but never emerging beyond the sporozoite-to-sporoblast contact site (a). Hemispindle microtubules were not visible, either due to the developmental stage shown with already fully pulled-in nuclei or due to the strong sMT signal overexposing the faint hemispindle signal. Sporozoites already showed their characteristic curvature at this stage of development. Moreover, nuclei were already pulled-in the emerging sporozoites, leading to stretched nuclei. Only little DNA was left inside the sporoblast. In contrast, the $\alpha 1(-)$ sporoblast showed very malformed emerging sporozoite-like structures (b). No microtubules (SiR-tubulin signal) were detectable inside the malformed sporozoites and $\alpha 1(-)$ sporozoites only rarely contained nuclei. The majority of nuclei were still present in the sporoblast, meaning, pulling nuclei inside the forming sporozoites was strongly impaired (**Figure 3.16** late oocyst, **Figure 3.17**).

To address the question, whether the 100-fold reduced $\alpha 2\text{-tubulin}$ expression levels are still sufficient to form hMTs, transmission electron microscopy of different developmental oocyst stages was performed. Among all images captured, no hMTs could be detected as shown with representative images in **Figure 3.18**.

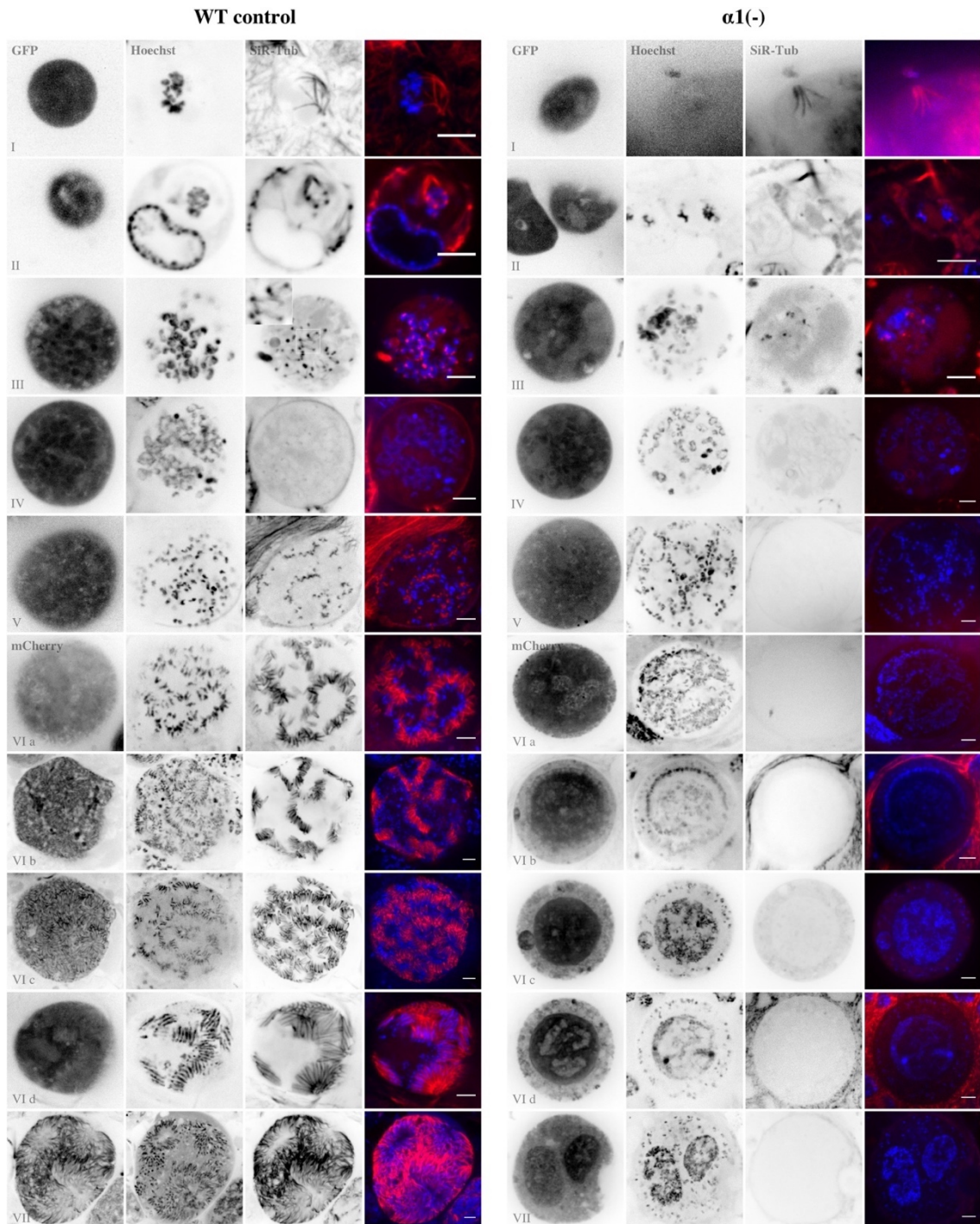


Figure 3.15. WT control and $\alpha 1(-)$ oocyst development in the mosquito midgut. Life images of oocysts expressing *efl* α -GFP (early and late oocysts) and *cs-mCherry* (late oocysts) to locate the oocyst cytoplasm. Microtubules were labeled with SiR-tubulin (red) and DNA with Hoechst 33342 (blue). Oocysts are shown in a chronological order from early to late development. Detailed information on WT development is mentioned in **Figure 3.6**. Note the missing SiR-tubulin signal in the $\alpha 1(-)$ oocysts. Only during very early development (I-II), microtubules are visible and most likely representing left-over sMTs of the ookinete stage. Furthermore, SiR-tubulin plaques next to nuclei were occasionally seen during very early stages. $\alpha 1(-)$ oocysts were still able to multiply and align their nuclei to the plasma membrane (V, VI a,b), however, nuclei retained predominantly within the sporoblast during sporozoite budding (VI, VII). Shown are single images or maximum z-projections (WT: I, 7.6 μ m; III, 2 μ m in z-direction; $\alpha 1(-)$: III, 2 μ m in z-direction). Scale bars: 5 μ m.

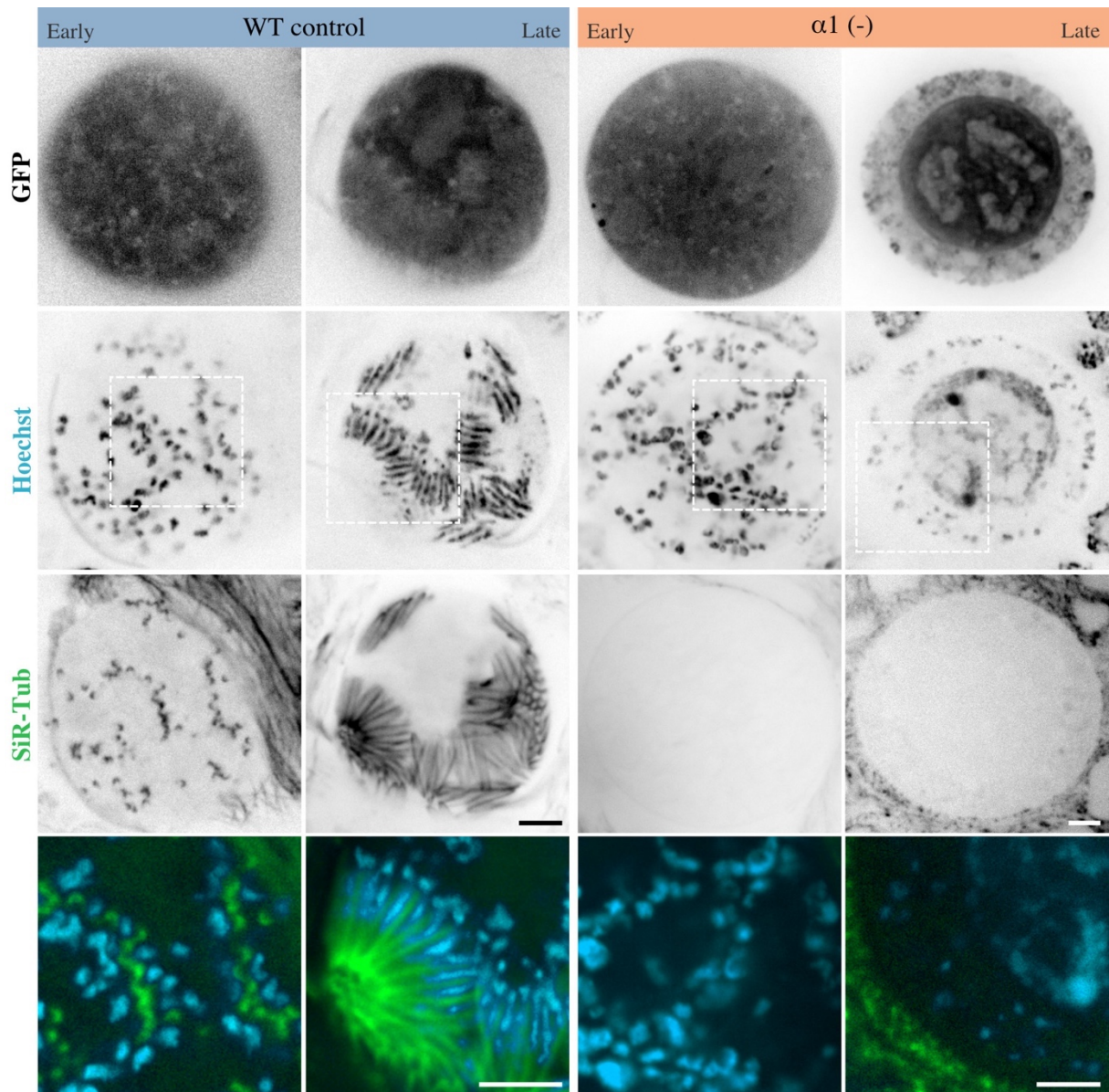


Figure 3.16. Nuclear shape and localization during sporogenesis in WT and $\alpha 1(-)$ oocysts. Early (10 days post feed) and late (12 days post feed) developing oocysts showed first, the nuclear alignment of nuclei (Hoechst, magenta) to the plasma membrane (not visible) and in case of late oocysts the pulling-in of the nuclei into the budding sporozoites. In contrast to WT, $\alpha 1(-)$ parasites managed to align nuclei, but the majority of nuclei were not pulled into the sporozoites and nuclei stayed round. Cytosolic GFP expressed from the *efla* promoter allocated the oocysts. SiR-tubulin (green) indicates microtubules. Scale bars: 5 μ m.

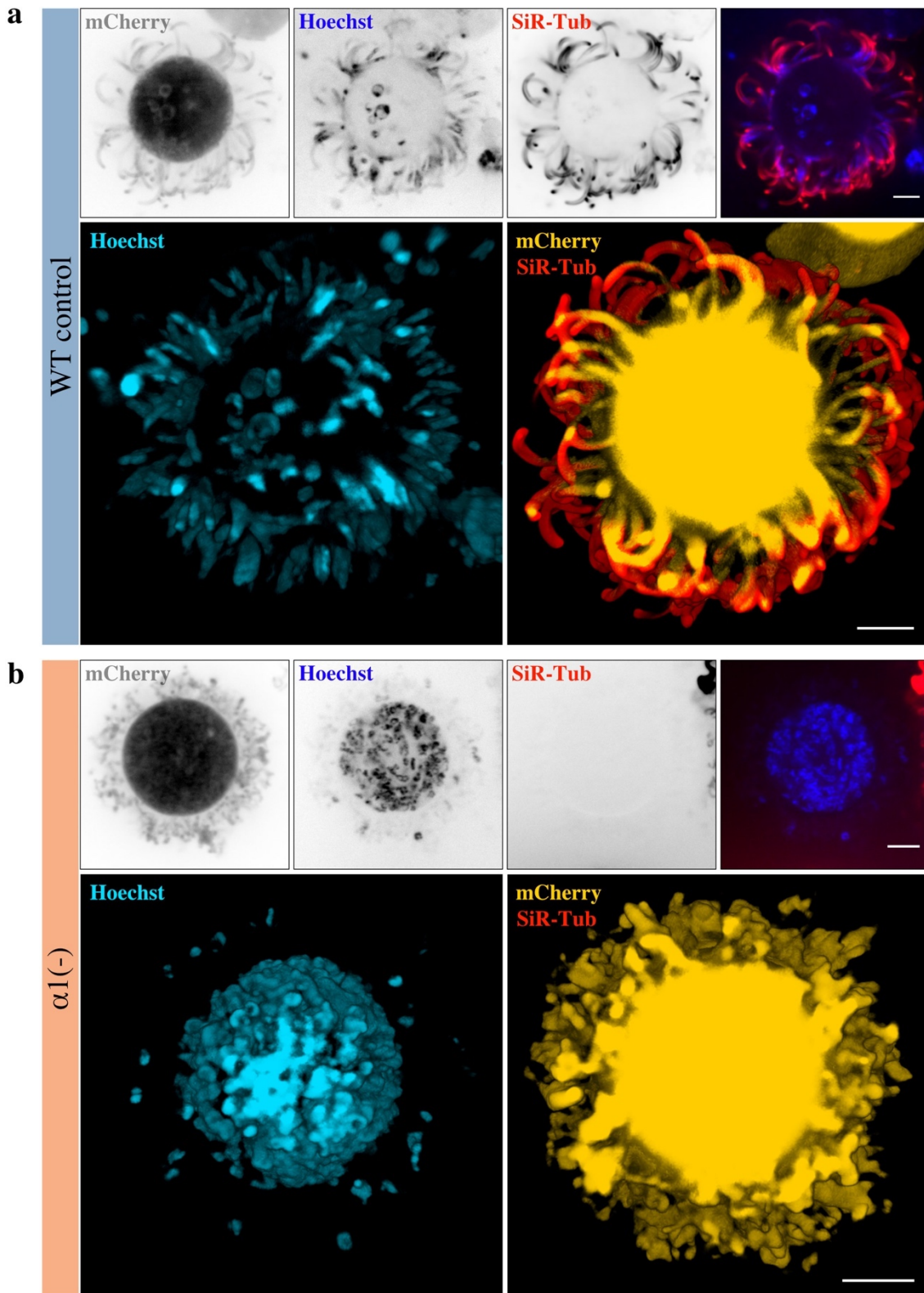


Figure 3.17. 3D reconstruction of sporoblasts with attached emerging sporozoites. Manually released sporoblasts are shown for WT (a) and $\alpha 1(-)$ (b) with attached emerging sporozoites. Cytoplasm is visualized in yellow (*cs-mCherry* expression), microtubules in red (SiR-tubulin labelling) and DNA in blue/cyan (Hoechst 33342 labelling). 3D reconstructions were rendered with Volocity 6.3 (3D Opacity) from z-stack images acquired with spinning disc confocal microscopy. On top of each 3D reconstruction, an example image from a selected plane is shown. 10 and 28 images with a z-distance of 1.5 μm and 1 μm were collated for WT and $\alpha 1(-)$ oocysts, respectively. Scale bars: 5 μm .

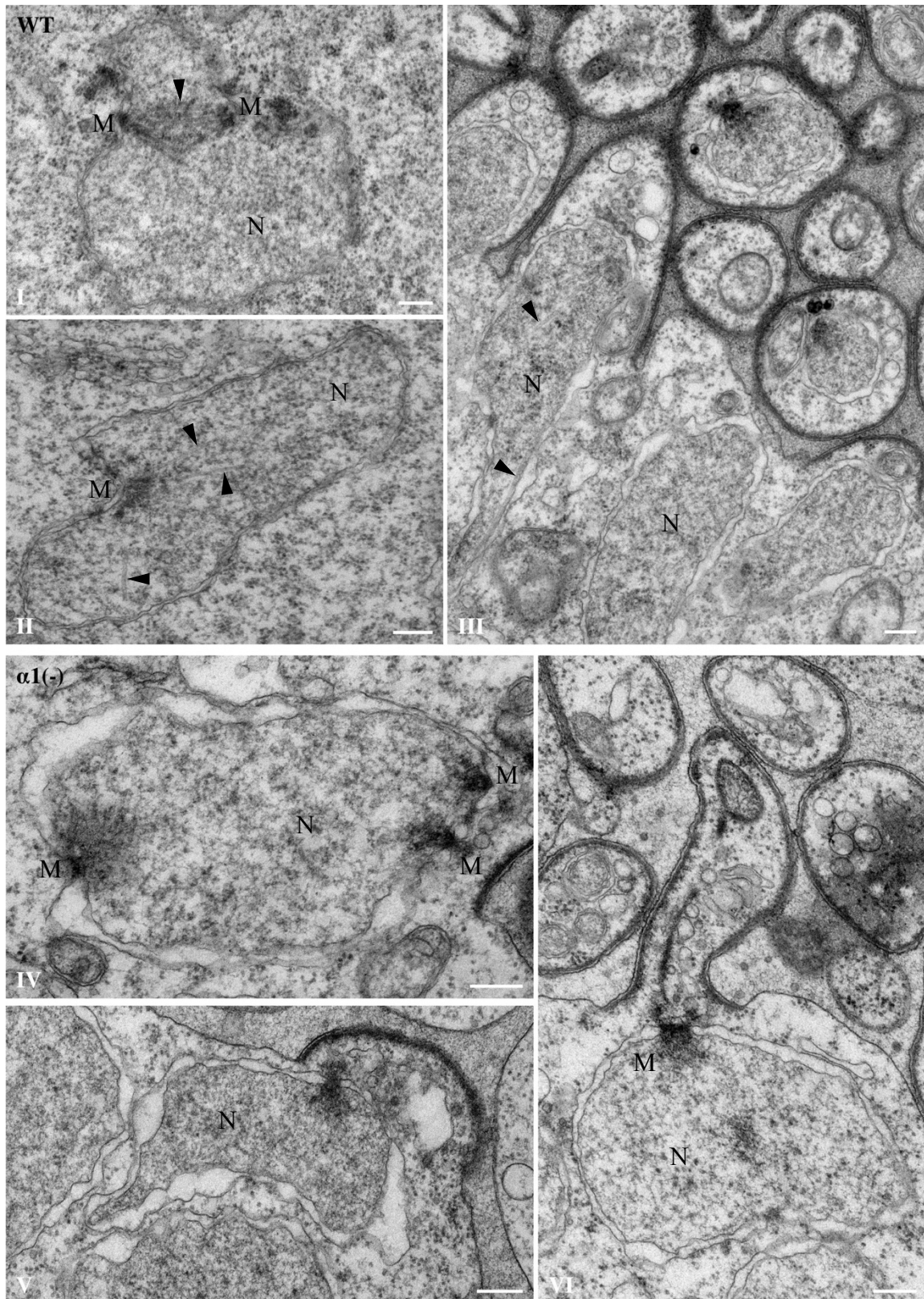


Figure 3.18. Hemispindle microtubules (hMTs) are absent in $\alpha 1(-)$ oocysts. During nuclear division and early sporozoite budding, hMTs (arrow heads) and microtubule organizing centers (MTOCs, M; also called spindle pole plaques) were seen in WT oocysts. Although, individual nuclei (N) and MTOCs were visible in $\alpha 1(-)$ oocysts, hMTs were absent. Transmission electron microscopy, 70 nm cuts. Scale bars: 0.2 μm .

3.3.4. Sporozoite budding is initiated and proceeds in *α1(-)* parasites which lack subpellicular and hemispindle microtubules resulting in aberrant sporozoites and life cycle arrest

As already partially described in the previous chapter, *α1(-)* parasites were capable to initiate sporozoite budding. In this chapter, I solely focus on sporozoite budding to dissect the impact of missing subpellicular microtubules (sMTs) on overall sporozoite integrity during early to late sporozoite development. In **Figure 3.19**, late developing oocysts are shown. For WT, longitudinal and cross sections of sporozoites were recognizable. Sporozoites can be identified by their inner membrane complex (IMC), only occurring within budding sporozoites but not at the sporoblast membrane. Furthermore, subpellicular or hemispindle microtubules attached to the IMC or located inside the nucleus, respectively, were visible in WT sporozoite cross sections (green arrow heads). Although *α1(-)* oocysts reached a very similar oocyst size, sporoblasts within oocysts were increased in late *α1(-)* oocysts (**Figure 3.19**, right). Sporozoites could also be identified in *α1(-)* oocysts via the IMC, but the overall structure of sporozoites was very malformed. Sporozoites contained numerous undefinable vesicular structures but no subpellicular or hemispindle microtubules.

Very early stages of sporozoite budding showed no obvious difference between WT and *α1(-)* oocysts besides missing hMTs when considering 2D images of transmission electron microscopy (TEM) (**Figure 3.20**, I & IV). However, 3D reconstructions from TEM serial sections revealed differences in the nuclei size and shape of nuclei (**Figure 3.21**). WT nuclei showed elongated nuclei with “spikes” facing towards the center of the sporoblast. Inside those “spikes”, hMTs were identified reaching all the way to the “spike” endings. In contrast to WT, *α1(-)* nuclei were missing hMTs and nuclei had a round shape. However, all analyzed early budding *α1(-)* sporozoites had a nucleus aligned to the sporoblast membrane.

Besides the nucleus shape, the early budding cone with its rhoptry (purple) and rootlet fiber (red) did not differ between WT and *α1(-)* sporozoites (**Figure 3.20**). Only after budding proceeded and sporozoites elongated, *α1(-)* sporozoites showed a bend (undular) formation instead of the straight shape observed in WT. The rootlet fiber was stretching from the apical end (possibly at the ring) to the spindle pole plaque in both lines. However, the nuclei were mostly not pulled inside the budding sporozoite but stayed within the sporoblast in *α1(-)* sporozoites. Micronemes (blue) were also missing in *α1(-)* sporozoites. Late budding WT sporozoites clearly showed sMTs (green) with elongated nuclei inside the sporozoites. *α1(-)* sporozoites did not contain any nucleus in most cases and were missing micronemes and microtubules. 3D reconstruction from TEM serial sections of very late (overaged) budding *α1(-)*

) sporozoites revealed a network of tubes and stacks connected at several sites to the sporoblast (**Figure 3.22**). Although we cannot fully exclude that sporozoites cannot bud off without microtubules, our 3D analysis showed that sporozoites in overaged oocysts (day 17 post blood meal) were still attached to the sporoblast. Furthermore, in many $\alpha I(-)$ oocysts, micronemes and other undefined vesicular structures were frequently seen inside the sporoblast whereas this phenomenon was only rarely seen for WT (**Figure 3.23**).

Overall, $\alpha I(-)$ infected mosquito midguts were as frequently infected as WT as shown in **Figure 3.12** and showed a very similar development early on (**Figure 3.24**, I, IV and **Figure 3.7**, III & VI) but abnormal development commenced when sporozoite budding started (II, III, V, VI). Apoptotic-looking oocysts (VII, VIII) were not seen more frequently in $\alpha I(-)$ than in WT and asynchronous development across oocysts (IX) appeared was similar to WT although I did not quantify this.

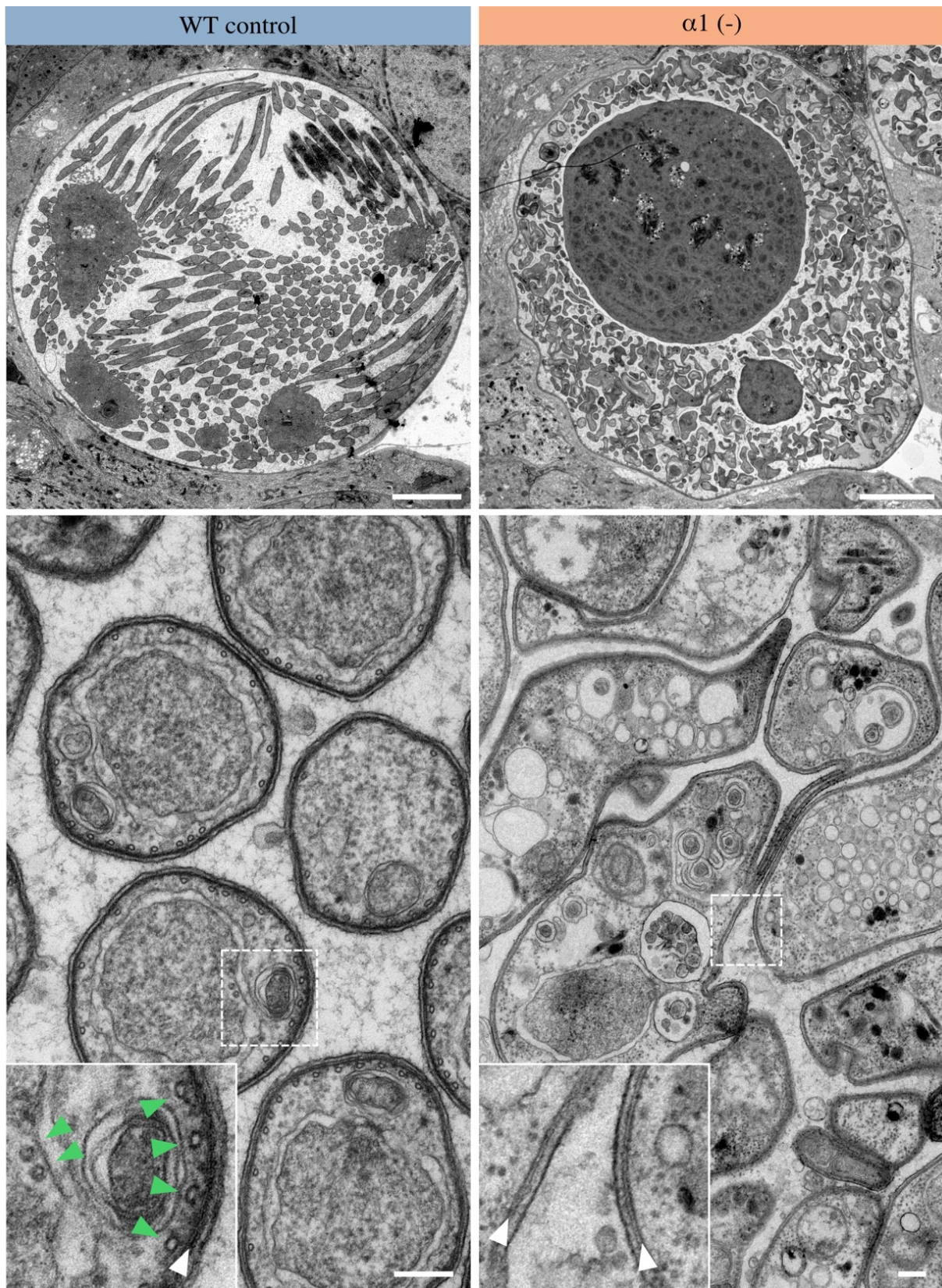


Figure 3.19. Transmission electron microscopy images of late WT and $\alpha 1(-)$ oocysts. (top) Overview of oocysts showing similarities in oocysts size and occurrence of differently sized sporoblasts as well as the malformed budding sporozoites in $\alpha 1(-)$ oocysts. (bottom) Detailed view of budding sporozoites showing size differences of sporozoites and malformations including many undefinable vesicles in the $\alpha 1(-)$ sporozoites. Close-up views show IMC (white arrow heads) and microtubules (green arrow heads). Slice thickness: 70 nm. Scale bars: top: 5 μm ; bottom: 0.2 μm .

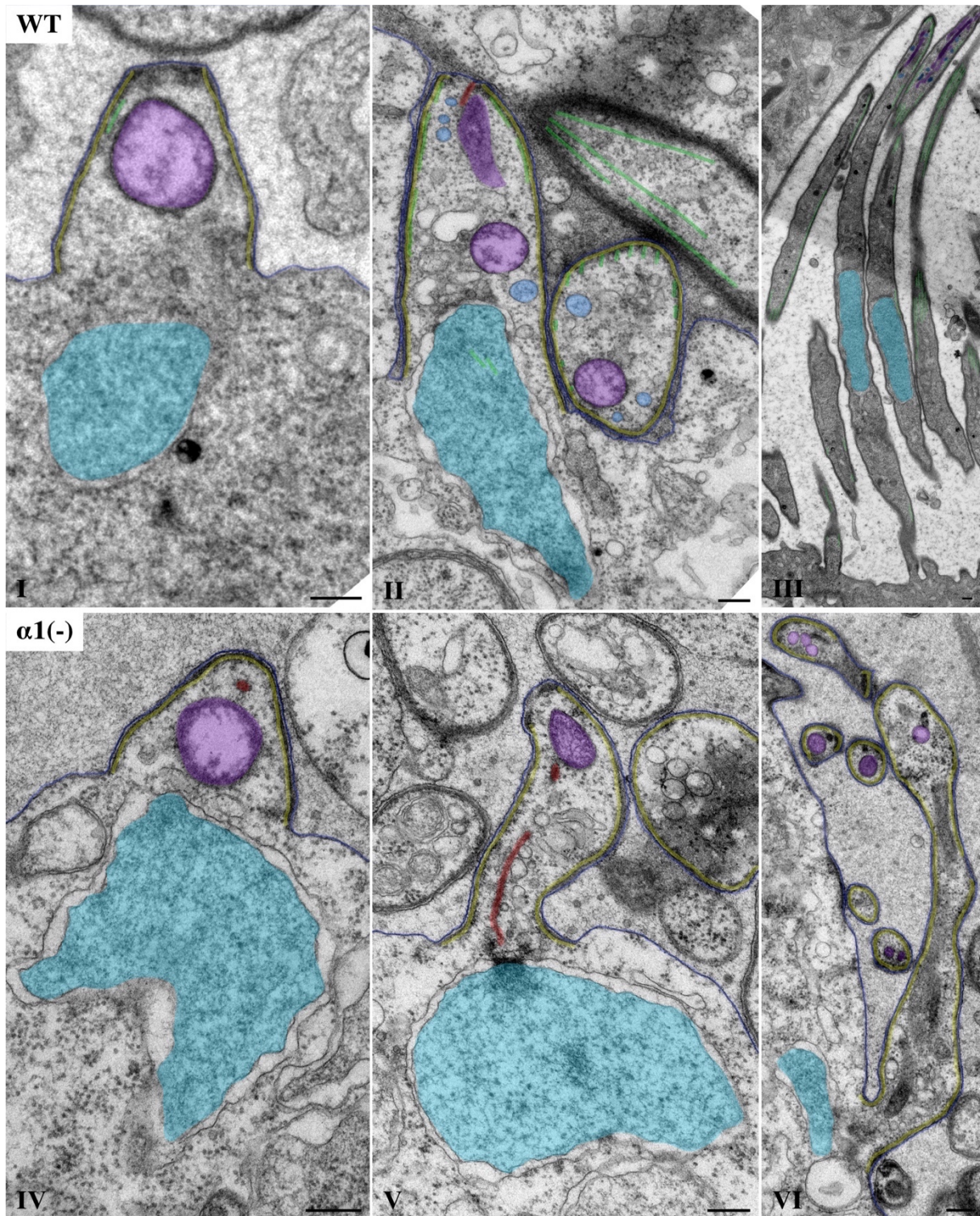


Figure 3.20. Sporozoite development of WT and $\alpha 1(-)$ parasite lines. Transmission electron micrographs of budding sporozoites. Early (I, IV), intermediate (II, V) and late sporozoite budding (III, VI) is shown. Note the missing hemispindle and sMTs (green), the nuclei (magenta) not pulled into the elongated sporozoites and the missing micronemes (blue) in $\alpha 1(-)$ sporozoites. The rootlet fiber (red) is seen in WT as well as $\alpha 1(-)$ intermediate budding sporozoites. Elongated $\alpha 1(-)$ sporozoites lose their straight shape and become wobbly and malformed. Slice thickness: 70 nm. Scale bars: 0.2 μm .

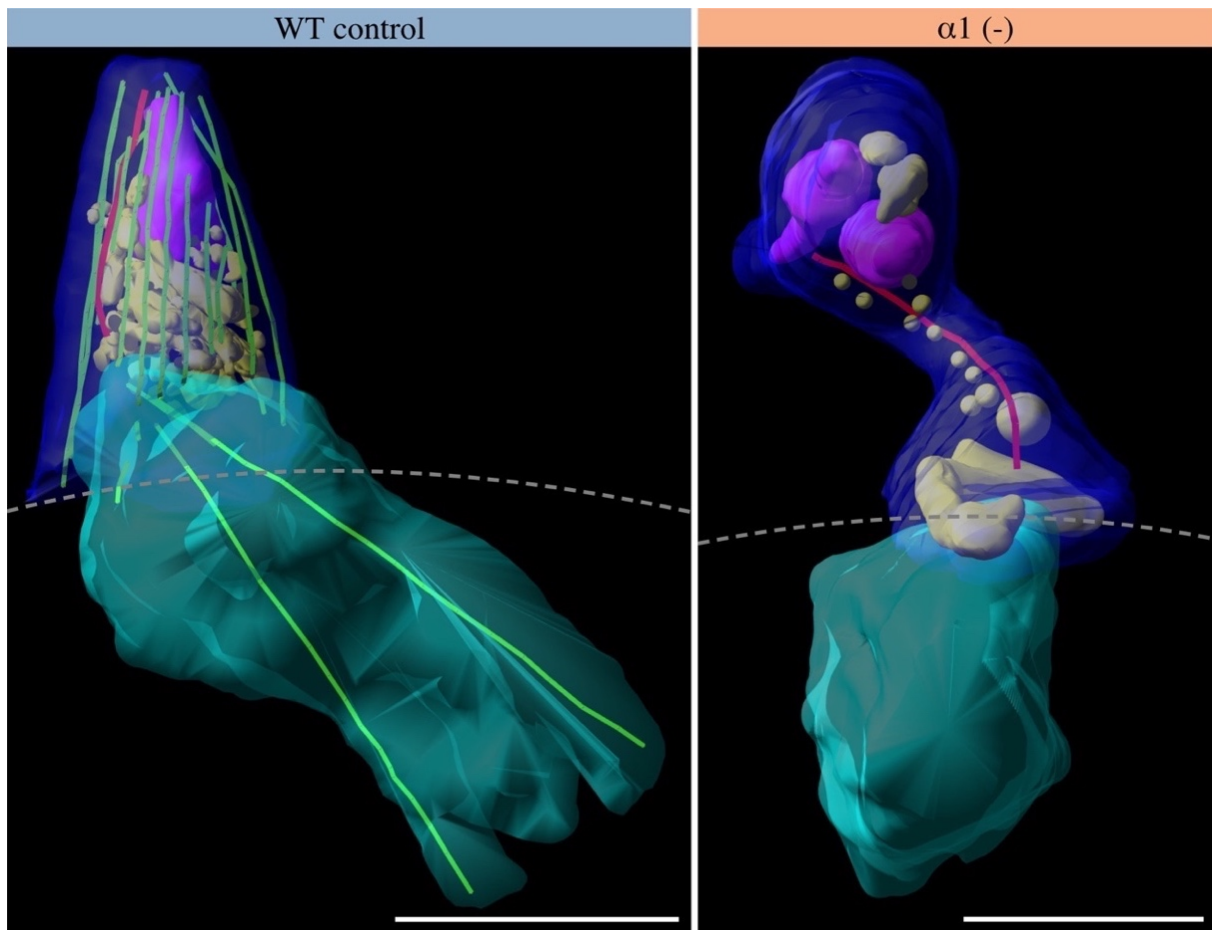


Figure 3.21 . 3D reconstructions from TEM serial sections of WT and $\alpha 1(-)$ early and late budding sporozoites. 3D reconstructions reveal that $\alpha 1(-)$ parasites fail to pull in nuclei and nuclei are missing “spike”-like nuclear elongations into the sporoblast. Furthermore, $\alpha 1(-)$ sporozoites show a wobbly shape. The dashed lines indicate the sporoblast membrane. 17 and 10 sections of 100 nm and 300 nm thickness were used to render the tomograms in WT and $\alpha 1(-)$ parasites, respectively. Samples were provided by me, images were taken by me, Marek Cyrklaff and Patrick Kübler and aligning and rendering the 3D reconstructions from the serial sections was performed by Patrick Kübler during his Bachelor thesis (Kübler, 2017). Rhoptries: purple; sporozoite plasma membrane and inner membrane complex (IMC): blue; microtubuli: green; endomembraneous vesicles: yellow; rootlet fiber: red; nucleus: cyan. Scale bars: 1 μm .

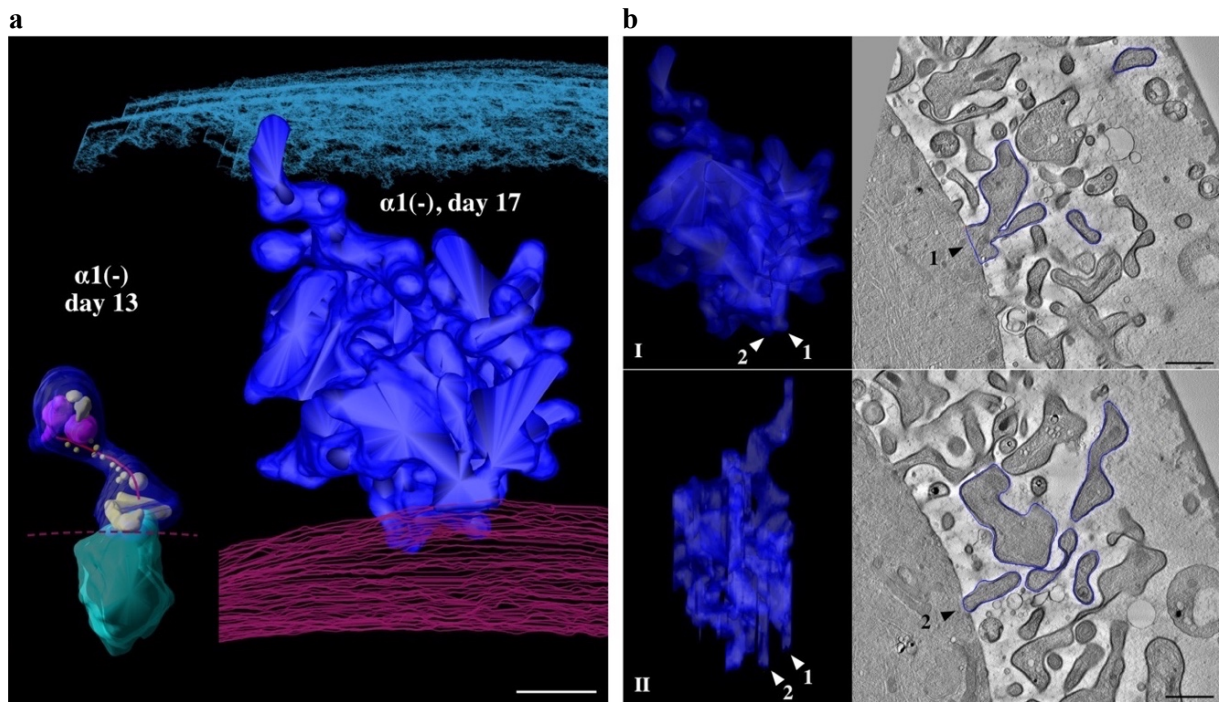


Figure 3.22. 3D reconstruction from TEM serial sections of a very late $\alpha 1(-)$ budding sporozoite. (a) 3D reconstructions reveal that very late $\alpha 1(-)$ sporozoites lose apical polarity, form a tubular network and are attached at several sites to the sporoblast (b). Samples were provided by me, images were taken by me, Marek Cyrklaff and Patrick Kübler and aligning and rendering the 3D reconstructions from the serial sections was performed by Patrick Kübler during his Bachelor thesis (Kübler, 2017). Scale bars: 1 μ m.

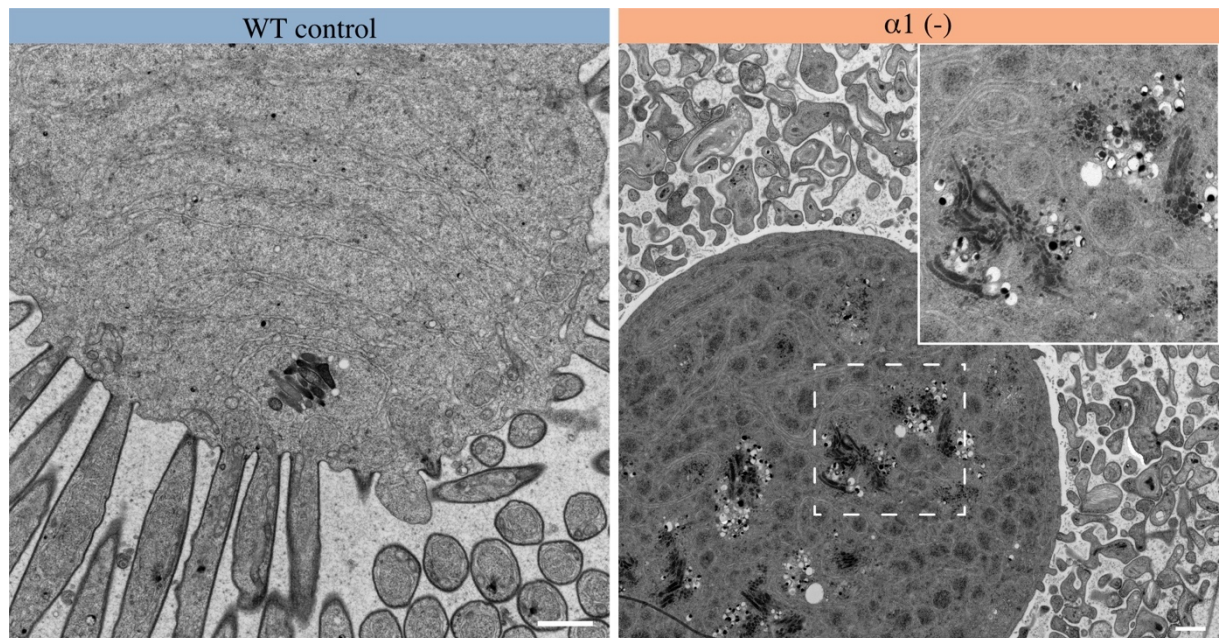
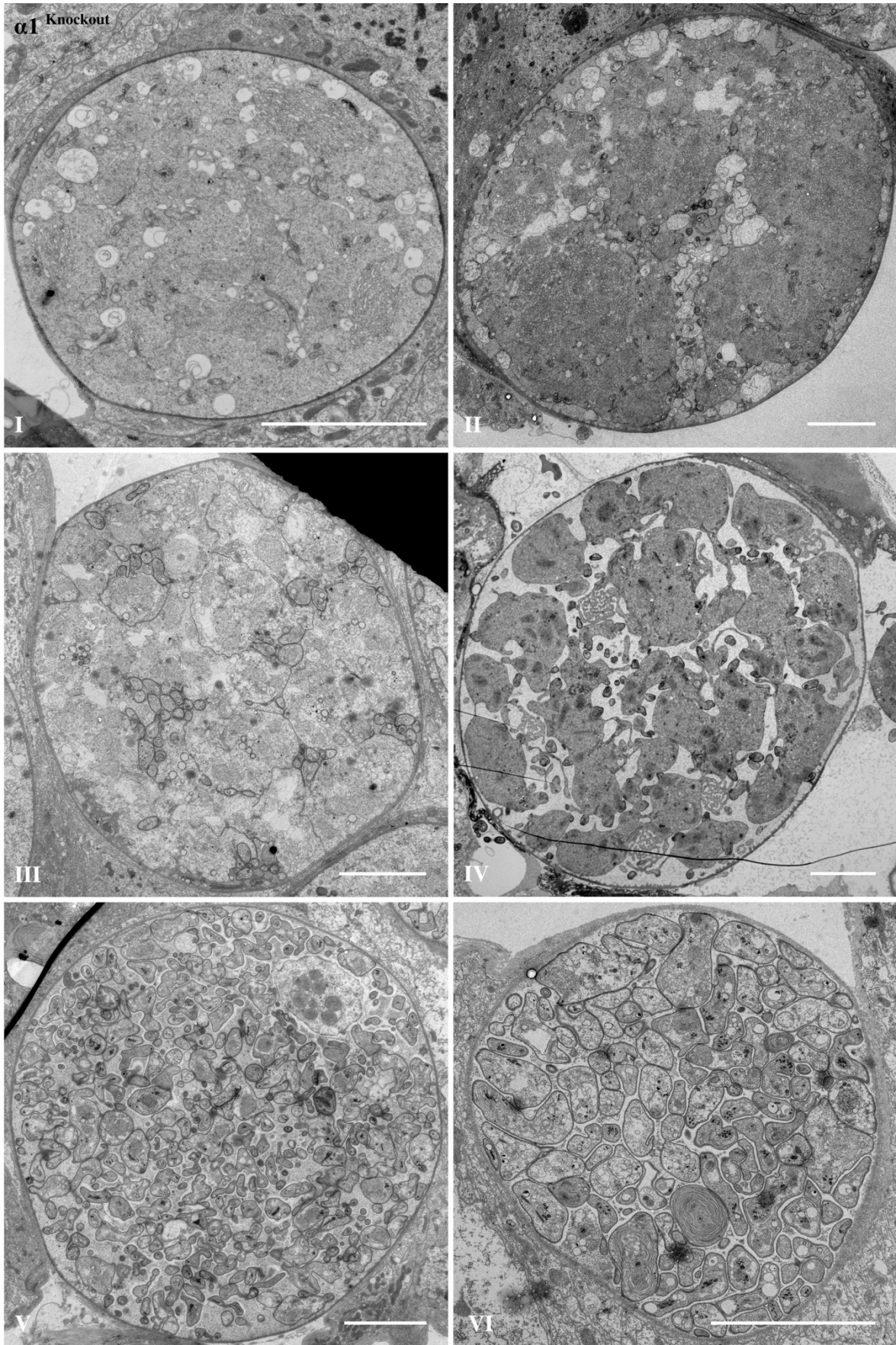


Figure 3.23. TEM images showing sporoblasts of late developed oocysts. In $\alpha 1(-)$ oocysts, increasing numbers of undefinable organelles and micronemes were found inside the sporoblast. The older the oocysts were, the more frequent this could be observed. For WT, this was only rarely seen. Representative pictures are shown. Slice thickness: 70 nm. Scale bars: 1 μ m.

Results



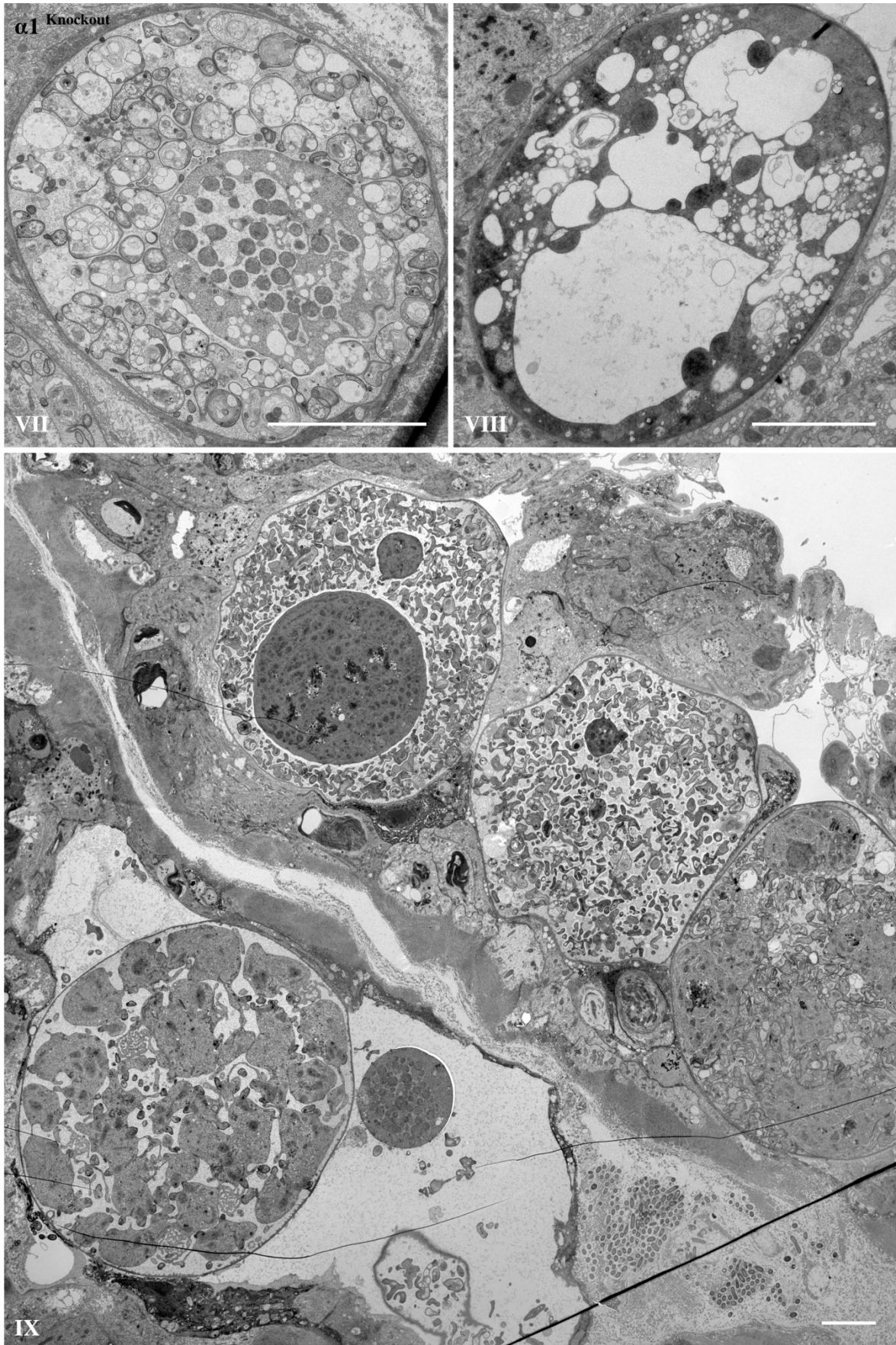


Figure 3.24. TEM images showing $\alpha I(-)$ oocysts from early to late oocyst development. Early development (I, IV) is very similar to WT (**Figure 3.7**, III & VI), but advanced sporozoite budding (II, III, V, VI) shows the abnormality of sporozoite formation in $\alpha I(-)$. (I) Nuclear replication; (II-IV) early sporozoite budding; (V, VI) late sporozoite budding; (VII, VIII) overaged and apoptotic-looking oocysts; (IX) overview of asynchronous oocyst development also seen for $\alpha I(-)$. Slice thickness: 70 nm. Scale bars: 5 μ m.

3.3.5. Complementation of $\alpha I(-)$ with wild-type αI -tubulin reverses the $\alpha I(-)$ phenotype

As described in chapter 3.1, we complemented the $\alpha I(-)$ parasite line with a WT αI -tubulin ORF. This line, called $\alpha I^{WTcompl.}$, did not show any phenotype, therefore, complementation restored the $\alpha I(-)$ phenotype completely (**Figure 3.25**). sMTs were visible during oocyst

	Parasite line	WT ANKA	WT ANKA (RG)	$\alpha I(-)$	WT compl.
Midgut sporozoites	Sporozoites / mosquito (n)	93,000 (42)	97,800 (39)	0 (70)	88,000 (64)
	N° of apical subpellicular microtubules (n)	16 (lit.)	16 (11)	0 (35)	16 (23)
	Sporozoite morphology	+++	+++	n.a.	+++
Salivary gland sporozoites	Sporozoites / mosquito (n)	19,100 (38)	20,400 (34)	0 (67)	20,600 (61)
	Salivary gland invasion ratio	0.21	0.21	n.a.	0.23
	Infected mice by 10 mosquito bites / total mice (prepatency)	n.d.	8/8 (4.3)	n.a.	7/8 (3.9)
	Infected mice by 10.000 sporozoites injected i.v. / total mice (prepatency)	n.d.	8/8 (3.9)	n.a.	11/12 (3.7)

Figure 3.25. Complementation of the $\alpha I(-)$ parasite line with wild-type $Pb \alpha I$ -tubulin. Quantifications (sporozoite numbers, sMT numbers, infectivity) of the $\alpha I^{WTcompl.}$ parasite line revealed no difference to WT ANKA or WT ANKA (RG) parasites.

development (**Figure 3.26**) and $\alpha I^{WTcompl.}$ sporozoites did not show any malformations as seen for $\alpha I(-)$ sporozoites. The characteristic SiR-tubulin signal (subpellicular microtubules) was restored at the apical side of hemispindle and salivary gland sporozoites (**Figure 3.27**). Quantification of sporozoite numbers revealed, that the complementation restored sporozoite numbers. Further, a median of 16 sMTs was found. Furthermore, infectivity assessed either by intravenous (*i.v.*) injections or by mosquito bite showed no difference to WT.

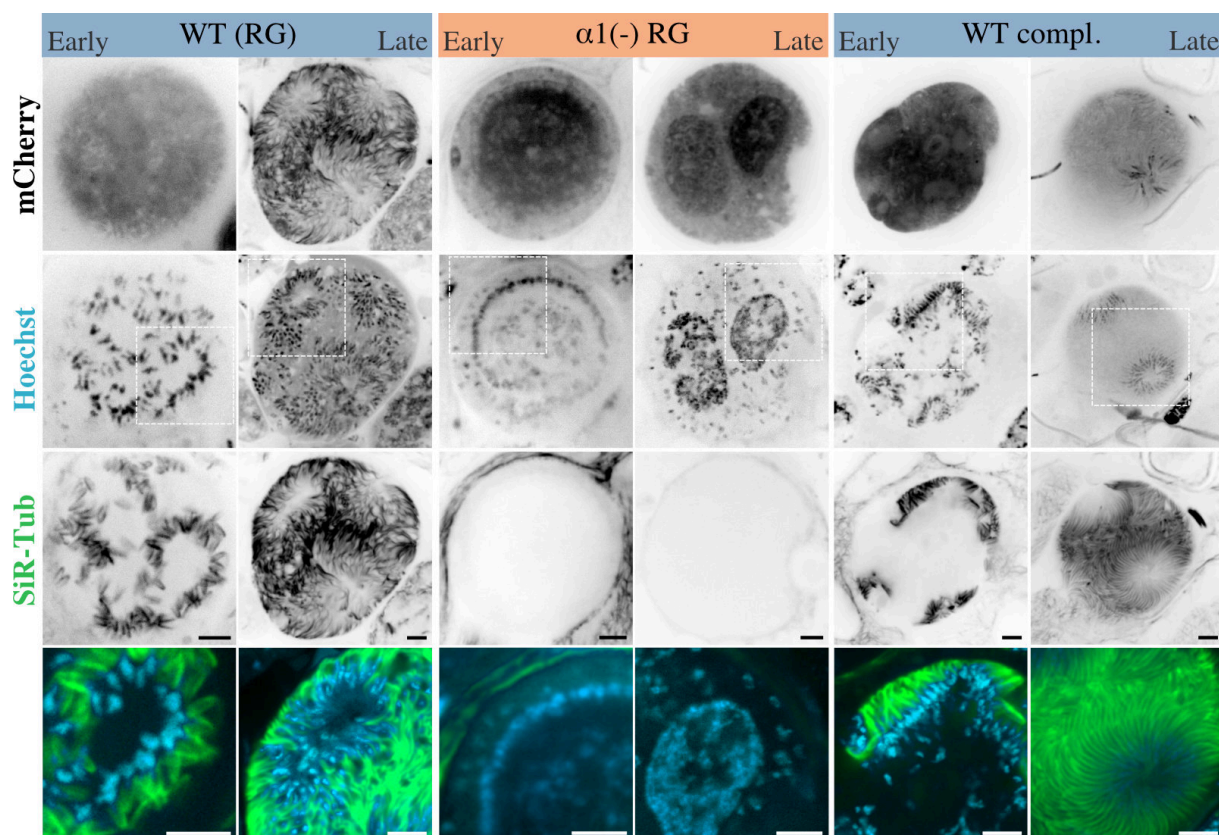


Figure 3.26. $\alpha 1^{WTcompl.}$ oocyst development reveals no difference to wild type (RG) parasites. Microtubule (SiR-tubulin stain, green) formation and nuclei shape (Hoechst, magenta) are restored in $\alpha 1^{WTcompl.}$ parasites during oocyst development. Scale bars indicate 5 μm .

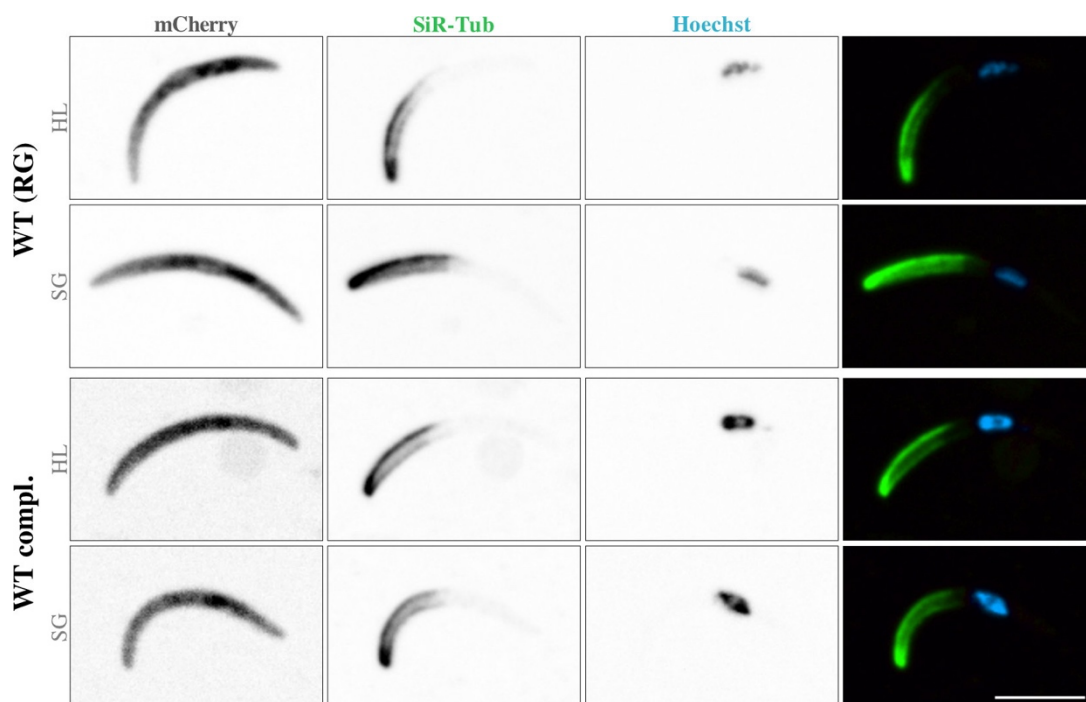


Figure 3.27. $\alpha 1^{WTcompl.}$ sporozoites show no malformations. $\alpha 1^{WTcompl.}$ hemolymph (HL) and salivary gland (SG) sporozoites do not show any malformations and reveal the characteristic SiR-tubulin stain at the apical side of the sporozoite. Scale bar indicates 5 μm .

3.4. Reduced expression of *α1-tubulin* leads to fewer subpellicular microtubules and aberrantly formed sporozoites

3.4.1. *α1-tubulin* expression can be reduced by deletion of introns and by codon modification of exons

Nucleation of microtubules is dependent on the $\alpha\beta$ -tubulin-heterodimer concentration as shown in *in vitro* studies (Kuchnir Fygenon et al., 1995; Flyvbjerg, Jobs, and Leibler, 1996). I therefore speculated, that a modulation of gene expression and subsequent changes in the α -tubulin protein concentrations could change the number of sMTs in sporozoites. *Plasmodium* has only one β -tubulin but two α -tubulins. The *α1-tubulin* deletion described previously revealed the importance of *α1-tubulin* for sMT and proper sporozoite development. Further, the qRT-PCR data showed that *α2-tubulin* is 100-fold less expressed than *α1-tubulin* during oocyst development. This supported the assumption, that *α2-tubulin* plays no or maybe only a minor role during sporozoite formation. Consequently, I choose to modify the *α1-tubulin* gene locus for expression level tuning. Two different parasite lines were generated with modifications on the *α1-tubulin* gene locus, which potentially disturb gene regulation and expression levels, a parasite line missing *α1-tubulin* introns ($\alpha1^{\Delta introns}$) and a parasite line missing introns combined with a codon modification of the exons ($\alpha1^{cm\&\Delta introns}$) (further described in chapter 3.1). Both

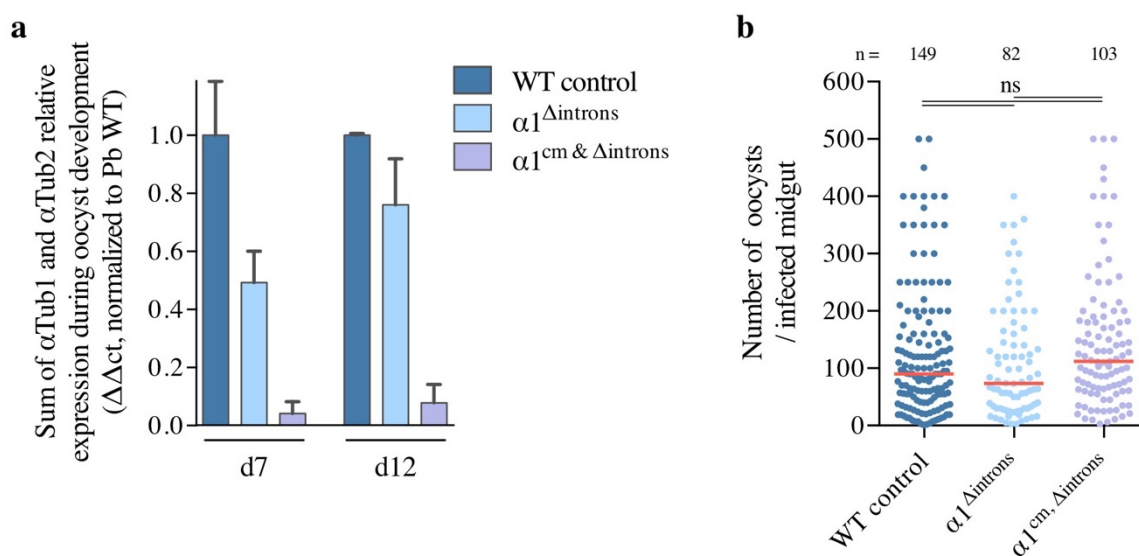


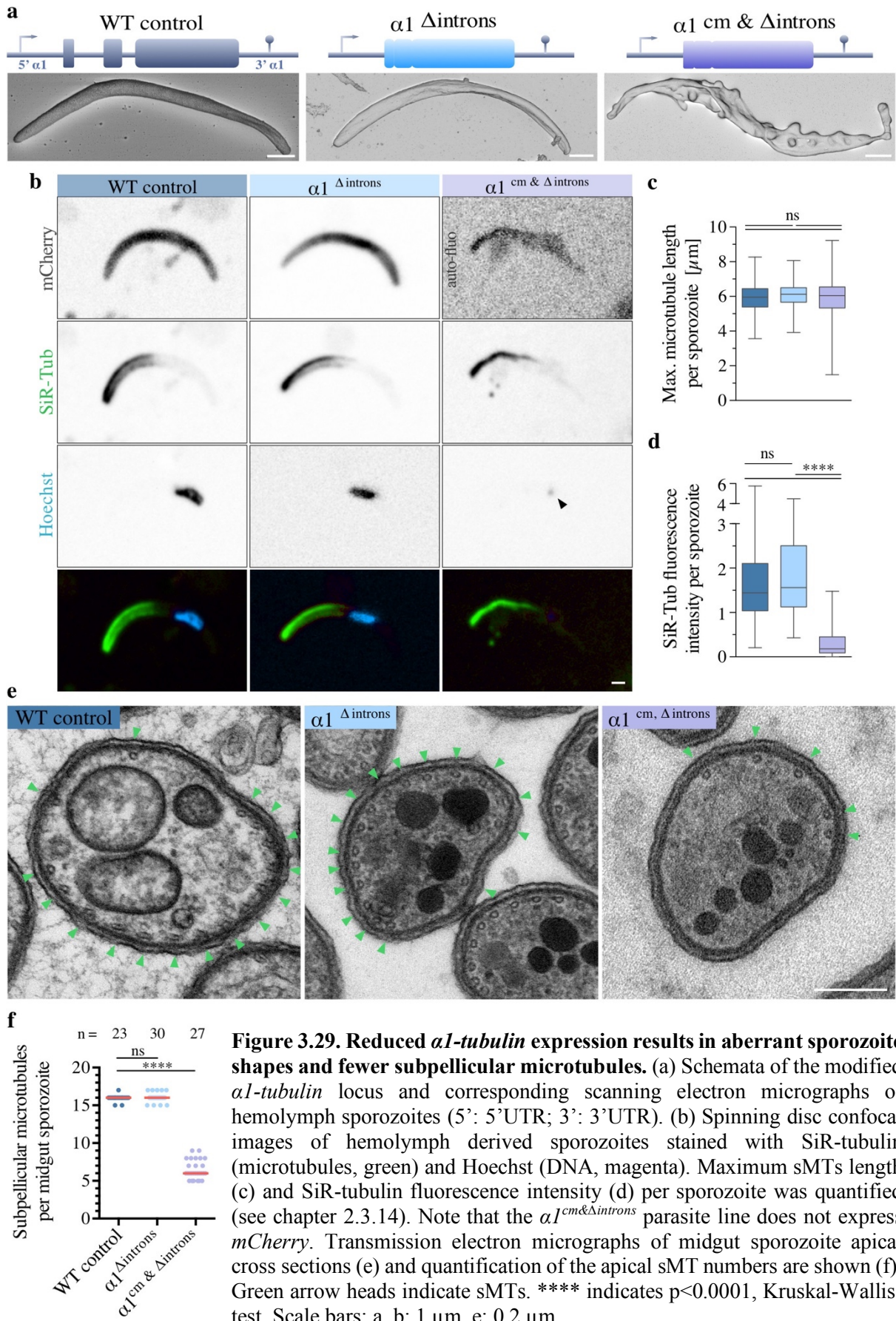
Figure 3.28. Modifications of the *α1-tubulin* gene locus results in expression level changes. (a) Relative expression was determined by quantitative real-time PCR by using the $\Delta\Delta ct$ method and normalization to 18S rRNA. Across-run variances were normalized by using a calibrator sample. $\alpha1^{\Delta introns}$ parasite line: deletion of the *α1*-introns; $\alpha1^{cm\&\Delta introns}$ parasite line: deletion of the *α1*-introns and codon modification of the exons. Data shows two biological replicates. (b) Oocyst numbers were not influenced by *α1-tubulin* modifications. Statistics were analyzed using a Kruskal-Wallis-test.

parasite lines showed reduced levels of expression during early oocyst development (d7, nuclear replication), but during late oocyst development (d12, sporozoite budding) only $\alpha I^{cm\&\Delta introns}$ showed a significant reduction in expression of about 20-fold compared to WT (**Figure 3.28**, a). Changes in expression levels had no significant impact on oocyst numbers (b).

3.4.2. Reduced αI -tubulin expression leads to malformed sporozoites with fewer subpellicular microtubules, variable sporozoite thickness and nuclei size

Reduced αI -tubulin expression levels had a strong impact on sporozoite morphology. Hemolymph $\alpha I^{cm\&\Delta introns}$ sporozoites were highly aberrant, showed undefinable extrusions and lost their typical crescent shape whereas $\alpha I^{\Delta introns}$ parasites did not show any morphological difference to WT (**Figure 3.29** a; gallery: **Figure 3.32**). Spinning disc confocal images revealed that $\alpha I^{cm\&\Delta introns}$ hemolymph sporozoites often only contained a faint nuclear stain (b) or two separated nuclei (gallery: **Figure 3.31**). Furthermore, quantification of the SiR-tubulin signal showed that malformed sporozoites had similar sMT maximum lengths (c) but a reduced SiR-tubulin fluorescence intensity (d). Strikingly, transmission electron micrographs of sporozoite cross sections revealed a reduced number of apical sMTs from 16 in WT and $\alpha I^{\Delta introns}$ to about 6 in $\alpha I^{cm\&\Delta introns}$ (**Figure 3.29** e, f; gallery: **Figure 3.33**). Overview oocyst images of the $\alpha I^{\Delta introns}$ parasite line showed no phenotype (**Figure 3.34**; I, II) but $\alpha I^{cm\&\Delta introns}$ (**Figure 3.34** IV, V, VI) oocysts depicted size differences in sporozoite diameter. Quantification for midgut sporozoites revealed an overall sporozoite diameter decrease in $\alpha I^{cm\&\Delta introns}$ parasites (**Figure 3.30** a). Differentiating between apical cross sections and nucleus cross sections showed a reduced diameter for apical and an increased diameter for nuclear cross sections in $\alpha I^{cm\&\Delta introns}$ parasites compared to WT (**Figure 3.30** b, c).

Results



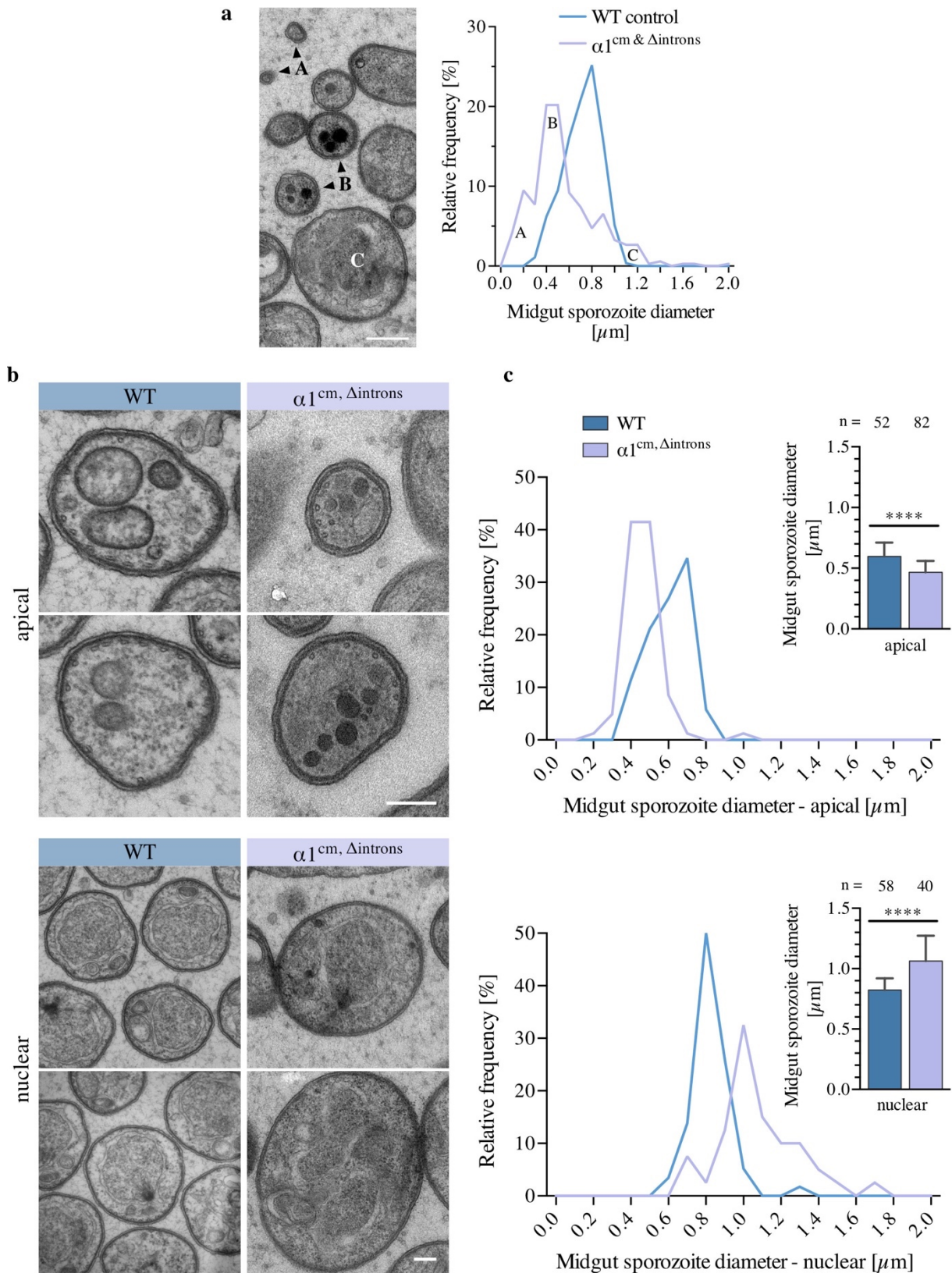
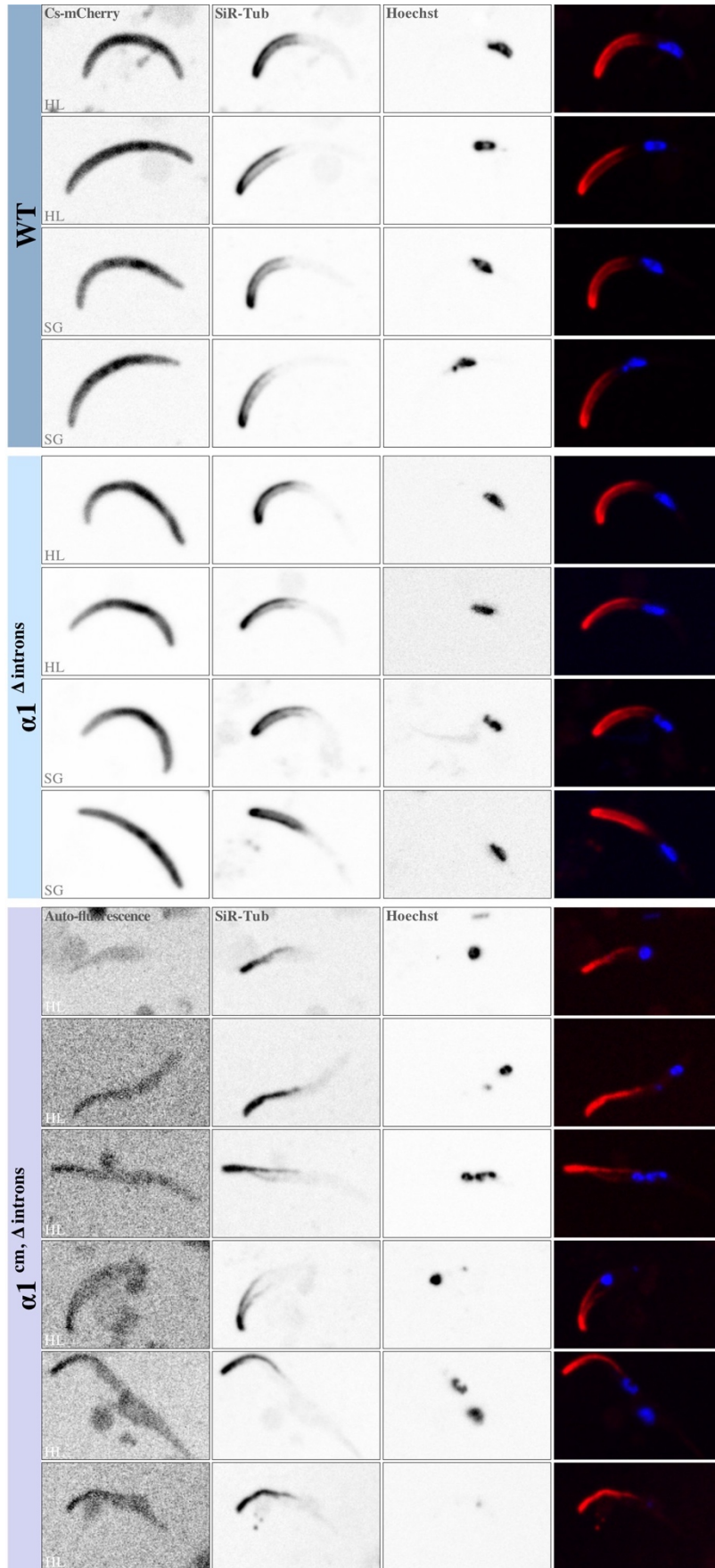


Figure 3.30. Sporozoites with fewer subpellicular microtubules show a greater variance in sporozoite diameter. (a) Sporozoite diameter is defined by the organelle located inside $\alpha 1^{\text{cm}} \Delta \text{introns}$ sporozoites. TEM image and quantification: A: undefined cut (no organelle); B: apical cut (rhoptries); C: nuclear cut (nucleus). (b) TEM images showing apical and nuclear sporozoite cross sections. (c) Quantification of apical and nuclear sporozoite thicknesses. $\alpha 1^{\text{cm}} \Delta \text{introns}$ sporozoites are less capable of keeping the optimal sporozoite diameter of $0,7 \mu\text{m}$. **** indicates $p < 0.0001$, Kruskal-Wallis-test. Scale bars: $0.2 \mu\text{m}$

Results



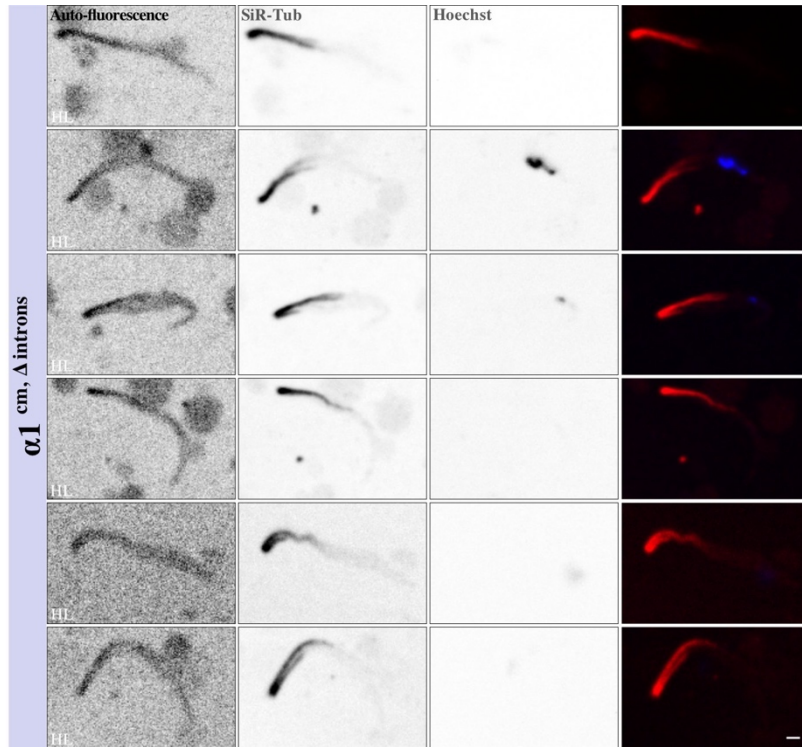


Figure 3.31. Fluorescence image gallery of *WT*, $\alpha 1^{\Delta introns}$ and $\alpha 1^{cm \& \Delta introns}$ sporozoites. Spinning disc confocal images of hemolymph (HL) and salivary gland (SG) sporozoites were stained with SiR-tubulin (microtubules, red) and Hoechst (DNA, blue). The cytoplasmic shape is identified by the *mCherry* expression in case of *WT* or $\alpha 1^{\Delta introns}$ parasites or by auto-fluorescence in case of $\alpha 1^{cm \& \Delta introns}$ parasites. Scale bars: 1 μ m.

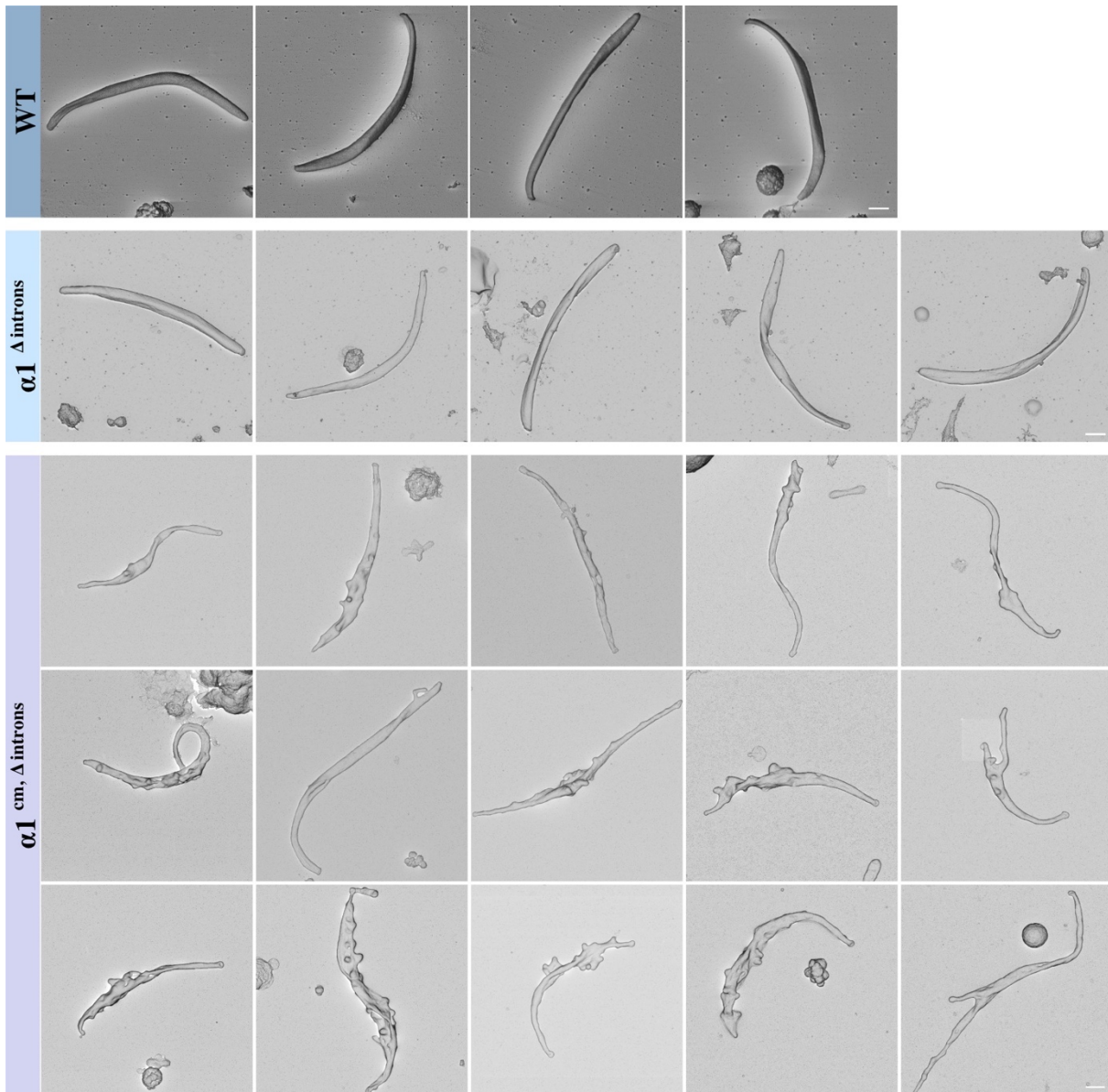


Figure 3.32. Scanning electron micrograph gallery of *WT*, $\alpha 1^{\Delta introns}$ and $\alpha 1^{cm \& \Delta introns}$ hemolymph sporozoites. Sporozoites with reduced numbers of sMTs ($\alpha 1^{cm \& \Delta introns}$) show strong malformations. Scale bars: 1 μ m.

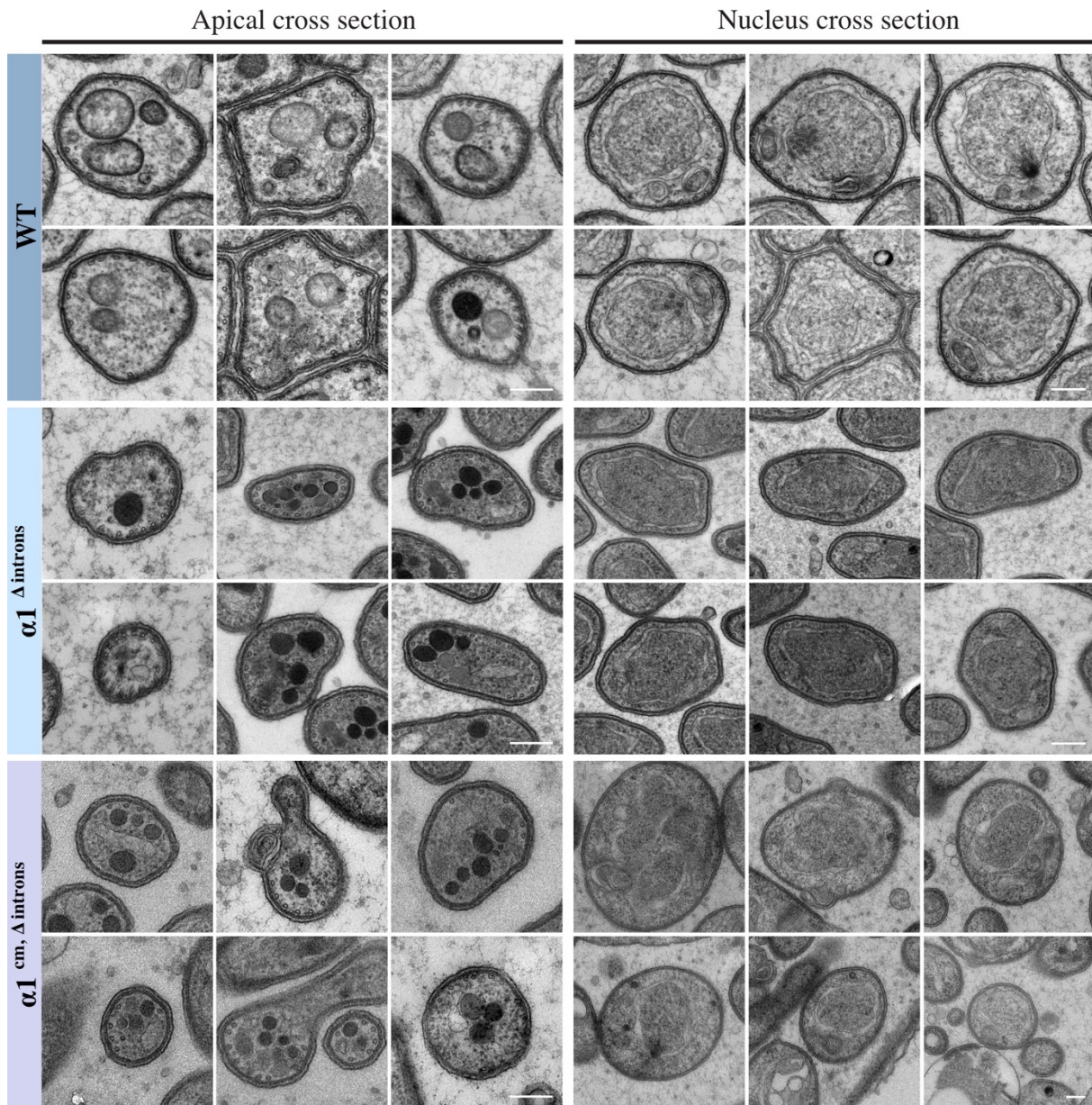


Figure 3.33. TEM gallery of *WT*, $\alpha 1^{\Delta introns}$ and $\alpha 1^{cm, \Delta introns}$ midgut sporozoites. Apical and nuclear cross sections of midgut sporozoites are shown. Slice thickness: 70 nm. Scale bars: 0.2 μm .

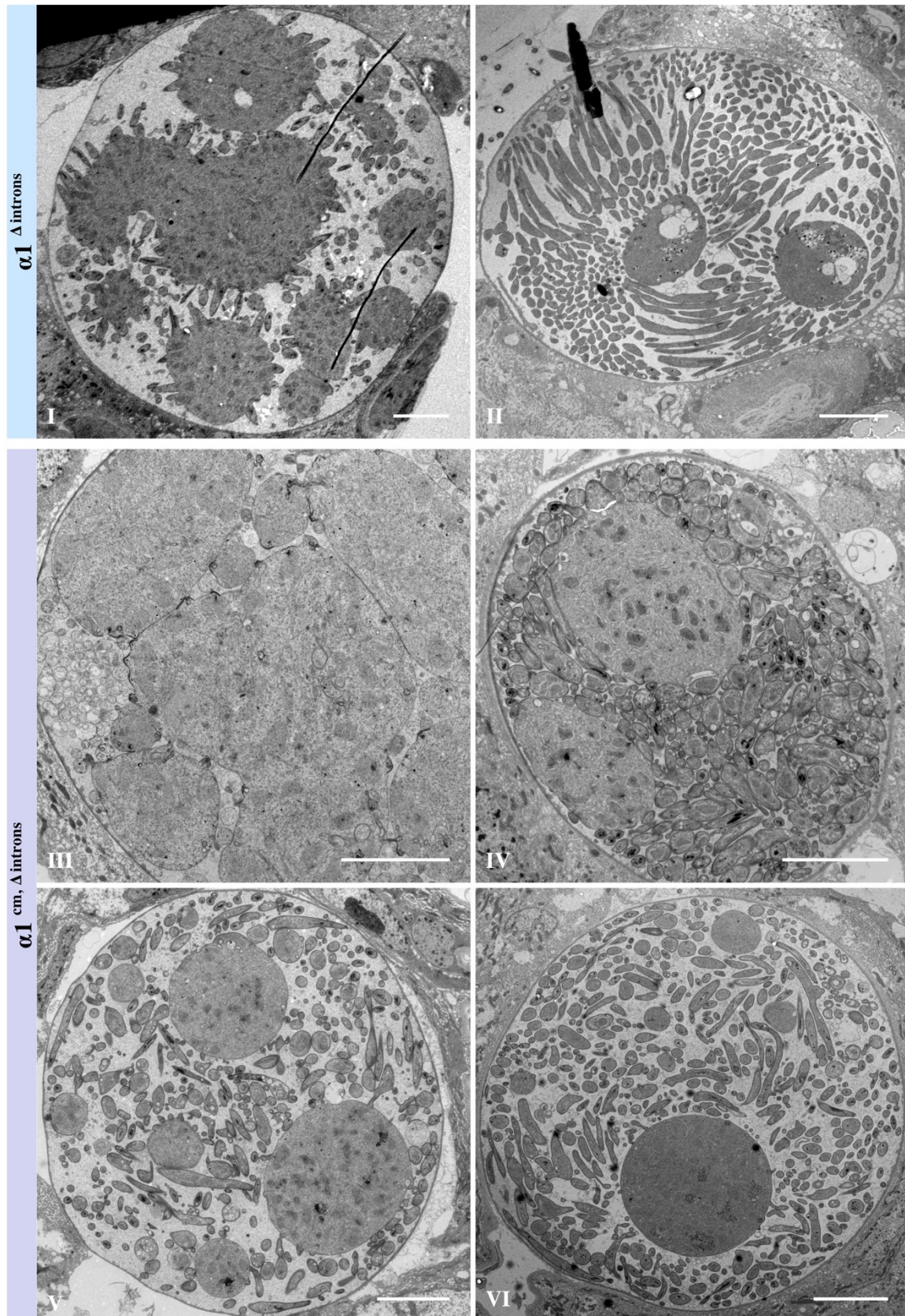


Figure 3.34. TEM images showing $\alpha 1^{\Delta introns}$ and $\alpha 1^{cm\&\Delta introns}$ early and late oocyst development. (I, III) Early sporozoite budding; (II, IV, V, VI) late sporozoite budding. Early development is very similar to WT (Figure 3.7, III & VI), but advanced sporozoite budding shows the abnormality of sporozoite formation in $\alpha 1^{cm\&\Delta introns}$ oocysts (IV, V, VI). Slice thickness: 70 nm. Scale bars: 5 μ m.

3.5. Specific α -tubulin amino acids define microtubule length whereas α -tubulin expression levels mediate microtubule numbers

$\alpha 1$ -tubulin and $\alpha 2$ -tubulin show 95% sequence identity with only few differences other than leucine to isoleucine changes (**Figure 1.8**). However, it could be shown, that tubulin isotypes can still have specific functions (Banerjee et al., 1990; Hoyle and Raff, 1990; Matthews, Rees, and Kaufman, 1993). To address functional differences between the two isotypes, we generated four different parasite lines where we exchanged or modified the introns, exons and 3'UTR of the $\alpha 1$ -tubulin gene either entirely or partially with corresponding $\alpha 2$ -tubulin elements (see chapter 3.1). All modifications were performed at the $\alpha 1$ -tubulin gene locus, meaning, all chimeras were regulated under the endogenous $\alpha 1$ -tubulin promoter. I designed several parasite lines expressing $\alpha 2$ -tubulin by either modifying $\alpha 1$ -tubulin by only minimal necessary point mutations such that an $\alpha 2$ -tubulin protein results (not considering leucine to isoleucine changes; $\alpha 2^+$) or by replacing the $\alpha 1$ -tubulin exons with $\alpha 2$ -tubulin exons ($\alpha 2^{++}$) or by replacing the entire ORF and 3'UTR of $\alpha 1$ -tubulin with the corresponding $\alpha 2$ -tubulin elements (see chapter 3.1 for detailed parasite generation). The parasite lines $\alpha 2^+$ and $\alpha 2^{++}$ were generated under my supervision by the Master students Claudia Di Biagio and Hannah Fleckenstein, respectively. Finally, I generated a parasite line only truncated at the $\alpha 1$ -tubulin C-terminus by its 3 additional amino acids ($\alpha 1^{\Delta c-term}$) therefore representing a $\alpha 2$ -tubulin C-terminus.

3.5.1. Introduction of $\alpha 2$ -tubulin elements does not affect oocyst numbers

Introduction of $\alpha 2$ -tubulin does not impair oocyst numbers (**Figure 3.35**) which is in line with the previous findings for $\alpha 1(-)$ and $\alpha 1^{cm\&\Delta introns}$ parasites (**Figure 3.12**, **Figure 3.28**).

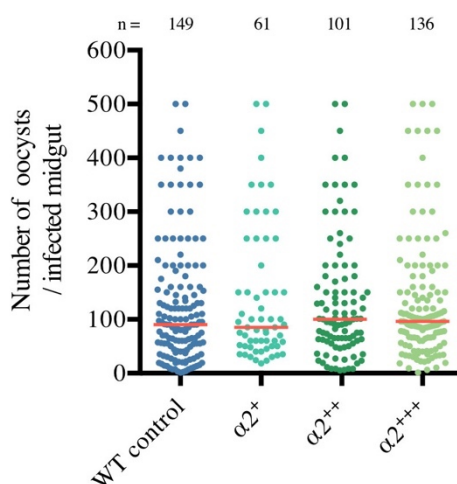


Figure 3.35. Oocyst numbers per infected mosquito midgut. No significant difference was found across different chimeras. Kruskal-Wallis test.

3.5.2. Complementation of the $\alpha 1(-)$ strain by a set of $\alpha 2$ -tubulin constructs results in grading aberrant sporozoites with less and shorter subpellicular microtubules

$\alpha 2$ -tubulin chimeras showed a set of gradient phenotypes. SEM images revealed that the introduction of $\alpha 2$ -tubulin regulatory DNA elements had a vast impact on sporozoite morphology (**Figure 3.36 a**). For instance, $\alpha 2^{++}$ and $\alpha 2^{+++}$ parasite lines both expressing wild-type $\alpha 2$ -tubulin and only differing by their introns and 3'UTRs show tremendous differences in sporozoite morphology (gallery: **Figure 3.38**). Turning $\alpha 1$ -tubulin into $\alpha 2$ -tubulin by minimal point mutations necessary (not considering leucine to isoleucine differences, $\alpha 2^+$) did not lead to any extrusions as seen occasionally for $\alpha 2^{++}$ and often for $\alpha 2^{+++}$ (SEM gallery: **Figure 3.38**) but to a reduced sporozoite length (quantified and described in detail in chapter 3.6.4). Only the truncation of the $\alpha 1$ -tubulin C-terminus had no impact on overall sporozoite morphology.

To understand the fundamental reasons leading to those phenotypes, I performed fluorescent assays to address sMT maximum length and microtubule amounts, qRT-PCR to indirectly estimate α -tubulin protein amounts via RNA levels and transmission electron microscopy to assess potential changes in the highly regulated number of sMTs. Analysis of sporozoite sMTs via spinning disc confocal images (gallery: **Figure 3.37**) revealed a general shortening of sMTs in case of $\alpha 2$ -tubulin expressing parasites (**Figure 3.36 b**). Additionally, the fluorescence intensity of the SiR-tubulin stain (representing microtubule amounts) was reduced even in the parasite line $\alpha 1^{\Delta c-term}$ (c). qRT-PCR analysis revealed an overall reduction of α -tubulin expression and the two lines showing extrusions ($\alpha 2^{++}$, $\alpha 2^{+++}$) had the lowest expression across all lines on day 12 when sporozoite budding is occurring (d). Sporozoite cross sections revealed a reduction in sMTs. While $\alpha 1^{\Delta c-term}$ and $\alpha 2^+$ sporozoites did not show any reduction in microtubule numbers, $\alpha 2^{++}$ and $\alpha 2^{+++}$ had only a median of 11 or 9 sMTs per sporozoite, respectively (e, f). Due to the indication that not all sMTs might reach the maximum length which arises when comparing the maximum length and number of sMTs with the SiR-tubulin fluorescence intensity, I tried to indirectly assess the individual sMT length by counting sMT numbers at different sporozoite cross sections - at apical, central or nuclear positions (**Figure 3.36 g, h, i**; gallery: **Figure 3.39**). This revealed that the number of sMTs did not drop for WT sporozoites when counting at central or nuclear cuts, however, in case of $\alpha 1^{\Delta c-term}$ as well as $\alpha 2^+$ sporozoites, sMTs numbers dropped. This means, that not all sMTs reach the maximum length in those two parasite lines.

$\alpha 1^{\Delta c-term}$ as well as $\alpha 2^+$ oocyst development showed no obvious difference to WT (**Figure 3.7, III & VI**; **Figure 3.40**) but late $\alpha 2^{++}$ oocysts showed an increase in sporozoite diameter variance

and this phenotype was even more pronounced in $\alpha 2^{+++}$ oocysts (**Figure 3.40** IX, X, XII). This is in line with the previous findings in $\alpha 1^{cm\&\Delta introns}$ sporozoites (**Figure 3.30**, **Figure 3.34**) and suggests a correlation of sMT numbers and increased sporozoite diameter variance.

Results

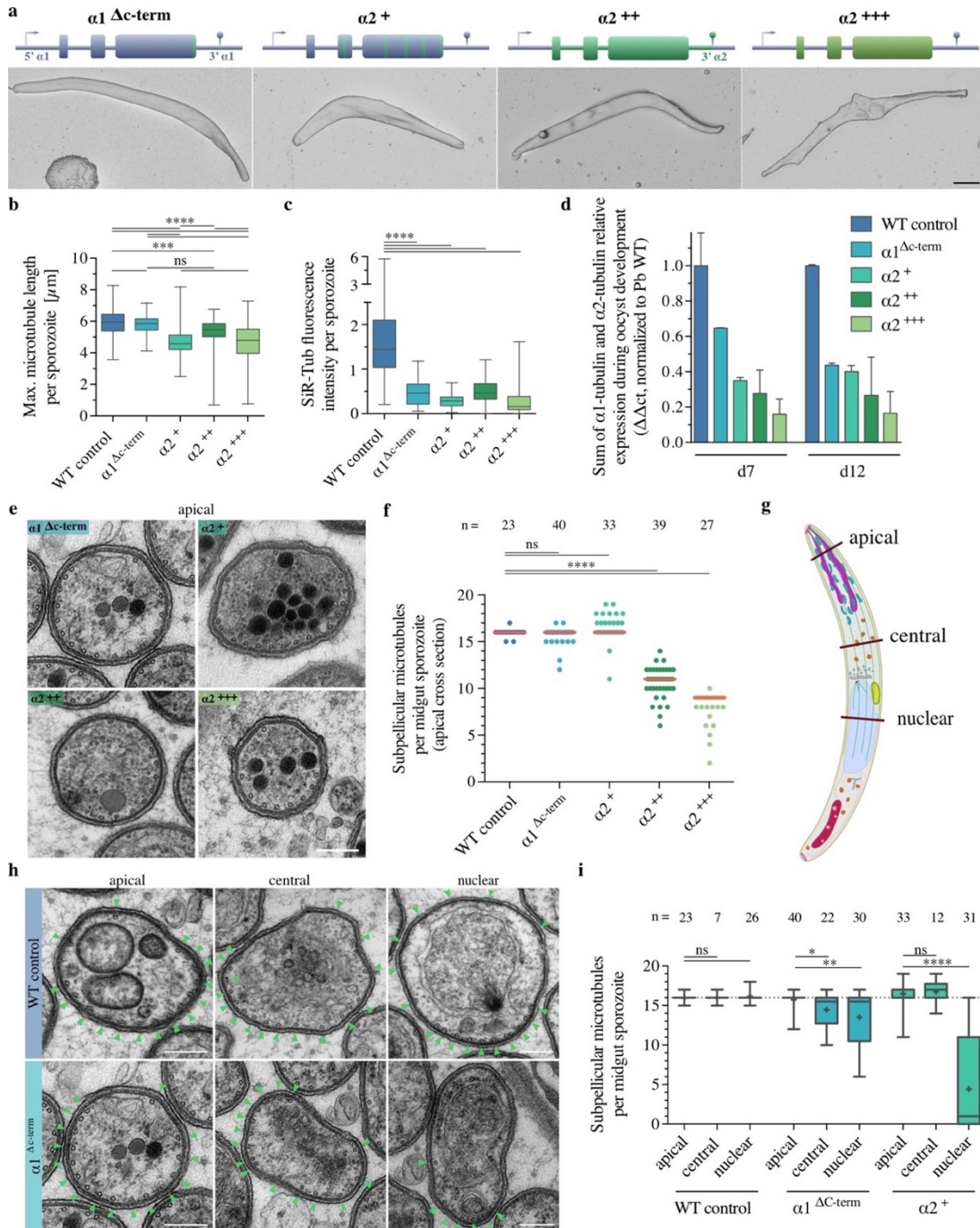
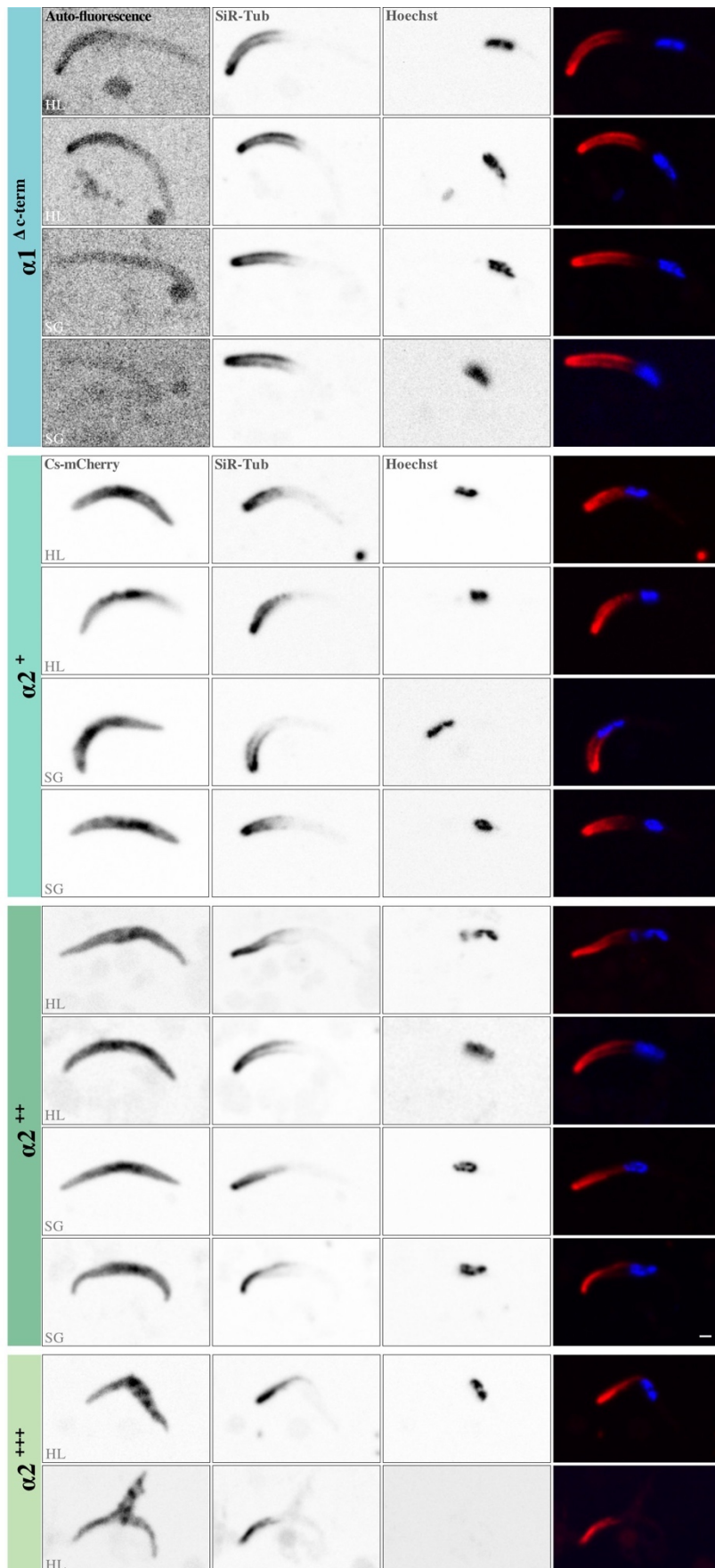


Figure 3.36. Complementation of the $\alpha 1(-)$ line by a set of $\alpha 2$ -tubulin chimeras results in grading aberrant sporozoites with less and shorter subpellicular microtubules. (a) Schemata of the modified $\alpha 1$ -tubulin locus (blue) and the introduced $\alpha 2$ -tubulin elements (green). Corresponding scanning electron micrographs of hemolymph sporozoites are shown below. (b, c) Quantifications of spinning disc confocal images of hemolymph derived sporozoites stained with SiR-tubulin. Maximum sMT length (b) and SiR-tubulin fluorescence intensity (c) per sporozoite was quantified (see chapter 2.3.14). (d) qRT-PCR analysis of two biological replicates are shown for day 7 and day 12 post mosquito blood meal. (e, f) Transmission electron micrographs (TEM) of midgut sporozoite apical cross sections (e) and quantification of the sMT numbers are shown (f). (g) Scheme of a sporozoite with highlighted cross section sites. (h, i) TEM images of apical, central and nuclear cross sections (h) and its quantification (i). Green arrow heads indicate sMTs. ****, ***, **, * indicate $p < 0.0001$, $p < 0.001$, $p < 0.01$ and $p < 0.05$, respectively. Kruskal-Wallis-test. Scale bars: a: 1 μm ; e, h: 0.2 μm .

Results



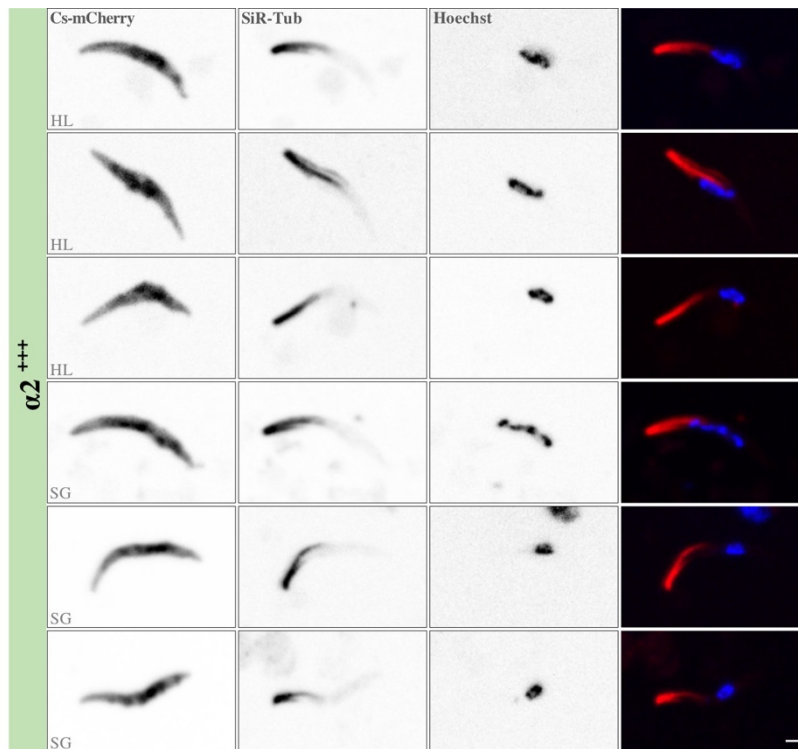


Figure 3.37. Fluorescence image gallery of $\alpha 1^{\Delta c-term}$, $\alpha 2^+$, $\alpha 2^{++}$ and $\alpha 2^{+++}$ sporozoites. Spinning disc confocal images of hemolymph (HL) and salivary gland (SG) sporozoites were stained with SiR-tubulin (microtubules, red) and Hoechst (DNA, blue). The cytoplasmic shape is identified by the *mCherry* expression in case of $\alpha 2^+$, $\alpha 2^{++}$ and $\alpha 2^{+++}$ sporozoites or by auto-fluorescence in $\alpha 1^{\Delta c-term}$ sporozoites. Scale bars: 1 μm .

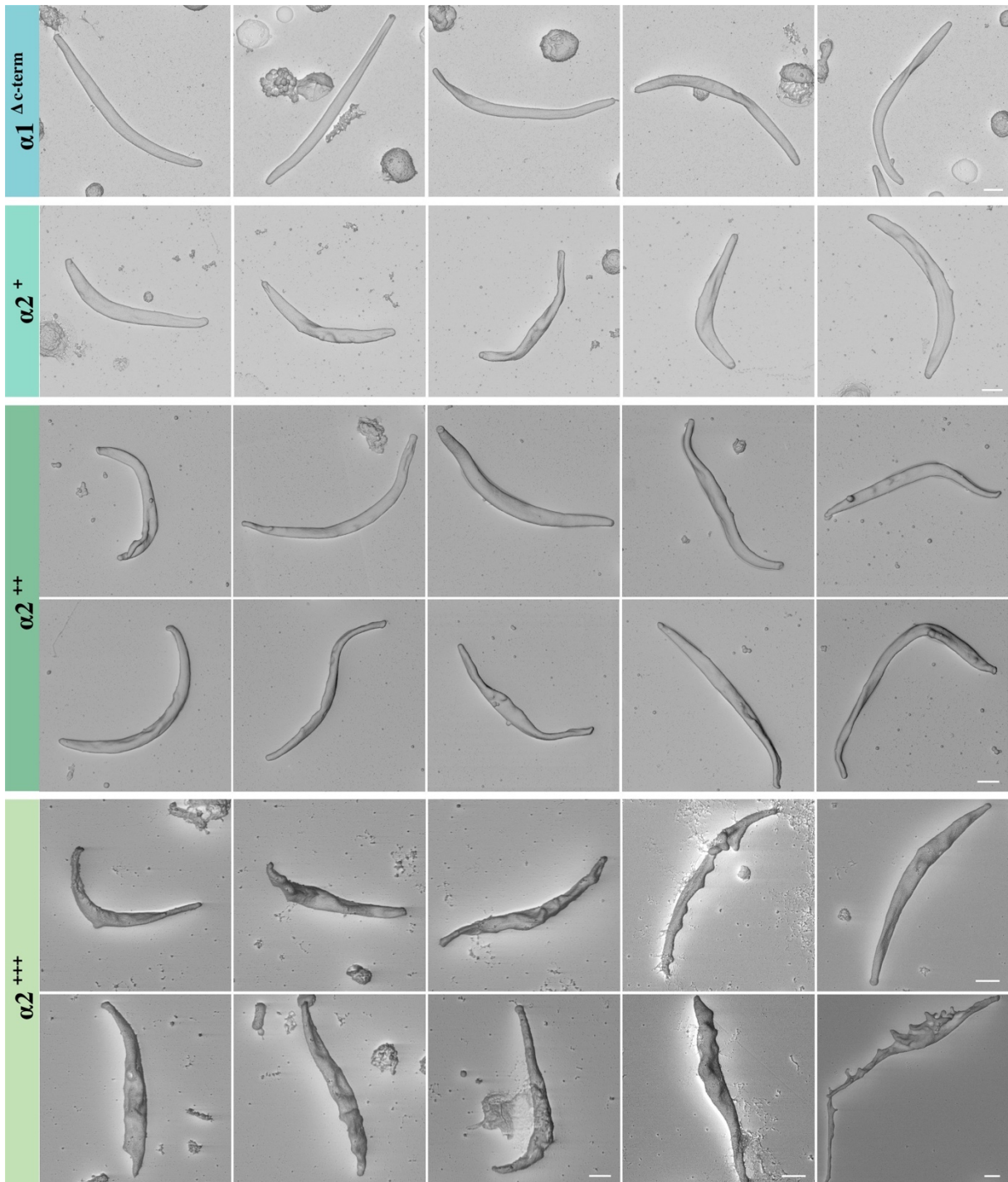


Figure 3.38. Scanning electron micrograph gallery of $\alpha 1^{\Delta c-term}$, $\alpha 2^+$, $\alpha 2^{++}$ and $\alpha 2^{+++}$ hemolymph sporozoites. $\alpha 1^{\Delta c-term}$ sporozoites show no difference to WT sporozoites (**Figure 3.32**). However, all $\alpha 2^{+++}$ sporozoites (median of 9 sMTs (sMTs), apical count) show extrusions and malformations whereas $\alpha 2^{++}$ sporozoites (median of 11 sMTs, apical count) are only occasionally malformed. $\alpha 2^+$ sporozoites (median of 16 sMTs, apical count) did not have any extrusions but sporozoite length was decreased (described in detail in chapter 3.6.4). Scale bars: 1 μ m.

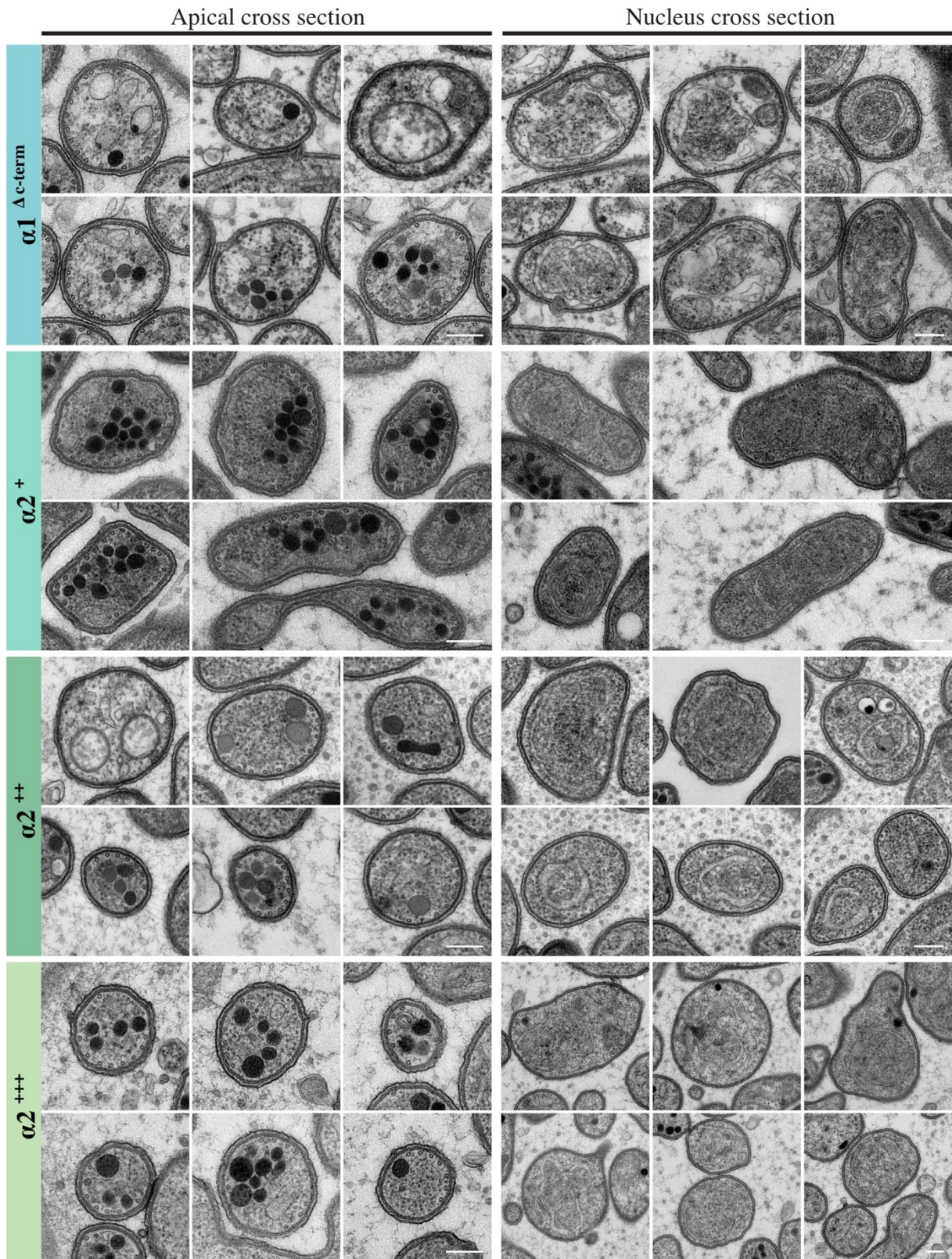
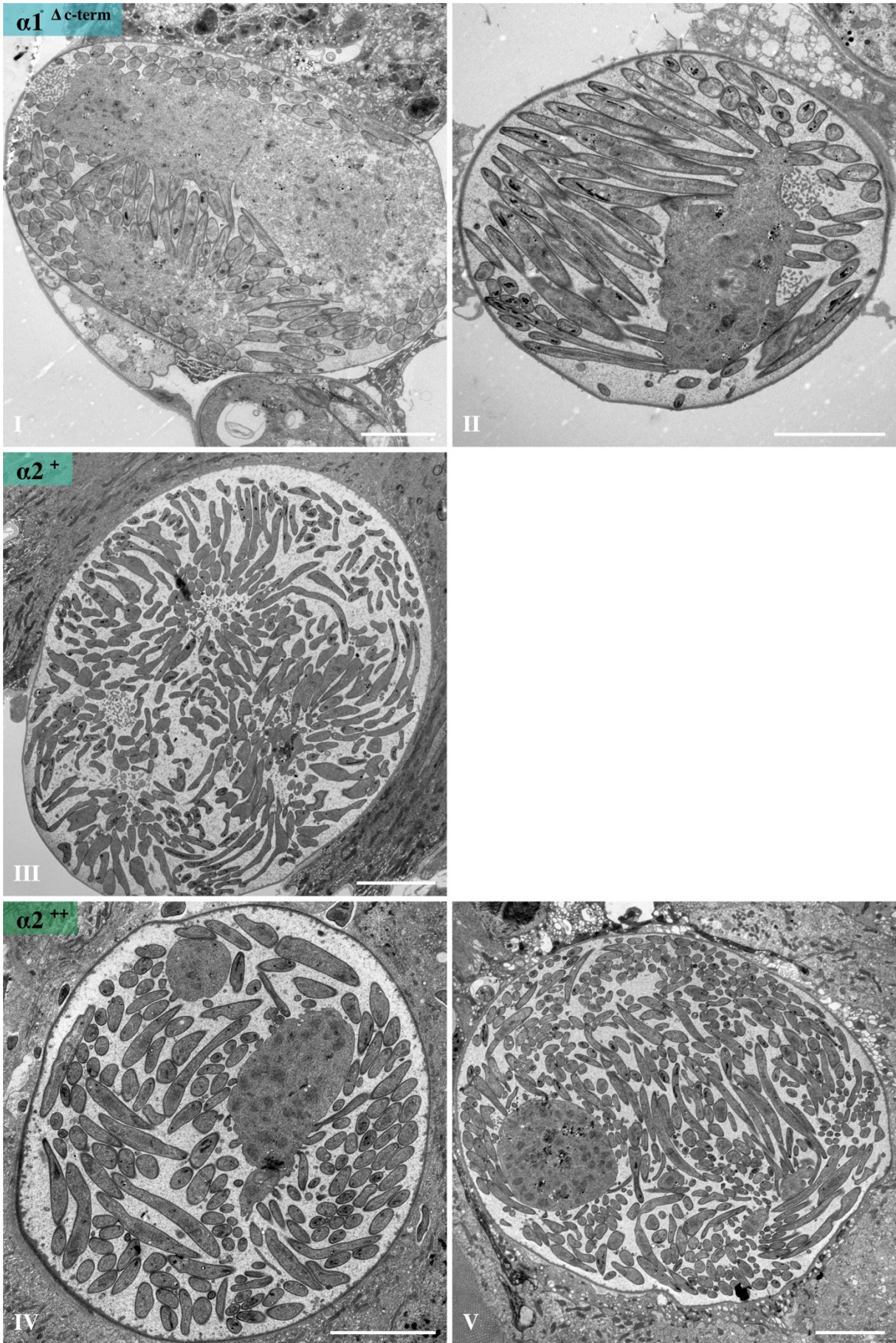
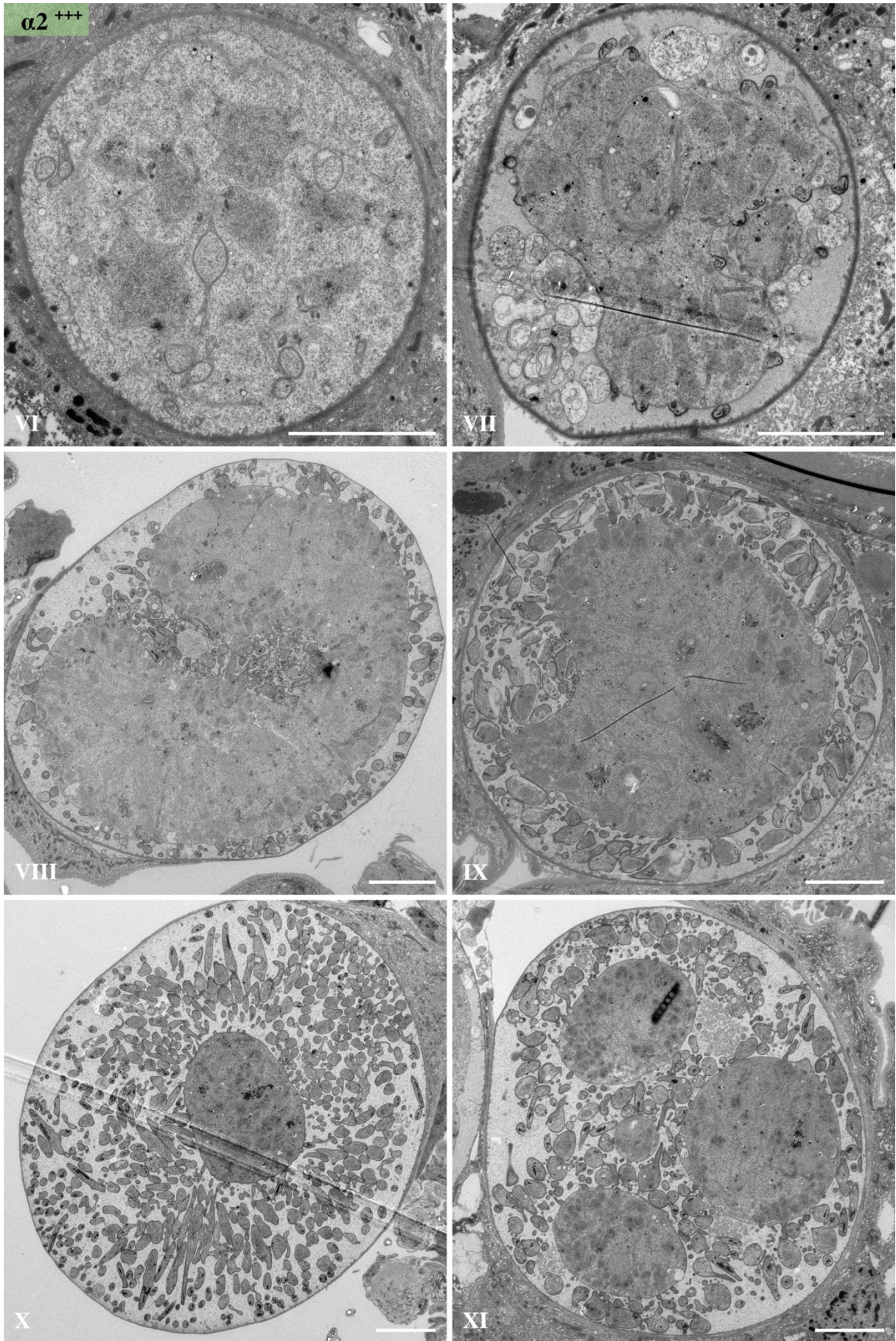


Figure 3.39. TEM gallery of $\alpha 1^{\Delta c-term}$, $\alpha 2^+$, $\alpha 2^{++}$ and $\alpha 2^{+++}$ midgut sporozoites. Apical and nuclear cross sections of midgut sporozoites are shown. Slice thickness: 70 nm. Scale bars: 0.2 μ m.





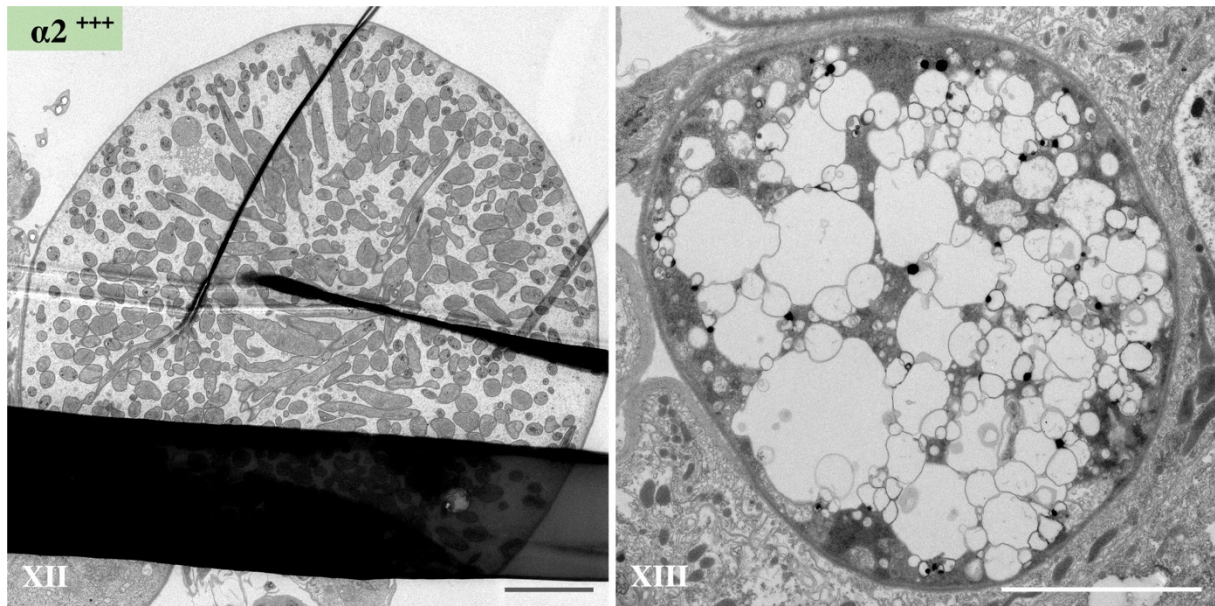


Figure 3.40. TEM images showing $\alpha 1^{\Delta c-term}$, $\alpha 2^+$, $\alpha 2^{++}$ and $\alpha 2^{+++}$ oocysts from different developmental stages. (VI, VII, VIII) Early sporozoite budding; (I, II, III, IV, V, IX, X, XI, XII) late sporozoite budding. (XIII) shows an apoptotic-looking oocyst. $\alpha 1^{\Delta c-term}$, $\alpha 2^+$ oocyst development shows no obvious difference to WT (**Figure 3.7**, III & VI) but late $\alpha 2^{++}$ oocysts already show an increase of sporozoite diameter variance and this was even more pronounced in $\alpha 2^{+++}$ oocysts (IX, X, XII). This is in line with the previous findings in $\alpha 1^{cm\&\Delta introns}$ sporozoites (**Figure 3.30**, **Figure 3.34**). Slice thickness: 70 nm. Scale bars: 5 μ m.

3.6. Subpellicular microtubule length and number define sporozoite overall morphology including length, curvature and thickness

3.6.1. Subpellicular microtubule numbers or $\alpha 2$ -tubulin expression have no impact on apical polar ring tilt

Tilting of the apical polar ring (APR) occurs during sporozoite budding in mosquito oocysts. Longitudinal TEM cuts of early budding sporozoites showed no APR tilt whereas late budding midgut sporozoites in WT did. WT sporozoites revealed a range between $\alpha = 11^\circ$ to 70° . $\alpha 2^{++}$,

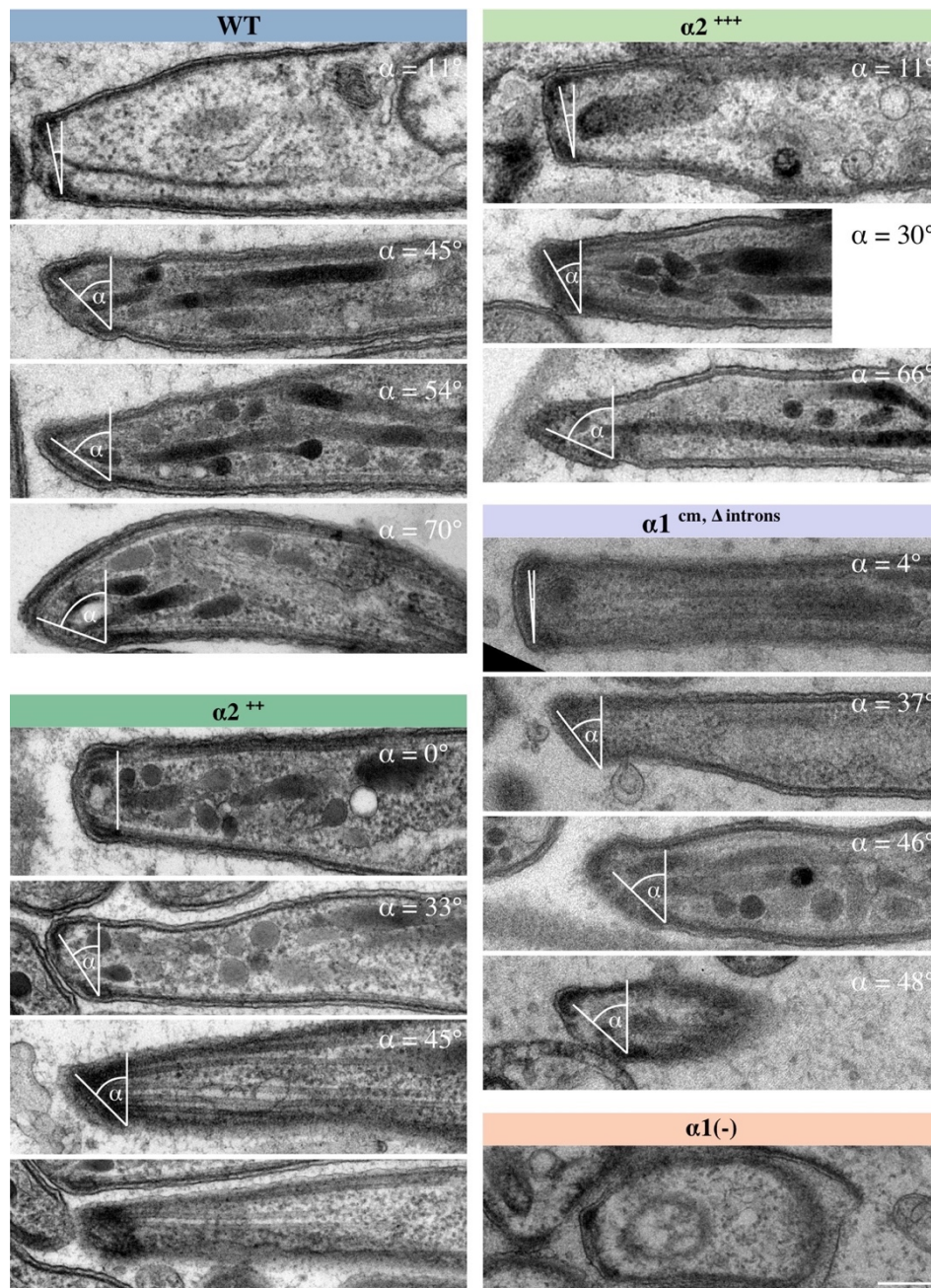


Figure 3.41. TEM longitudinal cut of WT, $\alpha 2^{++}$, $\alpha 2^{+++}$ and $\alpha 1^{cm\&\Delta introns}$ midgut sporozoites. Tilt of the apical polar ring (APR) is measured by the angle α . Scale bar: 0.2 μm .

$\alpha 2^{+++}$ and $\alpha 1^{cm\&\Delta introns}$ parasites also showed an APR tilt but with the tendency of being smaller than in WT (**Figure 3.41**). This would mean that a reduction of sMTs to either 6 sMTs ($\alpha 1^{cm\&\Delta introns}$) or sMTs formed with $\alpha 2$ -tubulin ($\alpha 2^{++}$, $\alpha 2^{+++}$) might influence APR tilt. However, analysis was limited to a very small number of longitudinal sporozoite cuts, therefore, this data might only be giving a hint about APR tilt. For $\alpha 1(-)$, sporozoites never showed an APR tilt, but classification into early and late sporozoite development was not possible. The stability of the tilt cannot be addressed with TEM analysis.

3.6.2. A reduced number of subpellicular microtubules leads to IMC & plasma membrane extrusions

Subpellicular microtubules are essential for sporozoite budding and sporozoites formed with a reduced number of sMTs lose their crescent shape, develop undefined malformations and cannot keep a constant sporozoite thickness as shown previously. To investigate the extrusions occurring in sporozoites in more detail (see **Figure 3.32** and **Figure 3.38**), I analyzed transmission electron micrographs of midgut sporozoites. Extrusions were formed of the inner membrane complex (IMC) and the plasma membrane (**Figure 3.42**). Plasma membrane extrusions without IMC were never spotted. For $\alpha 1(-)$ sporozoites, it was not possible to differentiate between the main sporozoite or extrusions in late developing oocysts. This is in line with the 3D reconstructions shown earlier on (**Figure 3.21**). $\alpha 1^{cm\&\Delta introns}$ sporozoites but also $\alpha 2^{+++}$ sporozoites showed many extrusions, especially located towards the back of the sporozoite. Although $\alpha 2^{+}$ did not show any malformations, the sporozoite width increased at the nucleus.

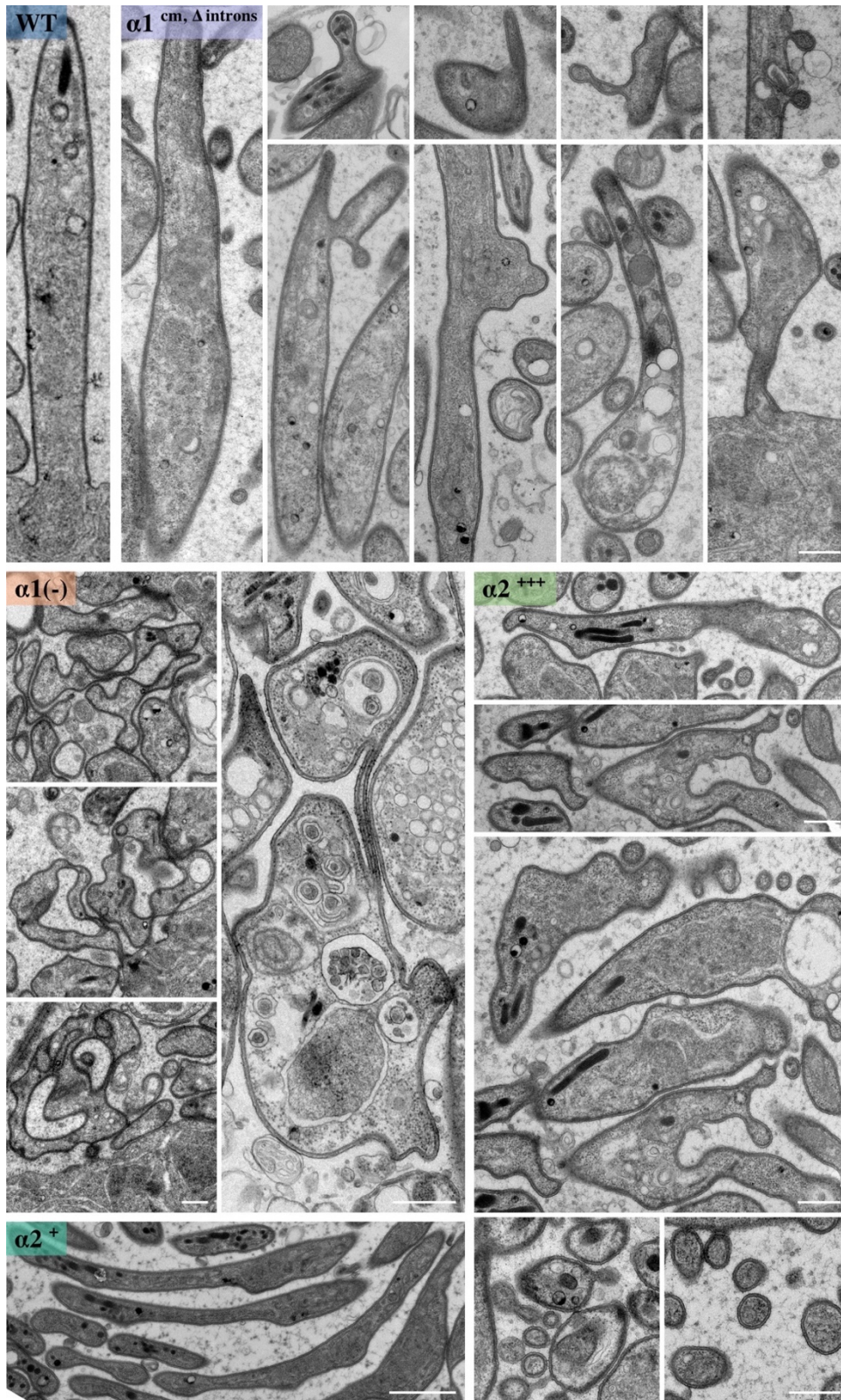


Figure 3.42. Transmission electron micrographs showing extrusions in midgut sporozoites. WT budding sporozoites (top left) show a straight formation. In contrast, $\alpha 1^{cm, \Delta introns}$ and $\alpha 2^{+++}$ sporozoites (top & center right) often show either an increased sporozoite width or extrusions formed by the plasma membrane and IMC. In late $\alpha 1^{-}$ sporozoites, differentiation between main sporozoite and extrusions was not possible (center left). Although $\alpha 2^{+}$ sporozoites did not show any extrusions, sporozoite width was increased at nuclear positions (bottom left). Scale bars: 0.5 μ m.

3.6.3. Subpellicular MTs stabilize the IMC and force nuclei into elongated formation

As described in the previous chapter, parasite lines which formed less than the 16 sMTs found in WT tended to form extrusions along sporozoites (**Figure 3.42**). To investigate what impact sMTs play in stabilizing the IMC, TEM pictures were analyzed for microtubule location and IMC/plasma membrane formation.

In WT, only at sites where microtubules were seen next to the IMC, the IMC/plasma membrane showed a very straight and smooth delineation (apical end of the budding sporozoite; **Figure 3.43 I**, left side). However, at sites where no microtubules were seen, the IMC/plasma membrane often appeared ‘wobbly’ (close to the sporozoite-to-sporoblast attachment site; **I**, right side). This phenomenon was not only seen at the outer front or back of a sporozoite but also when viewing the central or nuclear part of a sporozoite. The central part (**Figure 3.36**) is usually the area, where dorsoventral polarity of microtubules is fully accomplished (Kudryashev et al., 2012). In **Figure 3.43 II**, a longitudinal section of the central part of a sporozoite is shown with a smooth IMC/plasma membrane on top and a wobbled plasma membrane on the bottom. Microtubules are only seen on the top, but not at the bottom. This again supports the hypothesis, that microtubules stabilize the IMC and subsequently the plasma membrane. Furthermore, WT sporozoites keep their sporozoite width quite consistent even at the site of their nucleus and this is most likely performed by sMTs reaching beyond the nucleus (**III**). This observation could be supported with a parasite line ($\alpha 2^+$), which formed shorter sMTs and of those shorter microtubules only a small population reached the nucleus (**Figure 3.36 h**). In $\alpha 2^+$ sporozoites, increased sporozoite width was especially seen at sites of nuclei and sMTs were usually not found or only found at one side (top or bottom) next to nuclei (**IV**). This resulted in a straight IMC/plasma membrane at the side where the sMT was seen, but at the other side, a strong bend starting at the nucleus was found.

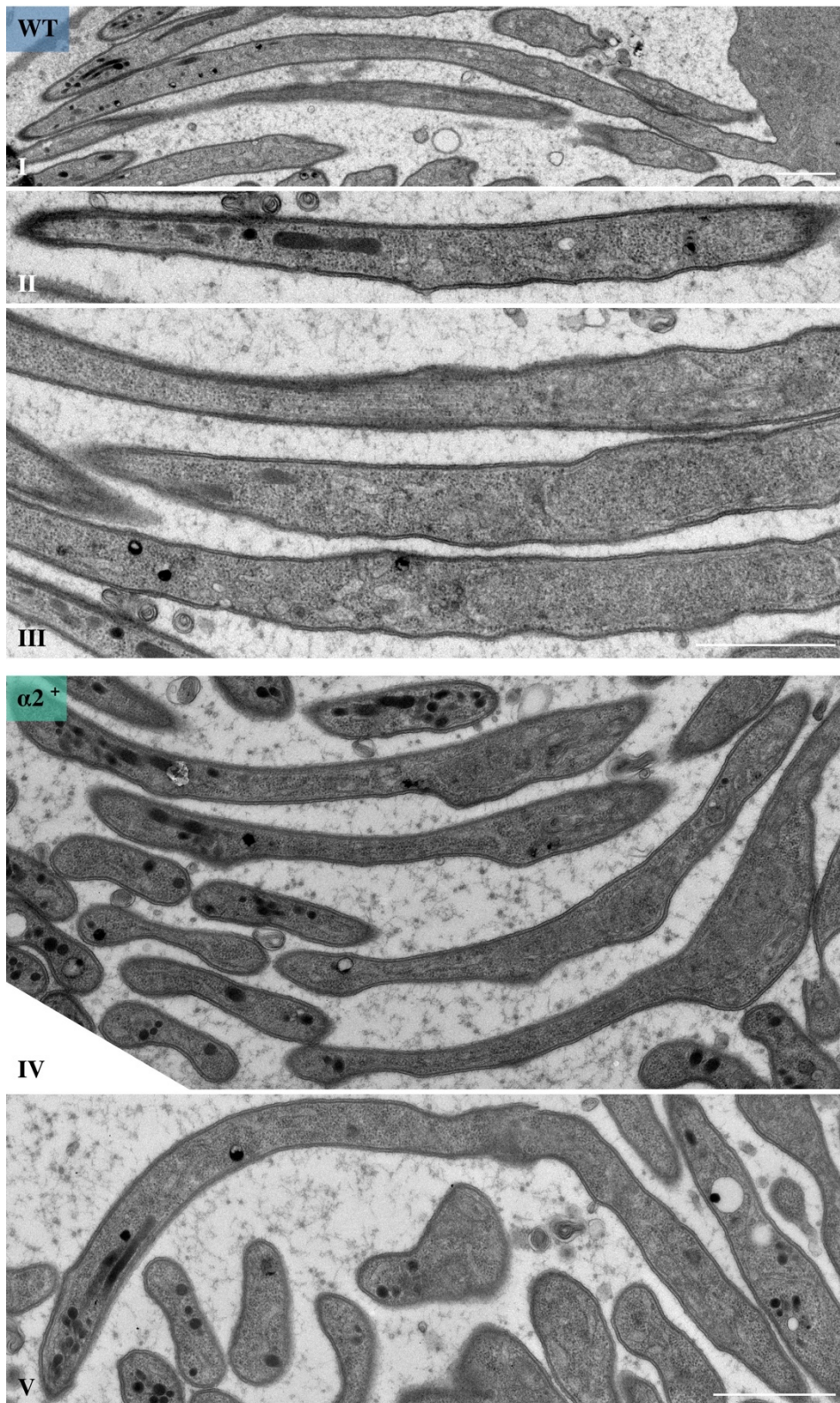


Figure 3.43. Transmission electron micrographs of longitudinal sporozoite cross sections. Sections support the hypothesis, that subpellicular MTs stabilize the IMC and force nuclei into an elongated shape. Scale bars: 1 μ m.

3.6.4. Parasite lines with short maximum microtubule length have shorter sporozoites

Analysis of hemolymph sporozoites revealed a reduced sMT maximum length and lower SiR-tubulin fluorescent levels in $\alpha 2$ -tubulin chimeras (Figure 3.36). This length difference and fluorescence decrease was also observed for salivary gland sporozoites for $\alpha 2$ -tubulin chimeras (Figure 3.44 a, b). Deletion of the $\alpha 1$ -tubulin C-terminus did not decrease the maximum microtubule length but showed a reduced fluorescence intensity of SiR-tubulin by about two-fold (a). This can be explained with the findings of (Figure 3.36 i), that not all sMTs reach full length. Interestingly, $\alpha 1^{\Delta introns}$ parasites showed a similar pattern, suggesting that also for this line only few microtubules reach the maximum length. Preliminary quantification of sporozoite nuclear cross sections revealed a median of 8 sMTs (n=7) (Figure 3.33).

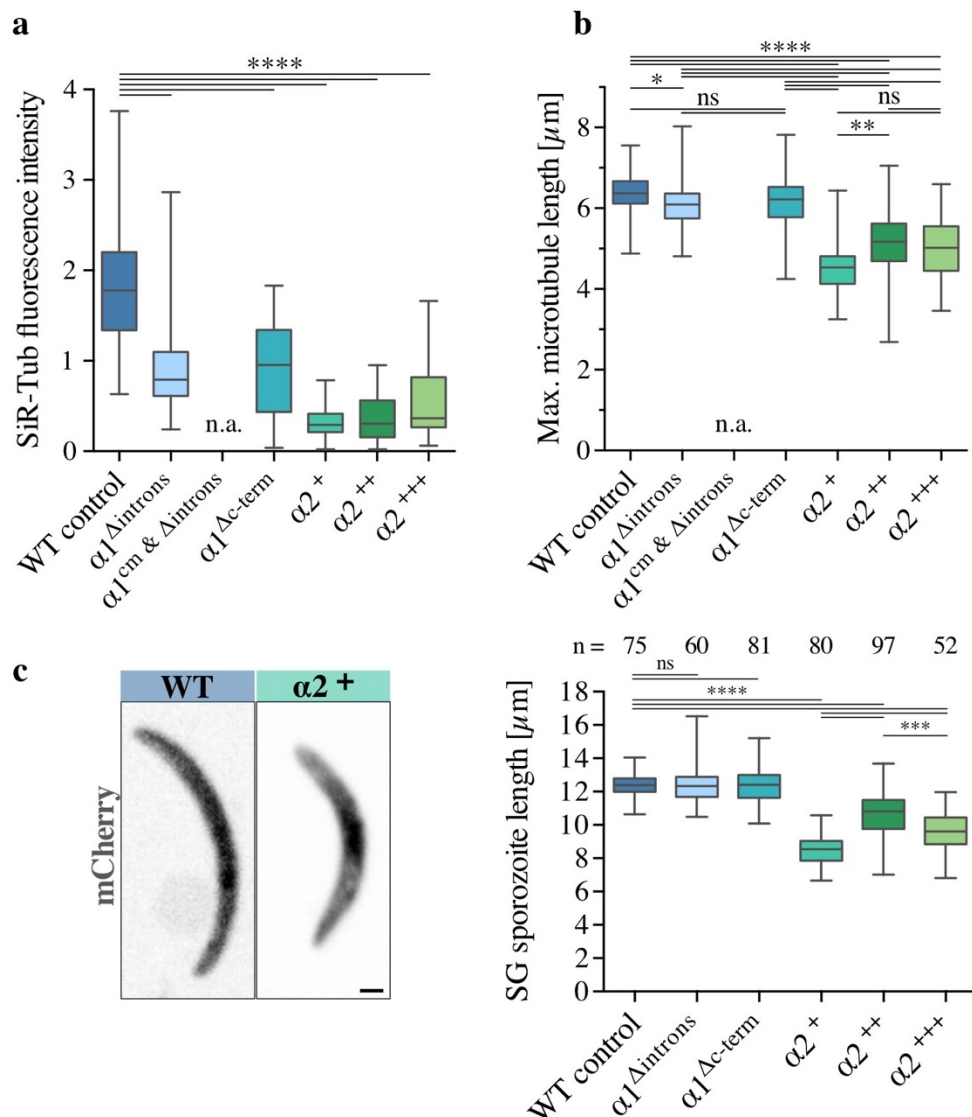


Figure 3.44. Quantifications of subpellicular microtubule length and sporozoite length for salivary gland derived sporozoites. SiR-tubulin fluorescence intensity (a) and maximum sMT length (b) per sporozoite was quantified from SiR-tubulin stained samples imaged via spinning disc confocal microscopy (for details see chapter 2.3.14). (c) Example images and quantification of salivary gland sporozoite length. Scale bar: 1 μm .

Besides the impact of $\alpha 2$ -tubulin on maximum sMT length, also the overall sporozoite length was reduced in $\alpha 2$ -tubulin expressing lines (Figure 3.44 c). $\alpha 2^+$ parasites had the shortest salivary gland sporozoites with only $\sim 8.5 \mu\text{m}$ in length compared to $\sim 12.4 \mu\text{m}$ in WT. Truncation of the $\alpha 1$ -tubulin C-terminus as well as missing introns did not affect sporozoite length.

3.6.5. $\alpha 2$ -tubulin chimeras have an increased sporozoite curvature

Parasite lines expressing $\alpha 2$ -tubulin or the C-terminal truncated version of $\alpha 1$ -tubulin ($\alpha 1^{\Delta\text{C-term}}$) showed a decrease in gliding circle diameter (Figure 3.45). Maximum z-projections of sporozoite gliding videos are shown (a). Measuring the circle diameter gives an easy read out for sporozoite curvature (see chapter 2.3.12 for more detail). $\alpha 2^+$ salivary gland sporozoites had the shortest diameter with $\sim 7.2 \mu\text{m}$ compared to $\sim 13.4 \mu\text{m}$ for WT sporozoites.

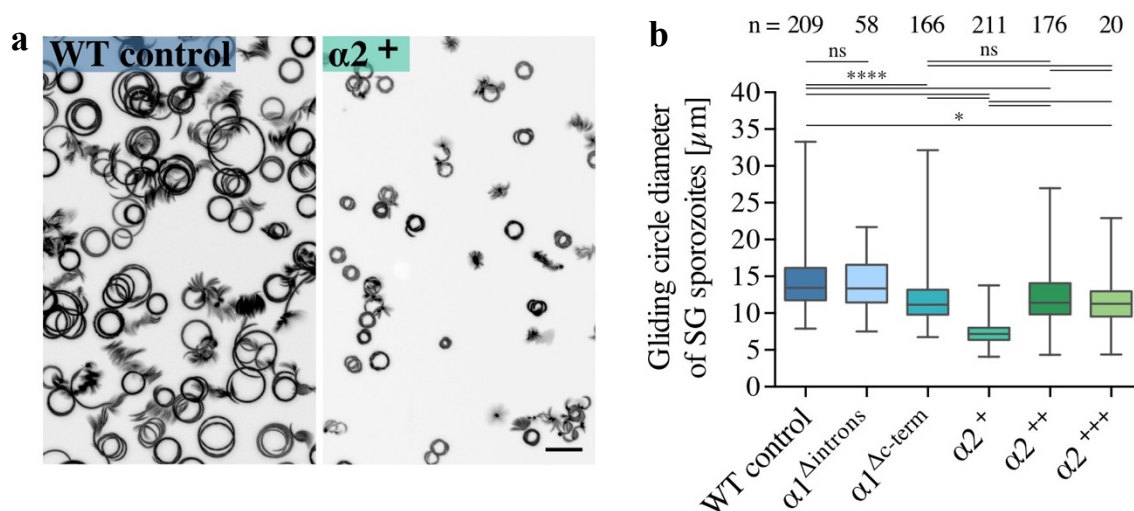


Figure 3.45. Gliding circle diameter of $\alpha 2$ -tubulin chimeras, WT and $\alpha 1^{\Delta\text{introns}}$ parasites. (a) Maximum z-projection images of sporozoite gliding assays are shown. Note the decreased size of the gliding circles for the $\alpha 2^+$ parasite line. (b) Quantification of the gliding circle diameter for the different lines. **** and * indicate $p < 0.0001$ and $p < 0.05$, respectively. Kruskal-Wallis-test. Scale bar: $20 \mu\text{m}$.

3.6.6. A reduced number of subpellicular microtubules negatively influences gliding motility of sporozoites

Not only sporozoite curvature but also the ability of sporozoite gliding and its direction can be determined. Approximately 70 – 80% of sporozoites were either capable of gliding or partially gliding. Only $\alpha 2^{+++}$ sporozoites had a reduced ability to move (32%) (Figure 3.46 a). As shown above, this line only showed a median of 9 sMTs per sporozoite and only very few $\alpha 2^{+++}$

Results

sporozoites were able to infect the mosquito salivary gland (**Table 4**). About 2% of WT sporozoites showed clockwise (CW) gliding but usually flipped over to continue in a counter-clockwise (CCW) direction after a short period of time (b). Intriguingly, parasites having a lower number of subpellicular MTs tended to more often continuously glide in a CW manner. 21.6% of $\alpha 2^{+++}$ sporozoites (median: 9 sMTs) and 10.3% of $\alpha 2^{++}$ sporozoites (median: 11 sMTs) were gliding in CW direction for at least 6 seconds during the 100 s video. Even $\alpha 2^{+}$ sporozoites, which have 16 but shorter sMTs showed an increase of 2-fold in CW movement.

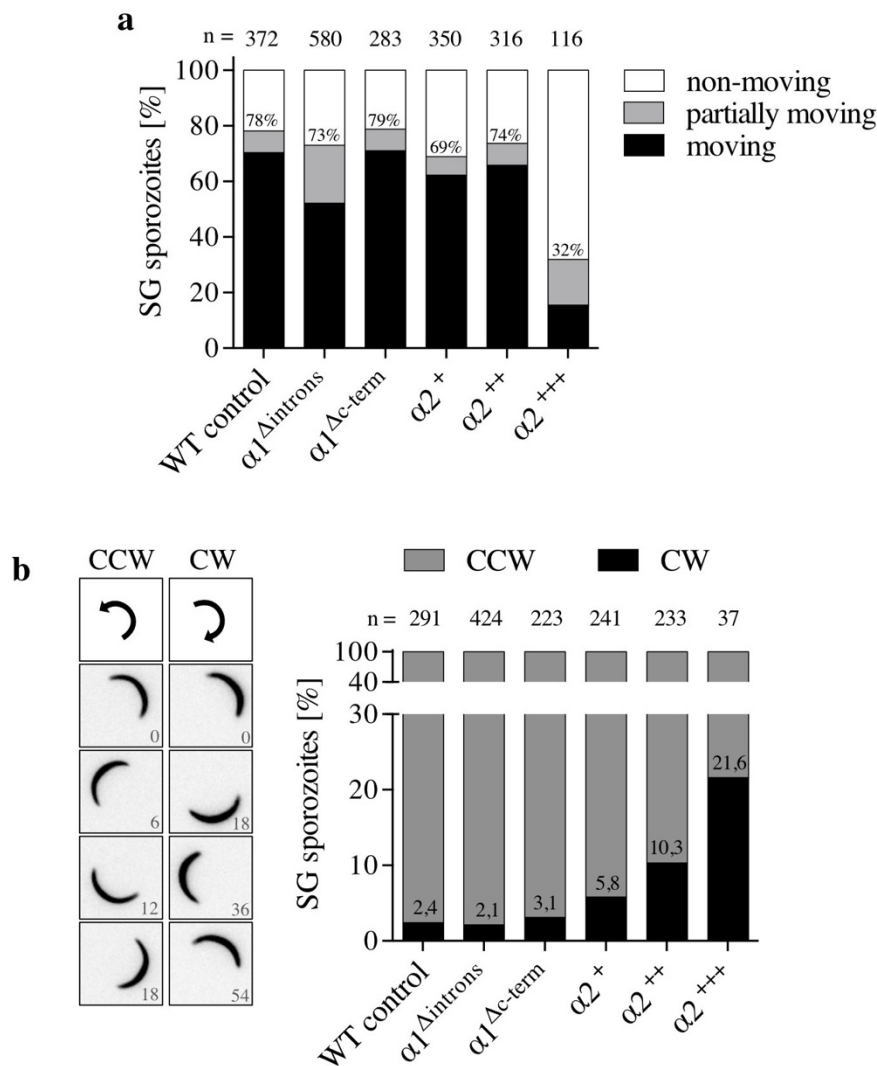


Figure 3.46 Moving/Gliding motility of the $\alpha 2$ -tubulin chimeras, WT, $\alpha 1^{\Delta c-term}$ and $\alpha 1^{\Delta introns}$ lines. (a) Gliding motility was categorized into three different patterns. Moving sporozoites moved at least a full circle during 100 seconds. Partially moving sporozoites moved for at least a sporozoite length and non-moving sporozoites were not moving at all. Non-moving also included attached, waving, twitching, patch gliding and floating sporozoites. (b) Moving sporozoites were further categorized into clockwise (CW) movers when sporozoites moved for at least two frames (6 seconds) in CW direction during the 100 s video. More details are found in chapter 2.3.12.

3.6.7. Attachment to the subpellicular network and the distance between neighboring subpellicular microtubules is changed in $\alpha 2$ -tubulin chimeras and $\alpha 1^{\Delta c-term}$

Among the high sequence identity, the C-terminus is one of the regions with major differences between the two α -tubulin isotypes (**Figure 1.8**). The C-terminus is sticking out from the microtubule lattice and is a key site for tubulin posttranslational modifications and MAP binding (Nogales et al., 1999; Janke, 2014; Magiera and Janke, 2014; Brouhard and Rice, 2018). Deletion of the three C-terminal amino acids might pinpoint the functional difference between the two α -tubulins and might explain the observation of shorter $\alpha 2$ -tubulin-formed sMTs (**Figure 3.36** and **Figure 3.44**). I generated a line with a truncated $\alpha 1$ -tubulin C-terminus subsequently representing $\alpha 1$ -tubulin with an $\alpha 2$ -tubulin C-terminus ($\alpha 1^{\Delta c-term}$). Analysis of midgut sporozoite cross sections revealed, that the equal and sometimes polar distribution of sMTs along the IMC is impaired in $\alpha 1^{\Delta c-term}$ sporozoites (**Figure 3.47**). The distance between neighboring sMTs is occasionally very narrow. In case of the $\alpha 2^+$ parasite line, similar observations were made and sometimes sMTs even detached of the IMC.

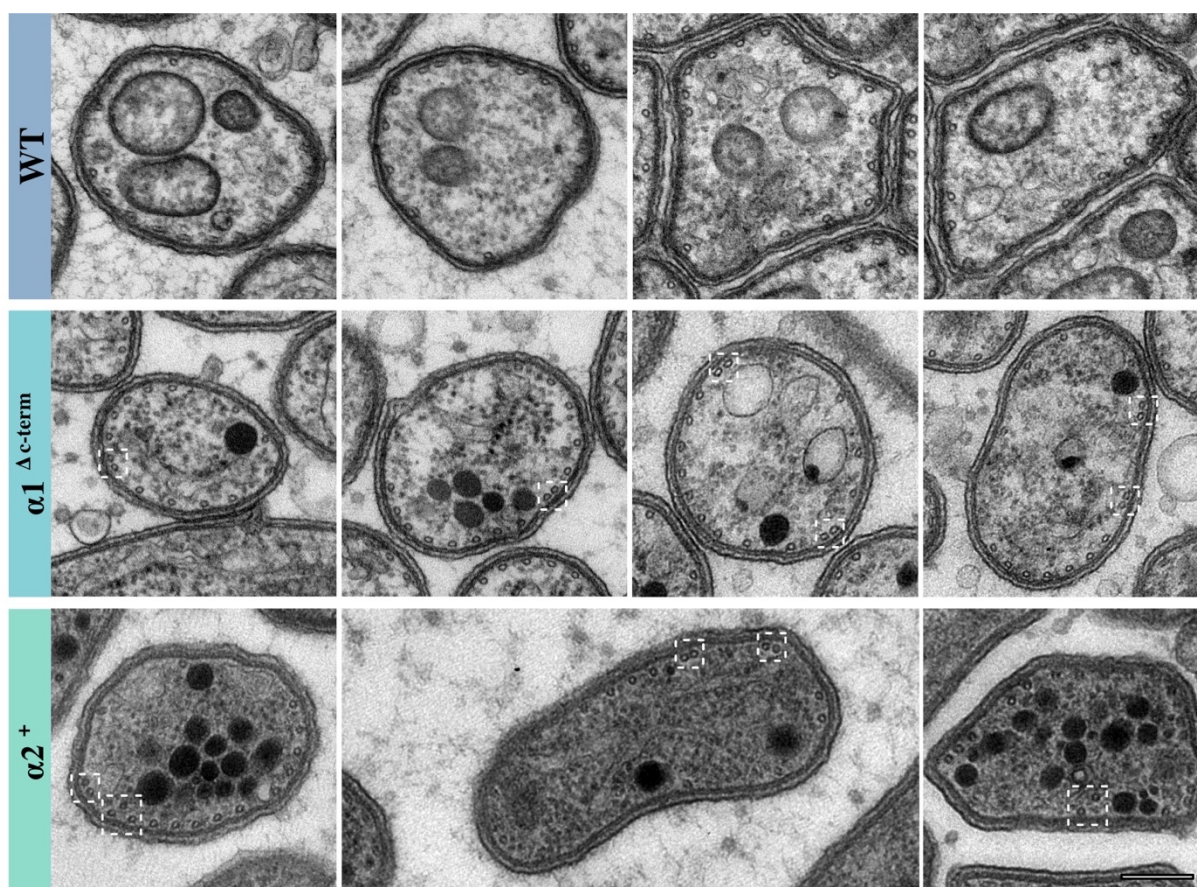


Figure 3.47. TEM cross sections of WT, $\alpha 1^{\Delta c-term}$ and $\alpha 2^+$ midgut sporozoites. Attachment and distribution of sMTs is impaired in $\alpha 1^{\Delta c-term}$ and $\alpha 2^+$ parasites, both having a truncated C-terminus. Scale bar: 0,2 μ m.

3.1. Subpellicular microtubule length and number define sporozoite infectivity

3.1.1. Subpellicular microtubule numbers define salivary gland invasion efficiency

To investigate the impact of morphological changes on sporozoite infectivity, midgut and salivary gland sporozoite numbers were counted (**Table 4**). Dividing the salivary gland sporozoite numbers by the midgut numbers gives an approximate measure of how efficient sporozoites can invade salivary glands. Numbers in **Table 4** are highlighted with a color code to make invasion phenotypes clearer. The $\alpha 1(-)$ parasite line was not able to form functional sporozoites (chapter 3.3), and accordingly, no sporozoites were found in midguts. Hence, parasite transmission was completely blocked. In case of the $\alpha 1^{cm\&\Delta introns}$ line, which formed malformed sporozoites with a median of only 6 sMTs but with normal length (chapter 3.4), no sporozoites were found in mosquito salivary glands. The very low number for salivary gland sporozoites counted is most likely due to a contamination with hemolymph sporozoites. The $\alpha 2^{+++}$ parasite line also showed malformed sporozoites, but with less extrusions and malformations than $\alpha 1^{cm\&\Delta introns}$ and sporozoites had a median of 9 sMTs (chapter 3.5). However, this slight increase in sMTs seemed to have been enough for at least a small sporozoite population to be able to invade salivary glands (0.3% of midgut sporozoites). $\alpha 2^{++}$ sporozoites and $\alpha 2^{+}$ both showed only a reduced invasion rate to about half (11-13%) the rate of WT (23%). In case of $\alpha 1^{\Delta c-term}$ and $\alpha 1^{\Delta introns}$, no phenotype in terms of salivary gland invasion was found.

Parasite line	Midgut sporozoites / mosquito (n)	Salivary gland sporozoites / mosquito (n)	Salivary gland invasion ratio
WT control	88,000 (64)	21,000 (61)	0.23
$\alpha 1^{\Delta introns}$	59,000 (34)	13,000 (34)	0.21
$\alpha 1^{\Delta c-term}$	88,000 (57)	30,000 (53)	0.34
$\alpha 2^{+}$	50,000 (65)	5,000 (66)	0.11
$\alpha 2^{++}$	92,000 (46)	12,000 (47)	0.13
$\alpha 2^{+++}$	96,000 (34)	300 (33)	0.003
$\alpha 1^{cm, \Delta introns}$	60,000 (89)	6 (87)	0.000
$\alpha 1(-)$	0 (70)	0 (67)	n.a.

Table 4. Sporozoite mosquito salivary gland invasion. n: indicates the number of investigated sporozoites; n.a.: not assessable; The means are shown. Sporozoite counts were performed between day 17-19 post mosquito feed.

3.1.2. At least 10 subpellicular MTs are necessary to invade mosquito salivary glands

As pointed out in the previous chapter, sMT numbers might play a very crucial role for salivary gland invasion. However, to address whether a specific threshold of sMTs is needed to invade salivary glands, sMT numbers have to be quantified from salivary gland sporozoites (**Figure 3.48**). I first analyzed the $\alpha 2^{+++}$ parasite line, because only very few sporozoites of this line reached the salivary gland (~ 300 per mosquito) indicating a strong selection pressure on the sporozoite population. However, it was not possible to find enough sporozoites for ultrastructural analysis. Per salivary gland cross section, approximately 20 sporozoites could be identified, whereas in general only one sporozoite in ~ 200 salivary gland sporozoites allows determination of microtubule numbers. As a consequence, this line could not be analyzed by EM inside the salivary gland. The $\alpha 2^{++}$ parasite line also showed a decreased salivary gland invasion ratio indicating a selection of the sporozoite population. Looking at several thousand sporozoites resulted in 37 sporozoites, which could be quantified. The mean of 10.6 sMTs (median: 11) found in midgut sporozoites was shifted to a mean of 11.4 sMTs (median: 11) in salivary gland sporozoites. Furthermore, the quantification revealed, that a minimum of 10 sMTs is needed to be able to enter mosquito salivary glands. This indicates, that a specific number of sMTs is critically important for sporozoite salivary gland invasion.

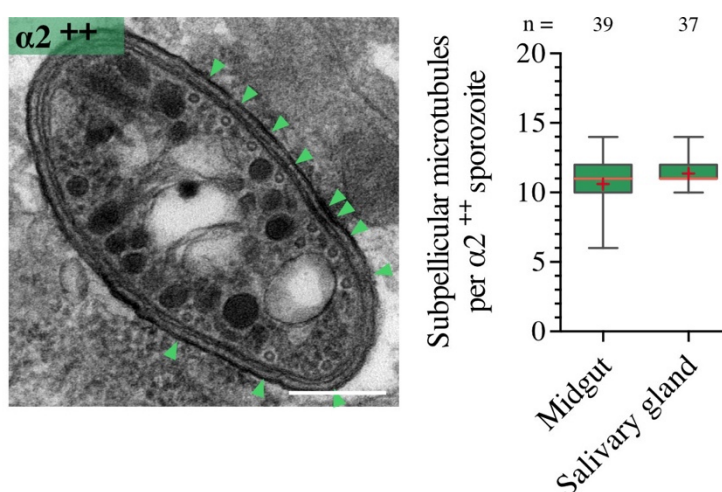


Figure 3.48. TEM cross section of a $\alpha 2^{++}$ salivary gland sporozoite and corresponding quantification. (Left) Example image of a sporozoite inside a mosquito salivary gland. Green arrow heads indicate sMTs. Section thickness: 70 nm. (Right) The quantification of subpellicular microtubules of midgut and salivary gland sporozoites of the $\alpha 2^{++}$ parasite line is shown. Note the upwards shift potentially indicating the selection pressure for entering the mosquito salivary glands. Red line: median; red cross: mean. Scale bar: 0.2 μ m.

3.1.3. A reduced number and shortening of subpellicular microtubules lowers parasite infectivity in mice

To test the impact of sMT modifications on infectivity, I infected mice by either injecting 10,000 salivary gland sporozoites intravenously (*i.v.*) to circumvent the skin phase of the host infection or by letting 10 infected mosquitos bite for 20 min. Parasite transmission by mosquito bite resulted in fewer positive mice in $\alpha 2^+$ and $\alpha 2^{++}$ lines and an increase in the time needed for first blood stage parasite detection for the $\alpha 2^+$ line (prepatency, **Figure 3.49 a**, **Table 5**). This prepatency delay was also found when mice were infected with 10,000 sporozoites *i.v.* (**Figure 3.49 b**, **Table 5**). In addition, none of the mice infected by the $\alpha 1^{cm\&\Delta introns}$ line got positive. This suggests, that both the number and the length play a crucial role for *Plasmodium* sporozoite infectivity.

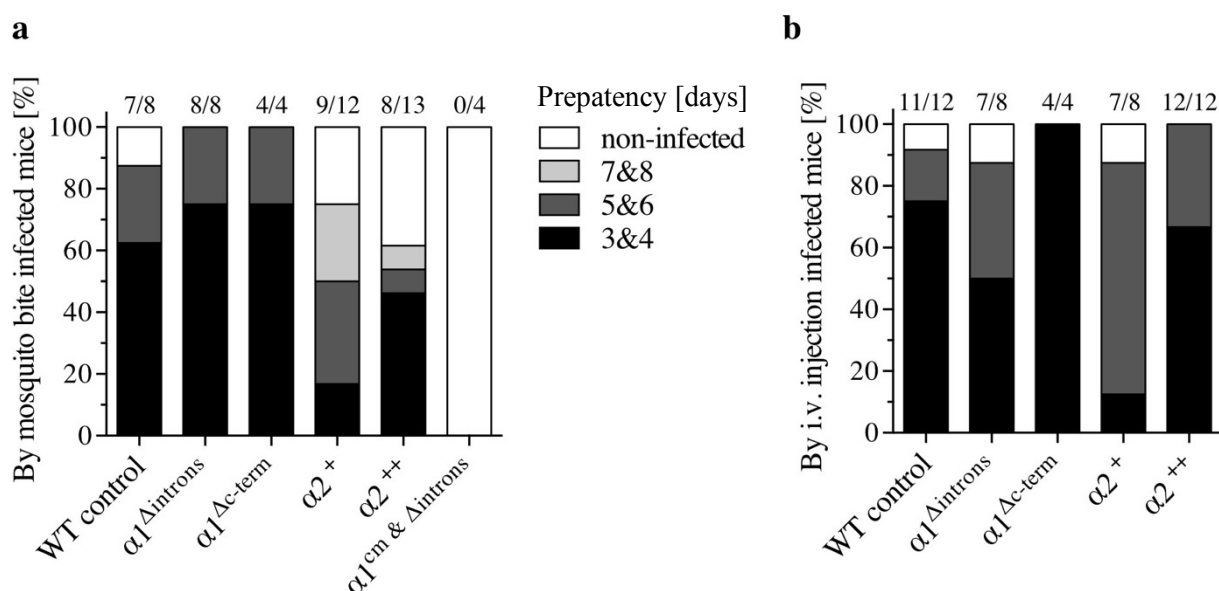


Figure 3.49. Ability of vector-to-host transmission of α -tubulin modified parasite lines. (a) Mice infection by mosquito bite: 10 infected mosquitos were allowed to bite on each NMRI mouse for 20 min. (b) Intravenous injection of sporozoites: 10,000 salivary gland sporozoites were injected intravenously (*i.v.*) per mouse. Parasitemia of mice was monitored daily from day 3 to day 8 post mosquito blood meal or post *i.v.* injection via blood smears stained with Giemsa solution. Numbers above bars indicate positive mice per total mice used. Grey scales indicate the prepatency in days, the time span until the first parasite was detected after mouse infection.

4. Discussion

Microtubules (MTs) are essential for many cellular processes, including intracellular transport, chromosome segregation, establishment and maintenance of polarity, and migration (Fojo, 2008; Alberts et al., 2014). In most eukaryotes, the number and length of microtubules is variable whereas the highly polarized and crescent shaped *Plasmodium* sporozoites contain microtubules that are well defined in number and length. However, the significance of both parameters has not been studied to date and little is known about the two α -tubulin isoforms existing in *Plasmodium*. Prior to my work it was not clear, which α -tubulin isoform is required for microtubule polymerization in sporozoites. Also, the influence of microtubule parameters (e.g. number, length, arrangement) on sporozoite development and infectivity has only been addressed in one study in *T. gondii* (Ma et al., 2007). In addition, hemispindle microtubules, suggested to be required for chromosome segregation during sporozoite budding, have been sparsely investigated due to difficulties in labelling MTs within insect stages. TEM approaches could reveal insights into sporozoite budding but addressing especially the function and whether length of microtubules is important during oocyst and sporozoite development was not feasible (Garnham, Bird, and Baker, 1960, 1963, Garnham et al., 1961, 1969; Vanderberg, Rdodin, and Yoeli, 1967; Sinden and Garnham, 1973; Sinden and Strong, 1978). Furthermore, the high amino acid sequence identity of the two *Plasmodium* α -tubulins combined with posttranslational modifications and mosquito α -tubulin sample contamination complicates specific detection, for example, via western blot or mass spectrometry (Fennell, Al-shatr, and Bell, 2008). Further, antibodies against tubulin are not capable of efficiently penetrating the oocyst wall to allow visualization of microtubules during sporozoite formation. Attempts to GFP-tag tubulin showed modification-dependent phenotypes and were not suitable for functional microtubule analysis (Kooij et al., 2005)(Singer M., data not shown). Therefore, the breakthrough to investigate microtubules within *Plasmodium* insect stages was a new live imaging dye called SiR-tubulin (Lukinavičius et al., 2014), which was able to penetrate the *Plasmodium* oocyst wall. Previously described observations of oocyst development acquired via TEM (Garnham, Bird, and Baker, 1960, 1963, Garnham et al., 1961, 1969; Vanderberg, Rdodin, and Yoeli, 1967; Sinden and Garnham, 1973; Schrével, Asfaux-Foucher, and Bafort, 1977; Sinden and Strong, 1978) could now be strengthened by *in vivo* imaging via SiR-tubulin. As an example, residual sMTs of ookinetes in early oocysts were observed up to 5 days post mosquito blood meal (**Figure 4.1**, **Figure 3.6**). This was previously suggested by (Garnham et al., 1969). In addition, oocyst development commenced in many cases inside a midgut epithelial cell as it was previously suggested by (Vanderberg, Rdodin, and Yoeli, 1967)(**Figure 3.6**).

However, the advantage of using SiR-tubulin is in quantifying e.g. the length of microtubules, which is almost impossible by TEM even using serial sectioning. The insights obtained by SiR-tubulin combined with SEM, TEM, 3D modelling of TEM serial sections and parasite transmission experiments performed during this study led to an understanding of the importance of microtubule numbers and length during *Plasmodium* sporozoite development and beyond.

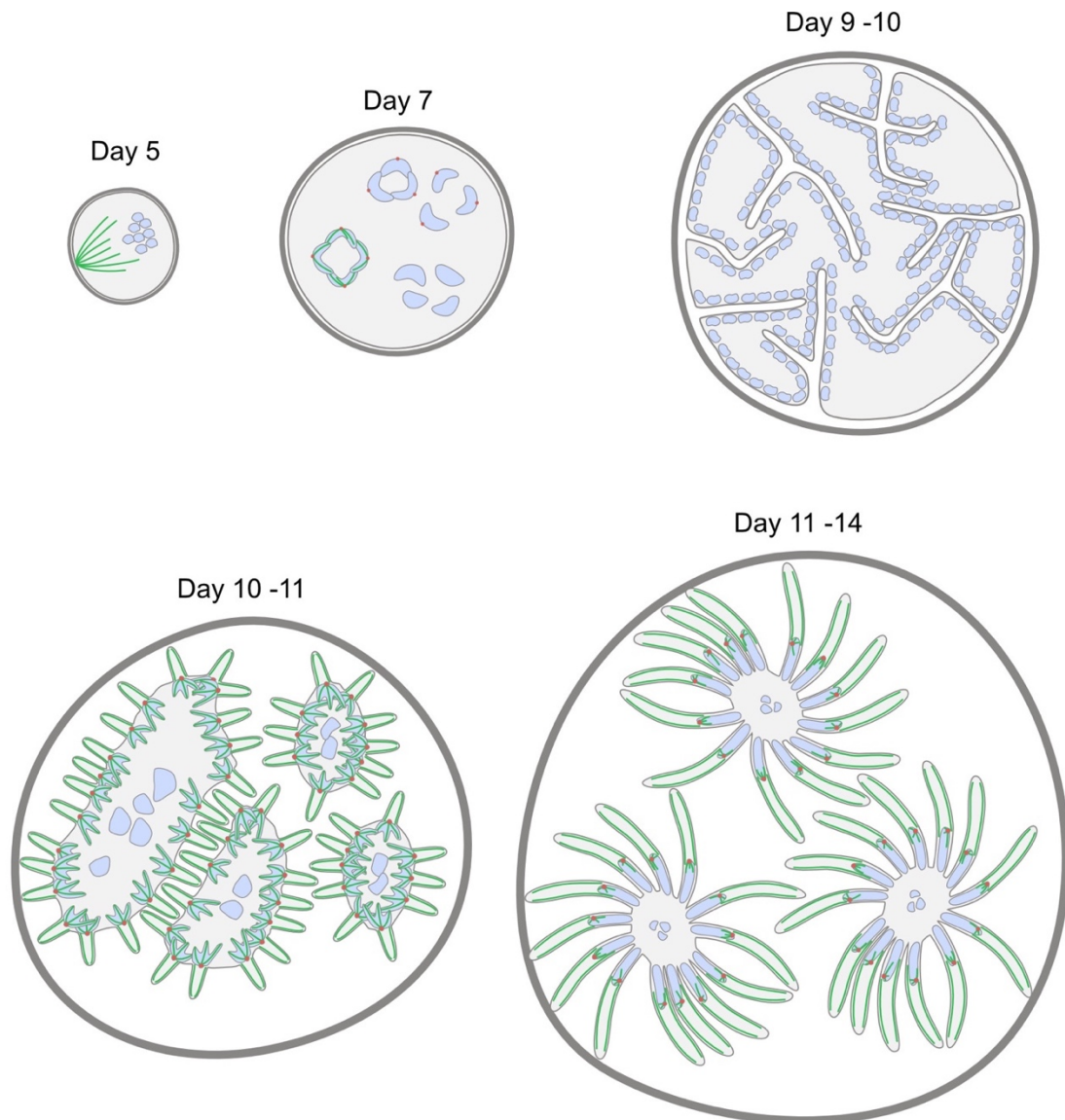


Figure 4.1. Schematic representation of a developing oocyst with a focus on microtubules. Oocysts still show left-over subpellicular microtubules (green) of the preceding ookinete stage up to 5 days post mosquito blood meal. Between day 5 and day 10, multiple asynchronous nuclear divisions in the absence of cytokinesis occur until approximately a thousand nuclei are formed within the multinucleate oocyst. Due to endomitosis which involves nuclei replication without disintegration of the nuclear membrane, hemispindle microtubules (green) are located inside the nucleus and are attached at a spindle pole plaque (red; also called centriolar plaque, MTOC) which is embedded in the nuclear membrane. From day 10 post blood meal, the plasma membrane invaginates followed by nuclei alignment to the membrane. Sporozoite budding including the formation of subpellicular microtubules starts from day 10 onwards. The nucleus is pulled into the budding sporozoite and hemispindle microtubules start to be disassembled after the sporozoite reaches approximately half its final length. It is estimated to take two to three days until fully formed sporozoites are released.

4.1. Nuclear segregation can occur in the absence of microtubules but microtubules are important to sustain nuclear integrity

The deletion of $\alpha 1$ -tubulin only showed a phenotype after nuclear division was already completed during oocyst development. Hemispindle microtubules (hMTs) were never found via fluorescence microscopy and TEM during mid and late $\alpha 1(-)$ oocyst development suggesting no complementation by $\alpha 2$ -tubulin (**Figure 3.18**). Only during nuclear replication in very early oocysts, SiR-tubulin plaques next to nuclei but no hMTs exceeding these plaques were identified in the $\alpha 1(-)$ (**Figure 3.15**). SiR-tubulin is based on docetaxel thus binding to β -tubulin and fluoresces when bound to microtubules (Lukinavičius et al., 2014) suggesting the occurrence of short microtubules within these SiR-tubulin plaques. Similar plaques are also identified for *P. falciparum* nuclei with different anti-microtubule reagents and are interpreted as tubulin-rich spindle pole plaques (SPP; also known as microtubule organizing centers (MTOCs) or centriolar plaques) which are also visible by TEM (Read et al., 1993; Fennell et al., 2006; Fennell, Al-shatr, and Bell, 2008; Arnot, Ronander, and Bengtsson, 2011; Gerald, Mahajan, and Kumar, 2011). These tubulin-rich plaques show similarities to centrin-labelling in *P. falciparum* (Mahajan et al., 2008), a protein located in SPPs. However, whether the SPPs seen in early $\alpha 1(-)$ oocysts contain short hMTs or whether the SiR-tubulin dye just labels the SPP itself is difficult to state. Furthermore, even in WT oocysts, hemispindles were only occasionally identified with SiR-tubulin due to their faint signal, which was overexposed by the strong microtubule signal of surrounding midgut cells. Attempts to detach very early oocysts from the mosquito midgut to reduce background signal were unsuccessful. TEM analysis never revealed any hMTs but only microtubule-free SPPs (**Figure 3.18**). SPPs were electron dense, therefore, very short microtubules might be difficult to be identified and the investigated numbers of early oocyst by TEM were low. As a consequence, it would be helpful to increase sample numbers of TEM, because this seems to be the only method appropriate to identify hMTs within early oocyst development.

Assuming that small hMTs occur in the SPPs, the question would still be what α -tubulin source is available during early oocyst development. Due to the deletion of $\alpha 1$ -tubulin, the predominant α -tubulin source was eliminated. However, other potential α -tubulin sources might exist: $\alpha 2$ -tubulin revealed very low expression levels during oocyst development ($\alpha 2$ -tubulin expression levels were ~ 100 -fold lower than $\alpha 1$ -tubulin, **Figure 3.11**). Whether this is sufficient for hemispindle formation is questionable. Another source of α -tubulin might be $\alpha\beta$ -tubulin heterodimers of the preceding ookinete stage. These could either be non-incorporated tubulin heterodimers or heterodimers, which are incorporated in the ookinete sMTs. Ookinete

sMTs were seen up to 5 days post blood meal (**Figure 3.15**). Once disassembled, these tubulin heterodimers could be used for hemispindle formation. Data on the half-life of tubulin in *Plasmodium* is not existing, but investigations on e.g. slime mold *Physarum* revealed, that the half-life of tubulin can strongly vary depending on the developmental stage from 1 hour to over 15 hours (Ducommun and Wright, 1989). This shows, that an organism can strongly regulate the half-life of a protein according to its needs. Therefore, $\alpha 2$ -tubulin of the preceding ookinete stage may last days and represent the source of α -tubulin during very early *al(-)* oocyst development.

Independent of this, SiR-tubulin plaques were never found during later nuclear replication in the *al(-)* parasite line although nuclear division took place. This suggests, that nuclear segregation in *Plasmodium* can occur in the absence of microtubules. However, no conclusions can be made so far on the integrity of chromosomes but performing fluorescent *in situ* hybridization (FISH) on nuclei of sporozoites would give further insights.

Similar observations were found in fission yeast (Castagnetti, Oliferenko, and Nurse, 2010) where nuclear division and progression into the next cell cycle takes place in the absence of mitotic spindles. However, it was also shown that fission yeast nuclear division requires filamentous actin therefore possibly reflecting a primitive nuclear division process independent of spindle microtubules. Whether this is also the case for *Plasmodium* cannot be stated to date. Further experiments on the role of actin during oocyst development would be necessary. In summary, both studies might change the overall understanding of how nuclear segregation can occur (Schneider and Lénárt, 2017).

4.1.1. Hemispindle microtubules are most likely important to sustain nuclear integrity

In previous reports, the total number of hMTs in wild type *P. falciparum* oocysts were determined via serial sections. Numbers varied from 35 to 60 per hemispindle (Sinden and Strong, 1978). In case of the 35-microtubule hemispindle, 14 microtubules were ending at kinetochores and thus correlated well with the number of chromosomes. However, this means that the majority of hMTs are involved in functions other than tethering the kinetochores. Using fluorescent microtubule labelling, long hMTs (2-4 μm) were first identified in *P. falciparum* blood-stages (Read et al., 1993; Fennell et al., 2006; Fennell, Al-shatr, and Bell, 2008). This was in contradiction to the previously detected size of early assembled hMTs by TEM, which only showed a maximum length of $\sim 1 \mu\text{m}$ (Aikawa and Beaudoin, 1968; Schrével, Asfaux-Foucher, and Bafort, 1977; Prensier and Slomianny, 1986; Sinou et al., 1998). It was proposed, that these elongated hMTs might represent later hMTs therefore increasing in size, but no

conclusions were made upon their function or whether these microtubules represent non-kinetochore microtubules. The main focus stayed on the kinetochore hMTs whereas non-kinetochore microtubules almost did not get any attention (Morrissette and Sibley, 2002b, 2002a; Striepen et al., 2007; Gerald, Mahajan, and Kumar, 2011; Suvorova et al., 2015).

It is very interesting in that context, that SiR-tubulin stained late oocysts revealed up to 14.5 μm long hMTs which originated from sporoblast membrane aligned nuclei into the sporoblast lumen where they ended at Hoechst stains (**Figure 3.9**). A similar observation was also found in tomograms and TEM images, where early WT budding sporozoites showed nuclei with “spike”-like extensions facing into the sporoblast (**Figure 3.20** and **Figure 3.21**) (Kübler, 2017). hMTs were identified within these nucleus extensions and ended at the nuclear envelope. Whether the microtubules were attached to the nuclear envelope via a linker protein could not be identified.

$\alpha 1(-)$ budding sporozoites were missing both, hMTs and the “spike”-like extensions (**Figure 3.20** and **Figure 3.21**). A loss of hemispindle and sMTs in $\alpha 1(-)$ parasites resulted in mostly nuclei-free budding sporozoites, however, nuclear alignment to the sporoblast membrane was not impaired (**Figure 3.15**, **Figure 3.16** and **Figure 3.20**). The nuclear alignment is most probably performed by the rootlet fiber, which is tethering the nucleus spindle pole plaque to the apical polar ring of the budding sporozoite (Francia et al., 2012). Therefore, missing hMTs might not impact nuclear alignment to the sporoblast surface but hMTs may have an important function in nuclei contraction and subsequent packaging into the budding sporozoites. As a result, besides the classical model that microtubules are important for chromosome segregation, hMTs in *Plasmodium* are most likely involved in nuclear organization and in maintaining nucleus integrity after the process of nuclear division. This would explain the excess amount of non-kinetochore microtubules found in hemispindle tomograms (Sinden and Strong, 1978) and the long hMTs identified in this study.

In case of sporozoites with fewer sMTs ($\alpha 1^{cm\&\Delta intrans}$, $\alpha 2^{+++}$), sporozoites contained nuclei with a wide range of sizes and sometimes, sporozoites did not even contain any nuclei (**Figure 3.31**). This again either suggests a partial malfunction in packaging the nucleus into the budding sporozoite or it could be explained by a reduced number or length of hMTs which only partially maintain integrity of nuclei during nuclear reorganization. As serial sections or tomography were not performed to assess hemispindle numbers for those parasite lines, it can only be speculated that parasites with reduced numbers or length of sMTs also show a reduced number or length for hMTs during sporozoite development.

4.1.2. Cell cycle checkpoints seem to be absent during oocyst development

The circumsporozoite protein (CSP) is the major surface protein of sporozoites (Yoshida et al., 1980, 1981; Aikawa et al., 1981) and the onset of strong CSP expression is adjusted to the time when sporozoite budding commences at around day 10 post blood meal (**Figure 3.11**). Therefore, it is a good indicator, whether oocyst development is delayed or stopped by e.g. activated cell cycle checkpoints. In this study, one *al(-)* parasite line was generated in a parasite line expressing mCherry under the control of the CSP promoter. mCherry was expressed with the onset of CSP expression during sporozoite budding. Hence, not just RT-PCR data could be analyzed, but also protein content and developmental progress via fluorescent microscopy. Fluorescence microscopy data showed, that CSP expression and oocysts development is delayed in *al(-)* parasites at day 12 post feed (**Figure 3.13**). Furthermore, RT-PCR showed a reduced CSP expression in *al(-)* oocysts on day 12 and day 14 post blood meal (**Figure 3.13**). These findings indicate a delay during late *al(-)* oocysts development and could be explained by a prolonged nuclear segregation or a prolonged nuclear alignment of nuclei to the sporoblast surface caused by missing hemispindle microtubules. Furthermore, sporozoite budding could still be identified until day 26 post blood meal and might even exist beyond this time point (data not shown) suggesting no checkpoint control during *Plasmodium* sporogony as previously suggested for *Plasmodium* schizogony (Gerald, Mahajan, and Kumar, 2011).

4.2. α 1-tubulin is essential for sporozoite formation but the deletion of α 1-tubulin can be partially rescued by α 2-tubulin

4.2.1. α 1-tubulin has no important function during blood stage development

Introduction of foreign DNA is performed on merozoites with selection during the asexual blood stage. Therefore, characterization of a genetically modified parasite line always starts with the analysis of blood stage parasites. Modification of the *α 1-tubulin* locus was shown to result in viable parasites with no impairment during blood stage growth but malformations during oocyst development (Konert, 2014). The deletion of the entire *α 1-tubulin* or *α 2-tubulin* gene locus was originally published to be lethal with no viable parasites formed (Kooij et al., 2005). In contrast, I showed here that *α 1(-)* parasites displayed no significant difference to WT for parasitic blood stage growth or mouse survival (**Figure 3.12**). This observation was confirmed by the recently published *in vivo* genetic knockout screen on *P. berghei* blood stages (Bushell et al., 2017). This means that α 1-tubulin is not needed during parasite blood stage development, although low levels of α 1-tubulin expression were found during RNA sequencing (Otto et al., 2014). Western immunoblotting approaches formerly reported a predominant expression of α 1-tubulin in asexual blood stages (Fennell, Al-shatr, and Bell, 2008) and α 2-tubulin to be only specifically expressed in sexual stages (Rawlings et al., 1992). However, this was already partially contested by the analysis of GFP expression controlled by the two α -tubulin promoters, which showed that α 2-tubulin is expressed throughout all blood stages and expression is highly increased in male gametocytes (Kooij et al., 2005). RNA sequencing revealed a predominant expression of *α 2-tubulin* throughout all blood stages (α 2/ α 1: gametocytes: ~50x, 4h ring: ~34x, 16h trophozoite: ~76x, 22h schizont: ~33x) (Otto et al., 2014), which would at least partially explain why a deletion of *α 1-tubulin* does not show any major fitness costs during blood stage development.

4.2.2. α 1-tubulin is essential for nuclei packaging and microneme positioning into sporozoites

Oocyst numbers were not reduced in *α 1(-)* parasites suggesting that exflagellation, zygote and ookinete formation and penetration of the midgut epithelial cells by ookinetes is not impaired in the absence of α 1-tubulin (**Figure 3.12**). Nuclear replication and segregation during oocyst development was comparable to WT and is therefore suggested to be functional (**Figure 3.14**, **Figure 3.15** and **Figure 3.16**). Nuclear alignment including the correct orientation of the nucleus with its spindle pole plaque facing towards the budding sporozoite, the Golgi apparatus,

the rootlet fiber with attached vesicles that are presumably transported to the front of the budding sporozoite and the *de novo* formation of the rhoptries at the apical tip of the sporozoites are all present in *al(-)* sporozoites (**Figure 3.20** and **Figure 3.21**) (Bannister et al., 2000; Schrevel et al., 2007). However, during later budding, wild type sporozoites elongated in a straight cone-like fashion, pulled in their nuclei after half of the budding had taken place and formed micronemes during final sporozoite budding (**Figure 3.20**, **Figure 3.21** and **Figure 3.22**) (Bannister et al., 2000, 2003; Schrevel et al., 2007). All these developments could not be observed for *al(-)* parasites. *al(-)* budding sporozoites were very malformed showing many extrusions, nuclei were not pulled into the budding sporozoites and stayed at the sporoblast/sporozoite interphase and micronemes could not be identified during later budding (**Figure 3.20**). This suggests that microtubules are essential for several processes during sporozoite budding: The loss of a straight sporozoite formation can be best explained by the loss of pellicle stabilization in case of no sMTs. However, the “stuck” nuclei at the sporoblast/sporozoite interphase is contradicting to a previous suggestion that the nucleus is only pulled into the budding sporozoite via the rootlet fiber (Sinden and Matuschewski, 2005). The *al(-)* results do not exclude that the rootlet fiber is involved in nuclear packaging, however, without the presence of microtubules no packaging occurs. Therefore, two possible ways of how to get the nucleus into the sporozoite are hypothesized: The nucleus could either be actively transported into the budding sporozoites by minus-directed motor proteins (dynein or kinesin) using sMTs as their intracellular tracks, or the nucleus could be passively transported only by its rootlet fiber tether. In the latter case, the pellicle and the microtubules would be built around the nucleus to squeeze it into an elongated shape fitting into the budding sporozoite. The force needed could be achieved by the rootlet fiber tether which does not elongate in length as fast as the pellicle and sMT formation (Schrevel et al., 2007) hence just keeping the nucleus in place until the pellicle is built around it. The counterforce and stability needed could be achieved by the sMTs. After the nucleus is inside the budding sporozoite, the rootlet fiber disappears (Schrevel et al., 2007). Tethering the nucleus to the subpellicular network would thus keep it in place during further budding and beyond. Indeed tethers linking the IMC to the nucleus were identified by cryo-electron tomography (Kudryashev et al., 2010). In case of missing or reduced numbers of sMTs, the already formed pellicle of an early budding sporozoite is not as stabilized and cannot raise the counterforce needed to get the nucleus into the budding sporozoite. Reduced microtubule numbers also result in fewer intracellular roads and therefore less motor force in case of active transport. Furthermore, a potential narrow entry site at the sporozoite/sporoblast interphase arising from a reduced-sized sMT “cage” might further

impede entry of the nucleus (**Figure 3.18** and **Figure 3.20**). However, independent of how the nucleus gets stuck at the sporozoite/sporoblast interphase in parasites lacking microtubules, the rootlet fiber tether prevents further sporozoite elongation until the rootlet fiber disappears during later sporozoite budding. During this time window, ongoing pellicle formation could lead to an excess amount of pellicle which would in turn explain the extrusion formation found in parasite lines with reduced SMTs.

Both hypotheses are plausible and it cannot be stated whether the nucleus is actively transported or passively pulled into the budding sporozoite with the current data. Indeed, both might occur. Hence, further experiments are necessary to gain more insights in nuclear packaging. Possible approaches would be to knockout either striated fiber assemblins (SFA) which form the rootlet fiber or minus-directed microtubule motor proteins. However, one problem of an SFA knockout could be that nuclei cannot be aligned to the sporoblast surface anymore hence excluding nuclear packaging into sporozoites. Long term *in vivo* imaging during sporozoite budding might also give insights. However, following live sporozoite budding within a packed oocyst which is still located in a mosquito midgut is almost impossible. A possibly better option might be, to squeeze sporoblasts with attached early sporozoites out of oocysts and image them separately. Whether sporozoite development is still ongoing outside the oocysts is not currently known and might necessitate the development of new media. Growing sporozoites *in vitro* from ookinetes might be the ultimate goal to allow a better understanding of how they are formed (Warburg and Miller, 1992).

The observation, that micronemes were not found within late budding sporozoites in *al(-)* parasites (**Figure 3.20**) is in line with previous suggestions that micronemes are actively transported along microtubules of sporozoites and merozoites (Bannister et al., 2003; Schrevel et al., 2007). Missing microtubules would therefore mean that micronemes cannot be transported to the front of the budding sporozoite. Further, late oocysts of the *al(-)* parasite line showed vesicular clusters within the sporoblast, which is only rarely seen in WT oocysts (**Figure 3.23**). These vesicular structures most likely represent micronemes accumulated in the sporoblast. This observation could have two explanations: The transport of micronemes towards the sporozoite apical end is prevented because of missing intracellular SMT tracks (Bannister et al., 2003; Schrevel et al., 2007). On the other hand, after degradation of the rootlet fiber, the nucleus is no longer attached or tethered to the budding sporozoite. Thus, nuclear localization might change and *de novo* synthesized micronemes may not be located within the sporozoite but within the sporoblast. Immunofluorescent labelling of micronemal proteins would give more insights here.

4.2.3. Sporozoite “budding” might be sporozoite “invagination”

Before, I discussed the potential underlying reasons of impaired nuclei packaging into budding sporozoites and microneme localization but not how overall sporozoite budding can happen: First, sporozoite budding could occur by pushing the emerging sporozoite outwards, meaning that the sporoblast membrane would be at a “fixed” position and sporoblast size would not directly reduce over time. In contrast, sporozoite formation could occur in the other direction by elongating the pellicle towards the inside of the sporoblast and tethering the plasma membrane to it. An assumable fixed sporoblast volume would indirectly force cytoplasmic content into the budding sporozoites. This would eventually lead to a continuous reduction of sporoblast size over time. WT oocysts showed a continuous reduction in sporoblast size and sporoblasts almost disappeared during late sporozoite budding while oocyst size only slightly increased (**Figure 3.7**). This suggests that sporozoite “budding” is more of an “invagination” of pellicle and sMTs. It could therefore be discussed whether budding is the correct term in this context.

4.2.4. Complementation of the *α1(-)* parasite line with WT *α1-tubulin* or a set of *α2-tubulin* constructs rescues sporozoite formation

The phenotypes described previously could be reversed by complementing the *α1(-)* parasite line with a wild type *α1-tubulin* gene suggesting that all morphological changes are due to the deletion of the *α1-tubulin* gene locus. Furthermore, the *α1(-)* parasite line was complemented with different versions of *α2-tubulin* ($\alpha 2^+$, $\alpha 2^{++}$, $\alpha 2^{+++}$), only differing in the amount of introduced *α2-tubulin* regulatory elements (introns, exons, 3'UTR). All three parasite lines expressed $\alpha 2$ -tubulin from two copies of *α2-tubulin*, one controlled by the *α1-tubulin* promoter and the other controlled by the *α2-tubulin* promoter. One has to keep in mind, that for the $\alpha 2^+$ parasite line valine to isoleucine differences between $\alpha 1$ -tubulin and $\alpha 2$ -tubulin were not considered (**Figure 1.8**). The $\alpha 2$ -tubulin complementations resulted in a range of phenotypes all located between the phenotype described for the *α1(-)* parasite line and wild type parasites (**Figure 3.36**, **Figure 3.37** and **Figure 3.38**). All $\alpha 2$ -tubulin expressing parasite lines were able to form sporozoites, whereas infectious sporozoites were only found for ($\alpha 2^+$, $\alpha 2^{++}$) (**Table 4** and **Table 5**). This can be explained by the reduced expression level of *α2-tubulin* in case of the $\alpha 2^{+++}$ parasite line and the correspondingly reduced numbers of sMTs leading to increased malformations and non-infectious sporozoites (**Figure 3.36**, **Figure 3.37**, **Figure 3.38** and **Figure 3.42**; further discussed in chapter 4.3). However, one common observation of all $\alpha 2$ -tubulin expressing parasites was a reduced length of sMTs (**Figure 3.44**, **Table 5**). This reduced

length of sMTs might be one of the reasons which led to a reduced infectivity by mosquito bite infections of naïve NMRI mice with $\alpha 2^+$, $\alpha 2^{++}$ parasites and a delay in prepatency in case of the $\alpha 2^+$ parasite line. However, this will be further discussed in chapter 4.9. Despite the reduced infectivity one can say, that $\alpha 2$ -tubulin can at least partially take over the function of $\alpha 1$ -tubulin when expressed at high enough levels.

4.3. Reduced α -tubulin expression levels lead to fewer subpellicular microtubules (sMTs) while the α -tubulin isotype expressed defines sMT length

4.3.1. $\alpha 1$ -tubulin introns might be important for base line tubulin expression

It was previously shown for *var* gene introns, that a deletion of introns leads to *var* gene promoter activation (Frank et al., 2006). We therefore speculated, that the deletion of $\alpha 1$ -tubulin introns might also affect tubulin expression levels. However, deletion of $\alpha 1$ -tubulin introns did not lead to any obvious phenotype in sporozoite morphology (**Figure 3.29**, **Figure 3.31** and **Figure 3.32**). Nevertheless, RT-PCR data revealed that during oocyst development at day 7 post blood meal, RNA levels were reduced to about 50% of wild type levels. This reduction was not observable at day 12 when sporozoite budding occurs (**Figure 3.28**). Maximum microtubule length slightly increased in wild type sporozoites from 6.0 μm (hemolymph, median) to 6.4 μm (salivary gland, median) during sporozoite maturation, although sporozoites were shrinking by about 0.5 μm in length. This increase was not seen for $\alpha 1^{\Delta\text{introns}}$ parasites (hemolymph: 6.1 μm , median; salivary glands: 6.1 μm , median) (**Figure 3.29** and **Figure 3.44**) and not all sMTs reached the full length in $\alpha 1^{\Delta\text{introns}}$ sporozoites as wild type parasites do. These observations potentially indicate, that $\alpha 1$ -tubulin introns play a function in maintaining base line expression levels of $\alpha 1$ -tubulin. Missing introns might consequently lead to a reduced expression level of $\alpha 1$ -tubulin during early oocyst development, when tubulin expression is still relatively low compared to day 12. However, to further test this hypothesis, either RT-PCR or Western blots would have to be performed on salivary gland sporozoites to identify base line RNA levels or α -tubulin protein amounts in intron deleted parasites, respectively.

4.3.2. $\alpha 1$ -tubulin codon modification strongly reduces $\alpha 1$ -tubulin RNA levels

Additional to the intron deletion, a modification of the exons by codon modification (Konert, 2014) resulted in a strong reduction of $\alpha 1$ -tubulin expression ($\alpha 1^{\text{cm}\&\Delta\text{introns}}$, day 7 p.i.: 25x less than WT; 12 days p.i.: 12.5x less than WT, **Figure 3.28**). This reduction in expression might have several causes. Codon modification could lead to a deletion of *cis*-regulatory sequences

which are recognized by transcription factors. It was shown before that *cis*-regulatory sequences can also be located in exon sequences (Ritter et al., 2012). Besides transcription factors, RNA binding proteins (RBPs) play a crucial role in many stages of the *Plasmodium* life cycle as described in more detail in the introduction section of this thesis. Destruction of target sequences might reduce or prevent RBP binding and subsequently reduce transcript stabilization. Furthermore, also antisense long non-coding RNAs (lncRNAs) or GC-rich non-coding RNAs (ncRNA) play important roles in e.g. *var* gene activation (Amit-Avraham et al., 2015; Guizzetti, Barcons-Simon, and Scherf, 2016). A similar activation could occur for tubulin expression during oocyst development. Besides the transcriptional control, effects of mRNA secondary structures, solubility and internal stability might be an alternative explanation as shown for *E. coli* (Kane, 1995; Wu et al., 2004). In case of highly translated transcripts, RNA stability can have a strong impact on RNA half-life and therefore indirectly reduce protein expression. To test RNA stability/half-life independent of identifying the underlying reason, RNA polymerase inhibitors can be used to inhibit new RNA synthesis and remaining RNA can be investigated over time via qRT-PCR. However, getting a drug to the site of action (within mosquito midgut and into the oocysts) might not be feasible. *In vitro* treatment of infected midguts could potentially be easier; however, long-term studies will not be possible due to limited time of viable midgut and midgut oocysts *in vitro*. Again, ultimately an *in vitro* ookinete to sporozoite conversion culture will be necessary to further these studies.

4.3.3. $\alpha 2$ -tubulin regulatory elements affect α -tubulin expression levels

Besides the $\alpha 1$ -tubulin gene locus modifications, three parasite lines expressing $\alpha 2$ -tubulin instead of $\alpha 1$ -tubulin were generated ($\alpha 2^+$, $\alpha 2^{++}$, $\alpha 2^{+++}$), which only differed in the kinds of $\alpha 2$ -tubulin regulatory elements such as introns, exons or 3'UTR. Intriguingly, the kinds of $\alpha 2$ -tubulin regulatory elements introduced showed different strong impacts on $\alpha 2$ -tubulin expression levels (**Figure 3.36**). However, one cannot simply state that the more $\alpha 2$ -tubulin elements introduced, the lower the RNA levels. The $\alpha 2^+$ parasite line contained theoretically no $\alpha 2$ -tubulin regulatory elements ($\alpha 1$ -tubulin is turned into $\alpha 2$ -tubulin by minimal necessary point mutations; valine to isoleucine differences were not considered) and had the highest expression levels on day 12 post feed (40% of WT levels; mean). This was followed by the $\alpha 2^{++}$ parasite line, which contained the entire ORF (exons and introns) and the 3'UTR of the $\alpha 2$ -tubulin locus (27% of WT levels; mean). The lowest expression was observed for the $\alpha 2^{+++}$ parasite line (16% of WT levels; mean), in which only the exons of $\alpha 1$ -tubulin were replaced with $\alpha 2$ -tubulin exons (**Figure 3.36**). However, one could speculate that $\alpha 2$ -tubulin introns/3'UTR and $\alpha 1$ -

tubulin exons have a positive effect on α -*tubulin* expression during oocyst development when compared to the corresponding regulatory elements of the other α -*tubulin*. The possible underlying reasons could be oocyst specific expression of RBPs or ncRNAs specific for α 1-*tubulin* as discussed in the previous chapter. On the other hand, α 2-*tubulin* introns or 3'UTR might contain a different set of activating *cis*-regulatory sequences recognized by transcription factors, which are also expressed during oocyst development, therefore actively promoting RNA polymerase binding by e.g. modifying the local chromatin structure. However, with the data at hand, it is difficult to conclude which regulatory element is specifically responsible for higher or lower expression. Further experiments addressing shorter stretches of DNA coupled with reverse experiments would give more in dept information about tubulin expression control during oocyst development.

4.3.4. α -*tubulin* expression levels highly correlate with the number of subpellicular microtubules

As discussed above, modifications of the α 1-*tubulin* locus resulted in reduced α -*tubulin* expression levels. Additionally, reduced numbers of sMTs could be counted at the apical tip of midgut sporozoites for several parasite lines (median sMT numbers: α 1^{cm& Δ introns} = 6; α 2⁺⁺⁺ = 9; α 2⁺⁺ = 11) (**Figure 3.29** and **Figure 3.36**). This brought up the assumption that expression levels could directly correlate with sMT numbers. Testing for correlation via a semilogarithmic regression revealed a $R^2 = 0.925$ (**Figure 4.2**, right), therefore not falsifying this hypothesis. Interestingly, the α 2⁺ and α 1 ^{Δ c-term} parasite lines, which had WT like sMT numbers also showed a reduction in expression by 40% and 44%, respectively. This suggests, that reduction of expression to about half the WT level does not impair sMT numbers, but a reduction to $\sim 1/3$ reduces sMT numbers (α 2⁺⁺ = 27% of WT expression). Nevertheless, one should be reminded that these parasite lines did not express α 1-tubulin, but α 2-tubulin or a C-terminally truncated α 1-tubulin in case of the α 1 ^{Δ c-term} parasite line. Hence, a good control would be to generate a parasite line expressing two separate copies of the codon modified α 1-*tubulin* gene and determine both mRNA expression and sMT number.

The correlation between expression levels and the number of sMTs can be explained as follows: Spontaneous microtubule nucleation is a kinetically restrained process, which needs to overcome a high energy barrier. Increasing tubulin concentrations therefore increase efficiency of nucleation (Kuchnir Fygenon et al., 1995). For mammalian tubulin, approximately $>20 \mu\text{M}$ tubulin is required for spontaneous nucleation. This concentration can be reduced by template-initiated nucleation (centrosomes with bound γ -tubulin ring complexes) which only needs

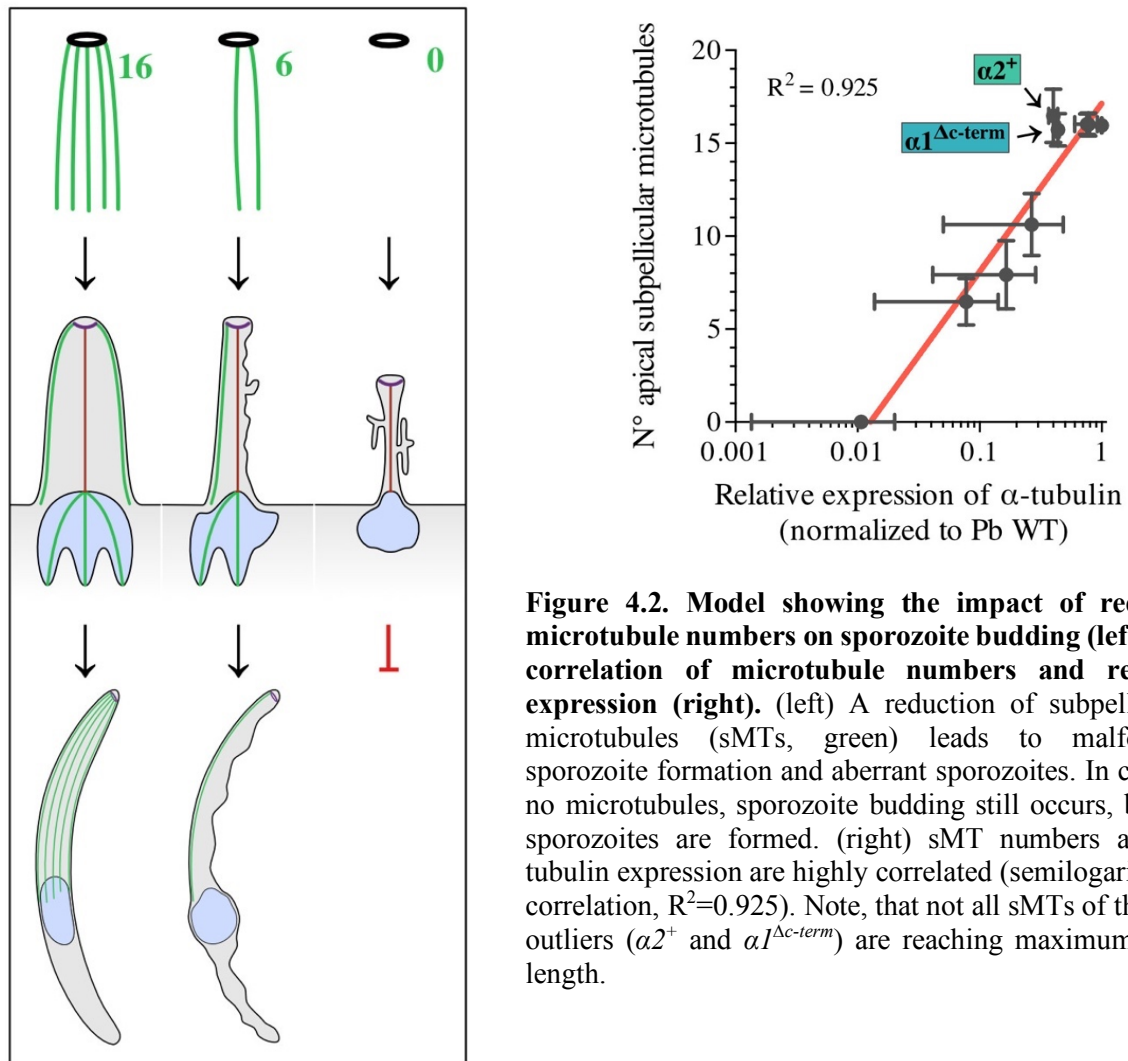


Figure 4.2. Model showing the impact of reduced microtubule numbers on sporozoite budding (left) and correlation of microtubule numbers and relative expression (right). (left) A reduction of subpellicular microtubules (sMTs, green) leads to malformed sporozoite formation and aberrant sporozoites. In case of no microtubules, sporozoite budding still occurs, but no sporozoites are formed. (right) sMT numbers and α -tubulin expression are highly correlated (semilogarithmic correlation, $R^2=0.925$). Note, that not all sMTs of the two outliers ($\alpha 2^+$ and $\alpha 1^{\Delta c-term}$) are reaching maximum sMT length.

approximately $>6 \mu\text{M}$ tubulin for nucleation. However, it is estimated that the elongation of existing microtubules only requires $>1 \mu\text{M}$ tubulin (Voter and Erickson, 1984; Wieczorek et al., 2015). In case of sporozoite budding, expression of tubulin leads to an increase of tubulin concentration over time. Once the concentration reaches the concentration needed for microtubule nucleation, nucleation will take place. Subsequent elongation of the newly nucleated microtubules will again reduce concentration levels below the level needed for nucleation. Due to the fact that elongation does not need as high concentrations, elongation can still occur while no more nucleation takes place. In case of higher expression levels, more tubulin and subsequently more nucleation events can occur in a given time, leading to an increased number of microtubules. Therefore, expression levels can directly influence the number of sMTs during sporozoite formation but only influence microtubule length when tubulin concentrations drop below a critical concentration, which is needed to keep the microtubule length in a steady state. This is in line with the findings that the length of sMTs did

not correlate with the expression levels measured (data not shown). The length seemed to be more dependent on the type of α -tubulin expressed as will be discussed in chapter 4.3.5.

Another interesting finding was that the $\alpha 2^+$ parasite line showed lower α -tubulin expression levels ($\sim 40\%$ less than WT on day 12 post blood meal) but higher maximum sMT numbers per sporozoite ($\alpha 2^+$: 19 sMTs; WT: 17 sMTs)(**Figure 3.36**). This might indicate a difference in nucleation or elongation kinetics between $\alpha 1$ -tubulin and $\alpha 2$ -tubulin which in turn might influence the time window in which nucleation can take place or reduce the nucleation barrier, therefore facilitating nucleation. This would match the needs for fast nucleation and assembly during gamete formation. Another possible explanation might be that the time point (day 12) used for RT-PCR is not ideal for capturing expression levels during microtubule nucleation. Analyzing midgut samples containing hundreds of oocysts with different developmental progress only gives an average value for a period of time. Thus, short increases or decreases in protein expression are not detectable. Analysis on a single oocyst level would be necessary but this is impossible to realize.

4.3.5. Isotypic differences between the two α -tubulins are suggested to define sMT length and the C-terminus might represent one major functional difference

Complementation of the $\alpha 1(-)$ line with $\alpha 2$ -tubulin constructs showed, that sMTs can be formed with $\alpha 2$ -tubulin with overall shorter length (**Table 5**). Statistics on testing whether the type of α -tubulin defines sMT length were not significant, most probably due to the low number of parasite lines available for comparison (three $\alpha 1$ -expressing parasite lines: WT, $\alpha 1^{\Delta introns}$, $\alpha 1^{cm\&\Delta introns}$; two to three $\alpha 2$ -expressing parasite lines: ($\alpha 2^+$), $\alpha 2^{++}$, $\alpha 2^{+++}$). However, it still suggests that $\alpha 2$ -tubulin incorporation into sMTs reduces the overall length of sMTs. This could indicate on the one hand that $\alpha 2$ -tubulin has different binding/polymerization properties influencing stability and microtubule catastrophe frequency at a given tubulin concentration. A similar effect could be shown for brain β -tubulin isotypes differing in their transitions to catastrophe 2-3-fold (Pamula, Ti, and Kapoor, 2016; Vemu et al., 2017). One possible explanation are differences in the GTP-hydrolysis rate. This was experimentally shown by introduced point mutations in the β -tubulin core, which reduced catastrophe frequencies by two-fold by keeping the GTP-state although GTP-hydrolysis has occurred (Geyer et al., 2015). Although GTP-hydrolysis is performed by β -tubulin, differences between α -tubulin isotypes might still result in conformational changes of tubulin heterodimers. Recent cryo-EM studies showed that GTP-hydrolysis leads to structural rearrangements in both α - and β -tubulin (Hyman et al., 1995; Alushin et al., 2014).

GTP-hydrolysis and subsequent catastrophe can also be accelerated by microtubule associated proteins (MAPs) such as end binding (EB) proteins (Komarova et al., 2002; Bieling et al., 2007). On the other hand, MAPs can also positively affect microtubule stability by binding across longitudinal and lateral tubulin interfaces (Roostalu, Cade, and Surrey, 2015; Zhang et al., 2017). Isozyme differences among amino acids presented on the tubulin surface might therefore affect the binding affinity and subsequently the stabilizing or destabilizing effect of MAPs. Ultrastructural studies in *T. gondii* revealed that sMTs are heavily decorated with MAP complexes and these complexes are suggested to collectively protect sMT stability (Morrissette, Murray, and Roos, 1997; Hu, Roos, and Murray, 2002; Liu et al., 2013, 2015).

Here, I showed TEM images that revealed $\alpha 2$ -formed sMT detachment from the subpellicular network and very close distances between adjacent sMTs (**Figure 3.47**). This suggests an impaired binding to MAPs or MAP complexes which in turn might influence the tether between $\alpha 2$ -formed sMTs to the subpellicular network. Classical TEM occasionally indicated connections between $\alpha 2$ -formed sMT and the SPN suggesting not a total loss of tethering (**Figure 3.47**). However, even in WT it is difficult to identify these connections. Cryo-electron tomography as performed by (Kudryashev et al., 2010) might give more detailed insights how efficiently $\alpha 2$ -formed sMTs are linked with the yet unknown linker protein to the subpellicular network, however quantitative analysis of tomograms might not be possible.

MAPs mostly bind to the C-terminus of tubulins which is highly negatively charged due to the abundance of aspartic and glutamic acid (**Figure 1.8**). The C-termini of α - and β -tubulins are sticking out of the tubule and are thus accessible for MAP binding (Nogales et al., 1999). Interestingly, one of the major differences between $\alpha 1$ -tubulin and $\alpha 2$ -tubulin in *Plasmodium* is the C-terminus, which is three amino acids shorter in case of $\alpha 2$ -tubulin. The last amino acid of $\alpha 1$ -tubulin is a tyrosine which is known for providing mechanical resistance to microtubules (Robison et al., 2016). Due to its location at the outermost tail of $\alpha 1$ -tubulin, it unlikely affects mechanical properties of microtubules, but it could do it indirectly by recruiting MAPs. This was e.g. shown for kinesin-13 family members which prefer tyrosinated microtubules as their substrate (Peris et al., 2009). Furthermore, a tyrosine kinase called Syk was shown to phosphorylate a yet unknown position in the α -tubulin C-terminus, possibly the ultimate tyrosine residue (Peters et al., 1996; Magiera and Janke, 2014).

To test whether a shortened C-terminus is leading to inefficient MAP binding and subsequently to impaired arrangements of sMTs, I generated a parasite line with a truncated *$\alpha 1$ -tubulin* C-terminus. This line showed the same phenotype as $\alpha 2$ -expressing parasite lines in terms of microtubule spacing, but no shortening in maximum microtubule length (**Figure 3.47**). This

suggests, that the C-terminus is important for MAP binding and tethering of the microtubules to the subpellicular network. However, this also suggests that the tether to the subpellicular network is not stabilizing the microtubule plus end and therefore has no influence on sMT length.

Any of the other differences between the two α -tubulin isotypes might be responsible for different binding/polymerization properties. However, during this study, those differences were not dissected in detail. A similar approach as the C-terminal truncation could be performed for all other divergent sites. Additionally, reverse experiments i.e. replacing elements of the $\alpha 2$ -*tubulin* locus by $\alpha 1$ -*tubulin* similar to the approach followed during this study could give further insights. However, due to the tremendous work and the potential difficulty of interpretation, a switch to tubulin *in vitro* assays might be a better option. *In vitro* studies would have the advantage to overcome the difficulty of addressing tubulin concentration levels for mosquito parasite stages which are only indirectly assessable via qRT-PCR which additionally only represents RNA levels of a pool of differently progressed oocysts. Furthermore, only *in vitro* assays would allow to precisely define differences in polymerization, stability and catastrophe frequency among tubulin isotypes.

4.4. Subpellicular microtubules stabilize sporozoite morphology

It was previously shown that sMTs are tethered to the subpellicular network by linker proteins (Kudryashev et al., 2010). Therefore, it is not surprising that reduced expression of α -*tubulin* and subsequently reduced sMTs had a strong impact on sporozoite morphology and infectivity. Reduced sMT numbers led to a spread of midgut sporozoite diameters measured along sporozoites. At the site of the nucleus, $\alpha 1^{cm\&\Delta introns}$ sporozoites showed a significant increase in sporozoite diameter whereas at the apical part (identified by rhoptries or micronemes), sporozoites were significantly narrower (**Figure 3.30**). Spinning disc imaging of hemolymph and salivary gland sporozoites showed that reduced sMT numbers also resulted in a loss of the characteristic crescent shape of sporozoites ($\alpha 1^{cm\&\Delta introns}$ and $\alpha 2^{+++}$ parasite lines; **Figure 3.31** and **Figure 3.37**). Many sporozoites showed straight or “S”-formations or had a strong curvature only at one side (**Figure 3.32**). Moreover, $\alpha 1^{cm\&\Delta introns}$ and $\alpha 2^{+++}$ sporozoites showed pellicle (plasma membrane, IMC, SPN) extrusions along sporozoites independent of the α -tubulin isotype used for sMT formation (**Figure 3.42**). TEM images of late budding WT parasites revealed that at sites where no microtubules were seen, the pellicle of a sporozoite got wobblier and loses its very straight formation (**Figure 3.43**). All these observations implicate, that sMTs must be important for stabilizing the sporozoite including its pellicle and giving it

the right curvature (further discussed in chapter 4.7). This suggests that a reduced sMT number results in larger areas of destabilized pellicle hence leading to the phenotypes mentioned above. These findings are summarized in combination with the $\alpha 1(-)$ data in a simplified model in (**Figure 4.2**, left). The formation of extrusions is suggested to happen during sporozoite budding as discussed in chapter 4.2.2.

4.5. The apical polar ring is not restricted to 17 microtubule nucleation sites

$\alpha 2^+$ sporozoites reached up to 19 sMTs per sporozoite (**Figure 3.36**). For WT, only up to 17 sMTs were counted. This suggests that the apical polar ring is not restricted to 17 nucleation sites. Further experiments such as cryo-electron tomography showing the apical polar ring with attached sMTs could give further insights on MT attachment and spacing in case of increased sMT numbers. Furthermore, overexpression of α -tubulin by an additional copy would show a possible maximum limit of nucleation sites.

4.6. Subpellicular microtubules are dynamic

It was long thought, that the dynamic instability naturally occurring in many microtubules is not present for sMTs in sporozoites (Cyrklaff et al., 2007). This was supported by unsuccessful attempts to target sMTs with microtubule disrupting drugs (Russell and Sinden, 1981; Bell, 1998; Morrissette and Sibley, 2002a). However, my investigations revealed that sMTs stretch along the entire length of budding sporozoites and reach up to 12.4 μm in length during very late midgut sporozoite development (median, **Figure 3.10**). However, hemolymph sporozoites only showed a sMT length of 6.0 μm (median) which then slightly increased again during sporozoite maturation in salivary gland sporozoites to 6.4 μm (median) (**Figure 3.10**). These observations demonstrate, that sMTs in sporozoites undergo some part of dynamic instability, which is defined as alternations between phases of growth and shortening.

4.7. Microtubule length mediates sporozoite length and curvature

sMTs formed with $\alpha 2$ -tubulin have the tendency to be shorter than sMTs formed with $\alpha 1$ -tubulin as discussed in chapter 4.3.5 (**Table 5**). Especially sporozoites of the $\alpha 2^+$ mutant showed a reduced maximum length of sMTs (**Figure 3.44**). Strikingly, $\alpha 2^+$ sporozoites themselves were also significantly shorter (**Figure 3.44**). This brings up the hypothesis, whether microtubules define sporozoite length. Linear regression of the maximum sMT length and sporozoite length including all characterized parasite lines revealed a strong correlation ($R^2 = 0.935$, **Figure 4.4**, right). However, this correlation does not reveal when sporozoite length is

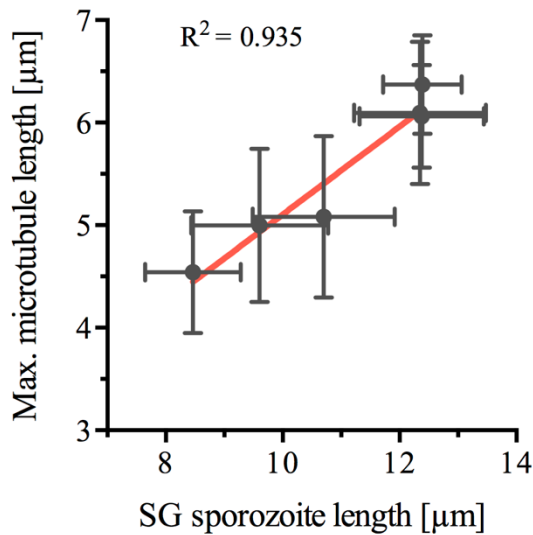


Figure 4.4. Correlation between maximum microtubule length and salivary gland (SG) sporozoite length. Linear regression was calculated with GraphPad Prism 6h. Each point represents the mean of a parasite line and the standard deviations.

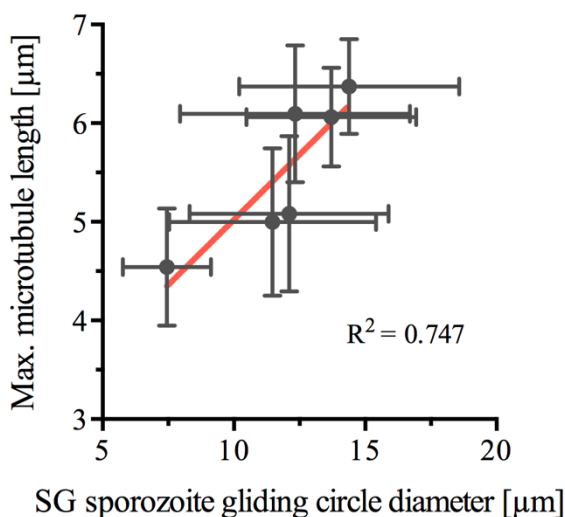


Figure 4.4. Correlation of maximum microtubule length and salivary gland (SG) gliding circle diameter. The gliding circle diameter represents sporozoite curvature. Linear regression was calculated with GraphPad Prism 6h. Each point represents the mean of a parasite line and the standard deviations.

defined by microtubules during budding. My findings that sMTs reach full sporozoite length during late sporozoite budding might be one possibility (**Figure 3.10**). On the other hand, sporozoite length could also be defined during sporozoite maturation occurring after budding. To test, whether the sporozoite length is defined by the maximum length of MTs during late budding, the $\alpha 2^+$ parasite line should be analyzed. This line had overall the shortest sMTs of all parasite lines investigated. A reduced length of sMTs in late budding $\alpha 2^+$ sporozoites compared to WT would indicate that *Plasmodium* sporozoite length is most likely defined by this maximum length during late budding. In case $\alpha 2^+$ sMTs reach WT levels during late budding, this hypothesis could be excluded. This experiment will be performed by a Bachelor student (Paul Rothhaar) and reported in his thesis, but data was not finally processed at time of writing this thesis.

Besides defining the sporozoite length, a change in sMT length also correlated with sporozoite curvature. However, this linear regression was not as significant ($R^2 = 0.747$) (**Figure 4.4**). One explanation could be that only the maximum sMT length was considered, but not all sMTs reached this maximum length (e.g. the $\alpha I^{\Delta C-term}$ parasite line). In this case, maximum sMT length is not the right measure, because it can be influenced by very few microtubules, which might not implement enough stability to affect sporozoite curvature (**Figure 4.5**). Whether microtubules directly define sporozoite curvature or whether other proteins of the subpellicular network are involved is difficult to state. However, as many spinning disc images of the $\alpha I^{cm\&\Delta introns}$ and $\alpha 2^{++}$ parasite lines (median of 6 and 9 sMTs, respectively) showed a complete or partial loss of the sporozoite crescent shape but almost all sporozoites of the parasite lines with more sMTs did, it is highly likely that microtubules are directly involved in defining sporozoite curvature (**Figure 3.31** and **Figure 3.37**). However, it cannot be excluded that it is an interplay of several components of the subpellicular network and the sMTs. It was previously shown, that sporozoite curvature establishes during sporozoite maturation during late midgut sporozoite development (Kudryashev et al., 2012). Sporozoites only showed a crescent shape when electron densities corresponding to the subpellicular network underneath the inner

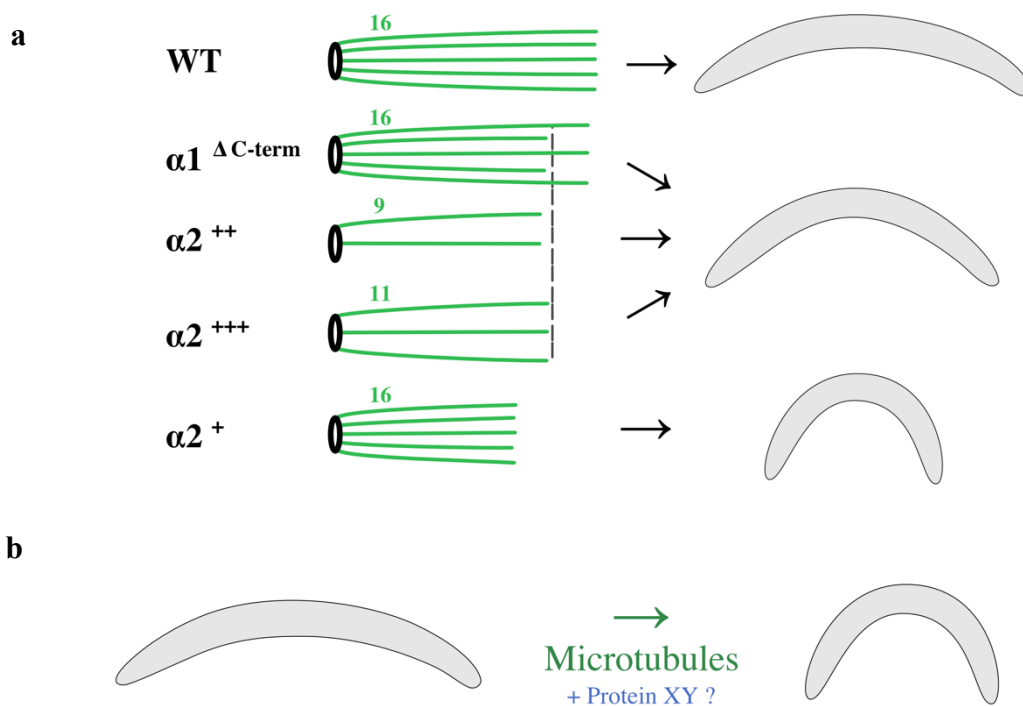


Figure 4.5. The length of subpellicular microtubules influence sporozoite curvature. (a) Model representing the hypothesis, that not the maximum length of few microtubules defines curvature, but the minimum length of many microtubules. Therefore, $\alpha I^{\Delta C-term}$ parasites show a similar curvature as the $\alpha 2$ -expressing parasites. Green numbers indicate the number of sMTs per sporozoite. (b) Microtubules play a crucial role in sporozoite curvature formation.

membrane complex were seen (Kudryashev et al., 2010). This would indicate an interplay between microtubules and proteins of the subpellicular network (SPN). PhIL1 is a protein found in the SPN of apicomplexans and was found to be important for tachyzoite morphology in *T. gondii* (Mann and Beckers, 2001). Disruption of PhIL1 resulted in shorter and wider tachyzoites (Barkhuff et al., 2011). Further, the deletion of IMC1a in *P. berghei* also revealed malformed sporozoites (Khater, Sinden, and Dessens, 2004). An interplay of such proteins with sMTs might result in the characteristic crescent shape of *Plasmodium* sporozoites.

Interestingly, sporozoite curvature is independent of the α -tubulin expressed, as sporozoites with $\alpha 2$ -tubulin formed sMTs also showed a crescent shape. This might indicate that the sporozoite curvature is independent of microtubule tethers to the subpellicular network.

4.8. Microtubule length and number influences sporozoite motility

Only the $\alpha 2^{+++}$ parasite line, which had a median of 9 sMTs per sporozoite showed a reduced ability to move (32% compared to 78% in WT) (**Figure 3.46 a**). Parasite lines with 11 or more sMTs had no significant defect (**Figure 3.46**). However, when considering the direction of movement, 21.6% of $\alpha 2^{+++}$ sporozoites and 10.3% of $\alpha 2^{++}$ sporozoites (median: 11 sMTs) were gliding in CW direction for at least 6 seconds during the 100 s video compared to 2% in WT (**Figure 3.46**). This indicates, that the number of sMTs have an impact on sporozoite gliding directionality when put onto a 2D surface. Microtubules originate at the apical polar ring in an equally spaced manner but show a polar dorsoventral distribution towards the center of the sporozoite (Kudryashev et al., 2012). When gliding on a 2D surface, the stretch of many microtubules is located at the bottom whereas the single microtubule is found at the top of the sporozoite (Kudryashev et al., 2012). Due to fewer microtubules, sporozoite dorsoventral polarity is perturbed. This might influence gliding machinery arrangements therefore leading to a shift in gliding direction more towards the 50% for each direction. Further, it was suggested that the apical polar ring tilt leads to a preference in gliding directionality (Kudryashev et al., 2012). Yet, tilting of the apical polar ring (APR) could also be found for parasite lines with fewer sMTs (**Figure 3.41**). However, the direction of the APR tilt and the stability to keep it in that position might be impaired when connected to fewer sMTs. Cryo-tomography of activated salivary gland sporozoites might be a good way of getting more insights here.

Moreover, not just the number of microtubules, but also the length or the composition of the sMTs may influence motility. As discussed in 4.3.5, the C-terminus differs between $\alpha 1$ -tubulin and $\alpha 2$ -tubulin by 3 amino acids. This might influence the affinity of microtubule associated proteins (MAPs) in the case of $\alpha 2$ -formed sMTs and subsequent tethering to the subpellicular

network (Kudryashev et al., 2010). $\alpha 2^+$ sporozoites showed differences in sMT spacing and sometimes even fully detached sMTs, which was never observed for WT sporozoites (**Figure 3.47**). A change in sMT spacing was also observed in $\alpha I^{\Delta c-term}$ sporozoites, indicating, that the C-terminus plays a major role for sMT attachment to the subpellicular network. This defect in proper sMT tethering might also impair proper dorsoventral microtubule polarity and subsequently gliding machinery anchorage. Therefore, not just the number of sMTs, but also the composition of sMTs with regard to the C-terminus might lead to improper sporozoite gliding behavior.

4.9. Subpellicular microtubule length and number define sporozoite infectivity

In the previous chapters, I pointed out the importance of sMTs on sporozoite formation and functionality. However, the effect on parasite fitness including the ability to proceed through its life cycle is of major interest. Compared to all other life cycle stages, sporozoites are the only stage, which have to cross several barriers including invasion of salivary glands, movement in the skin to actively find and invade host blood vessels and infection of hepatocytes. All other stages have to only cross one barrier or no barrier at all, e.g. merozoites have to invade erythrocytes by forming a parasitophorous vacuole and ookinetes have to cross the mosquito midgut epithelium. Therefore, decreases in sporozoite fitness may not only block or reduce transmission at one stage but can have an impact during different life cycle stages such as salivary gland invasion, movement in the host skin and liver infection. With a set of gradient sporozoite malformations generated via αI -*tubulin* modifications, it was possible to dissect important thresholds needed for successful sporozoite formation and sporozoite infectivity. To make correlations between the different quantifications more clear, morphological data combined with infectivity data is shown in (**Table 5**) and major deviations are highlighted with a green/yellow/red color code.

4.9.1. Microtubule numbers and length define salivary gland invasion efficiency

Table 5 summarizes the impact of reduced sMTs on sporozoite morphology and transmission. In short, missing sMTs completely blocked parasite transmission at the oocyst stage ($\alpha I(-)$). In case of reduced sMT numbers to a median of 6 sMTs but with normal length ($\alpha I^{cm\&\Delta introns}$), sporozoites were strongly malformed, not found in the salivary glands of mosquitos and mice infected via 10 mosquito bites stayed negative. An increase in sMT numbers to a median of 9 but with a reduced length of 4.8 μm compared to 6.0 μm in WT (median, $\alpha 2^{+++}$) resulted in

Parasite line	Midgut sporozoites			Hemolymph sporozoites				Salivary gland sporozoites							Infected mice by 10 mosquito bites / total mice (prepatency)		Infected mice by 10,000 sporozoites injected i.v. / total mice (prepatency)	
	Sporozoites / mosquito (n)	N° of apical subpellicular microtubules (n)	Subpellicular microtubule length in μm (n)	Sporozoite morphology	Sporozoites / mosquito (n)	Salivary gland invasion ratio	Subpellicular microtubule length in μm (n)	Sporozoite length (n)	Sporozoite gliding diameter (n)	Moving sporozoites (n)	Clockwise moving sporozoites (n)	Infected mice by 10 mosquito bites / total mice (prepatency)	Infected mice by 10,000 sporozoites injected i.v. / total mice (prepatency)					
WT control	88,000 (64)	16 (23)	6.0 (120)	+++	20,600 (61)	0.23	6.4 (122)	12.4 (75)	13.4 (209)	78 % (372)	2.4 % (291)	7/8 (3/9)	11/12 (3/7)					
$\alpha 1^{\Delta \text{intron}}$	59,200 (34)	16 (30)	6.1 (115)	+++	12,700 (34)	0.21	6.1 (127)	12.3 (60)	13.4 (58)	73 % (580)	2.1 % (424)	8/8 (4/4)	7/8 (4/4)					
$\alpha 1^{\Delta \text{C-term}}$	88,300 (57)	16 (40)	5.9 (69)	+++	30,000 (53)	0.34	6.2 (79)	12.4 (81)	11.2 (166)	79 % (283)	3.1 % (223)	4/4 (4/3)	4/4 (3/5)					
$\alpha 2^+$	49,700 (65)	16 (33)	4.6 (156)	++	5,400 (66)	0.11	4.5 (98)	8.5 (80)	7.2 (211)	69 % (350)	5.8 % (241)	9/12 (5/8)	7/8 (5/3)					
$\alpha 2^{++}$	92,400 (46)	11 (39)	5.5 (130)	++	12,200 (47)	0.13	5.2 (116)	10.8 (97)	11.4 (176)	74 % (316)	10.3 % (233)	8/13 (4/6)	12/12 (4/3)					
$\alpha 2^{+++}$	96,400 (34)	9 (27)	4.8 (130)	+	300 (33)	0.00	5.0 (69)	9.6 (52)	11.3 (20)	32 % (116)	21.6 % (37)	n.d.	n.d.					
$\alpha 1^{\text{cm, Amtrons}}$	59,600 (89)	6 (27)	6.1 (96)	-	6 (87)	0.00	n.a.	n.a.	n.a.	n.a.	n.a.	0/4 (∞)	n.a.					
$\alpha 1(-)$	0 (70)	0 (35)	n.a.	n.a.	0 (67)	n.a.	n.a.	n.a.	n.a.	n.a.	n.a.	n.a.	n.a.					

Table 5. Life cycle progression of all generated parasite lines. Major deviations from wild type are highlighted via a green/orange/red color code. Green numbers indicate similar values to wild type, orange indicates reduced values and red indicates strongly reduced values from wild type. n: indicates the number of investigated sporozoites; n.a.: not assessable; n.d.: not defined. The medians are shown except for sporozoite numbers (mean). Sporozoite counts and mice experiments were performed between day 17-19 post mosquito feed.

less malformed sporozoites but extrusions were still observable. Strikingly, the increase of three sMTs was enough that a small sporozoite population was able to invade salivary glands. A median of 11 sMTs per sporozoite ($\alpha 2^{++}$) even increased SG invasion rate to ~60% of WT rates (SG invasion ratio: $\alpha 2^+$: 0.3%; $\alpha 2^{++}$: 13%; WT: 23%). Addressing the sMT number of sporozoites which were able to enter the salivary glands revealed a threshold of 10 sMTs necessary to enter the glands (**Figure 3.48**). In summary, this illustrates the importance of microtubule numbers for parasite life cycle progression. Interestingly, all investigated species of *Plasmodium* form sporozoites with at least 11 sMTs (Garnham, Bird, and Baker, 1960, 1963; Garnham et al., 1961; Sinden and Strong, 1978). It suggests that the minimum number of 10 sMTs required to form infectious sporozoites in *P. berghei* determined in this study might also count for other *Plasmodium* species. This would mean, that some *Plasmodium* species have evolved their sporozoite microtubule numbers to be very close to the minimum number needed for functional and infective sporozoite formation. However, one cannot completely rule out that this minimum number differs across *Plasmodium* species. It seems to be very unlikely when considering the sporozoite requirements on stability needed to be able to cross several barriers during the *Plasmodium* life cycle.

Besides the importance of sMT numbers on sporozoite infectivity, also shorter sMTs showed a reduced SG invasion rate ($\alpha 2^+$, **Table 5**). A possible explanation could be the incorporation of $\alpha 2$ -tubulin which, resulted in detached sMTs. This suggests a lower stability of the subpellicular network and IMC possibly leading to a less stable anchorage of the gliding machinery. Myosin forces would not be fully transferred to sporozoite gliding but could be partially lost through internal “myosin/IMC movements”. A reduced gliding force would be the result which might affect salivary gland invasion efficacy. Measuring sporozoite forces via laser tweezers (Quadt et al., 2016) could give more insights.

4.9.2. Microtubule length defines sporozoite infectivity in mice

To test infectivity, we infected NMRI mice by either injecting 10,000 salivary gland sporozoites intravenously (*i.v.*) to circumvent the skin phase of sporozoite migration in the mammalian host or by letting 10 mosquitos bite per mouse. Sporozoite transmission by bite showed a decrease in infectivity for both, sporozoites with shorter sMTs ($\alpha 2^+$) and sporozoites with reduced sMT numbers ($\alpha 2^{++}$) while only $\alpha 2^+$ sporozoites showed a delay in prepatency, the onset of blood stage infection (**Table 5** and **Figure 3.49**). The prepatency delay in $\alpha 2^+$ parasites was also observed for *i.v.* infections and suggests a reduction of parasitic fitness during liver infection. As suggested previously, sporozoite curvature might be adjusted to the curvature of blood

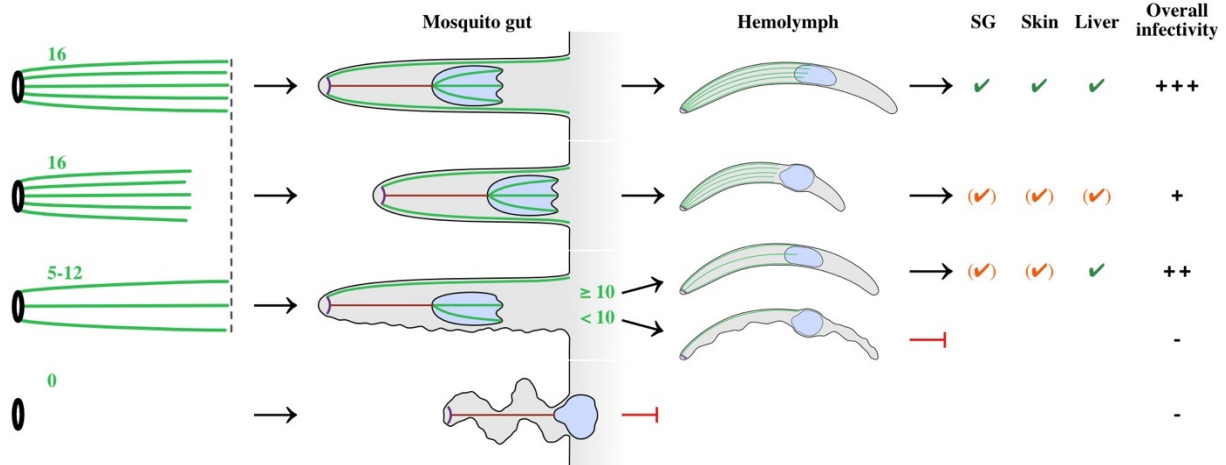


Figure 4.6. Summary model showing the impact of shorter microtubules or reduced numbers of microtubules on the formation and infectivity of sporozoites. (Left) The apical polar ring is shown in black and microtubules in green (numbers indicate microtubule numbers per sporozoite). In the mosquito gut, missing microtubules do not prevent budding, but no functional sporozoites are formed. The lower the microtubule number, the more malformations are observable. Sporozoites containing less than 10 microtubules are not able to infect the mosquito salivary gland, while sporozoites with at least 10 microtubules can enter salivary glands and be transmitted to the mammalian host. Reducing the length of microtubules leads to shorter sporozoites with increased curvature. A reduced length and a decreased number resulted in a decrease salivary gland infection rate. Both lines showed reduced infectivity in the skin, however, only reduced microtubule length reduced infectivity during liver infection. Note, that conclusions about infectivity are based on parasite lines expressing $\alpha 2$ -tubulin. Green numbers indicate the number of sMTs per sporozoite.

capillaries in the skin (Muthinja et al., 2017). A similar effect might also apply for the exit out of blood vessels in the liver. The reduced number of positive mice observed for by bite infections for both parasite lines ($\alpha 2^+$ and $\alpha 2^{++}$) suggests two independent reasons, however resulting in the same outcome. As mentioned above, $\alpha 2^+$ parasites are shorter and have an increased curvature. Curvature is suggested to play a role for identifying skin blood vessels (Muthinja et al., 2017). A change in curvature thus might reduce the probability to “run” into or associate with a capillary (smaller gliding diameter) and subsequently stay associated with it (sporozoite curvature does not match capillary curvature). Due to differences in curvature and potentially reduced amounts of gliding attachment sites, the forces needed to invade the capillary might not be as high. On the other hand, $\alpha 2^{++}$ sporozoites (median of 11 sMTs) tend to move 5 times more often in the “wrong” direction (CW) on 2D surfaces. This indicates, that a preferred direction in gliding is lost in case of fewer sMTs. In 3D environments, this could lead to a decreased displacement by an increased probability of consistent movement in a circle but not in a helical way as WT sporozoites do. This would decrease the chance of finding a blood capillary for the restricted time a sporozoite has in the skin. This might also partially apply to the $\alpha 2^+$ parasite line, which showed a two-fold increase in CW moving on 2D surfaces. Summarizing, an increase in curvature but also an increase in false directionality might lead to a decrease in infectivity in the mammalian skin. However, independent of the two hypotheses

discussed, $\alpha 2$ -tubulin incorporation into sMTs as discussed previously might also influence force transmission and sporozoite stability, and therefore efficient movement in the mammalian skin. Despite all that, one has to keep in mind, that both parasite lines had a reduced number of salivary gland sporozoites. It could therefore be that a lower number of sporozoites were injected by the 10 mosquito bites. Testing the sporozoites on their 3D-movement in e.g. Matrigel or in *in vivo* experiments within the mouse ear would give more insights on the importance of microtubule length and number for sporozoite motility in the mammalian skin. **Figure 4.6** summarizes the predominant effects of microtubule numbers and length on sporozoite formation in the midgut and hemolymph, and the impact on sporozoite infectivity on salivary glands (SG), skin and liver.

4.10. Do $\alpha 1$ -tubulin and $\alpha 2$ -tubulin have different functionalities?

Attempts to knockout *$\alpha 2$ -tubulin* resulted in non-viable parasites (Kooij et al., 2005; Bushell et al., 2017) suggesting that *$\alpha 2$ -tubulin* is essential for blood stage development. Replacement of the *$\alpha 2$ -tubulin* ORF by an *$\alpha 1$ -tubulin* ORF as performed by the Masters student Claudia Di Biagio revealed no growth rate phenotype in asexual blood stages but resulted in non-motile male gametes. The underlying mechanism is still to be investigated, but preliminary data revealed paralyzed flagella due to most probably improper axoneme formation (Biagio, 2017). Indeed, TEM showed that the axonemes were not properly assembled (Master thesis work of Nadine Renner). Only very few oocysts were found in mosquito midguts, but sporozoites were able to invade the salivary glands and subsequently re-infect naïve mice (Biagio, 2017). This strongly suggests that *$\alpha 1$ -tubulin* and *$\alpha 2$ -tubulin* can be both used for microtubule formation in asexual blood stages, but *$\alpha 1$ -tubulin* cannot substitute *$\alpha 2$ -tubulin* function during axonemal formation. On the other hand, *$\alpha 2$ -tubulin* can only partially surrogate *$\alpha 1$ -tubulin* function by forming sMTs. Thus, it is highly likely that both *α -tubulin* isotypes evolved in fulfilling highly specialized functions essential for stage specific requirements. In case of *$\alpha 2$ -tubulin*, the formation of axonemal microtubules during gametogenesis has to be finished within approximately three minutes and microtubules only have to last for ~ 30 minutes until zygote formation leads to microtubule disassembly (Sinden, Canning, and Spain, 1976; Rawlings et al., 1992). This likely requires pre-translated and stabilized mRNA and fast microtubule nucleation and assembly. On the other hand, *$\alpha 1$ -tubulin* is predominantly expressed during sporogenesis when *$\alpha 2$ -tubulin* expression is strongly reduced. Sporozoites likely form slowly over the course of 1 to 2 days, have to be able to cross several barriers (salivary gland, endothelium of blood capillaries, hepatocytes) and persist for weeks within the mosquito

salivary glands totally contrary to the requirements needed in male gametocytes. Here, stable and flexible microtubules are required, which can be tethered to the subpellicular network for stabilization of the IMC and subsequently the gliding machinery (Kudryashev et al., 2010). Hence the different sequences of $\alpha 1$ - and $\alpha 2$ -*tubulin* likely modulate rapid assembly ($\alpha 2$ -*tubulin*) versus slow assembly and persistence ($\alpha 1$ -*tubulin*).

An impaired tether to the SPN could be observed for sMTs formed from $\alpha 2$ -*tubulin* (**Figure 3.47**). In addition, $\alpha 2^+$ sporozoites showed up to 19 sMTs compared to maximum 17 found in WT although expression levels of $\alpha 2^+$ reached only 40% of WT levels (**Figure 3.36**). The increased sMT number could indicate a reduced nucleation barrier for $\alpha 2$ -*tubulin*, which would match the needs for fast nucleation and assembly during male gamete formation. As discussed in chapter 4.9, a carefully regulated microtubule number and length of sMTs is essential for efficient parasite transmission. It can therefore be suggested that a higher nucleation barrier for $\alpha 1$ -*tubulin* is advantageous to precisely regulate microtubule numbers and length to maximize sporozoite infectivity. In summary, these findings suggest a functional difference between the two α -*tubulin* isotypes.

4.11. Conclusion

The defined number of microtubules and their role in *Plasmodium* sporozoite biology have spiked my interest in finding out more about their specific function. In this study, I could show that $\alpha 1$ -*tubulin* is the isotype used for subpellicular microtubule formation in sporozoites. Furthermore, the deletion of $\alpha 1$ -*tubulin* and the subsequent absence of microtubules during sporogony did not prevent nuclear division suggesting an alternative mechanism of dividing chromosomes similar to the observations in fission yeast (Castagnetti, Oliferenko, and Nurse, 2010). Furthermore, I showed how important a precise number and length of subpellicular microtubules is for proper sporozoite formation and parasite transmission. Reducing the number in a step-wise manner by reducing the expression levels revealed a MT threshold necessary for sporozoite infectivity. Furthermore, my data suggests functional differences between the two α -*tubulin* isotypes and explains possible reasons why two α -*tubulin* isotypes have evolved. Taken together, my findings emphasize the importance of defined microtubule numbers and length in a unicellular organism to ensure efficient transmission and my data reveals functional and expressional differences of the two α -*tubulin* isotypes found in *Plasmodium*.

5. References

- Aikawa, M. (1967)** ‘Ultrastructure of the pellicular complex of *Plasmodium fallax*’, *The Journal of Cell Biology*, 35(1), pp. 103–113.
- Aikawa, M. et al. (1981)** ‘The protective antigen of malarial sporozoites (*Plasmodium berghei*) is a differentiation antigen’, *The Journal of Immunology*, 126(6), pp. 2494–2495.
- Aikawa, M. (1988)** ‘Fine structure of malaria parasites in the various stages of development’, in *Malaria: Principles and practice of malariology*. Churchill Livingstone, Edinburgh, UK, pp. 97–129.
- Aikawa, M. and Beaudoin, R. L. (1968)** ‘Studies on nuclear division of a malarial parasite under pyrimethamine treatment’, *The Journal of Cell Biology*, 39(3), pp. 749–754.
- Akella, J. S. et al. (2010)** ‘MEC-17 is an alpha-tubulin acetyltransferase’, *Nature*, 467(7312), pp. 218–22.
- Akhmanova, A. and Steinmetz, M. O. (2008)** ‘Tracking the ends: A dynamic protein network controls the fate of microtubule tips’, *Nature Reviews Molecular Cell Biology*, 9(4), pp. 309–322.
- Akhmanova, A. and Steinmetz, M. O. (2015)** ‘Control of microtubule organization and dynamics: Two ends in the limelight’, *Nature Reviews Molecular Cell Biology*, 16(12), pp. 711–726.
- Alberts, B. et al. (2014)** *Molecular Biology of the Cell*. 6th edn. New York: Garland Science.
- Alushin, G. M. et al. (2014)** ‘High-resolution microtubule structures reveal the structural transitions in $\alpha\beta$ -tubulin upon GTP hydrolysis’, *Cell*, 157(5), pp. 1117–29.
- Aly, A. S. I. and Matuschewski, K. (2005)** ‘A malarial cysteine protease is necessary for *Plasmodium* sporozoite egress from oocysts’, *The Journal of Experimental Medicine*, 202(2), pp. 225–230.
- Amino, R. et al. (2006)** ‘Quantitative imaging of *Plasmodium* transmission from mosquito to mammal’, *Nature Medicine*, 12(2), pp. 220–224.

- Amit-Avraham, I. et al. (2015)** ‘Antisense long noncoding RNAs regulate var gene activation in the malaria parasite *Plasmodium falciparum*’, *Proceedings of the National Academy of Sciences*, 112(9), pp. 982–991.
- Angrisano, F. et al. (2012)** ‘Malaria parasite colonisation of the mosquito midgut - Placing the *Plasmodium* ookinete centre stage’, *International Journal for Parasitology*, 42(6), pp. 519–527.
- Arnot, D. E., Ronander, E. and Bengtsson, D. C. (2011)** ‘The progression of the intra-erythrocytic cell cycle of *Plasmodium falciparum* and the role of the centriolar plaques in asynchronous mitotic division during schizogony’, *International Journal for Parasitology*, 41(1), pp. 71–80.
- Aurrecochea, C. et al. (2009)** ‘PlasmoDB: A functional genomic database for malaria parasites’, *Nucleic Acids Research*, 37(Database issue), pp. 539–543.
- Baer, K., Roosevelt, M., et al. (2007)** ‘Kupffer cells are obligatory for *Plasmodium yoelii* sporozoite infection of the liver’, *Cellular Microbiology*, 9(2), pp. 397–412.
- Baer, K., Klotz, C., et al. (2007)** ‘Release of hepatic *Plasmodium yoelii* merozoites into the pulmonary microvasculature’, *PLoS Pathogens*, 3(11), pp. 1651–1668.
- Balaji, S. et al. (2005)** ‘Discovery of the principal specific transcription factors of Apicomplexa and their implication for the evolution of the AP2-integrase DNA binding domains’, *Nucleic Acids Research*, 33(13), pp. 3994–4006.
- Balu, B. et al. (2011)** ‘CCR4-associated factor 1 coordinates the expression of *Plasmodium falciparum* egress and invasion proteins’, *Eukaryotic Cell*, 10(9), pp. 1257–1263.
- Banerjee, A. et al. (1990)** ‘Increased microtubule assembly in bovine brain tubulin lacking the type III isotype of β -tubulin’, *Journal of Biological Chemistry*, 265(3), pp. 1794–1799.
- Bannister, L. H. et al. (2000)** ‘Ultrastructure of rhoptry development in *Plasmodium falciparum* erythrocytic schizonts’, *Parasitology*, 121(3), pp. 273–287.
- Bannister, L. H. et al. (2003)** ‘*Plasmodium falciparum* apical membrane antigen 1 (PfAMA-1) is translocated within micronemes along subpellicular microtubules during merozoite development’, *Journal of Cell Science*, 116(18), pp. 3825–3834.

- Barkhuff, W. D. et al. (2011)** ‘Targeted disruption of TgPhiL1 in *Toxoplasma gondii* results in altered parasite morphology and fitness’, *PLoS One*, 6(8).
- Baum, J. et al. (2006)** ‘Regulation of apicomplexan actin-based motility’, *Nature Reviews Microbiology*, 4(8), pp. 621–628.
- Baum, J. et al. (2008)** ‘Host-cell invasion by malaria parasites: insights from *Plasmodium* and *Toxoplasma*’, *Trends in Parasitology*, 24(12), pp. 557–63.
- Bell, a. (1998)** ‘Microtubule inhibitors as potential antimalarial agents’, *Parasitology Today*, 14(6), pp. 234–240.
- Biagio, C. Di (2017)** *Unravelling functional and expressional differences between α -tubulin isoforms in Plasmodium berghei*. University of Heidelberg.
- Bieling, P. et al. (2007)** ‘Reconstitution of a microtubule plus-end tracking system in vitro’, *Nature*, 450(7172), pp. 1100–1105.
- Billker, O. et al. (1998)** ‘Identification of xanthurenic acid as the putative inducer of malaria development in the mosquito’, *Nature*, 392(6673), pp. 289–292.
- Bischoff, E. and Vaquero, C. (2010)** ‘In silico and biological survey of transcription-associated proteins implicated in the transcriptional machinery during the erythrocytic development of *Plasmodium falciparum*’, *BMC Genomics*, 11(1), p. 34.
- Boyle, M. J. et al. (2014)** ‘Sequential processing of merozoite surface proteins during and after erythrocyte invasion by *Plasmodium falciparum*’, *Infection and Immunity*, 82(3), pp. 924–936.
- Brouhard, G. J. and Rice, L. M. (2018)** ‘Microtubule dynamics: an interplay of biochemistry and mechanics’, *Nature Reviews Molecular Cell Biology*, pp. 1–13.
- Bullen, H. E. et al. (2009)** ‘A novel family of apicomplexan glideosome-associated proteins with an inner membrane-anchoring role’, *Journal of Biological Chemistry*, 284(37), pp. 25353–25363.
- Bunnik, E. M. et al. (2016)** ‘The mRNA-bound proteome of the human malaria parasite *Plasmodium falciparum*’, *Genome Biology*, 17(1), p. 147.

- Burda, P. C. et al. (2017)** ‘A *Plasmodium* plasma membrane reporter reveals membrane dynamics by live-cell microscopy’, *Scientific Reports*, 7(1), pp. 1–14.
- Bushell, E. et al. (2017)** ‘Functional profiling of a *Plasmodium* genome reveals an abundance of essential genes’, *Cell*, 170(2), pp. 260–272.
- Carrier, M. F. and Pantaloni, D. (1981)** ‘Kinetic analysis of guanosine 5'-triphosphate hydrolysis associated with tubulin polymerization’, *Biochemistry*, 20(7), pp. 1918–1924.
- Carlton, J. M. et al. (2008)** ‘Comparative genomics of the neglected human malaria parasite *Plasmodium vivax*’, *Nature*, 455(7214), pp. 757–763.
- Castagnetti, S., Oliferenko, S. and Nurse, P. (2010)** ‘Fission yeast cells undergo nuclear division in the absence of spindle microtubules’, *PLoS Biology*, 8(10), pp. 1–14.
- Coulson, R. M. R., Hall, N. and Ouzounis, C. A. (2004)** ‘Comparative genomics of transcriptional control in the human malaria parasite *Plasmodium falciparum*’, *Genome Research*, 14(8), pp. 1548–1554.
- Cyrklaff, M. et al. (2007)** ‘Cryoelectron tomography reveals periodic material at the inner side of subpellicular microtubules in apicomplexan parasites’, *The Journal of Experimental Medicine*, 204(6), pp. 1281–1287.
- Delves, C. J. et al. (1989)** ‘Cloning of a β -tubulin gene from *Plasmodium falciparum*’, *Molecular Microbiology*, 3(11), pp. 1511–1519.
- Dembélé, L. et al. (2014)** ‘Persistence and activation of malaria hypnozoites in long-term primary hepatocyte cultures’, *Nature Medicine*, 20(3), pp. 307–312.
- Dessens, J. T. et al. (1999)** ‘CTRP is essential for mosquito infection by malaria ookinetes’, *EMBO Journal*, 18(22), pp. 6221–6227.
- Douglas, R. G. et al. (2015)** ‘Active migration and passive transport of malaria parasites’, *Trends in Parasitology*, 31(8), pp. 357–362.
- Ducommun, B. and Wright, M. (1989)** ‘Variation of tubulin half-life during the cell cycle in the synchronous plasmodia of *Physarum polycephalum*’, *European Journal of Cell Biology*, 50(1), p. 48–55.

- Dvorak, J. A. et al. (1975)** ‘Invasion of erythrocytes by malaria merozoites’, *Science*, 187(4178), pp. 748–750.
- Elsworth, B. et al. (2014)** ‘PTEX is an essential nexus for protein export in malaria parasites’, *Nature*, 511(7511), pp. 587–591.
- Fennell, B. J. et al. (2006)** ‘Cellular and molecular actions of dinitroaniline and phosphorothioamidate herbicides on *Plasmodium falciparum*: tubulin as a specific antimalarial target’, *Molecular and Biochemical Parasitology*, 145(2), pp. 226–38.
- Fennell, B. J., Al-shatr, Z. A. and Bell, A. (2008)** ‘Isotype expression, post-translational modification and stage-dependent production of tubulins in erythrocytic *Plasmodium falciparum*’, *International Journal for Parasitology*, 38(5), pp. 527–39.
- Filarsky, M. et al. (2018)** ‘GDV1 induces sexual commitment of malaria parasites by antagonizing HP1-dependent gene silencing’, *Science*, 359(6381), pp. 1259–1263.
- Fleckenstein, H. (2016)** *α -tubulin isotype expression and specificity during sporozoite development of the rodent malaria causing parasite *Plasmodium berghei**. University of Heidelberg.
- Flyvbjerg, H., Jobs, E. and Leibler, S. (1996)** ‘Kinetics of self-assembling microtubules: An “inverse problem” in biochemistry’, *Proceedings of the National Academy of Sciences*, 93(12), pp. 5975–5979.
- Fojo, A. T. (2008)** *The Role of Microtubules in Cell Biology, Neurobiology, and Oncology*. 1st edn. Totowa, NJ: Humana Press.
- Fowler, R. E. et al. (1998)** ‘Microtubules in *Plasmodium falciparum* merozoites and their importance for invasion of erythrocytes’, *Parasitology*, 117(5), pp. 425–433.
- Francia, M. E. et al. (2012)** ‘Cell division in apicomplexan parasites is organized by a homolog of the striated rootlet fiber of algal flagella’, *PLoS Biology*, 10(12), pp. 1–14.
- Francia, M. E. and Striepen, B. (2014)** ‘Cell division in apicomplexan parasites’, *Nature Reviews Microbiology*, 12(2), pp. 125–36.

- Frank, M. et al. (2006)** ‘Strict pairing of var promoters and introns is required for var gene silencing in the malaria parasite *Plasmodium falciparum*’, *Journal of Biological Chemistry*, 281(15), pp. 9942–9952.
- Frevert, U. et al. (2005)** ‘Intravital observation of *Plasmodium berghei* sporozoite infection of the liver’, *PLoS Biology*, 3(6), pp. 1034–1046.
- Frischknecht, F. et al. (2004)** ‘Imaging movement of malaria parasites during transmission by *Anopheles* mosquitoes’, *Cellular Microbiology*, 6(7), pp. 687–694.
- Frischknecht, F., Hellmann, J. and Singer, M. (2011)** ‘Imaging motile malaria parasites’, *Imaging & Microscopy*.
- Frischknecht, F. and Matuschewski, K. (2017)** ‘*Plasmodium* sporozoite biology’, *Cold Spring Harbor Perspectives in Medicine*, 7(5).
- Fulton, C. and Simpson, P. A. (1976)** ‘Selective synthesis and utilization of flagellar tubulin. The multi-tubulin hypothesis’, *Cell Motility*, 3, pp. 987–1005.
- Garnham, P. C. C. et al. (1961)** ‘Electron microscope studies of motile stages of malaria parasites. II. The fine structure of the sporozoite of *Laverania* (= *Plasmodium*) *falcipara*’, *Transactions of the Royal Society of Tropical Medicine and Hygiene*, 55(1), pp. 98–102.
- Garnham, P. C. C. et al. (1969)** ‘Electron microscope studies on motile stages of malaria parasites VI. The ookinete of *Plasmodium berghei yoelii* and its transformation into the early oöcyst’, *Transactions of the Royal Society of Tropical Medicine and Hygiene*, 63(2), pp. 187–194.
- Garnham, P. C. C., Bird, R. G. and Baker, J. R. (1960)** ‘Electron microscope studies of motile stages of malaria parasites. I. The fine structure of the sporozoites of *Haemamoeba* (= *Plasmodium*) *gallinacea*’, *Transactions of the Royal Society of Tropical Medicine and Hygiene*, 54(3), pp. 274–278.
- Garnham, P. C. C., Bird, R. G. and Baker, J. R. (1962)** ‘Electron microscope studies of motile stages of malaria parasites III. The ookinetes of *Haemamoeba* and *Plasmodium*’, *Transactions of the Royal Society of Tropical Medicine and Hygiene*, 56(2), pp. 116–120.

- Garnham, P. C. C., Bird, R. G. and Baker, J. R. (1963)** ‘Electron microscope studies of motile stages of malaria parasites. IV. The fine structure of the sporozoites of four species of *Plasmodium*’, *Transactions of the Royal Society of Tropical Medicine and Hygiene*, 57(1), pp. 27–31.
- Gaskins, E. et al. (2004)** ‘Identification of the membrane receptor of a class XIV myosin in *Toxoplasma gondii*’, *Journal of Cell Biology*, 165(3), pp. 383–393.
- Gerald, N., Mahajan, B. and Kumar, S. (2011)** ‘Mitosis in the human malaria parasite *Plasmodium falciparum*’, *Eukaryotic Cell*, 10(4), pp. 474–82.
- Geyer, E. A. et al. (2015)** ‘A mutation uncouples the tubulin conformational and GTPase cycles, revealing allosteric control of microtubule dynamics’, *eLife*, 4, pp. 1–20.
- Ghosh, A. K. et al. (2009)** ‘Malaria parasite invasion of the mosquito salivary gland requires interaction between the *Plasmodium* TRAP and the *Anopheles* saglin proteins’, *PLoS Pathogens*, 5(1), pp. 1–13.
- Gomes-Santos, C. S. S. et al. (2011)** ‘Transition of *Plasmodium* sporozoites into liver stage-like forms is regulated by the RNA binding protein Pumilio’, *PLoS Pathogens*, 7(5).
- Guerreiro, A. et al. (2014)** ‘Genome-wide RIP-Chip analysis of translational repressor-bound mRNAs in the *Plasmodium* gametocyte’, *Genome Biology*, 15(11), p. 493.
- Guizetti, J., Barcons-Simon, A. and Scherf, A. (2016)** ‘Trans-acting GC-rich non-coding RNA at var expression site modulates gene counting in malaria parasite’, *Nucleic Acids Research*, 44(20), pp. 9710–9718.
- Hegge, S. et al. (2009)** ‘Automated classification of *Plasmodium* sporozoite movement patterns reveals a shift towards productive motility during salivary gland infection’, *Biotechnology Journal*, 4(6), pp. 903–913.
- Heintzelman, M. B. (2015)** ‘Gliding motility in apicomplexan parasites’, *Seminars in Cell and Developmental Biology*, 46, pp. 135–142.
- Hellmann, J. K. et al. (2011)** ‘Environmental constraints guide migration of malaria parasites during transmission’, *PLoS Pathogens*, 7(6), p. e1002080.

- van der Heyde, H. C. et al. (2006)** ‘A unified hypothesis for the genesis of cerebral malaria: sequestration, inflammation and hemostasis leading to microcirculatory dysfunction’, *Trends in Parasitology*, 22(11), pp. 503–508.
- Holloway, S. P. et al. (1989)** ‘Isolation of α -tubulin genes from the human malaria parasite, *Plasmodium falciparum*: sequence analysis of α -tubulin’, *Molecular Microbiology*, 3(11), pp. 1501–1510.
- Holloway, S. P. et al. (1990)** ‘The tubulin genes of the human malaria parasite *Plasmodium falciparum*, their chromosomal location and sequence analysis of the α -tubulin II gene’, *Molecular and Biochemical Parasitology*, 43(2), pp. 257–270.
- Hopp, C. S. et al. (2015)** ‘Longitudinal analysis of *Plasmodium* sporozoite motility in the dermis reveals component of blood vessel recognition’, *eLife*, 4, pp. 1–21.
- Howard, J. and Hyman, A. A. (2007)** ‘Microtubule polymerases and depolymerases’, *Current Opinion in Cell Biology*, 19(1), pp. 31–35.
- Hoyle, H. D. and Raff, E. C. (1990)** ‘Two *Drosophila* beta tubulin isoforms are not functionally equivalent’, *Journal of Cell Biology*, 111(3), pp. 1009–1026.
- Hu, K., Roos, D. S. and Murray, J. M. (2002)** ‘A novel polymer of tubulin forms the conoid of *Toxoplasma gondii*’, *Journal of Cell Biology*, 156, pp. 1039–1050.
- Hyman, A. A. et al. (1995)** ‘Structural changes accompanying GTP hydrolysis in microtubules: Information from a slowly hydrolyzable analogue guanylyl-(α,β)-methylene-diphosphonate’, *Journal of Cell Biology*, 128(1–2), pp. 117–125.
- Jacot, D. et al. (2016)** ‘An Apicomplexan actin-binding protein serves as a connector and lipid sensor to coordinate motility and invasion’, *Cell Host and Microbe*, 20(6), pp. 731–743.
- Janke, C. (2014)** ‘The tubulin code: Molecular components, readout mechanisms, functions’, *Journal of Cell Biology*, 206(4), pp. 461–472.
- Janke, C. and Chloë Bulinski, J. (2011)** ‘Post-translational regulation of the microtubule cytoskeleton: mechanisms and functions’, *Nature Reviews Molecular Cell Biology*, 12(12), pp. 773–786.

- Janse, C. J., van der Klooster, P. F. J., et al. (1986)** ‘DNA synthesis in *Plasmodium berghei* during asexual and sexual development’, *Molecular and Biochemical Parasitology*, 20(2), pp. 173–182.
- Janse, C. J., Van Der Klooster, P. F., et al. (1986)** ‘Rapid repeated dna replication during microgametogenesis and DNA synthesis in young zygotes of *Plasmodium berghei*’, *Transactions of the Royal Society of Tropical Medicine and Hygiene*, 80(1), pp. 154–157.
- Janse, C. J., Franke-Fayard, B. and Waters, A. P. (2006)** ‘Selection by flow-sorting of genetically transformed, GFP-expressing blood stages of the rodent malaria parasite, *Plasmodium berghei*’, *Nature Protocols*, 1(1), pp. 614–623.
- Josling, G. A. and Llinás, M. (2015)** ‘Sexual development in *Plasmodium* parasites: Knowing when it’s time to commit’, *Nature Reviews Microbiology*, 13(9), pp. 573–587.
- Kafsack, B. F. C. et al. (2014)** ‘A transcriptional switch underlies commitment to sexual development in malaria parasites’, *Nature*, 507(7491), pp. 248–252.
- Kane, J. F. (1995)** ‘Effects of rare codon clusters on high-level expression of heterologous proteins in *Escherichia coli*’, *Current Opinion in Biotechnology*, 6(suppl 7), pp. 494–500.
- Kantele, A. and Jokiranta, T. S. (2011)** ‘Review of cases with the emerging fifth human malaria parasite, *Plasmodium knowlesi*’, *Clinical Infectious Diseases*, 52(11), pp. 1356–1362.
- Kappe, S. H. I., Kaiser, K. and Matuschewski, K. (2003)** ‘The *Plasmodium* sporozoite journey: A rite of passage’, *Trends in Parasitology*, 19(3), pp. 135–143.
- Keeley, A. and Soldati, D. (2004)** ‘The glideosome: A molecular machine powering motility and host-cell invasion by Apicomplexa’, *Trends in Cell Biology*, 14(10), pp. 528–532.
- Khan, I. A. and Ludueña, R. F. (1996)** ‘Phosphorylation of β III -Tubulin’, *Biochemistry*, 35(12), pp. 3704–3711.
- Khater, E. I., Sinden, R. E. and Dessens, J. T. (2004)** ‘A malaria membrane skeletal protein is essential for normal morphogenesis, motility, and infectivity of sporozoites’, *Journal of Cell Biology*, 167(3), pp. 425–432.
- Kiernan, K. (2017)** *Functional studies of novel mosquito stage-specific genes in the malaria parasite Plasmodium berghei*. Loyola University Chicago.

- Kim, G.-W. et al. (2013)** ‘Mice lacking α -tubulin acetyltransferase 1 are viable but display α -tubulin acetylation deficiency and dentate gyrus distortion’, *The Journal of Biological Chemistry*, 288(28), pp. 20334–20350.
- Klug, D. and Frischknecht, F. (2017)** ‘Motility precedes egress of malaria parasites from oocysts’, *eLife*, 6, pp. 1–32.
- Komarova, Y. A. et al. (2002)** ‘Cytoplasmic linker proteins promote microtubule rescue in vivo’, *Journal of Cell Biology*, 159(4), pp. 589–599.
- Konert, M. (2014)** *K40-acetylation of subpellicular microtubules affects malaria parasite morphogenesis*. University of Heidelberg.
- De Koning-Ward, T. F. et al. (2016)** ‘*Plasmodium* species: Master renovators of their host cells’, *Nature Reviews Microbiology*, 14(8), pp. 494–507.
- Kooij, T. W. A. et al. (2005)** ‘*Plasmodium berghei* α -tubulin II: A role in both male gamete formation and asexual blood stages’, *Molecular and Biochemical Parasitology*, 144(1), pp. 16–26.
- Kremer, J. R., Mastrorarde, D. N. and McIntosh, J. R. (1996)** ‘Computer visualization of three-dimensional image data using IMOD’, *Journal of Structural Biology*, 116(1), pp. 71–76.
- Kübler, P. (2017)** *Electron Microscopy Analysis of Microtubules in Plasmodium Sporozoites*. University of Heidelberg.
- Kuchnir Fygenon, D. et al. (1995)** ‘Spontaneous nucleation of microtubules’, *Physical Review E*, 51(5), pp. 5058–5063.
- Kudryashev, M. et al. (2010)** ‘Positioning of large organelles by a membrane-associated cytoskeleton in *Plasmodium* sporozoites’, *Cellular Microbiology*, 12(3), pp. 362–371.
- Kudryashev, M. et al. (2012)** ‘Structural basis for chirality and directional motility of *Plasmodium* sporozoites’, *Cellular Microbiology*, 14(11), pp. 1757–1768.
- Kull, F. J. and Sloboda, R. D. (2014)** ‘A slow dance for microtubule acetylation’, *Cell*, 157(6), pp. 1255–6.

Lämmermann, T. et al. (2013) ‘Neutrophil swarms require LTB4 and integrins at sites of cell death in vivo’, *Nature*, 498(7454), pp. 371–375.

Langreth, S. G. and Peterson, E. (1985) ‘Pathogenicity, stability, and immunogenicity of a knobless clone of *Plasmodium falciparum* in colombian owl monkeys’, *Infection and Immunity*, 47(3), pp. 760–766.

Lasonder, E. et al. (2008) ‘Proteomic profiling of *Plasmodium* sporozoite maturation identifies new proteins essential for parasite development and infectivity’, *PLoS Pathogens*, 4(10), p. e1000195.

Lin, J. et al. (2011) ‘A novel “Gene Insertion/Marker Out” (GIMO) method for transgene expression and gene complementation in rodent malaria parasites’, *PLoS One*, 6(12).

Lindner, S. E. et al. (2013) ‘Perturbations of *Plasmodium* Puf2 expression and RNA-seq of Puf2-deficient sporozoites reveal a critical role in maintaining RNA homeostasis and parasite transmissibility’, *Cellular Microbiology*, 15(7), pp. 1266–1283.

Lindner, S. E. et al. (2013) ‘Total and putative surface proteomics of malaria parasite salivary gland sporozoites’, *Molecular & Cellular Proteomics*, 12(5), pp. 1127–1143.

Littauer, U. Z. et al. (1986) ‘Common and distinct tubulin binding sites for microtubule-associated proteins’, *Proceedings of the National Academy of Sciences of the United States of America*, 83(19), pp. 7162–7166.

Liu, J. et al. (2013) ‘Novel thioredoxin-like proteins are components of a protein complex coating the cortical microtubules of *Toxoplasma gondii*’, *Eukaryotic Cell*, 12, pp. 1588–1599.

Liu, J. et al. (2015) ‘An ensemble of specifically targeted proteins stabilizes cortical microtubules in the human parasite *Toxoplasma gondii*’, *Mol Biol Cell*, pp. 1–47.

Long, C. A. and Zavala, F. (2017) ‘Immune responses in malaria’, *Cold Spring Harbor Perspectives in Medicine*, 7(8).

Ludueña, R. F. and Banerjee, A. (2008) ‘The isotypes of tubulin’, in Fojo, T. (ed.) *The Role of Microtubules in Cell Biology, Neurobiology, and Oncology*. Totowa, NJ: Humana Press, pp. 123–175.

- Lukinavičius, G. et al. (2014)** ‘Fluorogenic probes for live-cell imaging of the cytoskeleton’, *Nature Methods*, 11(7), pp. 731–733.
- Ma, C. et al. (2007)** ‘Mutations in alpha-tubulin confer dinitroaniline resistance at a cost to microtubule function’, *Molecular Biology of the Cell*, 18(12), pp. 4711–4720.
- Magiera, M. M. and Janke, C. (2014)** ‘Post-translational modifications of tubulin’, *Current Biology*, 24(9), pp. 351–354.
- Mahajan, B. et al. (2008)** ‘Centrins, cell cycle regulation proteins in human malaria parasite *Plasmodium falciparum*’, *Journal of Biological Chemistry*, 283(46), pp. 31871–31883.
- Mair, G. R. et al. (2006)** ‘Regulation of sexual development of *Plasmodium* by translational repression’, *Science*, 313(5787), pp. 667–669.
- Mair, G. R. et al. (2010)** ‘Universal features of post-transcriptional gene regulation are critical for *Plasmodium* zygote development’, *PLoS Pathogens*, 6(2), p. e1000767.
- Mann, T. and Beckers, C. (2001)** ‘Characterization of the subpellicular network, a filamentous membrane skeletal component in the parasite *Toxoplasma gondii*’, *Molecular and Biochemical Parasitology*, 115(2), pp. 257–268.
- Mastrorarde, D. N. (2005)** ‘Automated electron microscope tomography using robust prediction of specimen movements’, *Journal of Structural Biology*, 152(1), pp. 36–51.
- Matsuoka, H. et al. (2002)** ‘A rodent malaria, *Plasmodium berghei*, is experimentally transmitted to mice by merely probing of infective mosquito, *Anopheles stephensi*’, *Parasitology International*, 51(1), pp. 17–23.
- Matthews, K. A., Rees, D. and Kaufman, T. C. (1993)** ‘A functionally specialized alpha-tubulin is required for oocyte meiosis and cleavage mitoses in *Drosophila*’, *Development*, 117(3), pp. 977–991.
- Medica, D. L. and Sinnis, P. (2005)** ‘Quantitative dynamics of *Plasmodium yoelii* sporozoite transmission by infected anopheline mosquitoes’, *Infection and Immunity*, 73(7), pp. 4363–4369.

- Meissner, M., Ferguson, D. J. P. and Frischknecht, F. (2013)** ‘Invasion factors of apicomplexan parasites: Essential or redundant?’, *Current Opinion in Microbiology*, 16(4), pp. 438–444.
- Ménard, R. et al. (1997)** ‘Circumsporozoite protein is required for development of malaria sporozoites in mosquitoes’, *Nature*, 385(6614), pp. 336–339.
- Mitchison, T. and Kirschner, M. (1984)** ‘Dynamic instability of microtubule growth’, *Nature*, 312(5991), pp. 237–242.
- Moll, K. et al. (2008)** *Methods in Malaria Research*. Paris, France: MR4/ATCC.
- Morahan, B. J., Wang, L. and Coppel, R. L. (2009)** ‘No TRAP, no invasion’, *Trends in Parasitology*, 25(2), pp. 77–84.
- Morrisette, N. S., Murray, J. M. and Roos, D. S. (1997)** ‘Subpellicular microtubules associate with an intramembranous particle lattice in the protozoan parasite *Toxoplasma gondii*’, *Journal of Cell Science*, 110 (Pt 1, pp. 35–42.
- Morrisette, N. S. and Sibley, L. D. (2002a)** ‘Cytoskeleton of apicomplexan parasites’, *Microbiology and Molecular Biology Reviews*, 66(1), pp. 21–38.
- Morrisette, N. S. and Sibley, L. D. (2002b)** ‘Disruption of microtubules uncouples budding and nuclear division in *Toxoplasma gondii*’, *Journal of Cell Science*, 115(Pt 5), pp. 1017–25.
- Mota, M. M. et al. (2001)** ‘Migration of *Plasmodium* sporozoites through cells before infection’, *Science*, 291(5501), pp. 141–144.
- Müller, K., Matuschewski, K. and Silvie, O. (2011)** ‘The Puf-family RNA-binding protein Puf2 controls sporozoite conversion to liver stages in the malaria parasite’, *PLoS One*, 6(5).
- Münter, S. et al. (2009)** ‘*Plasmodium* sporozoite motility is modulated by the turnover of discrete adhesion sites’, *Cell Host and Microbe*, 6(6), pp. 551–562.
- Muthinja, M. J. et al. (2017)** ‘Microstructured blood vessel surrogates reveal structural tropism of motile malaria parasites’, *Advanced Healthcare Materials*, 6(6), p. 1601178.
- Neumann, B. and Hilliard, M. a (2014)** ‘Loss of MEC-17 leads to microtubule instability and axonal degeneration’, *Cell Reports*. The Authors, 6(1), pp. 93–103.

- Nicastro, D. et al. (2006)** ‘The molecular architecture of axonemes revealed by cryoelectron tomography’, *Science*, 313(5789), pp. 944–948.
- Nogales, E. et al. (1999)** ‘High-resolution model of the microtubule’, *Cell*, 96(1), pp. 79–88.
- Olotu, A. et al. (2016)** ‘Seven-year efficacy of RTS,S/AS01 malaria vaccine among young african children’, *New England Journal of Medicine*, 374(26), pp. 2519–2529.
- Otto, T. D. et al. (2014)** ‘A comprehensive evaluation of rodent malaria parasite genomes and gene expression’, *BMC Biology*, 12(1), p. 86.
- Painter, H. J., Campbell, T. L. and Llinás, M. (2011)** ‘The apicomplexan AP2 family: Integral factors regulating *Plasmodium* development’, *Molecular and Biochemical Parasitology*, 176(1), pp. 1–7.
- Pamula, M. C., Ti, S. C. and Kapoor, T. M. (2016)** ‘The structured core of human β tubulin confers isotype-specific polymerization properties’, *Journal of Cell Biology*, 213(4), pp. 425–433.
- Peris, L. et al. (2009)** ‘Motor-dependent microtubule disassembly driven by tubulin tyrosination’, *Journal of Cell Biology*, 185(7), pp. 1159–1166.
- Peters, J. D. et al. (1996)** ‘Syk, activated by cross-linking the B-cell antigen receptor, localizes to the cytosol where it interacts with and phosphorylates α -tubulin on tyrosine’, *Journal of Biological Chemistry*, 271(9), pp. 4755–4762.
- Pimenta, P. F., Touray, M. and Miller, L. (1994)** ‘The journey of malaria sporozoites in the mosquito salivary gland’, *Journal of Eukaryotic Microbiology*, 41(6), pp. 608–624.
- Portran, D. et al. (2017)** ‘Tubulin acetylation protects long-lived microtubules against mechanical ageing’, *Nature Cell Biology*, 19(4), pp. 391–398.
- Prensier, G. and Slomianny, C. (1986)** ‘The karyotype of *Plasmodium falciparum* determined by ultrastructural serial sectioning and 3D reconstruction’, *Journal of Parasitology*, 72(5), pp. 731–736.
- Prudêncio, M., Rodriguez, A. and Mota, M. M. (2006)** ‘The silent path to thousands of merozoites: The *Plasmodium* liver stage’, *Nature Reviews Microbiology*, 4(11), pp. 849–856.

- Quadt, K. A. et al. (2016)** ‘Coupling of retrograde flow to force production during malaria parasite migration’, *ACS Nano*, 10(2), pp. 2091–2102.
- Ramasamy, R. (2014)** ‘Zoonotic malaria – global overview and research and policy needs’, *Frontiers in Public Health*, 2, p. 123.
- Rawlings, D. J. et al. (1992)** ‘ α -Tubulin II is a male-specific protein in *Plasmodium falciparum*’, *Molecular and Biochemical Parasitology*, 56(2), pp. 239–250.
- Read, M. et al. (1993)** ‘Microtubular organization visualized by immunofluorescence microscopy during erythrocytic schizogony in *Plasmodium falciparum* and investigation of post-translational modifications of parasite tubulin’, *Parasitology*, 106(3), pp. 223–232.
- Reddy, B. N. et al. (2015)** ‘A bioinformatic survey of RNA-binding proteins in *Plasmodium*’, *BMC Genomics*, 16(1), p. 890.
- Risco-Castillo, V. et al. (2015)** ‘Malaria sporozoites traverse host cells within transient vacuoles’, *Cell Host and Microbe*, 18(5), pp. 593–603.
- Ritter, D. I. et al. (2012)** ‘Transcriptional enhancers in protein-coding exons of vertebrate developmental genes’, *PLoS One*, 7(5).
- Robison, P. et al. (2016)** ‘Detyrosinated microtubules buckle and bear load in contracting cardiomyocytes’, *Science*, 352(6284).
- Rodriguez, M. H. and Hernández-Hernández, F. D. L. C. (2004)** ‘Insect-malaria parasites interactions: The salivary gland’, *Insect Biochemistry and Molecular Biology*, 34(7), pp. 615–624.
- Roostalu, J., Cade, N. I. and Surrey, T. (2015)** ‘Complementary activities of TPX2 and chTOG constitute an efficient importin-regulated microtubule nucleation module’, *Nature Cell Biology*, 17(11), pp. 1422–1434.
- RTS, S. P. C. T. (2015)** ‘Efficacy and safety of RTS,S/AS01 malaria vaccine with or without a booster dose in infants and children in Africa: Final results of a phase 3, individually randomised, controlled trial’, *The Lancet*, 386(9988), pp. 31–45.
- Russell, D. G. and Sinden, R. E. (1981)** ‘The role of the cytoskeleton in the motility of coccidian sporozoites’, *Journal of Cell Science*, 50, pp. 345–359.

- Sanders, P. R. et al. (2007)** ‘Identification of protein complexes in detergent-resistant membranes of *Plasmodium falciparum* schizonts’, *Molecular and Biochemical Parasitology*, 154(2), pp. 148–157.
- Schatz, P. J., Solomon, F. and Botstein, D. (1986)** ‘Genetically essential and nonessential alpha-tubulin genes specify functionally interchangeable proteins’, *Molecular and Cellular Biology*, 6(11), pp. 3722–3733.
- Schneider, I. and Lénárt, P. (2017)** ‘Chromosome segregation: Is the spindle all about microtubules?’, *Current Biology*, 27(21), pp. 1168–1170.
- Schrevel, J. et al. (2007)** ‘Vesicle trafficking during sporozoite development in *Plasmodium berghei*: Ultrastructural evidence for a novel trafficking mechanism’, *Parasitology*, 135(1), pp. 1–12.
- Schrével, J., Asfaux-Foucher, G. and Bafort, J. M. (1977)** ‘Etude ultrastructurale des mitoses multiples au cours de la sporogonie du *Plasmodium berghei*’, *Journal of Ultrastructure Research*, 59(3), pp. 332–350.
- Shida, T. et al. (2010)** ‘The major alpha-tubulin K40 acetyltransferase alphaTAT1 promotes rapid ciliogenesis and efficient mechanosensation’, *Proceedings of the National Academy of Sciences of the United States of America*, 107(50), pp. 21517–21522.
- Sidjanski, S. and Vanderberg, J. P. (1997)** ‘Delayed migration of *Plasmodium* sporozoites from the mosquito bite site to the blood’, *American Journal of Tropical Medicine and Hygiene*, 57(4), pp. 426–429.
- Sinden, R. E. et al. (1978)** ‘Gametocyte and gamete development in *Plasmodium falciparum*’, *Proceedings of the Royal Society of London - Biological Sciences*, 201(1145), pp. 375–399.
- Sinden, R. E., Canning, E. U. and Spain, B. (1976)** ‘Gametogenesis and fertilization in *Plasmodium yoelii nigeriensis*: a transmission electron microscope study’, *Proceedings of the Royal Society of London - Biological Sciences*, 193(1110), pp. 55–76.
- Sinden, R. E. and Croll, N. A. (1975)** ‘Cytology and kinetics of microgametogenesis and fertilization in *Plasmodium yoelii nigeriensis*’, *Parasitology*, 70(1), pp. 53–65.

- Sinden, R. E. and Garnham, P. C. C. (1973)** ‘A comparative study on the ultrastructure of *Plasmodium* sporozoites within the oocyst and salivary glands, with particular reference to the incidence of the micropore’, *Transactions of the Royal Society of Tropical Medicine and Hygiene*, 67(5), pp. 631–637.
- Sinden, R. E. and Matuschewski, K. (2005)** ‘The sporozoite’, in *Molecular Approaches to Malaria*. Washington, DC: ASM Press, pp. 169–190.
- Sinden, R. E. and Strong, K. (1978)** ‘An ultrastructural study of the sporogonic development of *Plasmodium falciparum* in *Anopheles gambiae*’, *Transactions of the Royal Society of Tropical Medicine and Hygiene*, 72(5), pp. 477–491.
- Singer, M. et al. (2015)** ‘Zinc finger nuclease-based double-strand breaks attenuate malaria parasites and reveal rare microhomology-mediated end joining’, *Genome Biology*, 16(1), pp. 1–18.
- Sinha, A. et al. (2014)** ‘A cascade of DNA-binding proteins for sexual commitment and development in *Plasmodium*’, *Nature*, 507(7491), pp. 253–257.
- Sinou, V. et al. (1998)** ‘Host cell and malarial targets for docetaxel (Taxotere) during the erythrocytic development of *Plasmodium falciparum*’, *Journal of Eukaryotic Microbiology*, 45(2), pp. 171–183.
- Skillman, K. M. et al. (2011)** ‘Evolutionarily divergent, unstable filamentous actin is essential for gliding motility in apicomplexan parasites’, *PLoS Pathogens*, 7(10).
- Smith, R. C. and Barillas-Mury, C. (2016)** ‘*Plasmodium* oocysts: Overlooked targets of mosquito immunity’, *Trends in Parasitology*, 32(12), pp. 979–990.
- Sorber, K., Dimon, M. T. and Derisi, J. L. (2011)** ‘RNA-Seq analysis of splicing in *Plasmodium falciparum* uncovers new splice junctions, alternative splicing and splicing of antisense transcripts’, *Nucleic Acids Research*, 39(9), pp. 3820–3835.
- Srinivasan, S. et al. (2006)** ‘Monoclonal antibody directed against neospora caninum tachyzoite carbohydrate epitope reacts specifically with apical complex-associated sialylated beta tubulin’, *Journal of Parasitology*, 92(6), pp. 1235–1243.
- Stanisic, D. I. and Good, M. F. (2015)** ‘Whole organism blood stage vaccines against malaria’, *Vaccine*, 33(52), pp. 7469–7475.

- Sterling, C. R., Aikawa, M. and Vanderberg, J. P. (1973)** ‘The passage of *Plasmodium berghei* sporozoites through the salivary glands of *Anopheles stephensi*: an electron microscope study’, *The Journal of Parasitology*, 59(4), pp. 593–605.
- Striepen, B. et al. (2007)** ‘Building the perfect parasite: Cell division in apicomplexa’, *PLoS Pathogens*, 3(6), pp. 0691–0698.
- Sturm, A. et al. (2006)** ‘Manipulation of host hepatocytes by the malaria parasite for delivery into liver sinusoids’, *Science*, 313(5791), pp. 1287–1290.
- Sulimenko, V. et al. (2017)** ‘Regulation of microtubule nucleation mediated by γ -tubulin complexes’, *Protoplasma*, 254(3), pp. 1187–1199.
- Suvorova, E. S. et al. (2015)** ‘A novel bipartite centrosome coordinates the apicomplexan cell cycle’, *PLoS Biology*, 13(3), p. e1002093.
- Szyk, A. et al. (2014)** ‘Molecular basis for age-dependent microtubule acetylation by tubulin acetyltransferase’, *Cell*, 157(6), pp. 1405–1415.
- Tavares, J. et al. (2013)** ‘Role of host cell traversal by the malaria sporozoite during liver infection’, *The Journal of Experimental Medicine*, 210(5), pp. 905–915.
- Terzakis, J. A., Sprinz, H. and Ward, R. A. (1967)** ‘The transformation of the *Plasmodium gallinaceum* oocyst in *Aedes aegypti* mosquitoes’, *The Journal of Cell Biology*, 34(1), pp. 311–326.
- Thathy, V. et al. (2002)** ‘Levels of circumsporozoite protein in the *Plasmodium* oocyst determine sporozoite morphology’, *EMBO Journal*, 21(7), pp. 1586–1596.
- Tilley, L., Dixon, M. W. A. and Kirk, K. (2011)** ‘The *Plasmodium falciparum*-infected red blood cell’, *International Journal of Biochemistry and Cell Biology*, 43(6), pp. 839–842.
- Tran, J. Q. et al. (2012)** ‘SPM1 stabilizes subpellicular microtubules in *Toxoplasma gondii*’, *Eukaryotic Cell*, 11(2), pp. 206–216.
- Vanderberg, J. P. (1974)** ‘Studies on the motility of *Plasmodium* sporozoites’, *The Journal of Protozoology*, 21(4), pp. 527–537.

- Vanderberg, J. P. and Frevert, U. (2004)** ‘Intravital microscopy demonstrating antibody-mediated immobilisation of *Plasmodium berghei* sporozoites injected into skin by mosquitoes’, *International Journal for Parasitology*, 34(9), pp. 991–996.
- Vanderberg, J., Rdodin, J. and Yoeli, M. (1967)** ‘Electron microscopic and histochemical studies of sporozoite formation in *Plasmodium berghei*’, *The Journal of Protozoology*, 14(1), pp. 82–103.
- Vanderberg, J. and Rhodin, J. (1967)** ‘Differentiation of nuclear and cytoplasmic fine structure during sporogonic development of *Plasmodium berghei*’, *Journal of Cell Biology*, 32(3).
- Vembar, S. S. et al. (2015)** ‘The PfAlba1 RNA-binding protein is an important regulator of translational timing in *Plasmodium falciparum* blood stages’, *Genome Biology*, 16(1), p. 212.
- Vemu, A. et al. (2017)** ‘Tubulin isoform composition tunes microtubule dynamics’, *Molecular Biology of the Cell*, 28(25), pp. 3564–3572.
- Vinetz, J. M. (2005)** ‘*Plasmodium* ookinete invasion of the mosquito midgut’, *Current Topics in Microbiology and Immunology*, 295, pp. 357–382.
- Vlachou, D. et al. (2006)** ‘The developmental migration of *Plasmodium* in mosquitoes’, *Current Opinion in Genetics and Development*, 16(4), pp. 384–391.
- Voter, W. a and Erickson, H. P. (1984)** ‘The kinetics of microtubule assembly. Evidence for a two-stage nucleation mechanism’, *Biological Chemistry*, 259(16), pp. 10430–10438.
- Warburg, A. and Miller, L. H. (1992)** ‘Sporogonic development of a malaria parasite in vitro’, *Science*, 255(5043), pp. 448–450.
- Wetzel, D., Håkansson, S. and Hu, K. (2003)** ‘Actin filament polymerization regulates gliding motility by apicomplexan parasites’, *Molecular Biology of the Cell*, 14(2), pp. 396–406.
- Whitelaw, J. A. et al. (2017)** ‘Surface attachment, promoted by the actomyosin system of *Toxoplasma gondii* is important for efficient gliding motility and invasion’, *BMC Biology*. BMC Biology, 15(1), p. 1.
- WHO (2017)** ‘World malaria report’, *World Health Organization*. Geneva, p. 196.

- Wieczorek, M. et al. (2015)** ‘Microtubule-associated proteins control the kinetics of microtubule nucleation’, *Nature Cell Biology*, 17(7), pp. 907–916.
- Wu, X. et al. (2004)** ‘Codon optimization reveals critical factors for high level expression of two rare codon genes in *Escherichia coli*: RNA stability and secondary structure but not tRNA abundance’, *Biochemical and Biophysical Research Communications*, 313(1), pp. 89–96.
- Yeoh, L. M. et al. (2017)** ‘Comparative transcriptomics of female and male gametocytes in *Plasmodium berghei* and the evolution of sex in alveolates’, *BMC Genomics*, 18(1), p. 734.
- Yoshida, N. et al. (1980)** ‘Hybridoma produces protective antibodies directed against the sporozoite stage of malaria parasite’, *Science*, 207(4426), pp. 71–73.
- Yoshida, N. et al. (1981)** ‘Biosynthesis of Pb44, the protective antigen of sporozoites of *Plasmodium berghei*’, *The Journal of Experimental Medicine*, 154(4), pp. 1225–1236.
- Zhang, M. et al. (2010)** ‘The *Plasmodium* eukaryotic initiation factor-2 α kinase IK2 controls the latency of sporozoites in the mosquito salivary glands’, *The Journal of Experimental Medicine*, 207(7), pp. 1465–1474.
- Zhang, R. et al. (2017)** ‘Structural insight into TPX2-stimulated microtubule assembly’, *eLife*, 6, pp. 1–22.

6. Publications

Benjamin Spreng, Hannah Fleckenstein, Patrick Kübler, Claudia Di Biagio, Madlen Benz, Pintu Patra, Ulrich S. Schwarz, Marek Cyrklaff and Friedrich Frischknecht. ‘Microtubule number and length determine malaria parasite shape and infectivity’, will be submitted to Cell Host & Microbe

7. Acknowledgements

Mein größter Dank gilt meinem Doktorvater Freddy. Du hast mir ermöglicht dieses vielseitige und spannende Projekt durchzuführen. Dankbar bin ich Dir nicht zuletzt für zahlreiche Stunden der anregenden Diskussion. Es ist kaum messbar, was ich in dieser Zeit alles gelernt habe. Zudem möchte ich mich für die Freiheit und unbeschränkten Möglichkeiten, die Du mir all die Jahre gewährt hast, und für dein Verständnis, als Schlaf eine Mangelware war, von Herzen bedanken.

Ganz besonders bedanken möchte ich mich bei meiner Frau Lena. Du hast mir so oft den Rücken freigehalten und ohne deine Hilfe wäre diese Arbeit schlichtweg nicht zu einem Ende gekommen. Danke auch für das endlose Verständnis dafür, dass Wissenschaft so einnehmend sein kann und wenig Zeit für anderes lässt. Danke auch für Dein immer offenes Ohr, ganz egal wie langweilig für Dich manche Detailergebnisse gewesen sein mögen.

Meine Kinder Juni und Joscha haben für so viel Ausgleich gesorgt und mir immer Freude bereitet. Dank Euch wuchs mir die Arbeit nie über den Kopf. Ihr wart so geduldig und ich werde nie vergessen, wie liebevoll ihr mich jeden Abend empfangen habt.

Natürlich möchte ich mich auch bei meinen Eltern Andrea und Gerd für Eure endlose Unterstützung bedanken, ohne die all das niemals möglich gewesen wäre. Es war bisweilen eine sehr intensive Zeit, es war und ist so wertvoll für mich, dass ich immer auf euch zählen kann.

Vielen Dank auch an die besten Brüder, die man sich vorstellen kann, Flo und Tim. Ihr habt mir stets viel Kraft und Ausgleich gegeben.

Insbesondere möchte ich auch Konrad danken. Du hast mir die Ankunft in Heidelberg so leicht gemacht. Danke für die vielen Botanik Sessions und Lachsnudel-Runden und deine einmaligen Partymanager-Qualitäten. Einen besseren Kollegen und Kumpel hätte ich mir nicht wünschen können.

Ich möchte außerdem dem gesamten Lab für das hilfreiche und gemeinschaftliche Zusammenarbeiten danken. Ross, dein Humor hat mir viele tolle Momente beschert und deine Hilfe bei allen möglichen Fragen war Gold wert. Mendi, vielen Dank für die entspannten Botanik-Runden, das Korrekturlesen und die Diskussionen über Gott und die Welt. Danke Marek für alles, was du mir beigebracht hast, für all die Stunden vor dem Elektronenmikroskop und für deine lockere, weltoffene und optimistische Art. Vielen Dank Julia für die lockeren Zeiten im Office und all deine Hilfe. Danke auch an Kartik und Hirdesh für die witzigen Zeiten im Labor. Ein großer Dank gilt auch all meinen hochmotivierten Studenten Claudia Di Biagio, Hannah Fleckenstein, Christian Sommerauer, Patrick Kübler, Paul Rothhaar, Serina Khater und Mona Rheinberger. Ihr habt dazu beigetragen, dass diese Arbeit ist, was sie ist. Vielen Dank auch an Saskia, Catherine, Mirko, Dennis, Markus, Katharina, Johanna, Miriam und Jessica für hilfreiche Tipps und anregende Diskussionen und eine entspannte Atmosphäre in Labor und Office.

Außerdem möchte ich Prof. Dr. Ulrich Schwarz als Erstgutachter und für eine erfolgreiche Kollaboration danken. Zudem danke ich Silvia Portugal und Petr Chlanda für die spontane Verfügbarkeit als Prüfer.

Ein großes Dankeschön gilt darüber hinaus all jenen, die mich in über vier Jahren Heidelberg begleitet haben und mir ein wirklich schönes Doktorandendasein ermöglichen konnten.

8. Appendix

8.1. Primers

8.1.1. Generation of $\alpha I^{cm\&\Delta introns}$

Number	Primer sequence (5' to 3')
766	ACGCGTCGACGGATATTTAATGTTTTTCAGTTTTTCCACT
767	GGAATTCTTTTACTTGTATATTATAAAATAAACAATTGTTTTTAAAATATAG
768	GGAATTCATGCGTGAGGTTATCTCTATCC
769	CCTTAATTAATTAGTAATCAGCTTCGTAACCC
770	CCTTAATTAATTATTTTCTTATCATTATAATGGTAAAAAAATTA AAAAAG
771	GATATCCTTATATATATTTATACATTTTCTAAAATTATTAAACTAAT
772	CCCAAGCTTATTATTTTCTTATCATTATAATGGTAAAAAAATTA AAAAAG
773	CCGCTCGAGGATAAAACAAAGACAACTAAATAAATATAAGATAAAG
838	CGCCGGATCAAGCCGGCCGTG
839	CACGGCCGGCTTGATCCGGCG

8.1.2. Generation of $\alpha I^{\Delta introns}$

Number	Primer sequence (5' to 3')
1289	CAATTGTTTATTTTATAATATACAAGTAAAAGCCTAGGATGAGAGAAGTAA TAAGTATACATGTAG
1290	TAATTTTTTTTACCATTATAATGATAAGAAAATAATGACGTCTTAATAGTCTG CCTCATATCC

8.1.3. Generation of $\alpha I^{WTcompl.}$

Number	Primer sequence (5' to 3')
1289	CAATTGTTTATTTTATAATATACAAGTAAAAGCCTAGGATGAGAGAAGTAA TAAGTATACATGTAG
1290	TAATTTTTTTTACCATTATAATGATAAGAAAATAATGACGTCTTAATAGTCTG CCTCATATCC

8.1.4. Generation of $\alpha 2^{+++}$

Number	Primer sequence (5' to 3')
767	GGAATTCTTTTACTTGTATATTATAAAATAAACAATTGTTTTTAAAATATAG
1277	GGATATGAATAAGACGTCATTATTTTCTTATCATTATAATGGTAAAAAAAT T
1278	TGATGTTTTTTCCTTCAATTTTCGATGGGTACCGATAAAACAAAGACAACT AAATAAATATAAG
1279	GCTGGTAATTAAGATATTATAATACTCTTGTATATCTTC

Appendix

1280	AAGCTCCCTAAAGAAAAATTAATTAGAATTTTGTAATAC
1281	AAACATGTAAGGAAATAAGAATTATATATATTTCAATAAT
1282	TCTAGGGACCTGTAAAATTTGATCAAATATATATATGTG
1283	ACAATTGTTTATTTTATAATATACAAGTAAAAGAATTCATGAGAGAAGTTA TTAGCATCC
1284	AGTATTATAATATCTTTAATTACCAGCAAGCATTCCGAT
1285	ATTCTAATTAATTTTCTTTAGGGAGCTTTTTGCCTAGA
1286	TGAAATATATATAATTCTTATTCCTTACATGTTTTCCAGCCCCAG
1287	TATTTGATCAAATTTTAACAGGTCCCTAGATGTGTATTCG
1288	AGAAAATAATGACGTCTTATTCATATCCTTCATCTTCTCC
1599	CGATCGGTCGACGTTTTATGTTTTCTTAATTGTTTCTGG
1600	GCTATGGGTACCATTGTCGTGGATTAGCAACG

8.1.5. Generation of $\alpha 2^{++}$

Number Primer sequence (5' to 3')

1283	ACAATTGTTTATTTTATAATATACAAGTAAAAGAATTCATGAGAGAAGTTA TTAGCATCC
1468	GTTTTTTCCTTCAATTCGATGGGTACCCAAATCACATGATAAAAATTATTAT GC

8.1.6. Generation of $\alpha 2^{+}$

Number Primer sequence (5' to 3')

1305	ACAATTGTTTATTTTATAATATACAAGTAAAAATGAGAGAAGTAATAAGTA TACATG
1306	ACCAGGTTGTGGCAGGTGGTGATGATGCTTTTAATACCTTTTTTTCAGA
1307	CACCACCTGCCACAACCTGGTCACTAGGCATTTGACCATC
1308	GGATGTTTATTATTAGAAAGATTGGCTATTGATTATGGAAAAAATCAAAG TTAAATTTTTGTTTCATGGCCATCACC
1309	GCCAATCTTTCTAATAATAAACATCCAAGTCCACTTCCAGTACCACCTCCA ACAGCATTAACATCAAAAATCC
1310	CAGCATTGGAACCAGCATCTATGATGGCAAATGTGATCC
1311	CACATTTTGCCATCATAGATGCTGGTTCAAATGCTGAG
1312	TATAAAAACGAAAAGATCTATTCAATTTGTTGATTGGTGC
1313	AATCAACAAATTGAATAGATCTTTTCGTTTTTATAGTGGC
1625	AATTTTTTTACCATTATAATGATAAGAAAATAATTTACTCATATCCTTCATC TTCTCC

8.1.7. Generation of $\alpha 1^{\Delta c-term}$

Number Primer sequence (5' to 3')

1305	ACAATTGTTTATTTTATAATATAACAAGTAAAAATGAGAGAAGTAATAAGTATACATG
1315	ATGATAAGAAAATAATTTACTCATATCCTTCATCTTCTCC

8.1.8. Genotyping primers

Number Primer sequence (5' to 3')

187	TTCTACTGAAGAGGTTGTGGTC
417	GCTACATTCACACATACATGCG
960	TAATTCAAAGGGACGAGG
1279	GCTGGTAATTAAGATATTATAAATACTCTTGTATATCTTC
1313	AATCAACAAATTGAATAGATCTTTTCGTTTTTATAGTGCC
1598	GCAGGCATATGTAGAGCC

8.1.9. qRT-PCR primers

Number Name Primer sequence (5' to 3')

1344	<i>18S rRNA</i>	AAGCATTAAATAAAGCGAATACATCCTTAC
1345	<i>18S rRNA</i>	GGAGATTGGTTTTGACGTTTATGTG
qP3	<i>CSP</i>	GTAAACAGATCAGGGATAGTATCACAGAGG
qP4	<i>CSP</i>	TTCAGTATCAATATCTTCTAAGGTCAAATCTTCTGC
qP31	<i>$\alpha 1$</i>	CCTCCTGACCAGGCTGGTAG
qP32	<i>$\alpha 1$</i>	GGGTGAAATAACTGGCGATATGTGC
qP33	<i>$\alpha 2$</i>	GCCCAGTGATCAAGTTGTGGC
qP34	<i>$\alpha 2$</i>	CAGGGTGAAATAATTGGCGATAGGTTC
qP43	<i>$\alpha 1-cm$</i>	TCAAGCCGGCCGTGCTAAC
qP44	<i>$\alpha 1-cm$</i>	GTTCCGGATGGAACAGTTGACG
qP45	<i>$\alpha 2^+$</i>	AGCTATTTTGTTTAGAACATGGTATACAGCCC
qP46	<i>$\alpha 2^+$</i>	GTTGGTTCTAAGTCAACAAAAACACAACGT

8.2. Macros

8.2.1. Crop of EM images

```

dirsave = "/directory/";
crop_width=1;
crop_height=1;
scalebar_length=1;
name_ori=getTitle
setTool("rectangle");
makeRectangle(318, 618, 780, 714);
run("Specify...", "width=crop_width height=crop_height x=0.43 y=0.84 scaled");
waitForUser( "Selection","Select the area you want to crop.\nPress OK when you are done");
run("Duplicate...", "duplicate");
run("Invert");
name_crop=getTitle;
name_crop=replace(name_crop, "-1.tif","");
name_crop=replace(name_crop, "-2.tif","");
name_crop=name_crop+"_"+crop_width+"x"+crop_height+"µm"+"_sporoCW";
path=dirsave+name_crop;
saveAs("Tiff", path);
run("Slice Keeper", "first=1 last=34 increment=2");
name_crop=getTitle;
name_crop=replace(name_crop, "-1.tif","");
name_crop=replace(name_crop, ".tif","");
path=dirsave+name_crop;
saveAs("Tiff", path);

```

8.2.2. Spinning Disc image analysis

```

// Workflow:
// 0.) copy name of file into line 13 and names which should be deleted in the following lines
// 1.) dir = folder where to save the pictures, hast to be adjusted every time
// 2.) crop width
// 3.) slice nr.
// 4.) for all channels: auto contrast or setMinAndMax (for manual fixed dynamic range settings)
// 5.) scale bar length
// keep in mind, when saving a picture, it always changes the name -> new "getTitle" is needed afterwards

//Import of .mvd2 file
// run("Bio-Formats Importer", "");
// not_cropped=getTitle
// not_cropped=replace(not_cropped, "file name","")
// rename(not_cropped)
// not_cropped=getTitle
// not_cropped=replace(not_cropped, "(cropped)","")
// rename(not_cropped)

//
// waitForUser( "Selection","Select a folder in which you want to save the cropped sporozoite
// images.\nPress OK when you are done");
// dir = getDirectory("Choose Source Directory ");
// dir=getDirectory("image");
// dir = "/Volumes/Macintosh HD 2/Analysis/9. Oocyst SiR Hoechst/2. intracell. Oocysts/";

run("Brightness/Contrast...");
waitForUser( "Selection","Adjust brightness/Contrast to see oocyst size.\n Press OK when you are
done");

```

```

crop_width=getNumber("Enter width [in µm] for crop selection", 20);
crop_height=getNumber("Enter height [in µm] for crop selection", 20);
setTool("rectangle");
run("Specify...", "width=crop_width height=crop_height x=0.43 y=0.84 scaled");
waitForUser("Selection", "Select the area you want to crop.\nPress OK when you are done");
run("Duplicate...", "duplicate");
cropped=getTitle
// selectWindow(not_cropped);
// run("Close");
cropped=replace(cropped, "-1", "_"+crop_width+"x"+crop_height+"µm")
rename(cropped)
cropped=getTitle
path=dir+cropped
saveAs("Tiff", path);
cropped2=getTitle

waitForUser("Selection", "Choose slice you want to keep. Transfer number.\nPress OK when you
are done");
slice_nr=getNumber("Enter width [in µm] for crop selection", 2);
run("Duplicate...", "duplicate channels=1-5 slices=slice_nr");

sliced=getTitle;
sliced=replace(sliced, "-1", "_slice"+slice_nr);
// sliced=replace(sliced, "-1", "_z-proj");
rename(sliced);
sliced2=getTitle;
path=dir+sliced2;
saveAs("Tiff", path);
sliced3=getTitle
selectWindow(cropped2);
run("Close");
selectWindow(sliced3);

//Split channels
sliced3=replace(sliced3, ".tif", "")
rename(sliced3)
run("Split Channels");

//enter channel prefixes
prefixSiRTub= "C1-"; prefixHOECHST= "C2-"; prefixGFP= "C3-";
SiRTub= prefixSiRTub + sliced3; HOECHST= prefixHOECHST + sliced3; GFP= prefixGFP +
sliced3;

//Adjust B&C for each channel (select between fixed values (setMinAndMax) or AutoContrast
selectWindow(SiRTub);
// setMinAndMax(550, 1700);
run("Enhance Contrast", "saturated=0.35");
run("8-bit");
SiRTub=getTitle;

selectWindow(HOECHST);
// setMinAndMax(400, 2500);
run("Enhance Contrast", "saturated=0.35");
run("8-bit");
HOECHST=getTitle;

selectWindow(GFP);
// setMinAndMax(300, 1500);

```

```

run("Enhance Contrast", "saturated=0.35");
run("8-bit");
GFP=getTitle;

//create merged image
//standard settings in ImageJ: C1=red; C2=green; C3=blue; C4=gray; C5=cyan; C6=magenta; C7=yellow
run("Merge Channels...", "c1=["+SiRTub+"] c2=["+GFP+"] c3=["+HOECHST+"] create keep");
merge8bit=getTitle
run("RGB Color");
mergeRGB=getTitle
mergeRGB=replace(mergeRGB, "Composite", "");
mergeRGB=sliced3+" b_RGBmerge";
rename(mergeRGB);
path=dir+mergeRGB;
saveAs("Tiff", path);
mergeRGB=replace(mergeRGB, ".tif", "")
rename(mergeRGB)
selectWindow(merge8bit);
run("Close");

//creat scale bar
scalebar_length=getNumber("Enter the desired length of the scale bar [in µm]", 5);
selectWindow(mergeRGB);
run("Scale Bar...", "width=scalebar_length height=4 font=20 color=White background=None
location=[Lower Right] bold hide");
mergeRGB=mergeRGB+"_"+scalebar_length+"µm"
rename(mergeRGB)
path=dir+mergeRGB;
saveAs("Tiff", path);
mergeRGBscale=getTitle
// run("Close");

//create merged image
//standard settings in ImageJ: C1=red; C2=green; C3=blue; C4=gray; C5=cyan; C6=magenta; C7=yellow
run("Merge Channels...", "c1=["+SiRTub+"] c3=["+HOECHST+"] create keep");
merge8bit=getTitle
run("RGB Color");
mergeRB=getTitle
mergeRB=replace(mergeRB, "Composite", "");
mergeRB=sliced3+" b_RBmerge";
rename(mergeRB);
path=dir+mergeRB;
saveAs("Tiff", path);
mergeRB=replace(mergeRB, ".tif", "")
rename(mergeRB)
selectWindow(merge8bit);
run("Close");

//creat scale bar
scalebar_length=getNumber("Enter the desired length of the scale bar [in µm]", 5);
selectWindow(mergeRB);
run("Scale Bar...", "width=scalebar_length height=4 font=20 color=White background=None
location=[Lower Right] bold hide");
mergeRB=mergeRB+"_"+scalebar_length+"µm"
rename(mergeRB)
path=dir+mergeRB;
saveAs("Tiff", path);
mergeRBscale=getTitle

```

```

run("Close");

//invert images for montage
selectWindow(SiRTub);
run("Invert");
SiRTub=getTitle
SiRTub=replace(SiRTub,""+prefixSiRTub+"", "")
rename(SiRTub);
SiRTub=SiRTub+" a_SiRTub";
rename(SiRTub);
path=dir+SiRTub;
saveAs("Tiff", path);
SiRTub=replace(SiRTub, ".tif", "")
rename(SiRTub)

run("Duplicate...", "duplicate");
SiRTubscale=getTitle
SiRTubscale=replace(SiRTubscale, "-1", "")
rename(SiRTubscale)
run("Scale Bar...", "width=scalebar_length height=4 font=20 color=Black background=None
location=[Lower Right] bold hide");
SiRTubscale=SiRTub+"_"+scalebar_length+"µm"
rename(SiRTubscale)
path=dir+SiRTubscale;
saveAs("Tiff", path);
SiRTubscale2=getTitle
close(SiRTubscale2);

selectWindow(HOECHST);
run("Invert");
HOECHST=getTitle
HOECHST=replace(HOECHST, ""+prefixHOECHST+"", "")
rename(HOECHST);
HOECHST=HOECHST+" a_HOECHST";
rename(HOECHST);
path=dir+HOECHST;
saveAs("Tiff", path);
HOECHST=replace(HOECHST, ".tif", "")
rename(HOECHST)
run("Duplicate...", "duplicate");
HOECHSTscale=getTitle
HOECHSTscale=replace(HOECHSTscale, "-1", "")
rename(HOECHSTscale)
run("Scale Bar...", "width=scalebar_length height=4 font=20 color=Black background=None
location=[Lower Right] bold hide");
HOECHSTscale=HOECHST+"_"+scalebar_length+"µm"
rename(HOECHSTscale)
path=dir+HOECHSTscale;
saveAs("Tiff", path);
HOECHSTscale2=getTitle
close(HOECHSTscale2);

selectWindow(GFP);
run("Invert");
GFP=getTitle
GFP=replace(GFP, ""+prefixGFP+"", "")
rename(GFP);
GFP=GFP+" a_GFP";
rename(GFP);

```

```
path=dir+GFP;
saveAs("Tiff", path);
GFP=replace(GFP, ".tif", "")
rename(GFP)

run("Duplicate...", "duplicate");
GFPscale=getTitle
GFPscale=replace(GFPscale, "-1", "")
rename(GFPscale)
run("Scale Bar...", "width=scalebar_length height=4 font=20 color=Black background=None
location=[Lower Right] bold hide");
GFPscale=GFP+" "+scalebar_length+"µm"
rename(GFPscale)
path=dir+GFPscale;
saveAs("Tiff", path);
GFPscale2=getTitle
close(GFPscale2);

close(SiRTub);
close(HOECHST);
close(GFP);
close(stack);
close(mergeRGBscale)
```